ARTICLES

Identification and analysis of functional elements in 1% of the human genome by the ENCODE pilot project

The ENCODE Project Consortium*

We report the generation and analysis of functional data from multiple, diverse experiments performed on a targeted 1% of the human genome as part of the pilot phase of the ENCODE Project. These data have been further integrated and augmented by a number of evolutionary and computational analyses. Together, our results advance the collective knowledge about human genome function in several major areas. First, our studies provide convincing evidence that the genome is pervasively transcribed, such that the majority of its bases can be found in primary transcripts, including non-protein-coding transcripts, and those that extensively overlap one another. Second, systematic examination of transcriptional regulation has yielded new understanding about transcription start sites, including their relationship to specific regulatory sequences and features of chromatin accessibility and histone modification. Third, a more sophisticated view of chromatin structure has emerged, including its inter-relationship with DNA replication and transcriptional regulation. Finally, integration of these new sources of information, in particular with respect to mammalian evolution based on inter- and intra-species sequence comparisons, has yielded new mechanistic and evolutionary insights concerning the functional landscape of the human genome. Together, these studies are defining a path for pursuit of a more comprehensive characterization of human genome function.

The human genome is an elegant but cryptic store of information. The roughly three billion bases encode, either directly or indirectly, the instructions for synthesizing nearly all the molecules that form each human cell, tissue and organ. Sequencing the human genome[1–3] provided highly accurate DNA sequences for each of the 24 chromosomes. However, at present, we have an incomplete understanding of the protein-coding portions of the genome, and markedly less understanding of both non-protein-coding transcripts and genomic elements that temporally and spatially regulate gene expression. To understand the human genome, and by extension the biological processes it orchestrates and the ways in which its defects can give rise to disease, we need a more transparent view of the information it encodes.

The molecular mechanisms by which genomic information directs the synthesis of different biomolecules has been the focus of much of molecular biology research over the last three decades. Previous studies have typically concentrated on individual genes, with the resulting general principles then providing insights into transcription, chromatin remodelling, messenger RNA splicing, DNA replication and numerous other genomic processes. Although many such principles seem valid as additional genes are investigated, they generally have not provided genome-wide insights about biological function.

The first genome-wide analyses that shed light on human genome function made use of observing the actions of evolution. The ever-growing set of vertebrate genome sequences[4–8] is providing increasing power to reveal the genomic regions that have been most and least acted on by the forces of evolution. However, although these studies convincingly indicate the presence of numerous genomic regions under strong evolutionary constraint, they have less power in identifying the precise bases that are constrained and provide little, if any, insight into why those bases are biologically important. Furthermore, although we have good models for how protein-coding regions

evolve, our present understanding about the evolution of other functional genomic regions is poorly developed. Experimental studies that augment what we learn from evolutionary analyses are key for solidifying our insights regarding genome function.

The Encyclopedia of DNA Elements (ENCODE) Project[9] aims to provide a more biologically informative representation of the human genome by using high-throughput methods to identify and catalogue the functional elements encoded. In its pilot phase, 35 groups provided more than 200 experimental and computational data sets that examined in unprecedented detail a targeted 29,998 kilobases (kb) of the human genome. These roughly 30 Mb—equivalent to ∼1% of the human genome—are sufficiently large and diverse to allow for rigorous pilot testing of multiple experimental and computational methods. These 30 Mb are divided among 44 genomic regions; approximately 15 Mb reside in 14 regions for which there is already substantial biological knowledge, whereas the other 15 Mb reside in 30 regions chosen by a stratified random-sampling method (see http://www.genome.gov/10506161). The highlights of our findings to date include:

● The human genome is pervasively transcribed, such that the majority of its bases are associated with at least one primary transcript and many transcripts link distal regions to established protein-coding loci.

● Many novel non-protein-coding transcripts have been identified, with many of these overlapping protein-coding loci and others located in regions of the genome previously thought to be transcriptionally silent.

● Numerous previously unrecognized transcription start sites have been identified, many of which show chromatin structure and sequence-specific protein-binding properties similar to well-understood promoters.

*A list of authors and their affiliations appears at the end of the paper.

● Regulatory sequences that surround transcription start sites are symmetrically distributed, with no bias towards upstream regions.

● Chromatin accessibility and histone modification patterns are highly predictive of both the presence and activity of transcription start sites.

● Distal DNaseI hypersensitive sites have characteristic histone modification patterns that reliably distinguish them from promoters; some of these distal sites show marks consistent with insulator function.

● DNA replication timing is correlated with chromatin structure.

● A total of 5% of the bases in the genome can be confidently identified as being under evolutionary constraint in mammals; for approximately 60% of these constrained bases, there is evidence of function on the basis of the results of the experimental assays performed to date.

● Although there is general overlap between genomic regions identified as functional by experimental assays and those under evolutionary constraint, not all bases within these experimentally defined regions show evidence of constraint.

● Different functional elements vary greatly in their sequence variability across the human population and in their likelihood of residing within a structurally variable region of the genome.

● Surprisingly, many functional elements are seemingly unconstrained across mammalian evolution. This suggests the possibility of a large pool of neutral elements that are biochemically active but provide no specific benefit to the organism. This pool may serve as a 'warehouse' for natural selection, potentially acting as the source of lineage-specific elements and functionally conserved but non-orthologous elements between species.

Below, we first provide an overview of the experimental techniques used for our studies, after which we describe the insights gained from analysing and integrating the generated data sets. We conclude with a perspective of what we have learned to date about this 1% of the human genome and what we believe the prospects are for a broader and deeper investigation of the functional elements in the human genome. To aid the reader, Box 1 provides a glossary for many of the abbreviations used throughout this paper.

Experimental techniques

Table 1 (expanded in Supplementary Information section 1.1) lists the major experimental techniques used for the studies reported here, relevant acronyms, and references reporting the generated data sets. These data sets reflect over 400 million experimental data points (603 million data points if one includes comparative sequencing bases). In describing the major results and initial conclusions, we seek to distinguish 'biochemical function' from 'biological role'. Biochemical function reflects the direct behaviour of a molecule(s), whereas biological role is used to describe the consequence(s) of this function for the organism. Genome-analysis techniques nearly always focus on biochemical function but not necessarily on biological role. This is because the former is more amenable to large-scale data-generation methods, whereas the latter is more difficult to assay on a large scale.

The ENCODE pilot project aimed to establish redundancy with respect to the findings represented by different data sets. In some instances, this involved the intentional use of different assays that were based on a similar technique, whereas in other situations, different techniques assayed the same biochemical function. Such redundancy has allowed methods to be compared and consensus data sets to be generated, much of which is discussed in companion papers, such as the ChIP-chip platform comparison[10,11]. All ENCODE data have been released after verification but before this publication, as befits a 'community resource' project (see http://www.wellcome.ac.uk/doc_wtd003208.html). Verification is defined as when the experiment is reproducibly confirmed (see Supplementary Information section 1.2). The main portal for ENCODE data is provided by the UCSC Genome Browser (http://genome.ucsc.edu/ENCODE/); this is

---

Box 1 | Frequently used abbreviations in this paper

AR Ancient repeat: a repeat that was inserted into the early mammalian lineage and has since become dormant; the majority of ancient repeats are thought to be neutrally evolving.

CAGE tag A short sequence from the 5' end of a transcript

CDS Coding sequence: a region of a cDNA or genome that encodes proteins

ChIP-chip Chromatin immunoprecipitation followed by detection of the products using a genomic tiling array

CNV Copy number variants: regions of the genome that have large duplications in some individuals in the human population

CS Constrained sequence: a genomic region associated with evidence of negative selection (that is, rejection of mutations relative to neutral regions)

DHS DNaseI hypersensitive site: a region of the genome showing a sharply different sensitivity to DNaseI compared with its immediate locale

EST Expressed sequence tag: a short sequence of a cDNA indicative of expression at this point

FAIRE Formaldehyde-assisted isolation of regulatory elements: a method to assay open chromatin using formaldehyde crosslinking followed by detection of the products using a genomic tiling array

FDR False discovery rate: a statistical method for setting thresholds on statistical tests to correct for multiple testing

GENCODE Integrated annotation of existing cDNA and protein resources to define transcripts with both manual review and experimental testing procedures

GSC Genome structure correction: a method to adapt statistical tests to make fewer assumptions about the distribution of features on the genome sequence. This provides a conservative correction to standard tests

HMM Hidden Markov model: a machine-learning technique that can establish optimal parameters for a given model to explain the observed data

Indel An insertion or deletion; two sequences often show a length difference within alignments, but it is not always clear whether this reflects a previous insertion or a deletion

PET A short sequence that contains both the 5' and 3' ends of a transcript

RACE Rapid amplification of cDNA ends: a technique for amplifying cDNA sequences between a known internal position in a transcript and its 5' end

RFBR Regulatory factor binding region: a genomic region found by a ChIP-chip assay to be bound by a protein factor

RFBR-Seqsp Regulatory factor binding regions that are from sequence-specific binding factors

RT–PCR Reverse transcriptase polymerase chain reaction: a technique for amplifying a specific region of a transcript

RxFrag Fragment of a RACE reaction: a genomic region found to be present in a RACE product by an unbiased tiling-array assay

SNP Single nucleotide polymorphism: a single base pair change between two individuals in the human population

STAGE Sequence tag analysis of genomic enrichment: a method similar to ChIP-chip for detecting protein factor binding regions but using extensive short sequence determination rather than genomic tiling arrays

SVM Support vector machine: a machine-learning technique that can establish an optimal classifier on the basis of labelled training data

TR50 A measure of replication timing corresponding to the time in the cell cycle when 50% of the cells have replicated their DNA at a specific genomic position

TSS Transcription start site

TxFrag Fragment of a transcript: a genomic region found to be present in a transcript by an unbiased tiling-array assay

Un.TxFrag A TxFrag that is not associated with any other functional annotation

UTR Untranslated region: part of a cDNA either at the 5' or 3' end that does not encode a protein sequence

---

augmented by multiple other websites (see Supplementary Information section 1.1).

A common feature of genomic analyses is the need to assess the significance of the co-occurrence of features or of other statistical tests. One confounding factor is the heterogeneity of the genome, which can produce uninteresting correlations of variables distributed across the genome. We have developed and used a statistical framework that mitigates many of these hidden correlations by adjusting the appropriate null distribution of the test statistics. We term this correction procedure genome structure correction (GSC) (see Supplementary Information section 1.3).

In the next five sections, we detail the various biological insights of the pilot phase of the ENCODE Project.

Transcription

Overview. RNA transcripts are involved in many cellular functions, either directly as biologically active molecules or indirectly by encoding other active molecules. In the conventional view of genome organization, sets of RNA transcripts (for example, messenger RNAs) are encoded by distinct loci, with each usually dedicated to a single biological role (for example, encoding a specific protein). However, this picture has substantially grown in complexity in recent years[12]. Other forms of RNA molecules (such as small nucleolar RNAs and micro (mi)RNAs) are known to exist, and often these are encoded by regions that intercalate with protein-coding genes. These observations are consistent with the well-known discrepancy between the levels of observable mRNAs and large structural RNAs

compared with the total RNA in a cell, suggesting that there are numerous RNA species yet to be classified[13–15]. In addition, studies of specific loci have indicated the presence of RNA transcripts that have a role in chromatin maintenance and other regulatory control. We sought to assay and analyse transcription comprehensively across the 44 ENCODE regions in an effort to understand the repertoire of encoded RNA molecules.

Transcript maps. We used three methods to identify transcripts emanating from the ENCODE regions: hybridization of RNA (either total or polyA-selected) to unbiased tiling arrays (see Supplementary Information section 2.1), tag sequencing of cap-selected RNA at the 5′ or joint 5′/3′ ends (see Supplementary Information sections 2.2 and S2.3), and integrated annotation of available complementary DNA and EST sequences involving computational, manual, and experimental approaches[16] (see Supplementary Information section 2.4). We abbreviate the regions identified by unbiased tiling arrays as TxFrags, the cap-selected RNAs as CAGE or PET tags (see Box 1), and the integrated annotation as GENCODE transcripts. When a TxFrag does not overlap a GENCODE annotation, we call it an Un.TxFrag. Validation of these various studies is described in papers reporting these data sets[17] (see Supplementary Information sections 2.1.4 and 2.1.5).

These methods recapitulate previous findings, but provide enhanced resolution owing to the larger number of tissues sampled and the integration of results across the three approaches (see Table 2). To begin with, our studies show that 14.7% of the bases represented in the unbiased tiling arrays are transcribed in at least one tissue sample. Consistent with previous work[14,15], many (63%) TxFrags reside outside of GENCODE annotations, both in intronic (40.9%) and intergenic (22.6%) regions. GENCODE annotations are richer than the more-conservative RefSeq or Ensembl annotations, with 2,608 transcripts clustered into 487 loci, leading to an average of 5.4 transcripts per locus. Finally, extensive testing of predicted protein-coding sequences outside of GENCODE annotations was positive in only 2% of cases[16], suggesting that GENCODE annotations cover nearly all protein-coding sequences. The GENCODE annotations are categorized both by likely function (mainly, the presence of an open reading frame) and by classification evidence (for example, transcripts based solely on ESTs are distinguished from other scenarios); this classification is not strongly correlated with expression levels (see Supplementary Information sections 2.4.2 and 2.4.3).

Analyses of more biological samples have allowed a richer description of the transcription specificity (see Fig. 1 and Supplementary Information section 2.5). We found that 40% of TxFrags are present in only one sample, whereas only 2% are present in all samples. Although exon-containing TxFrags are more likely (74%) to be expressed in more than one sample, 45% of unannotated TxFrags are also expressed in multiple samples. GENCODE annotations of separate loci often (42%) overlap with respect to their genomic coordinates, in particular on opposite strands (33% of loci). Further analysis of GENCODE-annotated sequences with respect to the positions of open reading frames revealed that some component exons do not have the expected synonymous versus non-synonymous substitution patterns of protein-coding sequence (see Supplement Information section 2.6) and some have deletions incompatible with

Table 1 | Summary of types of experimental techniques used in ENCODE

Feature class	Experimental technique(s)	Abbreviations	References	Number of experimental data points
Transcription	Tiling array, integrated annotation	TxFrag, RxFrag, GENCODE	117 118 19 119	63,348,656
5′ ends of transcripts*	Tag sequencing	PET, CAGE	121 13	864,964
Histone modifications	Tiling array	Histone nomenclature†, RFBR	46	4,401,291
Chromatin‡ structure	QT-PCR, tiling array	DHS, FAIRE	42 43 44 122	15,318,324
Sequence-specific factors	Tiling array, tag sequencing, promoter assays	STAGE, ChIP-Chip, ChIP-PET, RFBR	41,52 11,120 123 81 34,51 124 49 33 40	324,846,018
Replication	Tiling array	TR50	59 75	14,735,740
Computational analysis	Computational methods	CCI, RFBR cluster	80 125 10 16 126 127	NA
Comparative sequence analysis*	Genomic sequencing, multi-sequence alignments, computational analyses	CS	87 86 26	NA
Polymorphisms*	Resequencing, copy number variation	CNV	103 128	NA

* Not all data generated by the ENCODE Project.
† Histone code nomenclature follows the Brno nomenclature as described in ref. 129.
‡ Also contains histone modification.

Table 2 | Bases detected in processed transcripts either as a GENCODE exon, a TxFrag, or as either a GENCODE exon or a TxFrag

	GENCODE exon	TxFrag	Either GENCODE exon or TxFrag
Total detectable transcripts (bases)	1,776,157 (5.9%)	1,369,611 (4.6%)	2,519,280 (8.4%)
Transcripts detected in tiled regions of arrays (bases)	1,447,192 (9.8%)	1,369,611 (9.3%)	2,163,303 (14.7%)

Percentages are of total bases in ENCODE in the first row and bases tiled in arrays in the second row.

protein structure[18]. Such exons are on average less expressed (25% versus 87% by RT–PCR; see Supplementary Information section 2.7) than exons involved in more than one transcript (see Supplementary Information section 2.4.3), but when expressed have a tissue distribution comparable to well-established genes.

Critical questions are raised by the presence of a large amount of unannotated transcription with respect to how the corresponding sequences are organized in the genome—do these reflect longer transcripts that include known loci, do they link known loci, or are they completely separate from known loci? We further investigated these issues using both computational and new experimental techniques.

Unannotated transcription. Consistent with previous findings, the Un.TxFrags did not show evidence of encoding proteins (see Supplementary Information section 2.8). One might expect Un.TxFrags to be linked within transcripts that exhibit coordinated expression and have similar conservation profiles across species. To test this, we clustered Un.TxFrags using two methods. The first method[19] used expression levels in 11 cell lines or conditions, dinucleotide composition, location relative to annotated genes, and evolutionary conservation profiles to cluster TxFrags (both unannotated and annotated). By this method, 14% of Un.TxFrags could be assigned to annotated loci, and 21% could be clustered into 200 novel loci (with an average of ~7 TxFrags per locus). We experimentally examined these novel loci to study the connectivity of transcripts amongst Un.TxFrags and between Un.TxFrags and known exons. Overall, about 40% of the connections (18 out of 46) were validated by RT–PCR. The second clustering method involved analysing a time course (0, 2, 8 and 32 h) of expression changes in human HL60 cells following retinoic-acid stimulation. There is a coordinated program of expression changes from annotated loci, which can be shown by plotting Pearson correlation values of the expression levels of exons inside annotated loci versus unrelated exons (see Supplementary Information section 2.8.2). Similarly, there is coordinated expression of nearby Un.TxFrags, albeit lower, though still significantly different from randomized sets. Both clustering methods indicate that there is coordinated behaviour of many Un.TxFrags, consistent with them residing in connected transcripts.

Transcript connectivity. We used a combination of RACE and tiling arrays[20] to investigate the diversity of transcripts emanating from protein-coding loci. Analogous to TxFrags, we refer to transcripts detected using RACE followed by hybridization to tiling arrays as RxFrags. We performed RACE to examine 399 protein-coding loci (those loci found entirely in ENCODE regions) using RNA derived from 12 tissues, and were able to unambiguously detect 4,573 RxFrags for 359 loci (see Supplementary Information section 2.9). Almost half of these RxFrags (2,324) do not overlap a GENCODE exon, and most (90%) loci have at least one novel RxFrag, which often extends a considerable distance beyond the 5′ end of the locus. Figure 2 shows the distribution of distances between these new RACE-detected ends and the previously annotated TSS of each locus. The average distance of the extensions is between 50 kb and 100 kb, with many extensions (>20%) being more than 200 kb. Consistent with the known presence of overlapping genes in the human genome, our findings reveal evidence for an overlapping gene at 224 loci, with transcripts from 180 of these loci (~50% of the RACE-positive loci) appearing to have incorporated at least one exon from an upstream gene.

To characterize further the 5′ RxFrag extensions, we performed RT–PCR followed by cloning and sequencing for 550 of the 5′ RxFrags (including the 261 longest extensions identified for each locus). The approach of mapping RACE products using microarrays is a combination method previously described and validated in several studies[14,17,20]. Hybridization of the RT–PCR products to tiling arrays confirmed connectivity in almost 60% of the cases. Sequenced clones confirmed transcript extensions. Longer extensions were harder to clone and sequence, but 5 out of 18 RT–PCR-positive extensions over 100 kb were verified by sequencing (see Supplementary Information section 2.9.7 and ref. 17). The detection of numerous RxFrag extensions coupled with evidence of considerable intronic transcription indicates that protein-coding loci are more transcriptionally complex than previously thought. Instead of the traditional view that many genes have one or more alternative transcripts that code for alternative proteins, our data suggest that a given gene may both encode multiple protein products and produce other transcripts that include sequences from both strands and from neighbouring loci (often without encoding a different protein). Figure 3 illustrates such a case, in which a new fusion transcript is expressed in the small intestine, and consists of at least three coding exons from the *ATP5O* gene and at least two coding exons from the *DONSON*
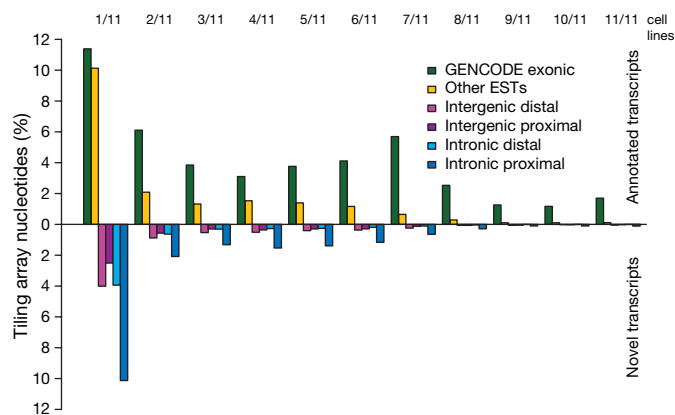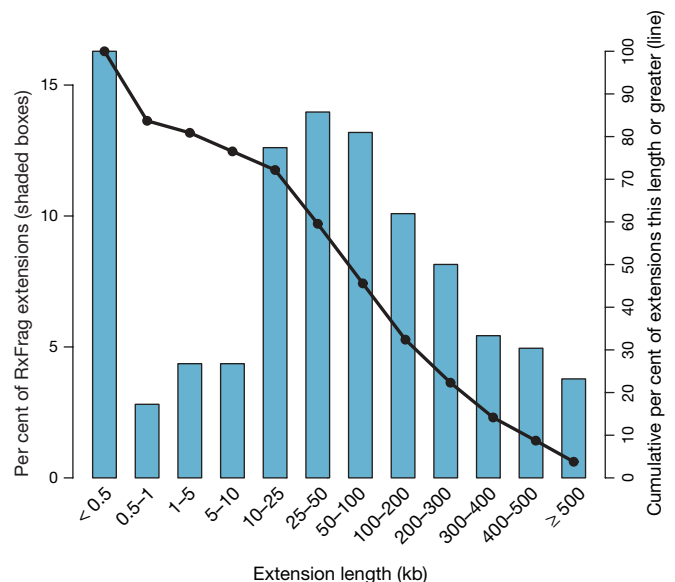

Figure 1 | Annotated and unannotated TxFrags detected in different cell lines. The proportion of different types of transcripts detected in the indicated number of cell lines (from 1/11 at the far left to 11/11 at the far right) is shown. The data for annotated and unannotated TxFrags are indicated separately, and also split into different categories based on GENCODE classification: exonic, intergenic (proximal being within 5 kb of a gene and distal being otherwise), intronic (proximal being within 5 kb of an intron and distal being otherwise), and matching other ESTs not used in the GENCODE annotation (principally because they were unspliced). The *y* axis indicates the per cent of tiling array nucleotides present in that class for that number of samples (combination of cell lines and tissues).

Figure 2 | Length of genomic extensions to GENCODE-annotated genes on the basis of RACE experiments followed by array hybridizations (RxFrags). The indicated bars reflect the frequency of extension lengths among different length classes. The solid line shows the cumulative frequency of extensions of that length or greater. Most of the extensions are greater than 50 kb from the annotated gene (see text for details).
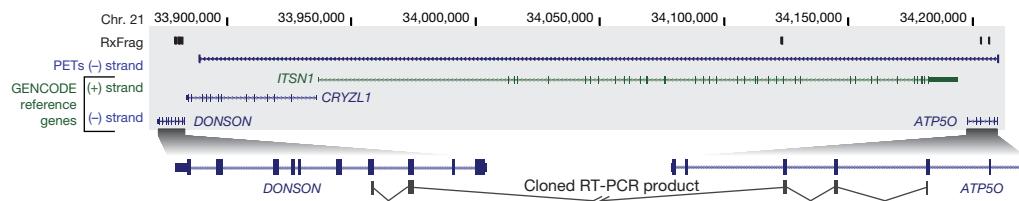
Figure 3 | Overview of RACE experiments showing a gene fusion. Transcripts emanating from the region between the *DONSON* and *ATP5O* genes. A 330-kb interval of human chromosome 21 (within ENm005) is shown, which contains four annotated genes: *DONSON, CRYZL1, ITSN1* and *ATP5O*. The 5′ RACE products generated from small intestine RNA and detected by tiling-array analyses (RxFrags) are shown along the top. Along the bottom is shown the placement of a cloned and sequenced RT–PCR product that has two exons from the *DONSON* gene followed by three exons from the *ATP5O* gene; these sequences are separated by a 300 kb intron in the genome. A PET tag shows the termini of a transcript consistent with this RT–PCR product.

gene, with no evidence of sequences from two intervening protein-coding genes (*ITSN1* and *CRYZL1*).

Pseudogenes. Pseudogenes, reviewed in refs 21 and 22, are generally considered non-functional copies of genes, are sometimes transcribed and often complicate analysis of transcription owing to close sequence similarity to functional genes. We used various computational methods to identify 201 pseudogenes (124 processed and 77 non-processed) in the ENCODE regions (see Supplementary Information section 2.10 and ref. 23). Tiling-array analysis of 189 of these revealed that 56% overlapped at least one TxFrag. However, possible cross-hybridization between the pseudogenes and their corresponding parent genes may have confounded such analyses. To assess better the extent of pseudogene transcription, 160 pseudogenes (111 processed and 49 non-processed) were examined for expression using RACE/tiling-array analysis (see Supplementary Information section 2.9.2). Transcripts were detected for 14 pseudogenes (8 processed and 6 non-processed) in at least one of the 12 tested RNA sources, the majority (9) being in testis (see ref. 23). Additionally, there was evidence for the transcription of 25 pseudogenes on the basis of their proximity (within 100 bp of a pseudogene end) to CAGE tags (8), PETs (2), or cDNAs/ESTs (21). Overall, we estimate that at least 19% of the pseudogenes in the ENCODE regions are transcribed, which is consistent with previous estimates[24,25].

Non-protein-coding RNA. Non-protein-coding RNAs (ncRNAs) include structural RNAs (for example, transfer RNAs, ribosomal RNAs, and small nuclear RNAs) and more recently discovered regulatory RNAs (for example, miRNAs). There are only 8 well-characterized ncRNA genes within the ENCODE regions (*U70, ACA36, ACA56, mir-192, mir-194-2, mir-196, mir-483* and *H19*), whereas representatives of other classes, (for example, box C/D snoRNAs, tRNAs, and functional snRNAs) seem to be completely absent in the ENCODE regions. Tiling-array data provided evidence for transcription in at least one of the assayed RNA samples for all of these ncRNAs, with the exception of mir-483 (expression of mir-483 might be specific to fetal liver, which was not tested). There is also evidence for the transcription of 6 out of 8 pseudogenes of ncRNAs (mainly snoRNA-derived). Similar to the analysis of protein-pseudogenes, the hybridization results could also originate from the known snoRNA gene elsewhere in the genome.

Many known ncRNAs are characterized by a well-defined RNA secondary structure. We applied two *de novo* ncRNA prediction algorithms—EvoFold and RNAz—to predict structured ncRNAs (as well as functional structures in mRNAs) using the multi-species sequence alignments (see below, Supplementary Information section 2.11 and ref. 26). Using a sensitivity threshold capable of detecting all known miRNAs and snoRNAs, we identified 4,986 and 3,707 candidate ncRNA loci with EvoFold and RNAz, respectively. Only 268 loci (5% and 7%, respectively) were found with both programs, representing a 1.6-fold enrichment over that expected by chance; the lack of more extensive overlap is due to the two programs having optimal sensitivity at different levels of GC content and conservation. We experimentally examined 50 of these targets using RACE/tiling-array analysis for brain and testis tissues (see Supplementary

Information sections 2.11 and 2.9.3); the predictions were validated at a 56%, 65%, and 63% rate for Evofold, RNAz and dual predictions, respectively.

Primary transcripts. The detection of numerous unannotated transcripts coupled with increasing knowledge of the general complexity of transcription prompted us to examine the extent of primary (that is, unspliced) transcripts across the ENCODE regions. Three data sources provide insight about these primary transcripts: the GENCODE annotation, PETs, and RxFrag extensions. Figure 4 summarizes the fraction of bases in the ENCODE regions that overlap transcripts identified by these technologies. Remarkably, 93% of bases are represented in a primary transcript identified by at least two independent observations (but potentially using the same technology); this figure is reduced to 74% in the case of primary transcripts detected by at least two different technologies. These increased spans are not mainly due to cell line rearrangements because they were present in multiple tissue experiments that confirmed the spans (see Supplementary Information section 2.12). These estimates assume that the presence of PETs or RxFrags defining the terminal ends of a transcript imply that the entire intervening DNA is transcribed and then processed. Other mechanisms, thought to be unlikely in the human genome, such as *trans*-splicing or polymerase jumping would also produce these long termini and potentially should be reconsidered in more detail.

Previous studies have suggested a similar broad amount of transcription across the human[14,15] and mouse[27] genomes. Our studies confirm these results, and have investigated the genesis of these transcripts in greater detail, confirming the presence of substantial intragenic and intergenic transcription. At the same time, many of the resulting transcripts are neither traditional protein-coding
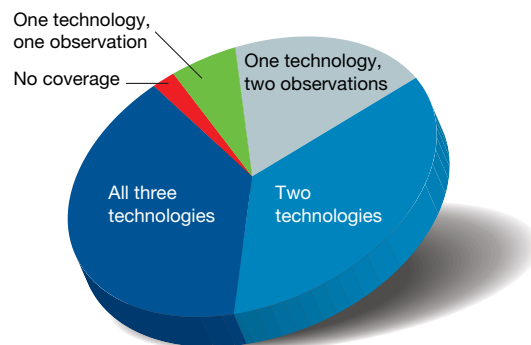

Figure 4 | Coverage of primary transcripts across ENCODE regions. Three different technologies (integrated annotation from GENCODE, RACE-array experiments (RxFrags) and PET tags) were used to assess the presence of a nucleotide in a primary transcript. Use of these technologies provided the opportunity to have multiple observations of each finding. The proportion of genomic bases detected in the ENCODE regions associated with each of the following scenarios is depicted: detected by all three technologies, by two of the three technologies, by one technology but with multiple observations, and by one technology with only one observation. Also indicated are genomic bases without any detectable coverage of primary transcripts.

transcripts nor easily explained as structural non-coding RNAs. Other studies have noted complex transcription around specific loci or chimaeric-gene structures (for example refs 28–30), but these have often been considered exceptions; our data show that complex inter-calated transcription is common at many loci. The results presented in the next section show extensive amounts of regulatory factors around novel TSSs, which is consistent with this extensive transcription. The biological relevance of these unannotated transcripts remains unanswered by these studies. Evolutionary information (detailed below) is mixed in this regard; for example, it indicates that unannotated transcripts show weaker evolutionary conservation than many other annotated features. As with other ENCODE-detected elements, it is difficult to identify clear biological roles for the majority of these transcripts; such experiments are challenging to perform on a large scale and, furthermore, it seems likely that many of the corresponding biochemical events may be evolutionarily neut-ral (see below).

Regulation of transcription

Overview. A significant challenge in biology is to identify the tran-scriptional regulatory elements that control the expression of each transcript and to understand how the function of these elements is coordinated to execute complex cellular processes. A simple, com-monplace view of transcriptional regulation involves five types of *cis*-acting regulatory sequences—promoters, enhancers, silencers, insulators and locus control regions[31]. Overall, transcriptional regu-lation involves the interplay of multiple components, whereby the availability of specific transcription factors and the accessibility of specific genomic regions determine whether a transcript is gener-ated[31]. However, the current view of transcriptional regulation is known to be overly simplified, with many details remaining to be established. For example, the consensus sequences of transcription factor binding sites (typically 6 to 10 bases) have relatively little information content and are present numerous times in the genome, with the great majority of these not participating in transcriptional regulation. Does chromatin structure then determine whether such a sequence has a regulatory role? Are there complex inter-factor inter-actions that integrate the signals from multiple sites? How are signals from different distal regulatory elements coupled without affecting all neighbouring genes? Meanwhile, our understanding of the repertoire of transcriptional events is becoming more complex, with an increas-ing appreciation of alternative TSSs[32,33] and the presence of non-coding[27,34] and anti-sense transcripts[35,36].

To better understand transcriptional regulation, we sought to begin cataloguing the regulatory elements residing within the 44 ENCODE regions. For this pilot project, we mainly focused on the binding of regulatory proteins and chromatin structure involved in transcriptional regulation. We analysed over 150 data sets, mainly from ChIP-chip[37–39], ChIP-PET and STAGE[40,41] studies (see Sup-plementary Information section 3.1 and 3.2). These methods use chromatin immunoprecipitation with specific antibodies to enrich for DNA in physical contact with the targeted epitope. This enriched DNA can then be analysed using either microarrays (ChIP-chip) or high-throughput sequencing (ChIP-PET and STAGE). The assays included 18 sequence-specific transcription factors and components of the general transcription machinery (for example, RNA polymer-ase II (Pol II), TAF1 and TFIIB/GTF2B). In addition, we tested more than 600 potential promoter fragments for transcriptional activity by transient-transfection reporter assays that used 16 human cell lines[33]. We also examined chromatin structure by studying the ENCODE regions for DNaseI sensitivity (by quantitative PCR[42] and tiling arrays[43,44], see Supplementary Information section 3.3), histone com-position[45], histone modifications (using ChIP-chip assays)[37,46], and histone displacement (using FAIRE, see Supplementary Information section 3.4). Below, we detail these analyses, starting with the efforts to define and classify the 5′ ends of transcripts with respect to their associated regulatory signals. Following that are summaries of

generated data about sequence-specific transcription factor binding and clusters of regulatory elements. Finally, we describe how this information can be integrated to make predictions about transcrip-tional regulation.

Transcription start site catalogue. We analysed two data sets to catalogue TSSs in the ENCODE regions: the 5′ ends of GENCODE-annotated transcripts and the combined results of two 5′-end-capture technologies—CAGE and PET-tagging. The initial results suggested the potential presence of 16,051 unique TSSs. However, in many cases, multiple TSSs resided within a single small segment (up to ~200 bases); this was due to some promoters con-taining TSSs with many very close precise initiation sites[47]. To nor-malize for this effect, we grouped TSSs that were 60 or fewer bases apart into a single cluster, and in each case considered the most frequent CAGE or PET tag (or the 5′-most TSS in the case of TSSs identified only from GENCODE data) as representative of that clus-ter for downstream analyses.

The above effort yielded 7,157 TSS clusters in the ENCODE regions. We classified these TSSs into three categories: known (pre-sent at the end of GENCODE-defined transcripts), novel (supported by other evidence) and unsupported. The novel TSSs were further subdivided on the basis of the nature of the supporting evidence (see Table 3 and Supplementary Information section 3.5), with all four of the resulting subtypes showing significant overlap with experimental evidence using the GSC statistic. Although there is a larger relative proportion of singleton tags in the novel category, when analysis is restricted to only singleton tags, the novel TSSs continue to have highly significant overlap with supporting evidence (see Supplemen-tary Information section 3.5.1).

Correlating genomic features with chromatin structure and tran-scription factor binding. By measuring relative sensitivity to DNaseI digestion (see Supplementary Information section 3.3), we identified DNaseI hypersensitive sites throughout the ENCODE regions. DHSs and TSSs both reflect genomic regions thought to be enriched for regulatory information and many DHSs reside at or near TSSs. We partitioned DHSs into those within 2.5 kb of a TSS (958; 46.5%) and the remaining ones, which were classified as distal (1,102; 53.5%). We then cross-analysed the TSSs and DHSs with data sets relating to histone modifications, chromatin accessibility and sequence-specific transcription factor binding by summarizing these signals in aggreg-ate relative to the distance from TSSs or DHSs. Figure 5 shows rep-resentative profiles of specific histone modifications, Pol II and selected transcription factor binding for the different categories of TSSs. Further profiles and statistical analysis of these studies can be found in Supplementary Information 3.6.

In the case of the three TSS categories (known, novel and unsup-ported), known and novel TSSs are both associated with similar signals for multiple factors (ranging from histone modifications through DNaseI accessibility), whereas unsupported TSSs are not.

Table 3 | Different categories of TSSs defined on the basis of support from different transcript-survey methods

Category	Transcript survey method	Number of TSS clusters (non-redundant)*	P value†	Singleton clusters‡ (%)
Known	GENCODE 5′ ends	1,730	2×10^{-70}	25 (74 overall)
Novel	GENCODE sense exons	1,437	6×10^{-39}	64
	GENCODE antisense exons	521	3×10^{-8}	65
	Unbiased transcription survey	639	7×10^{-63}	71
	CpG island	164	4×10^{-90}	60
Unsupported	None	2,666	-	83.4

* Number of TSS clusters with this support, excluding TSSs from higher categories.
† Probability of overlap between the transcript support and the PET/CAGE tags, as calculated by the Genome Structure Correction statistic (see Supplementary Information section 1.3).
‡ Per cent of clusters with only one tag. For the 'known' category this was calculated as the per cent of GENCODE 5′ ends with tag support (25%) or overall (74%).

The enrichments seen with chromatin modifications and sequence-specific factors, along with the significant clustering of this evidence, indicate that the novel TSSs do not reflect false positives and probably use the same biological machinery as other promoters. Sequence-specific transcription factors show a marked increase in binding across the broad region that encompasses each TSS. This increase is notably symmetric, with binding equally likely upstream or downstream of a TSS (see Supplementary Information section 3.7 for an explanation of why this symmetrical signal is not an artefact of the analysis of the signals). Furthermore, there is enrichment of SMARCC1 binding (a member of the SWI/SNF chromatin-modifying complex), which persists across a broader extent than other factors. The broad signals with this factor indicate that the ChIP-chip results reflect both specific enrichment at the TSS and broader enrichments across ~5-kb regions (this is not due to technical issues, see Supplementary Information section 3.8).

We selected 577 GENCODE-defined TSSs at the 5′ ends of a protein-coding transcript with over 3 exons, to assess expression status. Each transcript was classified as: (1) 'active' (gene on) or 'inactive' (gene off) on the basis of the unbiased transcript surveys, and (2) residing near a 'CpG island' or not ('non-CpG island') (see Supplementary Information section 3.17). As expected, the aggregate

signal of histone modifications is mainly attributable to active TSSs (Fig. 5), in particular those near CpG islands. Pronounced doublet peaks at the TSS can be seen with these large signals (similar to previous work in yeast[48]) owing to the chromatin accessibility at the TSS. Many of the histone marks and Pol II signals are now clearly asymmetrical, with a persistent level of Pol II into the genic region, as expected. However, the sequence-specific factors remain largely symmetrically distributed. TSSs near CpG islands show a broader distribution of histone marks than those not near CpG islands (see Supplementary Information section 3.6). The binding of some transcription factors (E2F1, E2F4 and MYC) is extensive in the case of active genes, and is lower (or absent) in the case of inactive genes.

Chromatin signature of distal elements. Distal DHSs show characteristic patterns of histone modification that are the inverse of TSSs, with high H3K4me1 accompanied by lower levels of H3K4Me3 and H3Ac (Fig. 5). Many factors with high occupancy at TSSs (for example, E2F4) show little enrichment at distal DHSs, whereas other factors (for example, MYC) are enriched at both TSSs and distal DHSs[49]. A particularly interesting observation is the relative enrichment of the insulator-associated factor CTCF[50] at both distal DHSs and TSSs; this contrasts with SWI/SNF components SMARCC2 and SMARCC1, which are TSS-centric. Such differential
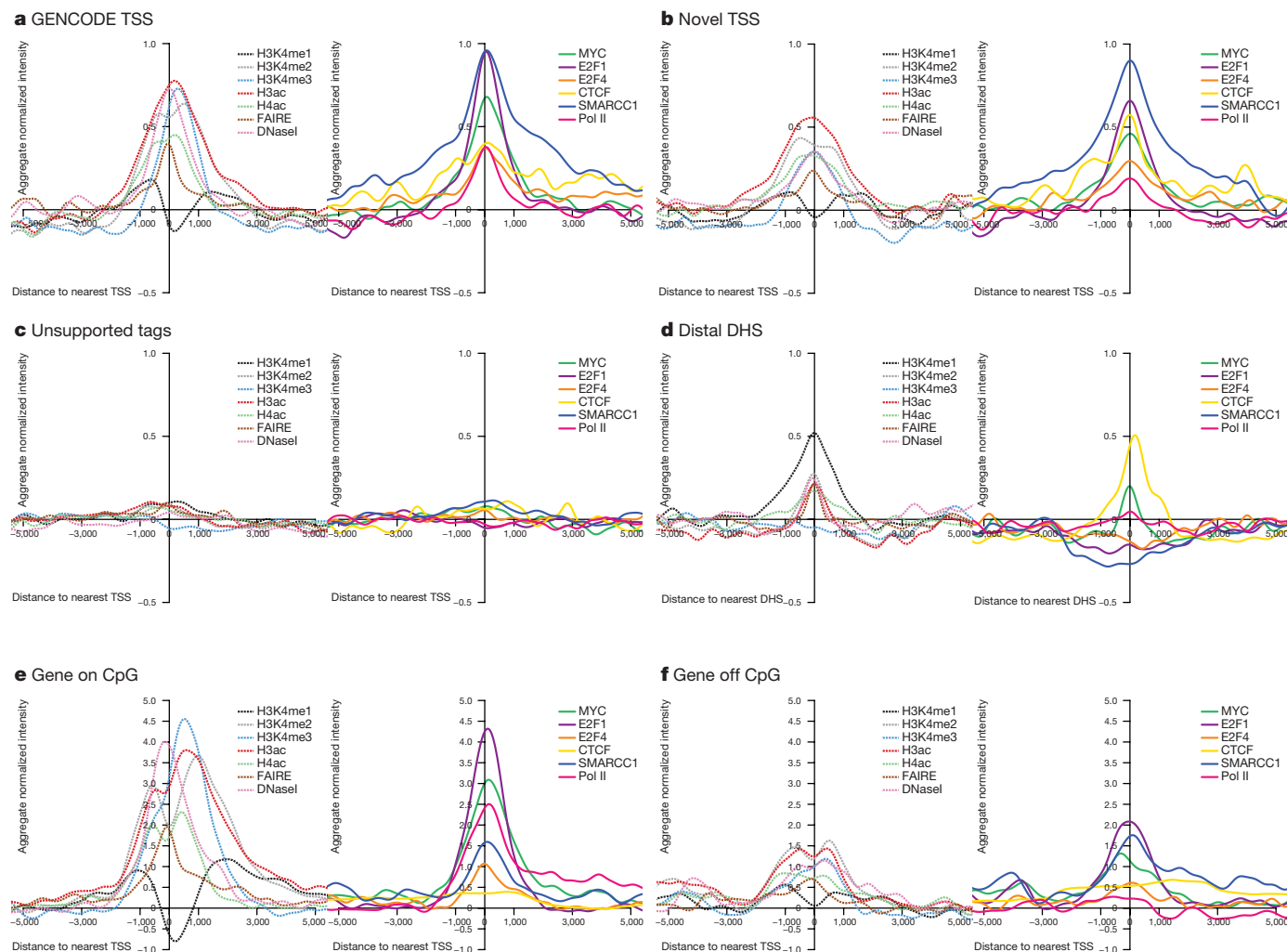

Figure 5 | Aggregate signals of tiling-array experiments from either ChIP-chip or chromatin structure assays, represented for different classes of TSSs and DHS. For each plot, the signal was first normalized with a mean of 0 and standard deviation of 1, and then the normalized scores were summed at each position for that class of TSS or DHS and smoothed using a kernel density method (see Supplementary Information section 3.6). For each class of sites there are two adjacent plots. The left plot depicts the data for general

factors: FAIRE and DNaseI sensitivity as assays of chromatin accessibility and H3K4me1, H3K4me2, H3K4me3, H3ac and H4ac histone modifications (as indicated); the right plot shows the data for additional factors, namely MYC, E2F1, E2F4, CTCF, SMARCC1 and Pol II. The columns provide data for the different classes of TSS or DHS (unsmoothed data and statistical analysis shown in Supplementary Information section 3.6).

805

behaviour of sequence-specific factors points to distinct biological differences, mediated by transcription factors, between distal regulatory sites and TSSs.

Unbiased maps of sequence-specific regulatory factor binding. The previous section focused on specific positions defined by TSSs or DHSs. We then analysed sequence-specific transcription factor binding data in an unbiased fashion. We refer to regions with enriched binding of regulatory factors as RFBRs. RFBRs were identified on the basis of ChIP-chip data in two ways: first, each investigator developed and used their own analysis method(s) to define high-enrichment regions, and second (and independently), a stringent false discovery rate (FDR) method was applied to analyse all data using three cut-offs (1%, 5% and 10%). The laboratory-specific and FDR-based methods were highly correlated, particularly for regions with strong signals[10,11]. For consistency, we used the results obtained with the FDR-based method (see Supplementary Information section 3.10). These RFBRs can be used to find sequence motifs (see Supplementary Information section S3.11).

RFBRs are associated with the 5′ ends of transcripts. The distribution of RFBRs is non-random (see ref. 10) and correlates with the positions of TSSs. We examined the distribution of specific RFBRs relative to the known TSSs. Different transcription factors and histone modifications vary with respect to their association with TSSs (Fig. 6; see Supplementary Information section 3.12 for modelling of random expectation). Factors for which binding sites are most enriched at the 5′ ends of genes include histone modifications, TAF1 and RNA Pol II with a hypo-phosphorylated carboxy-terminal domain[51]—confirming previous expectations. Surprisingly, we found that E2F1, a sequence-specific factor that regulates the expression of many genes at the G1 to S transition[52], is also tightly associated with TSSs[52]; this association is as strong as that of TAF1, the well-known TATA box-binding protein associated factor 1 (ref. 53). These results suggest that E2F1 has a more general role in transcription than previously suspected, similar to that for MYC[54–56]. In contrast, the large-scale assays did not support the promoter binding that was found in smaller-scale studies (for example, on SIRT1 and SPI1 (PU1)).

Integration of data on sequence-specific factors. We expect that regulatory information is not dispersed independently across the genome, but rather is clustered into distinct regions[57]. We refer to regions that contain multiple regulatory elements as 'regulatory clusters'. We sought to predict the location of regulatory clusters by
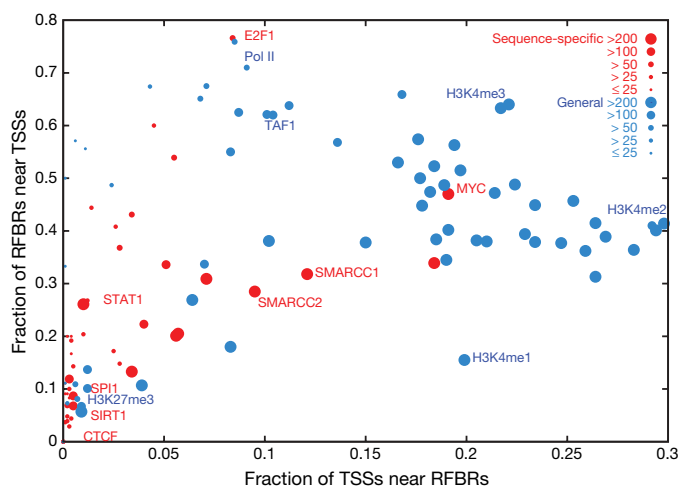
cross-integrating data generated using all transcription factor and histone modification assays, including results falling below an arbitrary threshold in individual experiments. Specifically, we used four complementary methods to integrate the data from 129 ChIP-chip data sets (see Supplementary Information section 3.13 and ref. 58. These four methods detect different classes of regulatory clusters and as a whole identified 1,393 clusters. Of these, 344 were identified by all four methods, with another 500 found by three methods (see Supplementary Information section 3.13.5). 67% of the 344 regulatory clusters identified by all four methods (or 65% of the full set of 1,393) reside within 2.5 kb of a known or novel TSS (as defined above; see Table 3 and Supplementary Information section 3.14 for a breakdown by category). Restricting this analysis to previously annotated TSSs (for example, RefSeq or Ensembl) reveals that roughly 25% of the regulatory clusters are close to a previously identified TSS. These results suggest that many of the regulatory clusters identified by integrating the ChIP-chip data sets are undiscovered promoters or are somehow associated with transcription in another fashion. To test these possibilities, sets of 126 and 28 non-GENCODE-based regulatory clusters were tested for promoter activity (see Supplementary Information section 3.15) and by RACE, respectively. These studies revealed that 24.6% of the 126 tested regulatory clusters had promoter activity and that 78.6% of the 28 regulatory clusters analysed by RACE yielded products consistent with a TSS[58]. The ChIP-chip data sets were generated on a mixture of cell lines, predominantly HeLa and GM06990, and were different from the CAGE/PET data, meaning that tissue specificity contributes to the presence of unique TSSs and regulatory clusters. The large increase in promoter proximal regulatory clusters identified by including the additional novel TSSs coupled with the positive promoter and RACE assays suggests that most of the regulatory regions identifiable by these clustering methods represent bona fide promoters (see Supplementary Information 3.16). Although the regulatory factor assays were more biased towards regions associated with promoters, many of the sites from these experiments would have previously been described as distal to promoters. This suggests that commonplace use of RefSeq- or Ensembl-based gene definition to define promoter proximity will dramatically overestimate the number of distal sites.

Predicting TSSs and transcriptional activity on the basis of chromatin structure. The strong association between TSSs and both histone modifications and DHSs prompted us to investigate whether the location and activity of TSSs could be predicted solely on the basis of chromatin structure information. We trained a support vector machine (SVM) by using histone modification data anchored around DHSs to discriminate between DHSs near TSSs and those distant from TSSs. We used a selected 2,573 DHSs, split roughly between TSS-proximal DHSs and TSS-distal DHSs, as a training set. The SVM performed well, with an accuracy of 83% (see Supplementary Information section 3.17). Using this SVM, we then predicted new TSSs using information about DHSs and histone modifications—of 110 high-scoring predicted TSSs, 81 resided within 2.5 kb of a novel TSS. As expected, these show a significant overlap to the novel TSS groups (defined above) but without a strong bias towards any particular category (see Supplementary Information section 3.17.1.5).

To investigate the relationship between chromatin structure and gene expression, we examined transcript levels in two cell lines using a transcript-tiling array. We compared this transcript data with the results of ChIP-chip experiments that measured histone modifications across the ENCODE regions. From this, we developed a variety of predictors of expression status using chromatin modifications as variables; these were derived using both decision trees and SVMs (see Supplementary Information section 3.17). The best of these correctly predicts expression status (transcribed versus non-transcribed) in 91% of cases. This success rate did not decrease dramatically when the predicting algorithm incorporated the results from one cell line to predict the expression status of another cell line. Interestingly, despite

Figure 6 | Distribution of RFBRs relative to GENCODE TSSs. Different RFBRs from sequence-specific factors (red) or general factors (blue) are plotted showing their relative distribution near TSSs. The *x* axis indicates the proportion of TSSs close (within 2.5 kb) to the specified factor. The *y* axis indicates the proportion of RFBRs close to TSSs. The size of the circle provides an indication of the number of RFBRs for each factor. A handful of representative factors are labelled.

the striking difference in histone modification enrichments in TSSs residing near versus those more distal to CpG islands (see Fig. 5 and Supplementary Information section 3.6), including information about the proximity to CpG islands did not improve the predictors. This suggests that despite the marked differences in histone modifications among these TSS classes, a single predictor can be made, using the interactions between the different histone modification levels.

In summary, we have integrated many data sets to provide a more complete view of regulatory information, both around specific sites (TSSs and DHSs) and in an unbiased manner. From analysing multiple data sets, we find 4,491 known and novel TSSs in the ENCODE regions, almost tenfold more than the number of established genes. This large number of TSSs might explain the extensive transcription described above; it also begins to change our perspective about regulatory information—without such a large TSS catalogue, many of the regulatory clusters would have been classified as residing distal to promoters. In addition to this revelation about the abundance of promoter-proximal regulatory elements, we also identified a considerable number of putative distal regulatory elements, particularly on the basis of the presence of DHSs. Our study of distal regulatory elements was probably most hindered by the paucity of data generated using distal-element-associated transcription factors; nevertheless, we clearly detected a set of distal-DHS-associated segments bound by CTCF or MYC. Finally, we showed that information about chromatin structure alone could be used to make effective predictions about both the location and activity of TSSs.

Replication

Overview. DNA replication must be carefully coordinated, both across the genome and with respect to development. On a larger scale, early replication in S phase is broadly correlated with gene density and transcriptional activity[59–66]; however, this relationship is not universal, as some actively transcribed genes replicate late and vice versa[61,64–68]. Importantly, the relationship between transcription and DNA replication emerges only when the signal of transcription is averaged over a large window (>100 kb)[63], suggesting that larger-scale chromosomal architecture may be more important than the activity of specific genes[69].

The ENCODE Project provided a unique opportunity to examine whether individual histone modifications on human chromatin can be correlated with the time of replication and whether such correlations support the general relationship of active, open chromatin with early replication. Our studies also tested whether segments showing interallelic variation in the time of replication have two different types of histone modifications consistent with an interallelic variation in chromatin state.

DNA replication data set. We mapped replication timing across the ENCODE regions by analysing Brd-U-labelled fractions from synchronized HeLa cells (collected at 2 h intervals throughout S phase) on tiling arrays (see Supplementary Information section 4.1). Although the HeLa cell line has a considerably altered karyotype, correlation of these data with other cell line data (see below) suggests the results are relevant to other cell types. The results are expressed as the time at which 50% of any given genomic position is replicated (TR50), with higher values signifying later replication times. In addition to the five 'activating' histone marks, we also correlated the TR50 with H3K27me3, a modification associated with polycomb-mediated transcriptional repression[70–74]. To provide a consistent comparison framework, the histone data were smoothed to 100-kb resolution, and then correlated with the TR50 data by a sliding window correlation analysis (see Supplementary Information section 4.2). The continuous profiles of the activating marks, histone H3K4 mono-, di-, and tri-methylation and histone H3 and H4 acetylation, are generally anti-correlated with the TR50 signal (Fig. 7a and Supplementary Information section 4.3). In contrast, H3K27me3 marks show a predominantly positive correlation with late-replicating segments (Fig. 7a; see Supplementary Information section 4.3 for additional analysis).

Although most genomic regions replicate in a temporally specific window in S phase, other regions demonstrate an atypical pattern of replication (Pan-S) where replication signals are seen in multiple parts of S phase. We have suggested that such a pattern of replication stems from interallelic variation in the chromatin structure[59,75]. If one allele is in active chromatin and the other in repressed chromatin, both types of modified histones are expected to be enriched in the Pan-S segments. An ENCODE region was classified as non-specific (or Pan-S) regions when $>60\%$ of the probes in a 10-kb window
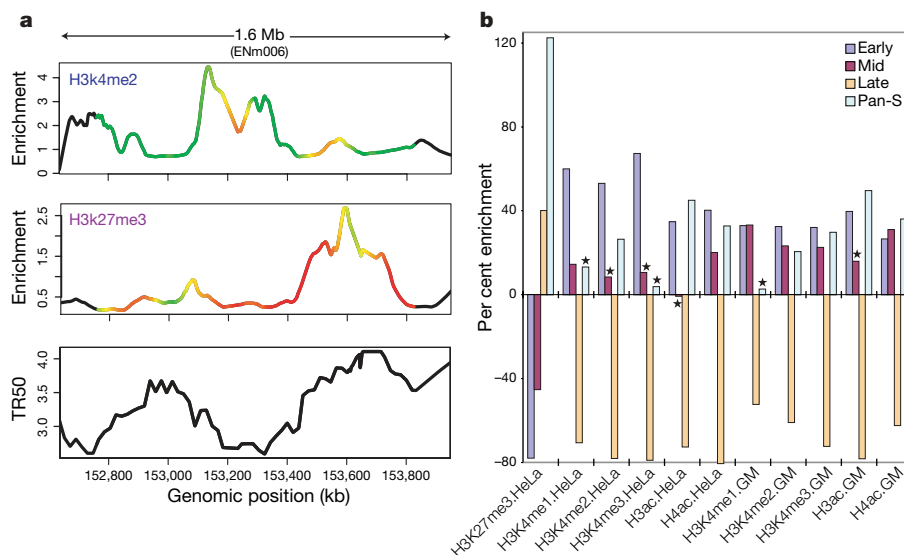

Figure 7 | Correlation between replication timing and histone modifications. a, Comparison of two histone modifications (H3K4me2 and H3K27me3), plotted as enrichment ratio from the Chip-chip experiments and the time for 50% of the DNA to replicate (TR50), indicated for ENCODE region ENm006. The colours on the curves reflect the correlation strength in a sliding 250-kb window. **b,** Differing levels of histone modification for different TR50 partitions. The amounts of enrichment or depletion of different histone modifications in various cell lines are depicted (indicated along the bottom as 'histone mark.cell line'; GM = GM06990). Asterisks indicate enrichments/depletions that are not significant on the basis of multiple tests. Each set has four partitions on the basis of replication timing: early, mid, late and Pan-S.

replicated in multiple intervals in S phase. The remaining regions were sub-classified into early-, mid- or late-replicating based on the average TR50 of the temporally specific probes within a 10-kb window[75]. For regions of each class of replication timing, we determined the relative enrichment of various histone modification peaks in HeLa cells (Fig. 7b; Supplementary Information section 4.4). The correlations of activating and repressing histone modification peaks with TR50 are confirmed by this analysis (Fig. 7b). Intriguingly, the Pan-S segments are unique in being enriched for both activating (H3K4me2, H3ac and H4ac) and repressing (H3K27me3) histones, consistent with the suggestion that the Pan-S replication pattern arises from interallelic variation in chromatin structure and time of replication[75]. This observation is also consistent with the Pan-S replication pattern seen for the H19/IGF2 locus, a known imprinted region with differential epigenetic modifications across the two alleles[76].

The extensive rearrangements in the genome of HeLa cells led us to ask whether the detected correlations between TR50 and chromatin state are seen with other cell lines. The histone modification data with GM06990 cells allowed us to test whether the time of replication of genomic segments in HeLa cells correlated with the chromatin state in GM06990 cells. Early- and late-replicating segments in HeLa cells are enriched and depleted, respectively, for activating marks in GM06990 cells (Fig. 7b). Thus, despite the presence of genomic rearrangements (see Supplementary Information section 2.12), the TR50 and chromatin state in HeLa cells are not far from a constitutive baseline also seen with a cell line from a different lineage. The enrichment of multiple activating histone modifications and the depletion of a repressive modification from segments that replicate early in S phase extends previous work in the field at a level of detail and scale not attempted before in mammalian cells. The duality of histone modification patterns in Pan-S areas of the HeLa genome, and the concordance of chromatin marks and replication time across two disparate cell lines (HeLa and GM06990) confirm the coordination of histone modifications with replication in the human genome.

Chromatin architecture and genomic domains

Overview. The packaging of genomic DNA into chromatin is intimately connected with the control of gene expression and other chromosomal processes. We next examined chromatin structure over a larger scale to ascertain its relation to transcription and other processes. Large domains (50 to >200 kb) of generalized DNaseI sensitivity have been detected around developmentally regulated gene clusters[77], prompting speculation that the genome is organized into 'open' and 'closed' chromatin territories that represent higher-order functional domains. We explored how different chromatin features, particularly histone modifications, correlate with chromatin structure, both over short and long distances.

Chromatin accessibility and histone modifications. We used histone modification studies and DNaseI sensitivity data sets (introduced above) to examine general chromatin accessibility without focusing on the specific DHS sites (see Supplementary Information sections 3.1, 3.3 and 3.4). A fundamental difficulty in analysing continuous data across large genomic regions is determining the appropriate scale for analysis (for example, 2 kb, 5 kb, 20 kb, and so on). To address this problem, we developed an approach based on wavelet analysis, a mathematical tool pioneered in the field of signal processing that has recently been applied to continuous-value genomic analyses. Wavelet analysis provides a means for consistently transforming continuous signals into different scales, enabling the correlation of different phenomena independently at differing scales in a consistent manner.

Global correlations of chromatin accessibility and histone modifications. We computed the regional correlation between DNaseI sensitivity and each histone modification at multiple scales using a wavelet approach (Fig. 8 and Supplementary Information section 4.2). To make quantitative comparisons between different histone modifications, we computed histograms of correlation values between DNaseI sensitivity and each histone modification at several scales and then tested these for significance at specific scales. Figure 8c shows the distribution of correlation values at a 16-kb scale, which is considerably larger than individual *cis*-acting regulatory elements. At this scale, H3K4me2, H3K4me3 and H3ac show similarly high correlation. However, they are significantly distinguished from H3K4me1 and H4ac modifications ($P < 1.5 \times 10^{-33}$; see Supplementary Information section 4.5), which show lower correlation with DNaseI sensitivity. These results suggest that larger-scale relationships between chromatin accessibility and histone modifications are dominated by sub-regions in which higher average DNaseI sensitivity is accompanied by high levels of H3K4me2, H3K4me3 and H3ac modifications.

Local correlations of chromatin accessibility and histone modifications. Narrowing to a scale of ~2 kb revealed a more complex situation, in which H3K4me2 is the histone modification that is best correlated with DNaseI sensitivity. However, there is no clear combination of marks that correlate with DNaseI sensitivity in a way that is analogous to that seen at a larger scale (see Supplementary Information section 4.3). One explanation for the increased
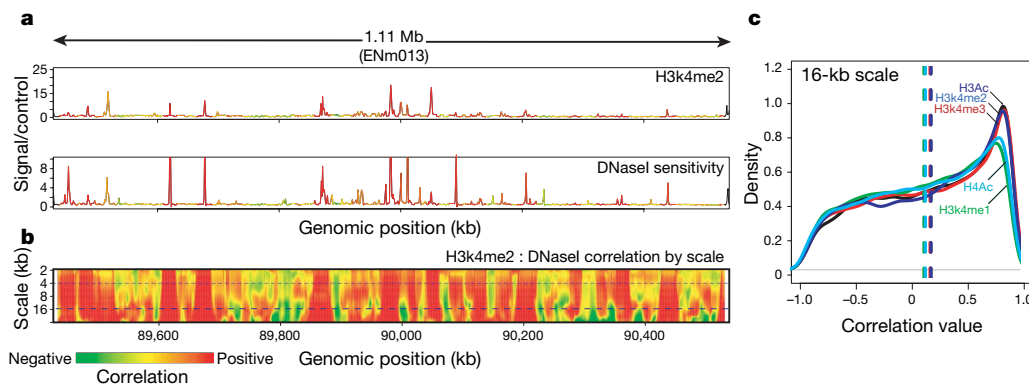

Figure 8 | Wavelet correlations of histone marks and DNaseI sensitivity. As an example, correlations between DNaseI sensitivity and H3K4me2 (both in the GM06990 cell line) over a 1.1-Mb region on chromosome 7 (ENCODE region ENm013) are shown. **a**, The relationship between histone modification H3K4me2 (upper plot) and DNaseI sensitivity (lower plot) is shown for ENCODE region ENm013. The curves are coloured with the strength of the local correlation at the 4-kb scale (top dashed line in panel **b**). **b**, The same data as in **a** are represented as a wavelet correlation. The

y axis shows the differing scales decomposed by the wavelet analysis from large to small scale (in kb); the colour at each point in the heatmap represents the level of correlation at the given scale, measured in a 20 kb window centred at the given position. **c**, Distribution of correlation values at the 16 kb scale between the indicated histone marks. The *y* axis is the density of these correlation values across ENCODE; all modifications show a peak at a positive-correlation value.

complexity at smaller scales is that there is a mixture of different classes of accessible chromatin regions, each having a different pattern of histone modifications. To examine this, we computed the degree to which local peaks in histone methylation or acetylation occur at DHSs (see Supplementary Information section 4.5.1). We found that 84%, 91% and 93% of significant peaks in H3K4 mono-, di- and tri-methylation, respectively, and 93% and 81% of significant peaks in H3ac and H4ac acetylation, respectively, coincided with DHSs (see Supplementary Information section 4.5). Conversely, a proportion of DHSs seemed not to be associated with significant peaks in H3K4 mono-, di- or tri-methylation (37%, 29% and 47%, respectively), nor with peaks in H3 or H4 acetylation (both 57%). Because only a limited number of histone modification marks were assayed, the possibility remains that some DHSs harbour other histone modifications. The absence of a more complete concordance between DHSs and peaks in histone acetylation is surprising given the widely accepted notion that histone acetylation has a central role in mediating chromatin accessibility by disrupting higher-order chromatin folding.

DNA structure at DHSs. The observation that distinctive hydroxyl radical cleavage patterns are associated with specific DNA structures[78] prompted us to investigate whether DHS subclasses differed with respect to their local DNA structure. Conversely, because different DNA sequences can give rise to similar hydroxyl radical cleavage patterns[79], genomic regions that adopt a particular local structure do not necessarily have the same nucleotide sequence. Using a Gibbs sampling algorithm on hydroxyl radical cleavage patterns of 3,150 DHSs[80], we discovered an 8-base segment with a conserved cleavage signature (CORCS; see Supplementary Information section 4.6). The underlying DNA sequences that give rise to this pattern have little primary sequence similarity despite this similar structural pattern. Furthermore, this structural element is strongly enriched in promoter-proximal DHSs (11.3-fold enrichment compared to the rest of the ENCODE regions) relative to promoter-distal DHSs (1.5-fold enrichment); this element is enriched 10.9-fold in CpG islands, but is higher still (26.4-fold) in CpG islands that overlap a DHS.

Large-scale domains in the ENCODE regions. The presence of extensive correlations seen between histone modifications, DNaseI

sensitivity, replication, transcript density and protein factor binding led us to investigate whether all these features are organized systematically across the genome. To test this, we performed an unsupervised training of a two-state HMM with inputs from these different features (see Supplementary Information section 4.7 and ref. 81). No other information except for the experimental variables was used for the HMM training routines. We consistently found that one state ('active') generally corresponded to domains with high levels of H3ac and RNA transcription, low levels of H3K27me3 marks, and early replication timing, whereas the other state ('repressed') reflected domains with low H3ac and RNA, high H3K27me3, and late replication (see Fig. 9). In total, we identified 70 active regions spanning 11.4 Mb and 82 inactive regions spanning 17.8 Mb (median size 136 kb versus 104 kb respectively). The active domains are markedly enriched for GENCODE TSSs, CpG islands and Alu repetitive elements ($P < 0.0001$ for each), whereas repressed regions are significantly enriched for LINE1 and LTR transposons ($P < 0.001$). Taken together, these results demonstrate remarkable concordance between ENCODE functional data types and provide a view of higher-order functional domains defined by a broader range of factors at a markedly higher resolution than was previously available[82].

Evolutionary constraint and population variability

Overview. Functional genomic sequences can also be identified by examining evolutionary changes across multiple extant species and within the human population. Indeed, such studies complement experimental assays that identify specific functional elements[83–85]. Evolutionary constraint (that is, the rejection of mutations at a particular location) can be measured by either (i) comparing observed substitutions to neutral rates calculated from multi-sequence alignments[86–88], or (ii) determining the presence and frequency of intra-species polymorphisms. Importantly, both approaches are indifferent to any specific function that the constrained sequence might confer.

Previous studies comparing the human, mouse, rat and dog genomes examined bulk evolutionary properties of all nucleotides in the genome, and provided little insight about the precise positions of constrained bases. Interestingly, these studies indicated that the
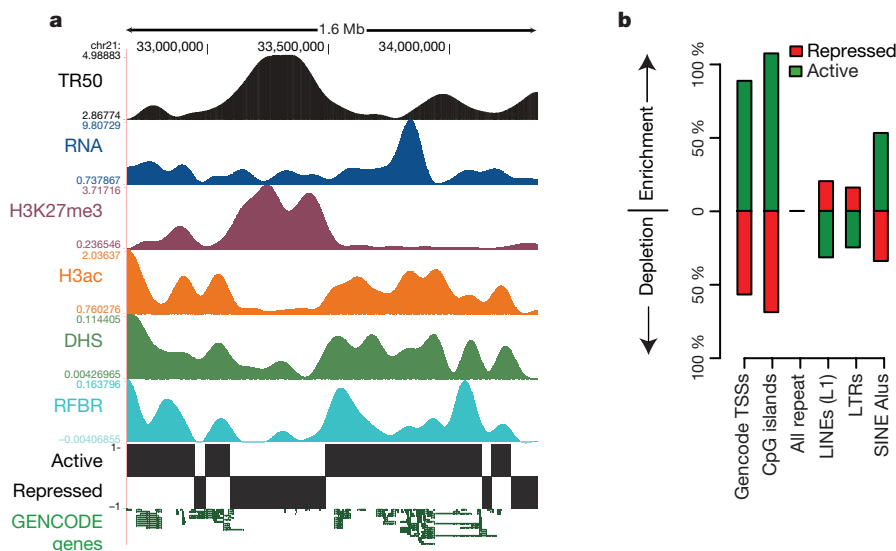

Figure 9 | Higher-order functional domains in the genome. The general concordance of multiple data types is shown for an illustrative ENCODE region (ENm005). **a**, Domains were determined by simultaneous HMM segmentation of replication time (TR50; black), bulk RNA transcription (blue), H3K27me3 (purple), H3ac (orange), DHS density (green), and RFBR density (light blue) measured continuously across the 1.6-Mb ENm005. All data were generated using HeLa cells. The histone, RNA, DHS and RFBR signals are wavelet-smoothed to an approximately 60-kb scale (see

Supplementary Information section 4.7). The HMM segmentation is shown as the blocks labelled 'active' and 'repressed' and the structure of GENCODE genes (not used in the training) is shown at the end. **b**, Enrichment or depletion of annotated sequence features (GENCODE TSSs, CpG islands, LINE1 repeats, Alu repeats, and non-exonic constrained sequences (CSs)) in active versus repressed domains. Note the marked enrichment of TSSs, CpG islands and Alus in active domains, and the enrichment of LINE and LTRs in repressed domains.

majority of constrained bases reside within the non-coding portion of the human genome. Meanwhile, increasingly rich data sets of polymorphisms across the human genome have been used extensively to establish connections between genetic variants and disease, but far fewer analyses have sought to use such data for assessing functional constraint[85].

The ENCODE Project provides an excellent opportunity for more fully exploiting inter- and intra-species sequence comparisons to examine genome function in the context of extensive experimental studies on the same regions of the genome. We consolidated the experimentally derived information about the ENCODE regions and focused our analyses on 11 major classes of genomic elements. These classes are listed in Table 4 and include two non-experimentally derived data sets: ancient repeats (ARs; mobile elements that inserted early in the mammalian lineage, have subsequently become dormant, and are assumed to be neutrally evolving) and constrained sequences (CSs; regions that evolve detectably more slowly than neutral sequences).

Comparative sequence data sets and analysis. We generated 206 Mb of genomic sequence orthologous to the ENCODE regions from 14 mammalian species using a targeted strategy that involved isolating[89] and sequencing[90] individual bacterial artificial chromosome clones. For an additional 14 vertebrate species, we used 340 Mb of orthologous genomic sequence derived from genome-wide sequencing efforts[3–8,91–93]. The orthologous sequences were aligned using three alignment programs: TBA[94], MAVID[95] and MLAGAN[96]. Four independent methods that generated highly concordant results[97] were then used to identify sequences under constraint (PhastCons[88], GERP[87], SCONE[98] and BinCons[86]). From these analyses, we developed a high-confidence set of 'constrained sequences' that correspond to 4.9% of the nucleotides in the ENCODE regions. The threshold for determining constraint was set using a FDR rate of 5% (see ref. 97); this level is similar to previous estimates of the fraction of the human genome under mammalian constraint[4,86–88] but the FDR rate was not chosen to fit this result. The median length of these constrained sequences is 19 bases, with the minimum being 8 bases—roughly the size of a typical transcription factor binding site. These analyses, therefore, provide a resolution of constrained sequences that is substantially better than that currently available using only whole-genome vertebrate sequences[99–102].

Intra-species variation studies mainly used SNP data from Phases I and II, and the 10 re-sequenced regions in ENCODE regions with 48 individuals of the HapMap Project[103]; nucleotide insertion or deletion (indel) data were from the SNP Consortium and HapMap. We also examined the ENCODE regions for the presence of overlaps with known segmental duplications[104] and CNVs.

Experimentally identified functional elements and constrained sequences. We first compared the detected constrained sequences with the positions of experimentally identified functional elements. A total of 40% of the constrained bases reside within protein-coding exons and their associated untranslated regions (Fig. 10) and, in agreement with previous genome-wide estimates, the remaining constrained bases do not overlap the mature transcripts of protein-coding genes[4,5,88,105,106]. When we included the other experimental annotations, we found that an additional 20% of the constrained bases overlap experimentally identified non-coding functional regions, although far fewer of these regions overlap constrained sequences compared to coding exons (see below). Most experimental annotations are significantly different from a random expectation for both base-pair or element-level overlaps (using the GSC statistic, see Supplementary Information section 1.3), with a more striking deviation when considering elements (Fig. 11). The exceptions to this are pseudogenes, Un.TxFrags and RxFrags. The increase in significance moving from base-pair measures to the element level suggests that discrete islands of constrained sequence exist within experimentally identified functional elements, with the surrounding bases apparently not showing evolutionary constraint. This notion is discussed in greater detail in ref. 97.

We also examined measures of human variation (heterozygosity, derived allele-frequency spectra and indel rates) within the sequences of the experimentally identified functional elements (Fig. 12). For these studies, ARs were used as a marker for neutrally evolving sequence. Most experimentally identified functional elements are associated with lower heterozygosity compared to ARs, and a few have lower indel rates compared with ARs. Striking outliers are 3′ UTRs, which have dramatically increased indel rates without an obvious cause. This is discussed in more depth in ref. 107.

These findings indicate that the majority of the evolutionarily constrained, experimentally identified functional elements show evidence of negative selection both across mammalian species and within the human population. Furthermore, we have assigned at least one molecular function to the majority (60%) of all constrained bases in the ENCODE regions.

Conservation of regulatory elements. The relationship between individual classes of regulatory elements and constrained sequences varies considerably, ranging from cases where there is strong evolutionary constraint (for example, pan-vertebrate ultraconserved regions[108,109]) to examples of regulatory elements that are not conserved between orthologous human and mouse genes[110]. Within the ENCODE regions, 55% of RFBRs overlap the high-confidence

Table 4 | Eleven classes of genomic elements subjected to evolutionary and population-genetics analyses

| Abbreviation	Description
CDS	Coding exons, as annotated by GENCODE
5′ UTR	5′ untranslated region, as annotated by GENCODE
3′ UTR	3′ untranslated region, as annotated by GENCODE
Un.TxFrag	Unannotated region detected by RNA hybridization to tiling array (that is, unannotated TxFrag)
RxFrag	Region detected by RACE and analysis on tiling array
Pseudogene	Pseudogene identified by consensus pseudogene analysis
RFBR	Regulatory factor binding region identified by ChIP-chip assay
RFBR-SeqSp	Regulatory factor binding region identified only by ChIP-chip assays for factors with known sequence-specificity
DHS	DNaseI hypersensitive sites found in multiple tissues
FAIRE	Region of open chromatin identified by the FAIRE assay
TSS	Transcription start site
AR	Ancient repeat inserted early in the mammalian lineage and presumed to be neutrally evolving
CS	Constrained sequence identified by analysing multi-sequence alignments
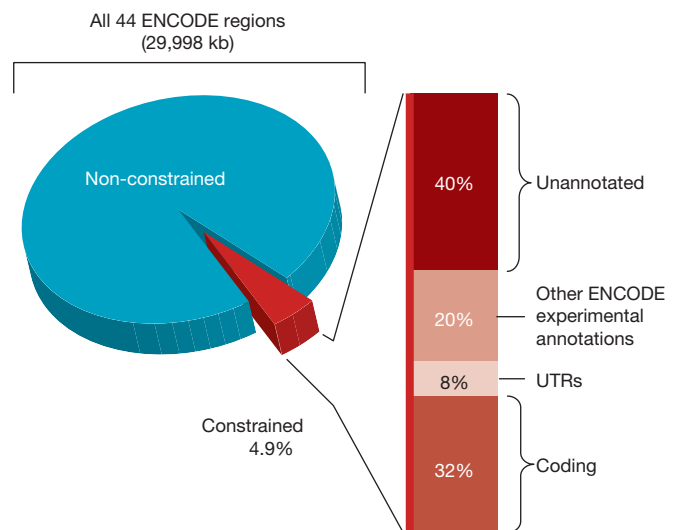
Figure 10 | Relative proportion of different annotations among constrained sequences. The 4.9% of bases in the ENCODE regions identified as constrained is subdivided into the portions that reflect known coding regions, UTRs, other experimentally annotated regions, and unannotated sequence.

constrained sequences. As expected, RFBRs have many unconstrained bases, presumably owing to the small size of the specific binding site. We investigated whether the binding sites in RFBRs could be further delimited using information about evolutionary constraint. For 7 out of 17 factors with either known TRANSFAC or Jaspar motifs, our ChIP-chip data revealed a marked enrichment of the appropriate motif within the constrained versus the unconstrained portions of the RFBRs (see Supplementary Information section 5.1). This enrichment was seen for levels of stringency used for defining ChIP-chip-positive sites (1% and 5% FDR level), indicating that combining sequence constraint and ChIP-chip data may provide a highly sensitive means for detecting factor binding sites in the human genome.

Experimentally identified functional elements and genetic variation. The above studies focus on purifying (negative) selection. We used nucleotide variation to detect potential signals of adaptive (positive) selection. We modified the standard McDonald–Kreitman test (MK-test[111,112]) and the Hudson–Kreitman–Aguade (HKA)[113] test (see Supplementary Information section 5.2.1), to examine whether an entire set of sequence elements shows an excess of polymorphisms or an excess of inter-species divergence. We found that constrained sequences and coding exons have an excess of polymorphisms (consistent with purifying selection), whereas 5′ UTRs

show evidence of an excess of divergence (with a portion probably reflecting positive selection). In general, non-coding genomic regions show more variation, with both a large number of segments that undergo purifying selection and regions that are fast evolving.

We also examined structural variation (that is, CNVs, inversions and translocations[114]; see Supplementary Information section 5.2.2). Within these polymorphic regions, we encountered significant over-representation of CDSs, TxFrags, and intra-species constrained sequences ($P < 10^{-3}$, Fig. 13), and also detected a statistically significant under-representation of ARs ($P = 10^{-3}$). A similar overrepresentation of CDSs and intra-species constrained sequences was found within non-polymorphic segmental duplications.

Unexplained constrained sequences. Despite the wealth of complementary data, 40% of the ENCODE-region sequences identified as constrained are not associated with any experimental evidence of function. There is no evidence indicating that mutational cold spots account for this constraint; they have similar measures of constraint to experimentally identified elements and harbour equal proportions of SNPs. To characterize further the unexplained constrained sequences, we examined their clustering and phylogenetic distribution. These sequences are not uniformly distributed across most ENCODE regions, and even in most ENCODE regions the distribution is different from constrained sequences within experimentally identified functional elements (see Supplementary Information section 5.3). The large fraction of constrained sequence that does not match any experimentally identified elements is not surprising considering that only a limited set of transcription factors, cell lines and biological conditions have thus far been examined.

Unconstrained experimentally identified functional elements. In contrast, an unexpectedly large fraction of experimentally identified functional elements show no evidence of evolutionary constraint ranging from 93% for Un.TxFrags to 12% for CDS. For most types of non-coding functional elements, roughly 50% of the individual elements seemed to be unconstrained across all mammals.

There are two methodological reasons that might explain the apparent excess of unconstrained experimentally identified functional elements: the underestimation of sequence constraint or overestimation of experimentally identified functional elements. We do not believe that either of these explanations fully accounts for the large and varied levels of unconstrained experimentally functional sequences. The set of constrained bases analysed here is highly accurate and complete due to the depth of the multiple alignment. Both by bulk fitting procedures and by comparison of SNP frequencies to constraint there is clearly a proportion of constrained bases not captured in the defined 4.9% of constrained sequences, but it is small (see
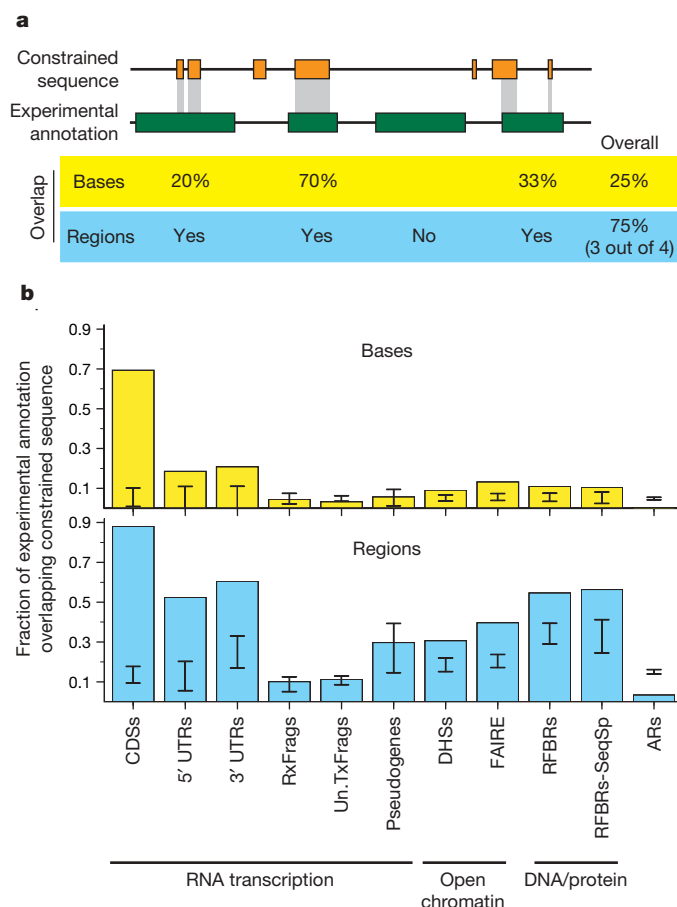

Figure 11 | Overlap of constrained sequences and various experimental annotations. a, A schematic depiction shows the different tests used for assessing overlap between experimental annotations and constrained sequences, both for individual bases and for entire regions. **b**, Observed fraction of overlap, depicted separately for bases and regions. The results are shown for selected experimental annotations. The internal bars indicate 95% confidence intervals of randomized placement of experimental elements using the GSC methodology to account for heterogeneity in the data sets. When the bar overlaps the observed value one cannot reject the hypothesis that these overlaps are consistent with random placements.
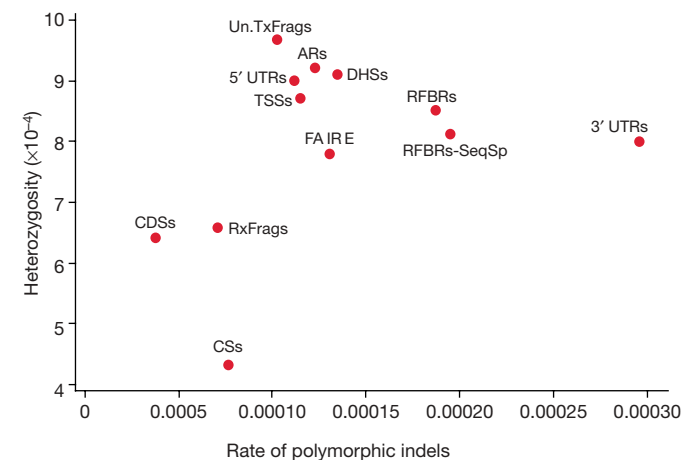

Figure 12 | Relationship between heterozygosity and polymorphic indel rate for a variety of experimental annotations. 3′ UTRs are an expected outlier for the indel measures owing to the presence of low-complexity sequence (leading to a higher indel rate).

Supplementary Information section 5.4 and S5.5). More aggressive schemes to detect constraint only marginally increase the overlap with experimentally identified functional elements, and do so with considerably less specificity. Similarly, all experimental findings have been independently validated and, for the least constrained experimentally identified functional elements (Un.TxFrags and binding sites of sequence-specific factors), there is both internal validation and cross-validation from different experimental techniques. This suggests that there is probably not a significant overestimation of experimentally identified functional elements. Thus, these two explanations may contribute to the general observation about unconstrained functional elements, but cannot fully explain it.

Instead, we hypothesize five biological reasons to account for the presence of large amounts of unconstrained functional elements. The first two are particular to certain biological assays in which the elements being measured are connected to but do not coincide with the analysed region. An example of this is the parent transcript of an miRNA, where the current assays detect the exons (some of which are not under evolutionary selection), whereas the intronic miRNA actually harbours the constrained bases. Nevertheless, the transcript sequence provides the critical coupling between the regulated promoter and the miRNA. The sliding of transcription factors (which might bind a specific sequence but then migrate along the DNA) or the processivity of histone modifications across chromatin are more exotic examples of this. A related, second hypothesis is that delocalized behaviours of the genome, such as general chromatin accessibility, may be maintained by some biochemical processes (such as transcription of intergenic regions or specific factor binding) without the requirement for specific sequence elements. These two explanations of both connected components and diffuse components related to, but not coincident with, constrained sequences are particularly relevant for the considerable amount of unannotated and unconstrained transcripts.

The other three hypotheses may be more general—the presence of neutral (or near neutral) biochemical elements, of lineage-specific functional elements, and of functionally conserved but non-orthologous elements. We believe there is a considerable proportion of neutral biochemically active elements that do not confer a selective advantage or disadvantage to the organism. This neutral pool of sequence elements may turn over during evolutionary time,

emerging via certain mutations and disappearing by others. The size of the neutral pool would largely be determined by the rate of emergence and extinction through chance events; low information-content elements, such as transcription factor-binding sites[110] will have larger neutral pools. Second, from this neutral pool, some elements might occasionally acquire a biological role and so come under evolutionary selection. The acquisition of a new biological role would then create a lineage-specific element. Finally, a neutral element from the general pool could also become a peer of an existing selected functional element and either of the two elements could then be removed by chance. If the older element is removed, the newer element has, in essence, been conserved without using orthologous bases, providing a conserved function in the absence of constrained sequences. For example, a common HNF4A binding site in the human and mouse genomes may not reflect orthologous human and mouse bases, though the presence of an HNF4A site in that region was evolutionarily selected for in both lineages. Note that both the neutral turnover of elements and the 'functional peering' of elements has been suggested for cis-acting regulatory elements in Drosophila[115,116] and mammals[110]. Our data support these hypotheses, and we have generalized this idea over many different functional elements. The presence of conserved function encoded by conserved orthologous bases is a commonplace assumption in comparative genomics; our findings indicate that there could be a sizable set of functionally conserved but non-orthologous elements in the human genome, and that these seem unconstrained across mammals. Functional data akin to the ENCODE Project on other related species, such as mouse, would be critical to understanding the rate of such functionally conserved but non-orthologous elements.

Conclusion

The generation and analyses of over 200 experimental data sets from studies examining the 44 ENCODE regions provide a rich source of functional information for 30 Mb of the human genome. The first conclusion of these efforts is that these data are remarkably informative. Although there will be ongoing work to enhance existing assays, invent new techniques and develop new data-analysis methods, the generation of genome-wide experimental data sets akin to the ENCODE pilot phase would provide an impressive platform for future genome exploration efforts. This now seems feasible in light of throughput improvements of many of the assays and the ever-declining costs of whole-genome tiling arrays and DNA sequencing. Such genome-wide functional data should be acquired and released openly, as has been done with other large-scale genome projects, to ensure its availability as a new foundation for all biologists studying the human genome. It is these biologists who will often provide the critical link from biochemical function to biological role for the identified elements.

The scale of the pilot phase of the ENCODE Project was also sufficiently large and unbiased to reveal important principles about the organization of functional elements in the human genome. In many cases, these principles agree with current mechanistic models. For example, we observe trimethylation of H3K4 enriched near active genes, and have improved the ability to accurately predict gene activity based on this and other histone modifications. However, we also uncovered some surprises that challenge the current dogma on biological mechanisms. The generation of numerous intercalated transcripts spanning the majority of the genome has been repeatedly suggested[13,14], but this phenomenon has been met with mixed opinions about the biological importance of these transcripts. Our analyses of numerous orthogonal data sets firmly establish the presence of these transcripts, and thus the simple view of the genome as having a defined set of isolated loci transcribed independently does not seem to be accurate. Perhaps the genome encodes a network of transcripts, many of which are linked to protein-coding transcripts and to the majority of which we cannot (yet) assign a biological role. Our perspective of transcription and genes may have to evolve and also poses
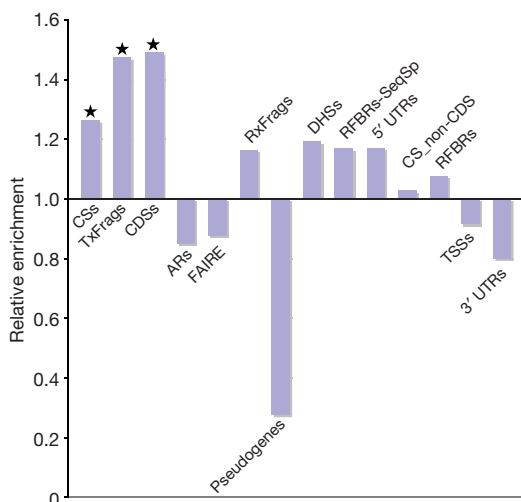
Figure 13 | CNV enrichment. The relative enrichment of different experimental annotations in the ENCODE regions associated with CNVs. CS_non-CDS are constrained sequences outside of coding regions. A value of 1 or less indicates no enrichment, and values greater than 1 show enrichment. Starred columns are cases that are significant on the basis of this enrichment being found in less than 5% of randomizations that matched each element class for length and density of features.

some interesting mechanistic questions. For example, how are splicing signals coordinated and used when there are so many overlapping primary transcripts? Similarly, to what extent does this reflect neutral turnover of reproducible transcripts with no biological role?

We gained subtler but equally important mechanistic findings relating to transcription, replication and chromatin modification. Transcription factors previously thought to primarily bind promoters bind more generally, and those which do bind to promoters are equally likely to bind downstream of a TSS as upstream. Interestingly, many elements that previously were classified as distal enhancers are, in fact, close to one of the newly identified TSSs; only about 35% of sites showing evidence of binding by multiple transcription factors are actually distal to a TSS. This need not imply that most regulatory information is confined to classic promoters, but rather it does suggest that transcription and regulation are coordinated actions beyond just the traditional promoter sequences. Meanwhile, although distal regulatory elements could be identified in the ENCODE regions, they are currently difficult to classify, in part owing to the lack of a broad set of transcription factors to use in analysing such elements. Finally, we now have a much better appreciation of how DNA replication is coordinated with histone modifications.

At the outset of the ENCODE Project, many believed that the broad collection of experimental data would nicely dovetail with the detailed evolutionary information derived from comparing multiple mammalian sequences to provide a neat 'dictionary' of conserved genomic elements, each with a growing annotation about their biochemical function(s). In one sense, this was achieved; the majority of constrained bases in the ENCODE regions are now associated with at least some experimentally derived information about function. However, we have also encountered a remarkable excess of experimentally identified functional elements lacking evolutionary constraint, and these cannot be dismissed for technical reasons. This is perhaps the biggest surprise of the pilot phase of the ENCODE Project, and suggests that we take a more 'neutral' view of many of the functions conferred by the genome.

METHODS

The methods are described in the Supplementary Information, with more technical details for each experiment often found in the references provided in Table 1. The Supplementary Information sections are arranged in the same order as the manuscript (with similar headings to facilitate cross-referencing). The first page of Supplementary Information also has an index to aid navigation. Raw data are available in ArrayExpress, GEO or EMBL/GenBank archives as appropriate, as detailed in Supplementary Information section 1.1. Processed data are also presented in a user-friendly manner at the UCSC Genome Browser's ENCODE portal (http://genome.ucsc.edu/ENCODE/).

1. International Human Genome Sequencing Consortium. Initial sequencing and analysis of the human genome. *Nature* **409**, 860–921 (2001).
2. Venter, J. C. *et al.* The sequence of the human genome. *Science* **291**, 1304–1351 (2001).
3. International Human Genome Sequencing Consortium. Finishing the euchromatic sequence of the human genome. *Nature* **431**, 931–945 (2004).
4. Mouse Genome Sequencing Consortium. Initial sequencing and comparative analysis of the mouse genome. *Nature* **420**, 520–562 (2002).
5. Rat Genome Sequencing Project Consortium. Genome sequence of the Brown Norway rat yields insights into mammalian evolution. *Nature* **428**, 493–521 (2004).
6. Lindblad-Toh, K. *et al.* Genome sequence, comparative analysis and haplotype structure of the domestic dog. *Nature* **438**, 803–819 (2005).
7. International Chicken Genome Sequencing Consortium. Sequence and comparative analysis of the chicken genome provide unique perspectives on vertebrate evolution. *Nature* **432**, 695–716 (2004).
8. Chimpanzee Sequencing and Analysis Consortium. Initial sequence of the chimpanzee genome and comparison with the human genome. *Nature* **437**, 69–87 (2005).
9. ENCODE Project Consortium. The ENCODE (ENCyclopedia Of DNA Elements) Project. *Science* **306**, 636–640 (2004).
10. Zhang, Z. D. *et al.* Statistical analysis of the genomic distribution and correlation of regulatory elements in the ENCODE regions. *Genome Res.* **17**, 787–797 (2007).
11. Euskirchen, G. M. *et al.* Mapping of transcription factor binding regions in mammalian cells by ChIP: comparison of array and sequencing based technologies. *Genome Res.* **17**, 898–909 (2007).
12. Willingham, A. T. & Gingeras, T. R. TUF love for "junk" DNA. *Cell* **125**, 1215–1220 (2006).
13. Carninci, P. *et al.* Genome-wide analysis of mammalian promoter architecture and evolution. *Nature Genet.* **38**, 626–635 (2006).
14. Cheng, J. *et al.* Transcriptional maps of 10 human chromosomes at 5-nucleotide resolution. *Science* **308**, 1149–1154 (2005).
15. Bertone, P. *et al.* Global identification of human transcribed sequences with genome tiling arrays. *Science* **306**, 2242–2246 (2004).
16. Guigó, R. *et al.* EGASP: the human ENCODE Genome Annotation Assessment Project. *Genome Biol.* **7**, (Suppl. 1; S2) 1–31 (2006).
17. Denoeud, F. *et al.* Prominent use of distal 5′ transcription start sites and discovery of a large number of additional exons in ENCODE regions. *Genome Res.* **17**, 746–759 (2007).
18. Tress, M. L. *et al.* The implications of alternative splicing in the ENCODE protein complement. *Proc. Natl Acad. Sci. USA* **104**, 5495–5500 (2007).
19. Rozowsky, J. *et al.* The DART classification of unannotated transcription within ENCODE regions: Associating transcription with known and novel loci. *Genome Res.* **17**, 732–745 (2007).
20. Kapranov, P. *et al.* Examples of the complex architecture of the human transcriptome revealed by RACE and high-density tiling arrays. *Genome Res.* **15**, 987–997 (2005).
21. Balakirev, E. S. & Ayala, F. J. Pseudogenes: are they "junk" or functional DNA? *Annu. Rev. Genet.* **37**, 123–151 (2003).
22. Mighell, A. J., Smith, N. R., Robinson, P. A. & Markham, A. F. Vertebrate pseudogenes. *FEBS Lett.* **468**, 109–114 (2000).
23. Zheng, D. *et al.* Pseudogenes in the ENCODE regions: Consensus annotation, analysis of transcription and evolution. *Genome Res.* **17**, 839–851 (2007).
24. Zheng, D. *et al.* Integrated pseudogene annotation for human chromosome 22: evidence for transcription. *J. Mol. Biol.* **349**, 27–45 (2005).
25. Harrison, P. M., Zheng, D., Zhang, Z., Carriero, N. & Gerstein, M. Transcribed processed pseudogenes in the human genome: an intermediate form of expressed retrosequence lacking protein-coding ability. *Nucleic Acids Res.* **33**, 2374–2383 (2005).
26. Washietl, S. *et al.* Structured RNAs in the ENCODE selected regions of the human genome. *Genome Res.* **17**, 852–864 (2007).
27. Carninci, P. *et al.* The transcriptional landscape of the mammalian genome. *Science* **309**, 1559–1563 (2005).
28. Runte, M. *et al.* The IC-*SNURF–SNRPN* transcript serves as a host for multiple small nucleolar RNA species and as an antisense RNA for *UBE3A. Hum. Mol. Genet.* **10**, 2687–2700 (2001).
29. Seidl, C. I., Stricker, S. H. & Barlow, D. P. The imprinted *Air* ncRNA is an atypical RNAPII transcript that evades splicing and escapes nuclear export. *EMBO J.* **25**, 3565–3575 (2006).
30. Parra, G. *et al.* Tandem chimerism as a means to increase protein complexity in the human genome. *Genome Res.* **16**, 37–44 (2006).
31. Maston, G. A., Evans, S. K. & Green, M. R. Transcriptional regulatory elements in the human genome. *Annu. Rev. Genomics Hum. Genet.* **7**, 29–59 (2006).
32. Trinklein, N. D., Aldred, S. J., Saldanha, A. J. & Myers, R. M. Identification and functional analysis of human transcriptional promoters. *Genome Res.* **13**, 308–312 (2003).
33. Cooper, S. J., Trinklein, N. D., Anton, E. D., Nguyen, L. & Myers, R. M. Comprehensive analysis of transcriptional promoter structure and function in 1% of the human genome. *Genome Res.* **16**, 1–10 (2006).
34. Cawley, S. *et al.* Unbiased mapping of transcription factor binding sites along human chromosomes 21 and 22 points to widespread regulation of noncoding RNAs. *Cell* **116**, 499–509 (2004).
35. Yelin, R. *et al.* Widespread occurrence of antisense transcription in the human genome. *Nature Biotechnol.* **21**, 379–386 (2003).
36. Katayama, S. *et al.* Antisense transcription in the mammalian transcriptome. *Science* **309**, 1564–1566 (2005).
37. Ren, B. *et al.* Genome-wide location and function of DNA binding proteins. *Science* **290**, 2306–2309 (2000).
38. Iyer, V. R. *et al.* Genomic binding sites of the yeast cell-cycle transcription factors SBF and MBF. *Nature* **409**, 533–538 (2001).
39. Horak, C. E. *et al.* GATA-1 binding sites mapped in the β-globin locus by using mammalian CHIp-chip analysis. *Proc. Natl Acad. Sci. USA* **99**, 2924–2929 (2002).
40. Wei, C. L. *et al.* A global map of p53 transcription-factor binding sites in the human genome. *Cell* **124**, 207–219 (2006).
41. Kim, J., Bhinge, A. A., Morgan, X. C. & Iyer, V. R. Mapping DNA–protein interactions in large genomes by sequence tag analysis of genomic enrichment. *Nature Methods* **2**, 47–53 (2005).
42. Dorschner, M. O. *et al.* High-throughput localization of functional elements by quantitative chromatin profiling. *Nature Methods* **1**, 219–225 (2004).
43. Sabo, P. J. *et al.* Genome-scale mapping of DNase I sensitivity *in vivo* using tiling DNA microarrays. *Nature Methods* **3**, 511–518 (2006).
44. Crawford, G. E. *et al.* DNase-chip: a high-resolution method to identify DNase I hypersensitive sites using tiled microarrays. *Nature Methods* **3**, 503–509 (2006).
45. Hogan, G. J., Lee, C. K. & Lieb, J. D. Cell cycle-specified fluctuation of nucleosome occupancy at gene promoters. *PLoS Genet.* **2**, e158 (2006).

46. Koch, C. M. *et al.* The landscape of histone modifications across 1% of the human genome in five human cell lines. *Genome Res.* **17**, 691–707 (2007).

47. Smale, S. T. & Kadonaga, J. T. The RNA polymerase II core promoter. *Annu. Rev. Biochem.* **72**, 449–479 (2003).

48. Mito, Y., Henikoff, J. G. & Henikoff, S. Genome-scale profiling of histone H3.3 replacement patterns. *Nature Genet.* **37**, 1090–1097 (2005).

49. Heintzman, N. D. *et al.* Distinct and predictive chromatin signatures of transcriptional promoters and enhancers in the human genome. *Nature Genet.* **39**, 311–318 (2007).

50. Yusufzai, T. M., Tagami, H., Nakatani, Y. & Felsenfeld, G. CTCF tethers an insulator to subnuclear sites, suggesting shared insulator mechanisms across species. *Mol. Cell* **13**, 291–298 (2004).

51. Kim, T. H. *et al.* Direct isolation and identification of promoters in the human genome. *Genome Res.* **15**, 830–839 (2005).

52. Bieda, M., Xu, X., Singer, M. A., Green, R. & Farnham, P. J. Unbiased location analysis of E2F1-binding sites suggests a widespread role for E2F1 in the human genome. *Genome Res.* **16**, 595–605 (2006).

53. Ruppert, S., Wang, E. H. & Tjian, R. Cloning and expression of human TAF$_{II}$250: a TBP-associated factor implicated in cell-cycle regulation. *Nature* **362**, 175–179 (1993).

54. Fernandez, P. C. *et al.* Genomic targets of the human c-Myc protein. *Genes Dev.* **17**, 1115–1129 (2003).

55. Li, Z. *et al.* A global transcriptional regulatory role for c-Myc in Burkitt's lymphoma cells. *Proc. Natl Acad. Sci. USA* **100**, 8164–8169 (2003).

56. Orian, A. *et al.* Genomic binding by the *Drosophila* Myc, Max, Mad/Mnt transcription factor network. *Genes Dev.* **17**, 1101–1114 (2003).

57. de Laat, W. & Grosveld, F. Spatial organization of gene expression: the active chromatin hub. *Chromosome Res.* **11**, 447–459 (2003).

58. Trinklein, N. D. *et al.* Integrated analysis of experimental datasets reveals many novel promoters in 1% of the human genome. *Genome Res.* **17**, 720–731 (2007).

59. Jeon, Y. *et al.* Temporal profile of replication of human chromosomes. *Proc. Natl Acad. Sci. USA* **102**, 6419–6424 (2005).

60. Woodfine, K. *et al.* Replication timing of the human genome. *Hum. Mol. Genet.* **13**, 191–202 (2004).

61. White, E. J. *et al.* DNA replication-timing analysis of human chromosome 22 at high resolution and different developmental states. *Proc. Natl Acad. Sci. USA* **101**, 17771–17776 (2004).

62. Schubeler, D. *et al.* Genome-wide DNA replication profile for *Drosophila melanogaster*: a link between transcription and replication timing. *Nature Genet.* **32**, 438–442 (2002).

63. MacAlpine, D. M., Rodriguez, H. K. & Bell, S. P. Coordination of replication and transcription along a *Drosophila* chromosome. *Genes Dev.* **18**, 3094–3105 (2004).

64. Gilbert, D. M. Replication timing and transcriptional control: beyond cause and effect. *Curr. Opin. Cell Biol.* **14**, 377–383 (2002).

65. Schwaiger, M. & Schubeler, D. A question of timing: emerging links between transcription and replication. *Curr. Opin. Genet. Dev.* **16**, 177–183 (2006).

66. Hatton, K. S. *et al.* Replication program of active and inactive multigene families in mammalian cells. *Mol. Cell. Biol.* **8**, 2149–2158 (1988).

67. Gartler, S. M., Goldstein, L., Tyler-Freer, S. E. & Hansen, R. S. The timing of *XIST* replication: dominance of the domain. *Hum. Mol. Genet.* **8**, 1085–1089 (1999).

68. Azuara, V. *et al.* Heritable gene silencing in lymphocytes delays chromatid resolution without affecting the timing of DNA replication. *Nature Cell Biol.* **5**, 668–674 (2003).

69. Cohen, S. M., Furey, T. S., Doggett, N. A. & Kaufman, D. G. Genome-wide sequence and functional analysis of early replicating DNA in normal human fibroblasts. *BMC Genomics* **7**, 301 (2006).

70. Cao, R. *et al.* Role of histone H3 lysine 27 methylation in Polycomb-group silencing. *Science* **298**, 1039–1043 (2002).

71. Muller, J. *et al.* Histone methyltransferase activity of a *Drosophila* Polycomb group repressor complex. *Cell* **111**, 197–208 (2002).

72. Bracken, A. P., Dietrich, N., Pasini, D., Hansen, K. H. & Helin, K. Genome-wide mapping of Polycomb target genes unravels their roles in cell fate transitions. *Genes Dev.* **20**, 1123–1136 (2006).

73. Kirmizis, A. *et al.* Silencing of human polycomb target genes is associated with methylation of histone H3 Lys 27. *Genes Dev.* **18**, 1592–1605 (2004).

74. Lee, T. I. *et al.* Control of developmental regulators by Polycomb in human embryonic stem cells. *Cell* **125**, 301–313 (2006).

75. Karnani, N., Taylor, C., Malhotra, A. & Dutta, A. Pan-S replication patterns and chromosomal domains defined by genome tiling arrays of human chromosomes. *Genome Res.* **17**, 865–876 (2007).

76. Delaval, K., Wagschal, A. & Feil, R. Epigenetic deregulation of imprinting in congenital diseases of aberrant growth. *Bioessays* **28**, 453–459 (2006).

77. Dillon, N. Gene regulation and large-scale chromatin organization in the nucleus. *Chromosome Res.* **14**, 117–126 (2006).

78. Burkhoff, A. M. & Tullius, T. D. Structural details of an adenine tract that does not cause DNA to bend. *Nature* **331**, 455–457 (1988).

79. Price, M. A. & Tullius, T. D. How the structure of an adenine tract depends on sequence context: a new model for the structure of T$_n$A$_n$ DNA sequences. *Biochemistry* **32**, 127–136 (1993).

80. Greenbaum, J. A., Parker, S. C. J. & Tullius, T. D. Detection of DNA structural motifs in functional genomic elements. *Genome Res.* **17**, 940–946 (2007).

81. Thurman, R. E., Day, N., Noble, W. S. & Stamatoyannopoulos, J. A. Identification of higher-order functional domains in the human ENCODE regions. *Genome Res.* **17**, 917–927 (2007).

82. Gilbert, N. *et al.* Chromatin architecture of the human genome: gene-rich domains are enriched in open chromatin fibers. *Cell* **118**, 555–566 (2004).

83. Nobrega, M. A., Ovcharenko, I., Afzal, V. & Rubin, E. M. Scanning human gene deserts for long-range enhancers. *Science* **302**, 413 (2003).

84. Woolfe, A. *et al.* Highly conserved non-coding sequences are associated with vertebrate development. *PLoS Biol.* **3**, e7 (2005).

85. Drake, J. A. *et al.* Conserved noncoding sequences are selectively constrained and not mutation cold spots. *Nature Genet.* **38**, 223–227 (2006).

86. Margulies, E. H., Blanchette, M., NISC Comparative Sequencing Program, Haussler D. & Green, E. D. Identification and characterization of multi-species conserved sequences. *Genome Res.* **13**, 2507–2518 (2003).

87. Cooper, G. M. *et al.* Distribution and intensity of constraint in mammalian genomic sequence. *Genome Res.* **15**, 901–913 (2005).

88. Siepel, A. *et al.* Evolutionarily conserved elements in vertebrate, insect, worm, and yeast genomes. *Genome Res.* **15**, 1034–1050 (2005).

89. Thomas, J. W. *et al.* Parallel construction of orthologous sequence-ready clone contig maps in multiple species. *Genome Res.* **12**, 1277–1285 (2002).

90. Blakesley, R. W. *et al.* An intermediate grade of finished genomic sequence suitable for comparative analyses. *Genome Res.* **14**, 2235–2244 (2004).

91. Aparicio, S. *et al.* Whole-genome shotgun assembly and analysis of the genome of *Fugu rubripes. Science* **297**, 1301–1310 (2002).

92. Jaillon, O. *et al.* Genome duplication in the teleost fish *Tetraodon nigroviridis* reveals the early vertebrate proto-karyotype. *Nature* **431**, 946–957 (2004).

93. Margulies, E. H. *et al.* An initial strategy for the systematic identification of functional elements in the human genome by low-redundancy comparative sequencing. *Proc. Natl Acad. Sci. USA* **102**, 4795–4800 (2005).

94. Blanchette, M. *et al.* Aligning multiple genomic sequences with the threaded blockset aligner. *Genome Res.* **14**, 708–715 (2004).

95. Bray, N. & Pachter, L. MAVID: constrained ancestral alignment of multiple sequences. *Genome Res.* **14**, 693–699 (2004).

96. Brudno, M. *et al.* LAGAN and Multi-LAGAN: efficient tools for large-scale multiple alignment of genomic DNA. *Genome Res.* **13**, 721–731 (2003).

97. Margulies, E. H. *et al.* Relationship between evolutionary constraint and genome function for 1% of the human genome. *Genome Res.* **17**, 760–774 (2007).

98. Asthana, S., Roytberg, M., Stamatoyannopoulos, J. A. & Sunyaev, S. Analysis of sequence conservation at nucleotide resolution. *PLoS Comp. Biol.* (submitted).

99. Cooper, G. M., Brudno, M., Green, E. D., Batzoglou, S. & Sidow, A. Quantitative estimates of sequence divergence for comparative analyses of mammalian genomes. *Genome Res.* **13**, 813–820 (2003).

100. Eddy, S. R. A model of the statistical power of comparative genome sequence analysis. *PLoS Biol.* **3**, e10 (2005).

101. Stone, E. A., Cooper, G. M. & Sidow, A. Trade-offs in detecting evolutionarily constrained sequence by comparative genomics. *Annu. Rev. Genomics Hum. Genet.* **6**, 143–164 (2005).

102. McAuliffe, J. D., Jordan, M. I. & Pachter, L. Subtree power analysis and species selection for comparative genomics. *Proc. Natl Acad. Sci. USA* **102**, 7900–7905 (2005).

103. International HapMap Consortium. A haplotype map of the human genome. *Nature* **437**, 1299–1320 (2005).

104. Cheng, Z. *et al.* A genome-wide comparison of recent chimpanzee and human segmental duplications. *Nature* **437**, 88–93 (2005).

105. Cooper, G. M. *et al.* Characterization of evolutionary rates and constraints in three Mammalian genomes. *Genome Res.* **14**, 539–548 (2004).

106. Dermitzakis, E. T., Reymond, A. & Antonarakis, S. E. Conserved non-genic sequences - an unexpected feature of mammalian genomes. *Nature Rev. Genet.* **6**, 151–157 (2005).

107. Clark, T. G. *et al.* Small insertions/deletions and functional constraint in the ENCODE regions. *Genome Biol.* (submitted) (2007).

108. Bejerano, G. *et al.* Ultraconserved elements in the human genome. *Science* **304**, 1321–1325 (2004).

109. Woolfe, A. *et al.* Highly conserved non-coding sequences are associated with vertebrate development. *PLoS Biol.* **3**, e7 (2005).

110. Dermitzakis, E. T. & Clark, A. G. Evolution of transcription factor binding sites in Mammalian gene regulatory regions: conservation and turnover. *Mol. Biol. Evol.* **19**, 1114–1121 (2002).

111. McDonald, J. H. & Kreitman, M. Adaptive protein evolution at the *Adh* locus in *Drosophila. Nature* **351**, 652–654 (1991).

112. Andolfatto, P. Adaptive evolution of non-coding DNA in *Drosophila. Nature* **437**, 1149–1152 (2005).

113. Hudson, R. R., Kreitman, M. & Aguade, M. A test of neutral molecular evolution based on nucleotide data. *Genetics* **116**, 153–159 (1987).

114. Feuk, L., Carson, A. R. & Scherer, S. W. Structural variation in the human genome. *Nature Rev. Genet.* **7**, 85–97 (2006).

115. Ludwig, M. Z. *et al.* Functional evolution of a *cis*-regulatory module. *PLoS Biol.* **3**, e93 (2005).

116. Ludwig, M. Z. & Kreitman, M. Evolutionary dynamics of the enhancer region of even-skipped in *Drosophila. Mol. Biol. Evol.* **12**, 1002–1011 (1995).

117. Harrow, J. *et al.* GENCODE: producing a reference annotation for ENCODE. *Genome Biol.* **7**, (Suppl. 1; S4) 1–9 (2006).

118. Emanuelsson, O. *et al.* Assessing the performance of different high-density tiling microarray strategies for mapping transcribed regions of the human genome. *Genome Res.* advance online publication, doi: 10.1101/gr.5014606 (21 November 2006).

119. Kapranov, P. *et al.* Large-scale transcriptional activity in chromosomes 21 and 22. *Science* 296, 916–919 (2002).

120. Bhinge, A. A., Kim, J., Euskirchen, G., Snyder, M. & Iyer, V. R. Mapping the chromosomal targets of STAT1 by Sequence Tag Analysis of Genomic Enrichment (STAGE). *Genome Res.* 17, 910–916 (2007).

121. Ng, P. *et al.* Gene identification signature (GIS) analysis for transcriptome characterization and genome annotation. *Nature Methods* 2, 105–111 (2005).

122. Giresi, P. G., Kim, J., McDaniell, R. M., Iyer, V. R. & Lieb, J. D. FAIRE (Formaldehyde-Assisted Isolation of Regulatory Elements) isolates active regulatory elements from human chromatin. *Genome Res.* 17, 877–885 (2006).

123. Rada-Iglesias, A. *et al.* Binding sites for metabolic disease related transcription factors inferred at base pair resolution by chromatin immunoprecipitation and genomic microarrays. *Hum. Mol. Genet.* 14, 3435–3447 (2005).

124. Kim, T. H. *et al.* A high-resolution map of active promoters in the human genome. *Nature* 436, 876–880 (2005).

125. Halees, A. S. & Weng, Z. PromoSer: improvements to the algorithm, visualization and accessibility. *Nucleic Acids Res.* 32, W191–W194 (2004).

126. Bajic, V. B. *et al.* Performance assessment of promoter predictions on ENCODE regions in the EGASP experiment. *Genome Biol.* 7, (Suppl 1; S3) 1–13 (2006).

127. Zheng, D. & Gerstein, M. B. A computational approach for identifying pseudogenes in the ENCODE regions. *Genome Biol.* 7, S13.1–S13.10 (2006).

128. Stranger, B. E. *et al.* Genome-wide associations of gene expression variation in humans. *PLoS Genet.* 1, e78 (2005).

129. Turner, B. M. Reading signals on the nucleosome with a new nomenclature for modified histones. *Nature Struct. Mol. Biol.* 12, 110–112 (2005).

The ENCODE Project Consortium

Analysis Coordination Ewan Birney[1], John A. Stamatoyannopoulos[2], Anindya Dutta[3], Roderic Guigó[4,5], Thomas R. Gingeras[6], Elliott H. Margulies[7], Zhiping Weng[8,9], Michael Snyder[10,11] & Emmanouil T. Dermitzakis[12]

Chromatin and Replication John A. Stamatoyannopoulos[2], Robert E. Thurman[2,13], Michael S. Kuehn[2,13], Christopher M. Taylor[3], Shane Neph[2], Christoph M. Koch[12], Saurabh Asthana[14], Ankit Malhotra[3], Ivan Adzhubei[14], Jason A. Greenbaum[15], Robert M. Andrews[12], Paul Flicek[1], Patrick J. Boyle[3], Hua Cao[13], Nigel P. Carter[12], Gayle K. Clelland[12], Sean Davis[16], Nathan Day[2], Pawandeep Dhami[12], Shane C. Dillon[12], Michael O. Dorschner[2], Heike Fiegler[12], Paul G. Giresi[17], Jeff Goldy[2], Michael Hawrylycz[18], Andrew Haydock[2], Richard Humbert[2], Keith D. James[12], Brett E. Johnson[13], Ericka M. Johnson[13], Tristan T. Frum[13], Elizabeth R. Rosenzweig[13], Neerja Karnani[3], Kirsten Lee[2], Gregory C. Lefebvre[12], Patrick A. Navas[13], Fidencio Neri[2], Stephen C. J. Parker[15], Peter J. Sabo[2], Richard Sandstrom[2], Anthony Shafer[2], David Vetrie[12], Molly Weaver[2], Sarah Wilcox[12], Man Yu[13], Francis S. Collins[7], Job Dekker[19], Jason D. Lieb[17], Thomas D. Tullius[15], Gregory E. Crawford[20], Shamil Sunyaev[14], William S. Noble[2], Ian Dunham[12] & Anindya Dutta[3]

Genes and Transcripts Roderic Guigó[4, 5], France Denoeud[5], Alexandre Reymond[21,22], Philipp Kapranov[6], Joel Rozowsky[11], Deyou Zheng[11], Robert Castelo[5], Adam Frankish[12], Jennifer Harrow[12], Srinka Ghosh[6], Albin Sandelin[23], Ivo L. Hofacker[24], Robert Baertsch[25,26], Damian Keefe[1], Paul Flicek[1], Sujit Dike[6], Jill Cheng[6], Heather A. Hirsch[27], Edward A. Sekinger[27], Julien Lagarde[5], Josep F. Abril[5,28], Atif Shahab[29], Christoph Flamm[24,30], Claudia Fried[30], Jörg Hackermüller[32], Jana Hertel[30], Manja Lindemeyer[30], Kristin Missal[30,31], Andrea Tanzer[24,30], Stefan Washietl[24], Jan Korbel[11], Olof Emanuelsson[11], Jakob S. Pedersen[26], Nancy Holroyd[12], Ruth Taylor[12], David Swarbreck[12], Nicholas Matthews[12], Mark C. Dickson[33], Daryl J. Thomas[25,26], Matthew T. Weirauch[25], James Gilbert[12], Jorg Drenkow[6], Ian Bell[6], XiaoDong Zhao[34], K.G. Srinivasan[34], Wing-Kin Sung[34], Hong Sain Ooi[34], Kuo Ping Chiu[34], Sylvain Foissac[4], Tyler Alioto[4], Michael Brent[35], Lior Pachter[36], Michael L. Tress[37], Alfonso Valencia[37], Siew Woh Choo[34], Chiou Yu Choo[34], Catherine Ucla[22], Caroline Manzano[22], Carine Wyss[22], Evelyn Cheung[6], Taane G. Clark[38], James B. Brown[39], Madhavan Ganesh[6], Sandeep Patel[6], Hari Tammana[6], Jacqueline Chrast[21], Charlotte N. Henrichsen[21], Chikatoshi Kai[23], Jun Kawai[23,40], Ugrappa Nagalakshmi[10], Jiaqian Wu[10], Zheng Lian[41], Jin Lian[41], Peter Newburger[42], Xueqing Zhang[42], Peter Bickel[43], John S. Mattick[44], Piero Carninci[40], Yoshihide Hayashizaki[23,40], Sherman Weissman[41], Emmanouil T. Dermitzakis[12], Elliott H. Margulies[7], Tim Hubbard[12], Richard M. Myers[33], Jane Rogers[12], Peter F. Stadler[24,30,45], Todd M. Lowe[25], Chia-Lin Wei[34], Yijun Ruan[34], Michael Snyder[10,11], Ewan Birney[1], Kevin Struhl[27], Mark Gerstein[11,46,47], Stylianos E. Antonarakis[22] & Thomas R. Gingeras[6]

Integrated Analysis and Manuscript Preparation James B. Brown[39], Paul Flicek[1], Yutao Fu[8], Damian Keefe[1], Ewan Birney[1], France Denoeud[5], Mark Gerstein[11,46,47], Eric D. Green[7,48], Philipp Kapranov[6], Ulaş Karaöz[8], Richard M. Myers[33], William S. Noble[2], Alexandre Reymond[21,22], Joel Rozowsky[11], Kevin Struhl[27], Adam Siepel[25, 26]†, John A. Stamatoyannopoulos[2], Christopher M. Taylor[3], James Taylor[49,50], Robert E. Thurman[2,13], Thomas D. Tullius[15], Stefan Washietl[24] & Deyou Zheng[11]

Management Group Laura A. Liefer[51], Kris A. Wetterstrand[51], Peter J. Good[51], Elise A. Feingold[51], Mark S. Guyer[51] & Francis S. Collins[52]

Multi-species Sequence Analysis Elliott H. Margulies[7], Gregory M. Cooper[33]†, George Asimenos[53], Daryl J. Thomas[25,26], Colin N. Dewey[54], Adam Siepel[25,26]†, Ewan Birney[1], Damian Keefe[1], Minmei Hou[49,50], James Taylor[49,50], Sergey Nikolaev[22], Juan I. Montoya-Burgos[55], Ari Löytynoja[1], Simon Whelan[1]†, Fabio Pardi[1], Tim Massingham[1], James B. Brown[39], Haiyan Huang[43], Nancy R. Zhang[43,56], Peter Bickel[43], Ian Holmes[57], James C. Mullikin[7,48], Abel Ureta-Vidal[1], Benedict Paten[1], Michael Seringhaus[11], Deanna Church[58], Kate Rosenbloom[26], W. James Kent[25,26], Eric A. Stone[33], NISC Comparative Sequencing Program*, Baylor College of Medicine Human Genome Sequencing Center*, Washington University Genome Sequencing Center*, Broad Institute*, Children's Hospital Oakland Research Institute*, Mark Gerstein[11,46,47], Stylianos E. Antonarakis[22], Serafim Batzoglou[53], Nick Goldman[1], Ross C. Hardison[50,59], David Haussler[25,26,60], Webb Miller[49,50,61], Lior Pachter[36], Eric D. Green[7,48] & Arend Sidow[33,62]

Transcriptional Regulatory Elements Zhiping Weng[8,9], Nathan D. Trinklein[33]†, Yutao Fu[8], Zhengdong D. Zhang[11], Ulaş Karaöz[8], Leah Barrera[68], Rhona Stuart[68], Deyou Zheng[11], Srinka Ghosh[6], Paul Flicek[1], David C. King[50, 59], James Taylor[49, 50], Adam Ameur[69], Stefan Enroth[69], Mark C. Bieda[70], Christoph M. Koch[12], Heather A. Hirsch[27], Chia-Lin Wei[34], Jill Cheng[6], Jonghwan Kim[71], Akshay A. Bhinge[71], Paul G. Giresi[17], Nan Jiang[72], Jun Liu[34], Fei Yao[34], Wing-Kin Sung[34], Kuo Ping Chiu[34], Vinsensius B. Vega[34], Charlie W.H. Lee[34], Patrick Ng[34], Atif Shahab[29], Edward A. Sekinger[27], Annie Yang[27], Zarmik Moqtaderi[27], Zhou Zhu[27], Xiaoqin Xu[70], Sharon Squazzo[70], Matthew J. Oberley[73], David Inman[73], Michael A. Singer[72], Todd A. Richmond[72], Kyle J. Munn[72,74], Alvaro Rada-Iglesias[74], Ola Wallerman[74], Jan Komorowski[69], Gayle K. Clelland[12], Sarah Wilcox[12], Shane C. Dillon[12], Robert M. Andrews[12], Joanna C. Fowler[12], Phillippe Couttet[12], Keith D. James[12], Gregory C. Lefebvre[12], Alexander W. Bruce[12], Oliver M. Dovey[12], Peter D. Ellis[12], Pawandeep Dhami[12], Cordelia F. Langford[12], Nigel P. Carter[12], David Vetrie[12], Philipp Kapranov[6], David A. Nix[6], Ian Bell[6], Sandeep Patel[6], Joel Rozowsky[11], Ghia Euskirchen[10], Stephen Hartman[10], Jin Lian[41], Jiaqian Wu[10], Alexander E. Urban[10], Peter Kraus[10], Sara Van Calcar[68], Nate Heintzman[68], Tae Hoon Kim[68], Kun Wang[68], Chunxu Qu[68], Gary Hon[68], Rosa Luna[75], Christopher K. Glass[75], M. Geoff Rosenfeld[75], Shelley Force Aldred[33], Sara J. Cooper[33], Anason Halees[8], Jane M. Lin[9], Hennady P. Shulha[9], Xiaoling Zhang[8], Mousheng Xu[8], Jaafar N. S. Haidar[9], Yong Yu[9], Ewan Birney*[1], Sherman Weissman[41], Yijun Ruan[34], Jason D. Lieb[17], Vishwanath R. Iyer[71], Roland D. Green[72], Thomas R. Gingeras[6], Claes Wadelius[74], Ian Dunham[12], Kevin Struhl[27], Ross C. Hardison[50,59], Mark Gerstein[11,46,47], Peggy J. Farnham[70], Richard M. Myers[33] Bing Ren[68] & Michael Snyder[10,11]

UCSC Genome Browser Daryl J. Thomas[25,26], Kate Rosenbloom[26], Rachel A. Harte[26], Angie S. Hinrichs[26], Heather Trumbower[26], Hiram Clawson[26], Jennifer Hillman-Jackson[26], Ann S. Zweig[26], Kayla Smith[26], Archana Thakkapallayil[26], Galt Barber[26], Robert M. Kuhn[26], Donna Karolchik[26], David Haussler[25,26,60] & W. James Kent[25,26]

Variation Emmanouil T. Dermitzakis[1,2], Lluis Armengol[76], Christine P. Bird[12], Taane G. Clark[38], Gregory M. Cooper[33]†, Paul I. W. de Bakker[77], Andrew D. Kern[26], Nuria Lopez-Bigas[5], Joel D. Martin[50,59], Barbara E. Stranger[12], Daryl J. Thomas[25,26], Abigail Woodroffe[78], Serafim Batzoglou[53], Eugene Davydov[53], Antigone Dimas[12], Eduardo Eyras[5], Ingileif B. Hallgrímsdóttir[79], Ross C. Hardison[50,59], Julian Huppert[12], Arend Sidow[33,62], James Taylor[49,50], Heather Trumbower[26], Michael C. Zody[77], Roderic Guigó[4,5], James C. Mullikin[7], Gonçalo R. Abecasis[78], Xavier Estivill[76,80] & Ewan Birney[1].

*NISC Comparative Sequencing Program** Gerard G. Bouffard[7,48], Xiaobin Guan[48], Nancy F. Hansen[48], Jacquelyn R. Idol[7], Valerie V.B. Maduro[7], Baishali Maskeri[48], Jennifer C. McDowell[48], Morgan Park[48], Pamela J. Thomas[48], Alice C. Young[48] & Robert W. Blakesley[7,48] **Baylor College of Medicine, Human Genome Sequencing Center** Donna M. Muzny[63], Erica Sodergren[63], David A. Wheeler[63], Kim C. Worley[63], Huaiyang Jiang[63], George M. Weinstock[63] & Richard A. Gibbs[63]; **Washington University Genome Sequencing Center** Tina Graves[64], Robert Fulton[64], Elaine R. Mardis[64] & Richard K. Wilson[64] **Broad Institute** Michele Clamp[65], James Cuff[65], Sante Gnerre[65], David B. Jaffe[65], Jean L. Chang[65], Kerstin Lindblad-Toh[65] & Eric S. Lander[65,66] **Children's Hospital Oakland Research Institute** Maxim Koriabine[67], Mikhail Nefedov[67], Kazutoyo Osoegawa[67], Yuko Yoshinaga[67], Baoli Zhu[67] & Pieter J. de Jong[67]

Affiliations for participants: [1]EMBL-European Bioinformatics Institute, Wellcome Trust Genome Campus, Hinxton, Cambridge, CB10 1SD, UK. [2]Department of Genome Sciences, 1705 NE Pacific Street, Box 357730, University of Washington, Seattle, Washington 98195, USA. [3]Department of Biochemistry and Molecular Genetics, Jordan 1240, Box 800733, 1300 Jefferson Park Ave, University of Virginia School of Medicine, Charlottesville, Virginia 22908, USA. [4]Genomic Bioinformatics Program, Center for Genomic Regulation, [5]Research Group in Biomedical Informatics, Institut Municipal d'Investigació Mèdica/Universitat Pompeu Fabra, c/o Dr. Aiguader 88, Barcelona Biomedical Research Park Building, 08003 Barcelona, Catalonia, Spain. [6]Affymetrix, Inc., Santa Clara, California 95051, USA. [7]Genome Technology Branch, National Human Genome Research Institute, National Institutes of Health, Bethesda, Maryland 20892, USA. [8]Bioinformatics Program, Boston University, 24 Cummington St., Boston, Massachusetts 02215, USA. [9]Biomedical Engineering Department, Boston University, 44 Cummington St., Boston, Massachusetts 02215, USA. [10]Department of Molecular, Cellular, and Developmental Biology, Yale University, New Haven, Connecticut 06520, USA. [11]Department of Molecular Biophysics and Biochemistry, Yale University, PO Box 208114, New Haven, Connecticut 06520, USA. [12]The Wellcome Trust Sanger Institute, Wellcome Trust Genome Campus, Hinxton, Cambridge, CB10 1SA, UK. [13]Division of Medical Genetics, 1705 NE Pacific Street, Box 357720, University of Washington, Seattle, Washington 98195, USA. [14]Division of Genetics, Brigham and Women's Hospital and Harvard Medical School, 77 Avenue Louis Pasteur, Boston, Massachusetts 02115, USA. [15]Department of Chemistry and Program in Bioinformatics, Boston University, 590 Commonwealth Avenue, Boston, Massachusetts 02215, USA. [16]Genetics Branch, Center for Cancer Research, National Cancer Institute, National Institutes of Health, Bethesda, Maryland 20892, USA. [17]Department of Biology and Carolina Center for Genome Sciences, CB# 3280, 202 Fordham Hall, The University of North Carolina at Chapel Hill, Chapel Hill, North Carolina 27599, USA. [18]Allen Institute for Brain Sciences, 551 North 34th Street, Seattle, Washington 98103, USA. [19]Program in Gene Function and Expression and Department of Biochemistry and Molecular Pharmacology, University of Massachusetts Medical School, 364 Plantation Street, Worcester, Massachusetts 01605, USA. [20]Institute for Genome Sciences & Policy and Department of Pediatrics, 101 Science Drive, Duke University, Durham, North Carolina 27708, USA. [21]Center for Integrative Genomics, University of Lausanne, Genopode building, 1015 Lausanne, Switzerland. [22]Department of Genetic Medicine and Development, University of Geneva Medical School, 1211 Geneva, Switzerland. [23]Genome Exploration Research Group, RIKEN Genomic Sciences Center (GSC), RIKEN Yokohama Institute, 1-7-22, Suehiro-cho, Tsurumi-ku, Yokohama, Kanagawa, 230-0045, Japan. [24]Institute for Theoretical Chemistry, University of Vienna, Währingerstraße 17, A-1090 Wien, Austria. [25]Department of Biomolecular Engineering, University of California, Santa Cruz, 1156 High Street, Santa Cruz, California 95064, USA. [26]Center for Biomolecular Science and Engineering, Engineering 2, Suite 501, Mail Stop CBSE/ITI, University of California, Santa Cruz, California 95064, USA. [27]Department of Biological Chemistry & Molecular Pharmacology, Harvard Medical School, 240 Longwood Avenue, Boston, Massachusetts 02115, USA. [28]Department of Genetics, Facultat de Biologia, Universitat de Barcelona, Av Diagonal, 645, 08028, Barcelona, Catalonia, Spain. [29]Bioinformatics Institute, 30 Biopolis Street, #07-01 Matrix, Singapore, 138671, Singapore. [30]Bioinformatics Group, Department of Computer Science, [31]Interdisciplinary Center of Bioinformatics, University of Leipzig, Härtelstraße 16-18, D-04107 Leipzig, Germany. [32]Fraunhofer Institut für Zelltherapie und Immunologie - IZI, Deutscher Platz 5e, D-04103 Leipzig, Germany. [33]Department of Genetics, Stanford University School of Medicine, Stanford, California 94305, USA. [34]Genome Institute of Singapore, 60 Biopolis Street, Singapore 138672, Singapore. [35]Laboratory for Computational Genomics, Washington University, Campus Box 1045, Saint Louis, Missouri 63130, USA. [36]Department of Mathematics and Computer Science, University of California, Berkeley, California 94720, USA. [37]Spanish National Cancer Research Centre, CNIO, Madrid, E-28029, Spain. [38]Department of Epidemiology and Public Health, Imperial College, St Mary's Campus, Norfolk Place, London W2 1PG, UK. [39]Department of Applied Science & Technology, University of California, Berkeley, California 94720, USA. [40]Genome Science Laboratory, Discovery and Research Institute, RIKEN Wako Institute, 2-1 Hirosawa, Wako, Saitama, 351-0198, Japan. [41]Department of Genetics, Yale University School of Medicine, 333 Cedar Street, New Haven, Connecticut 06510, USA. [42]Department of Pediatrics, University of Massachusetts Medical School, 55 Lake Avenue, North Worcester, Massachusetts 01605, USA. [43]Department of Statistics, University of California, Berkeley, California 94720, USA. [44]Institute for Molecular Bioscience, University of Queensland, St. Lucia, QLD 4072, Australia. [45]The Santa Fe Institute, 1399 Hyde Park Road, Santa Fe, New Mexico 87501, USA. [46]Department of Computer Science, Yale University, PO Box 208114, New Haven, Connecticut 06520-8114, USA. [47]Program in Computational Biology & Bioinformatics, Yale University, PO Box 208114, New Haven, Connecticut 06520-8114, USA. [48]NIH Intramural Sequencing Center, National Human Genome Research Institute, National Institutes of Health, Bethesda, Maryland 20892, USA. [49]Department of Computer Science and Engineering, The Pennsylvania State University, University Park, Pennsylvania 16802, USA. [50]Center for Comparative Genomics and Bioinformatics, Huck Institutes for Life Sciences, The Pennsylvania State University, University Park, Pennsylvania 16802, USA. [51]Division of Extramural Research, National Human Genome Research Institute, National Institute of Health, 5635 Fishers Lane, Suite 4076, Bethesda, Maryland 20892-9305, USA. [52]Office of the Director, National Human Genome Research Institute, National Institute of Health, 31 Center Drive, Suite 4B09, Bethesda, Maryland 20892-2152, USA. [53]Department of Computer Science, Stanford University, Stanford, California 94305, USA. [54]Department of Biostatistics and Medical Informatics, University of Wisconsin-Madison, 6720 MSC, 1300 University Ave, Madison, Wisconsin 53706, USA. [55]Department of Zoology and Animal Biology, Faculty of Sciences, University of Geneva, 1205 Geneva, Switzerland. [56]Department of Statistics, Stanford University, Stanford, California 94305, USA. [57]Department of Bioengineering, University of California, Berkeley, California 94720-1762, USA. [58]National Center for Biotechnology Information, National Institutes of Health, Bethesda, Maryland 20894, USA. [59]Department of Biochemistry and Molecular Biology, Huck Institutes of Life Sciences, The Pennsylvania State University, University Park, Pennsylvania 16802, USA. [60]Howard Hughes Medical Institute, University of California, Santa Cruz, California 95064, USA. [61]Department of Biology, The Pennsylvania State University, University Park, Pennsylvania 16802, USA. [62]Department of Pathology, Stanford University School of Medicine, Stanford, California 94305, USA. [63]Human Genome Sequencing Center and Department of Molecular and Human Genetics, Baylor College of Medicine, Houston, Texas 77030, USA. [64]Genome Sequencing Center, Washington University School of Medicine, Campus Box 8501, 4444 Forest Park Avenue, Saint Louis, Missouri 63108, USA. [65]Broad Institute of Harvard University and Massachusetts Institute of Technology, 320 Charles Street, Cambridge, Massachusetts 02141, USA. [66]Whitehead Institute for Biomedical Research, 9 Cambridge Center, Cambridge, Massachusetts 02142, USA. [67]Children's Hospital Oakland Research Institute, BACPAC Resources, 747 52nd Street, Oakland, California 94609, USA. [68]Ludwig Institute for Cancer Research, 9500 Gilman Drive, La Jolla, California 92093-0653, USA. [69]The Linnaeus Centre for Bioinformatics, Uppsala University, BMC, Box 598, SE-75124 Uppsala, Sweden. [70]Department of Pharmacology and the Genome Center, University of California, Davis, California 95616, USA. [71]Institute for Cellular & Molecular Biology, The University of Texas at Austin, 1 University Station A4800, Austin, Texas 78712, USA. [72]NimbleGen Systems, Inc., 1 Science Court, Madison, Wisconsin 53711, USA. [73]University of Wisconsin Medical School, Madison, Wisconsin 53706, USA. [74]Department of Genetics and Pathology, Rudbeck Laboratory, Uppsala University, SE-75185 Uppsala, Sweden. [75]University of California, San Diego School of Medicine, 9500 Gilman Drive, La Jolla, California 92093, USA. [76]Genes and Disease Program, Center for Genomic Regulation, c/o Dr. Aiguader 88, Barcelona Biomedical Research Park Building, 08003 Barcelona, Catalonia, Spain. [77]Broad Institute of MIT and Harvard, 7 Cambridge Center, Cambridge, Massachusetts 02142, USA. [78]Center for Statistical Genetics, Department of Biostatistics, SPH II, 1420 Washington Heights, Ann Arbor, Michigan 48109-2029, USA. [79]Department of Statistics, University of Oxford, Oxford OX1 3TG, UK. [80]Universitat Pompeu Fabra, c/o Dr. Aiguader 88, Barcelona Biomedical Research Park Building, 08003 Barcelona, Catalonia, Spain. †Present addresses: Department of Genome Sciences, University of Washington School of Medicine, Seattle, Washington 98195, USA (G.M.C.); Department of Biological Statistics & Computational Biology, Cornell University, Ithaca, New York 14853, USA (A.S.); Faculty of Life Sciences, University of Manchester, Michael Smith Building, Oxford Road, Manchester, M13 9PT, UK (S.W.); SwitchGear Genomics, 1455 Adams Drive, Suite 2015, Menlo Park, California 94025, USA (N.D.T.; S.F.A.).

Identification and analysis of functional elements in 1% of the human genome by the ENCODE pilot project

This supplement contains methods of data generation and analysis as well as other technical information on the ENCODE project publication.

S1 ENCODE Project Technical Details

S1.1 Summary of Data Sets and Data Access

In addition to the ENCODE data portal at the UCSC genome browser (see Supplement S1.1.2) the ENCODE data are also being integrated with other genome browsers, such as Ensembl (http://www.ensembl.org/index.html) and NCBI Map Viewer (http://www.ncbi.nlm.nih.gov/mapview/). Archived raw microarray data and other numerical-valued data are available via the NCBI Gene Expression Omnibus (GEO) (http://www.ncbi.nlm.nih.gov/geo/) or the EBI ArrayExpress (http://www.ebi.ac.uk/arrayexpress/), and sequence-tag data have been submitted to EMBL/GenBank/DDBJ

S1.1.1   Datasets, acronyms, cell lines, references

The table below lists the ENCODE datasets, acronyms used, cell lines, and references for each ENCODE dataset.

Dataset	Description	Source	Cell lines	Abbreviation	Biological Samples	Biological Reps	Technical Rept	Array/data points size	Total points	Accession Numbers	References
BU ORChID	ORChID (OH Radical Cleavage Intensity Database)	BU (Tullius)	Computational	CCI (Calculated cleavage intensity)	NA	NA	NA	30,000,000	30,000,000		Greenbaum et al[1],
NHGRI DNaseI	DNaseI-Hypersensitive Sites	Duke/NHGRI	CD4, GM06990, Hela S3, HepG2	DHS	4	3	3 (different Dnase concentrations)	382,884	13,782,324		Crawford et al[2]
UNC FAIRE	Formaldehyde Assisted Isolation of Regulatory Elements	Univ N Carolina	2091Fib	RFBR	1 cell line, 4 independent samples from independent cultures	4	0	384,000	1,536,000	GEO: GSE4886	Giresi et al[3]
UW DNaseI	UW QCP DNaseI	UW/Regulome	GM06990, HELA, CACO2, SKNSH, CD4, HEPG2, HUH7, EryAdult, EryFetal, K562, PANC1, NHBE, CALU3, SAEC, HMEC,	DHS	16	Pooling 4-8 replicates	4-8	7.5 million qPCR reactions ~119,000 amplicons	7,620,000	GEO: GSE4334	Dorschner et al[4]

			HRE								
UW DNaseI	UW DNase-array		GM06990	DHS	1	2	N/A	384.000	768,000		Sabo *et al*[5]
GERP Cons	GERP conservation and conserved elements	Stanford (Sidow)	Computational		NA	NA	NA				Cooper *et al*[6]
BinCons Cons	BinCons conservation and conserved elements	NHGRI (Marguli es)	Computational		NA	NA	NA				
Consens Elements	Consensus Constrained Elements	ENCOD E MSA	Computational	MCS	NA	NA	NA				
DLESS	Detection of Lineage-Specific Selection	UC Santa Cruz	Computational		NA	NA	NA				
MAVID Alignme nt	MAVID Multiple Sequence Alignments	UC Berkeley (Pachter)	Computational		NA	NA	NA				
MLAGA N Alignme nt	MLAGAN Multiple Sequence Alignments	Stanford (Batzogl ou)	Computational		NA	NA	NA				
PhastCon s Cons	PhastCons Conservatio n and Conserved Elements	UC Santa Cruz			NA	NA	NA				

SCONE Cons	SCONE Conservation and Conserved Elements	Harvard (Sunyaev)	Computational		NA	NA	NA				
TBA Alignment	TBA Multiple Sequence Alignments	Penn State /NHGRI	Computational		NA	NA	NA				
Uva DNA Rep	Temporal Profiling of DNA Replication	Univ Virginia	HeLa	TR50	5	2	2	continous data set, 736,787 probes (25mer each) on affymetrix ENCODE array	14,735,740	E-MEXP-708	Jeon et al[7]
Uva DNA Rep Ori	DNA Replication Origins	Univ Virginia		TR50 minima	5	2	2		229	E-MEXP-708	Karnani et al[8]
BU First Exon	First Exon Activity	BU (Weng)	Computational		NA	NA					Ding & Cantor[9] Ding & Cantor[10] Halees et al[11] Halees & Weng[12]
LI ChIP	Ludwig Institute/UCSD ChIP/Chip	Ludwig Inst/UCSD	HeLa, IMR90, HCT116, THP1	RFBR	27	3	1	24046	1,947,726	GDS876, GSE2672, GSE2801, GSE2730, GSE2072, GSE1778	Kim et al[13] Kim el al[14]
LI Ng ChIP	Ludwig Institute/UCSD Nimblegen ChIP/Chip	Ludwig Inst/UCSD	HeLa, IMR90,	RFBR	11	3	1	385,000	12,705,000	GSE2813	Heintzman et al[15]

Sanger ChIP1	Histone Modification ChIP/chip	Sanger	GM06990, HeLaS3, HFL1, K562, MOLT4, PTR8	RFBR	27	3	2	24005	3,816,795	Arrayexpress: E-MEXP-269, E-TABM-140	Koch et al[16]
UT-Austin STAGE	Sequence Tag Analysis of Genomic Enrichment identification of c-Myc and STAT1 targets	UT Austin	HeLa	RFBR	2	1		238708	238,708	GSE6312	Bhinge et al[17]
Stanf ChIP	ChIP/Chip with Sp1, Sp3	Stanford (Myers)		RFBR	6	3			2		
Stanf Meth	Methylation Digest	Stanford (Myers)	Be2C, CRL1690, HCT116, HT1080, HepG2, JEG3, Snu182, U87		8	3			2		
Stanf Promoter	Promoter Activity	Stanford (Myers)	AGS, BE(2)C, T98G, G402, HCT116, HMCB, HT1080, SKNSH, HeLa, HepG2, JEG3, MG63, MRC5, PANC1, SNU182, U87MG		16						Cooper et al[18]

[1] Not all factors were done in all cell lines, some factor/cell line combinations have only one technical replicate

UCD Ng ChIP	ChIP/Chip of E2F1, C-Myc	UC Davis	HeLa	RFBR	2	3	1	384,000	2,304,000	GSE4354, GSE4306	Bieda et al[19]
Uppsala ChIP	ChIP/chip in HepG2	Univ Uppsala	HepG2	RFBR	9	3	1	21648	584,496	Arrayexpress E-MEXP-452	Rada-Iglesias et al[20]
UT-Austin ChIP	ChIP/Chip of C-Myc, E2F4	UT Austin	HeLa, 2091 fibroblast	RFBR	4	3		384,000	4,608,000		ENCODE Project Consortium[21]
Yale ChIP Sig	ChIP/Chip of STAT1, BAF, JUN, FOS	Yale	HeLa	RFBR	5	3-5	1	384,000	7,296,000	GSE2714, GSE3448, GSE3449, GSE3549, GSE3550	Euskirchen et al[22]
2Harvard /AFFX ChIP-chip	ChIP-chip signal	Harvard (Struhl) AFFX	HL-60, Me180	RFBR	47	3-5	2	732,046	295,746,584	GPL1789	Cawley et al[23]
3Yale RFBR Clusters	RFBR Enriched / Depleted regions	Yale (Gerstein)	Computational		NA	NA	NA		1415		Zhang et al[24]
Affy RNA Signal	PolyA+ RNA Signal	Affymetrix	HL60, HeLa, GM06990	TxFrag	6	3	2	732,046	26,353,656	GPL3111	Kapranov et al[25]
EGASP	EGASP promoter, protein coding, and pseudo gene predictions	EGASP	Computational		NA	NA	NA		126,8394		Guigo et al[26] Bajic et al[27] Zheng & Gerstein[28]
GENCODE Genes	Gene Annotations	GENCODE		GENCODE							Harrow et al[29]
Yale 5' RACE	Yale 5' RACE	Yale	NB4	5' RACE	1	N/A	N/A	3106	3106		Trinklein et al[30]

[2] Not all factors were done in both cell lines, not all factors were done for the same time points, not all factors were done in the same number of replicates.

[3] http://dart.gersteinlab.org

[4] Consists of 122,038 predicted exons, 4600 predicted promoters, 201 predicted pseudogenes

	product end sequencing										
GIS ChIP-PET	ChIP-PET of STAT1, p53	GI Singapore	HeLa, HCT116	Chip-PET	1	1	1	N/A	1,238,753		Wei et al[31]
GIS PET RNA	PETof PolyA+ RNA	GI Singapore	MCF7, HCT116	GIS-PET	1	1	1	N/A	864,964		Ng et al[32]
RIKEN CAGE	CAGE Predicted Gene Start Sites	RIKEN		CAGE	39	1	1			[5]ABAAA0000001-ABAAA0345530 ABAAB0000001-ABAAB0349735 ABAAC0000001-ABAAC0081282 ABAAD0000001-ABAAD0067015 ABAAE0000001-ABAAE0143179 ABAAF0000001-ABAAF0080664 ABAAG0000001-ABAAG0038560 ABAAH0000001-ABAAH0069492 ABAAI0000001-ABAAI0048328 ABAAJ0000001-ABAAJ0074930 ABAAM0000001-ABAAM0402473 ABAAN0000001-ABAAN0138842	Carninci et al[33]

---

[5] DDBJ accession numbers listed are not restricted to CAGE tags mapping to the ENCODE regions. Sequenced CAGE tags form a specific category ("MGA") in the DDBJ database accessible at ftp://ftp.ddbj.nig.ac.jp/database/mga/

| | | | | | | | | | | ABAAO0000001-ABAAO0248911 ABAAP0000001-ABAAP0023693 ABAAQ0000001-ABAAQ0268395 ABAAR0000001-ABAAR0014605 ABAAS0000001-ABAAS0035057 ABAAT0000001-ABAAT0035935 ABAAU0000001-ABAAU0049424 ABAAV0000001-ABAAV0037683 ABAAZ0000001-ABAAZ0022849 ABABA0000001-ABABA0100977 ABABB0000001-ABABB0055212 ABABD0000001-ABABD0010632 ABABE0000001-ABABE0179630 ABABF0000001-ABABF0125171 ABABG0000001-ABABG0024354 ABABJ0000001-ABABJ0033204 ABABL0000001-ABABL0029329 ABABM0000001-ABABM0025571 ABABN0000001-ABABN0145808 ABABO0000001-ABABO0030699 ABABP0000001-ABABP0065654 ABABQ0000001-ABABQ0321486 ABABR0000001- | |

										ABABR0059492 ABABS0000001- ABABS0148007 ABABT0000001- ABABT0039592 ABABU0000001- ABABU0408819 ABABV0000001- ABABV0069939	
Stanf RTPCR	Endogenous Transcript Levels	Stanford (Myers)	HCT116								
RNA Secondary Structure prodiction	EvoFold and RNAz Predictions of RNA Secondary Structure Using TBA	UC Santa Cruz (EvoFold) and University of Vienna (RNAz)	Computational		NA	NA	NA				Washietl et al[34]
Yale RNA	RNA Transcript Map	Yale	Neut,Plcnta, NB4	TxFrag	5	3-10	2-3	755.000	36.995.000	GSE2671, GSE2678, GSE2679	Emanuelsson et al[35] Rozowsky et al[36]
HapMap Coverage	Resequencing Coverage	HapMap			4						
HapMap SNPs	Minor and Derived Allele Frequencies	HapMap			4						International HapMap Consortium[37]
NHGRI DIPs	Deletion/Insertion Polymorphisms	NHGRI (Mulliken)									
Sanger Assoc	Genotype-Expression Association	Sanger	GM06990		60	1	6	700	4200		Stranger et al[38]
SNP Recomb Hots	Recombination Hotspots from Resequencing and SNP	Oxford			270						International HapMap Consortium[37]

	Data										
SNP Recomb Rates	Recombination Rates from Resequencing and SNP Data	Oxford			270						International HapMap Consortium[37]

S1.1.2   Data Repository at UC Santa Cruz

The ENCODE Project at UCSC web site (http://genome.ucsc.edu/ENCODE) is the main portal for sequence based data produced as part of the ENCODE Project. The site provides researchers with a number of tools that allows visualization and analysis of the data as well as the ability to download data for local analyses.   Details and examples of the new ENCODE-related features are available elsewhere[39], which describes the portal to the data, highlights the data that has been made available, and presents the tools that have been developed within the ENCODE project. These features are integrated with the UCSC Genome Browser[40], Genome Browser Database[41], and Table Browser[42].

As the primary data repository for sequence based data, the roles of UC Santa Cruz are (i) to collect the experimental data and analyses, (ii) to perform basic quality assurance (QA) on the submitted data, (iii) to publicly release the data with comprehensive descriptions, (iv) to provide interactive displays for integrating the ENCODE data with existing genome-wide data and (v) to provide interactive tools for analysis.

S1.1.3   Data deposition, access and analysis through Galaxy system

To facilitate data exchange among different ENCODE groups during the analysis process we implemented a data repository at http://encode-upload.g2.bx.psu.edu. The repository is a web application designed to (1) provide user-friendly interface for data upload, (2) standardize naming of data files according to ENCODE guidelines, (3) automatically fragment the data into ENCODE analysis partitions, and (4) store the data so it can be accesses through the Galaxy web site (http://main.g2.bx.psu.edu).

S1.2 Experimental reproducibility and confirmation

To ascertain the reliability of the data produced by the ENCODE Project, the Consortium has established two levels of data quality evaluation: data verification and data validation. "Data verification" refers to assessing the reproducibility of data recording a biochemical event assayed by a high throughput method. "Data validation" refers to confirming the biochemical function of the DNA elements identified using another, preferably independent, method on a subset of the verified data. For example, for the ChIP-chip technology, data verification involves performing at least 3 biological replicates where the top targets identified in each replica are significantly correlated. ChIP-chip validation is done by quantitative PCR (qPCR) on 48 ChIP-chip targets selected across a range of signal intensities. In the spirit of the Human Genome Project's practice of rapid data release, the ENCODE Project requires the immediate release of verified data into the appropriate public databases, with the subsequent release of validated data. For more information on the ENCODE data release policy, see: http://www.genome.gov/12513440.

S1.3 Genome Structure Correction

The type of question that we primarily address in this supplement is: Given two features of genome position, e.g. "conservation between species" and "transcription start sites" and a measure of the relatedness of these two features, e.g. base or region percentage overlap; how

significant is the observed value of the measure? How does it compare with that which might be observed "at random"?

The essential difficulty in dealing with these questions is to determine the appropriate interpretation of randomness for the genome, since we observe only one of the multitudes of possible genomes that evolution might have produced for our and other species.

We postulate that genomes or stretches of genomes that we observe (1) Can be thought of as a number of regions, each of which is homogenous in a sense we describe mathematically below, (2) The number of regions is small compared to the total length of the genomic segments we consider, (3) Bases that are very far from each other on the average have little to do with each other, and (4) The size of at most all but one homogenous region is small compared to the stretch that we observe. This last assumption is needed for the method we describe, but an alternative approach, which is more computationally intensive, can avoid it.

There is considerable evidence for (1), (2), and (4) in the literature[43-48] and (3) is clearly plausible. When we translate this into mathematical terms we obtain a formulation more general than the patently incorrect assumption that, in the homogeneous regions, bases are independent and identically distributed (the multinomial model). In fact, our formulation is more general and hence more conservative than any of the models advanced for convenience in genomics, such as Markov models and HMMs. Remarkably, it enables us to use the genomic data we have to estimate the parameters we need to perform the task(s) we outlined earlier. The formulation, for the homogenous pieces, is a well studied one in the context of time series[49].

The question of association for two features is now interpretable: Within the given sequence dependency structure, are the assignments of feature A and feature B to individual bases made independently?

The conceptual basis of the approach is that, under our assumptions, we expect that the distribution of our statistic (over all possible genomes for this species), for a stretch of length n of the genome, can be approximated, after some renormalization by the distribution of the statistic as defined for stretches of length L where L is large, but small compared to n. This enables us to estimate the quantities we need using the empirical distribution of the values of the statistic for the n-L stretches of length L present in the data. We now sketch the actual implementation and associated statistics of the methodology. A fuller, more mathematical account is in preparation.

Suppose we want to test the hypothesis that two features F and G are not associated. For example, in the expanding human transcriptome, novel sets of transcripts are regularly recorded; one can ask the question, do the base-pairs (bps) corresponding to one such set of transcripts tend to overlap with a comprehensive set of bps ostensibly conserved between multiple species more than expected at random?

To answer this question, we consider the bivariate time series ("time" here being the position in the sequence in bps), $\left(I\left(t\right), J\left(t\right)\right)$ with n data points corresponding to the length of the

sequence. Here, $I(t) = 1$ iff the bp t belongs to an instance of feature F and $J(t) = 1$ iff t belongs to feature G. We assume that this time series is approximately piecewise stationary.

That is, for all sets of k positions $t_1, \ldots, t_k$ in a region $R_i, i = 1, \ldots, M$, possible configurations $(a_1, b_1), \ldots, (a_k, b_k)$ of 0,1-valued pairs, and all h,

1) $P\left[I(t_j + h) = a_j, J(t_j + h) = b_j, 1 \le j \le k \middle| R_i \right] = P\left[I(t_j) = a_j, J(t_j) = b_j, 1 \le j \le k \middle| R_i \right]$

Note that there is no assumption on the relation between regional boundaries. Within regions this covers Markov Chains of any order, HMMs, etc. The second assumption is that,

2) $M \ll n$ where n is the total length of the region(s) under study.

3) The process $(I(t), J(t))$ is strongly mixing in a suitable sense – see Doukhan[50].

We can now represent percent bp overlap:

$$S = \frac{\sum I(t) J(t)}{\sum I(t)}$$

and a symmetrized version of percent regional overlap, essentially as

$$R = \frac{\sum I(t) J(t) \left(1 - I(t+1) J(t+1)\right)}{\sum I(t) \left(1 - I(t+1)\right)}$$

The essential point is that, S and R and all the other statistics we discuss below are smooth functions of linear statistics, $T_j, j = 1, 2, \ldots$ For instance,

$S = \dfrac{T_1}{T_2}$, where

$T_1 = n^{-1} \sum I(t) J(t)$

$T_2 = n^{-1} \sum I(t)$

It is well known (see Doukhan, Chapter Theorem 3, p. 48)[50], that under conditions which include the type of module we've considered, and the linear statistics we need, the distribution of $\dfrac{T - E(T)}{SD(T)}$ is approximated by a standard normal, and that $E(T) = \mu$, $SD(T) = \dfrac{\sigma}{\sqrt{n}}$ to a first approximation, where μ and σ don't depend on n.

It is also standard that, by the delta method, smooth functions S of linear statistics have the same approximations and $E(S) = \upsilon$, $SD(S) = \dfrac{\tau}{\sqrt{n}}$ where υ and τ are expressible in terms of he means, variances, and covariances of the component linear statistics (see Bickel and Doksum, Theorem 5.3.4)[51].

To test the hypothesis of no association, we need estimates of the expectations of these quantities, $\hat{S}$ and $\hat{R}$ under "randomness", and then the null distributions of $S - \hat{S}$ and $R - \hat{R}$. To do this we rely on the following principle, whose rationale becomes apparent in the context of time series in Politis, Romano, and Wolf[52].

1. The distribution of statistics such as S_n and R_n based on the whole segment of length n can be approximated by a suitably renormalized version of the distribution of S_L and R_L, where the subscript L denotes that the statistic is computed on a sub-segment of length L, where L is $<< n$, but large compared to the size of a homogeneous subregion[51], or by concatenating in order $\dfrac{n}{L}$ randomly sampled subsegments as above[52].

2. The distribution of S_L and R_L may be approximated by the empirical distribution of the statistic as defined on all n-L possible sub-segments of length L.

Relevant results are theorem 4.2.1 in Politis et al[52] and theorem 3.5 and discussion in Kunsch[53].

Strictly speaking, the principle applies in the inhomogeneous case only if the size weighted variation between the means of the homogeneous regions is small when compared to the total variability from within the homogeneous regions after normalization of the latter by the maximum total homogeneous region size. However, if this is not the case, the analysis we pursue below is even more conservative than if the assumption holds. For regional overlap statistics we apply a Poisson approximation to the block statistics, which again does not require the above negligibility hypothesis. Fortunately, it is possible, in any case, to check whether the variability assumption is adequate by using an analytical formula for the variance of the statistics we use (Doukhan, Theorem 2, p. 47)[50]. This expression can be estimated correctly from the data still subject to a regularization parameter, such as L, even if the between means variability is large.

Evidently, application of these methods, choosing the appropriate L in particular, is delicate. Some principles for the choice of L are discussed in Politis et al. (Ch. 12, p. 249)[52], and Buhlmann and Kunsch[54]. We check these approaches and choices of L for internal consistency below.

Testing

This is not enough to give us $\hat{S}$, $\hat{R}$ and the null distribution. We formulate the hypothesis that feature G is not enriched for feature F. No enrichment means that F and G were placed on the sequence independent of each other, but with cognizance of sequence structure. While arbitrary piecewise stationarity is assumed, note that only the two features are assumed independent.

All that is assumed for the sequence is still just piecewise stationarity. In particular, this would mean that, in a block of length L occurrences of feature F are approximately independent of feature G occurrences in a distant block of length L. This suggests that for a pair of blocks of length L, under the null, if we ascribe the feature F status of position t for $1 \leq t \leq L$ in the first block to the bps in the second, which we denote $\left(I^{(1)}(t), J^{(2)}(t)\right)$, then the overlap we would observe between the 'dummy' feature F and the true feature G would have the same distribution as the overlap we would observe between the genuine annotations in a block of length L. Hence, for a pair of blocks of length L, we have two observations of true overlap, and two observations of this 'dummy' overlap. In the basepair case, the true overlap is just:

$$S_{2L} = \frac{\sum I^{(1)}(t) J^{(1)}(t) + \sum I^{(2)}(t) J^{(2)}(t)}{\sum I^{(1)}(t) + \sum I^{(2)}(t)}$$ the 'dummy' overlap is just:

$$\hat{S}_{2L} = \frac{\sum I^{(1)}(t) J^{(2)}(t) + \sum I^{(2)}(t) J^{(1)}(t)}{\sum I^{(1)}(t) + \sum I^{(2)}(t)}.$$ Then, the null corresponds to the expected value of

$\hat{d} = S_{2L} - \hat{S}_{2L}$ being 0.

Now, suppose we draw B pairs of blocks of length L and for each pair b compute $S_{2Lb} - \hat{S}_{2Lb}$, where we use the subscript to indicate that the quantity is computed based only on the two blocks, as above. $\hat{S} = \frac{1}{B} \sum_{b=1}^{B} \hat{S}_{2Lb}$

The empirical distribution of these B numbers is an approximation to the null distribution of $S_L - \hat{S}_L$ (whose mean is 0, but whose variance is too large). We now compute $\hat{S} = \frac{1}{B} \sum_{b=1}^{B} \hat{S}_{2Lb}$.

If $B >> L$, this is an adequate approximation to the value we would obtain under the hypothesis of independence of F and G. The theoretical basis for this assertion is based on the following principle. For any pair of blocks, under the null hypothesis, we know that $\{I(t): t = b_1 + 1, ..., b_1 + L, b_2 + 1, ..., b_2 + L\}$ and $\{J(t): t = b_1 + 1, ..., b_1 + L, b_2 + 1, ..., b_2 + L\}$ are independent, where $b_1 + 1$ and $b_2 + 1$ are the start positions of the two blocks. Of course, our data does not have this property unless the null is true, but we can postulate that the marginal distributions of $\{I(t): t = b_1 + 1, ..., b_1 + L\}$ and $\{I(t): t = b_2 + 1, ..., b_2 + L\}$ are the same as under the null, and similarly for J. In the formulation of our statistic, we are making use of the fact that, if $|b_1 - b_2|$ is large, $\{(I(t), J(t)): t = b_1 + 1, ..., b_1 + L\}$ and $\{(I(t), J(t)): t = b_2 + 1, ..., b_2 + L\}$ are approximately independent, whether the null is true or not. If they were exactly independent, then indeed $\hat{S}_{2L}$ has the correct null distribution. However, if $L << n$, we expect that $|b_1 - b_2|$ is large compared to L, so that the approximation is justified.

The simplest renormalization is to multiply the statistics $S_L - \hat{S}_L$ by $\sqrt{\dfrac{n}{2L}}$, and then refer $S_n - \hat{S}$ to the empirical distribution of the B renormalized $S_{2Lb} - \hat{S}_{2Lb}$ for a p-value.

A somewhat more sophisticated argument needed for regional statistics leads to estimating the covariance of the numerator $R - \hat{R}$:

$$N_R = \sum \left(I^{(1)}(t) J^{(1)}(t) \left(1 - I^{(1)}(t+1) J^{(1)}(t+1)\right) - I^{(2)}(t) J^{(1)}(t) \left(1 - I^{(2)}(t+1) J^{(1)}(t+1)\right)\right)$$
$$+ \sum \left(I^{(2)}(t) J^{(2)}(t) \left(1 - I^{(2)}(t+1) J^{(2)}(t+1)\right) - I^{(1)}(t) J^{(2)}(t) \left(1 - I^{(1)}(t+1) J^{(2)}(t+1)\right)\right) \text{ and the}$$

denominator:

$$D_R = \sum \left(I^{(1)}(t) J^{(1)}(t) \left(1 - I^{(1)}(t+1) J^{(1)}(t+1)\right)\right) + \sum \left(I^{(2)}(t) J^{(2)}(t) \left(1 - I^{(2)}(t+1) J^{(2)}(t+1)\right)\right)$$

based on blocks of length L, renormalized as before, but base the computation on the identity $P\left[R - \hat{R} \leq t \right] = P\left[N_R - N_{\hat{R}} \leq t D_R \right]$. The choice of L is important in these approximations.

Fortunately, in practice there is computationally negligible change in the mean or variance of the empirical distributions of $S_{Lb} - \hat{S}_{Lb}$ for a wide range of L. To address the regional and bp overlap statistics, for each feature F,G pairing, we formed the $S_{Lb} - \hat{S}_{Lb}$ for many L ranging from 10 times the largest feature instance to 1/5th the total sequence length, n, and selected L approximately in the center of the largest region of stability, which provided an unambiguous choice in each case.

A Demonstration of the Method via Simulation

In order to clearly present the importance of accounting for genomic structure in the estimation of the significance of association between two features, we have simulated two dummy features. These features occur in 100 homogeneous stretches, (with an average length of 100Kb and standard deviation 20Kb) which we concatenated to form an inhomogeneous 10Mb region. The first feature, Feature 1, is somewhat sparse, but densely clustered. Instances of this feature are around 20bps. The second, Feature 2, is ubiquitous and also densely clustered. Both features occur frequently in some homogeneous subregions, and rarely in others. On average, there are 1000 instances of Feature 1 in the 10Mb, and 10,000 instances of Feature 2. We simulated 10,000 times in order to compute the empirical distribution of feature overlap (the fraction of Feature 2 instances covered by Feature 1). This distribution was approximately Gaussian, as expected.
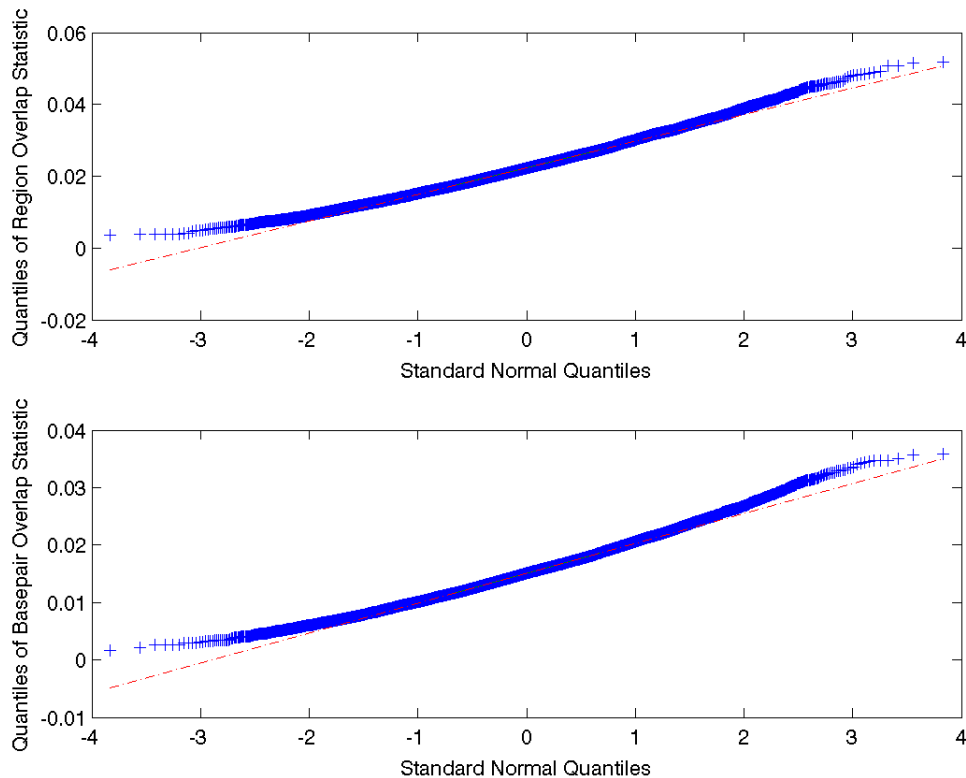
Supplementary Figure 1: QQplot demonstrating the approximate gaussianity of the overlap statistics from simulation

We selected one pair of features from these simulation runs to treat as our observed data, which was at the 99.9th percentile of both basepair and region overlap. We employed five methods to recapitulate the simulation distribution from this single observation. Those methods were (1) GSC, (2) independent randomization of start-sites and inter-feature-instance distances, (3) modeling features and inter-feature-instance distances with alternating exponentials (i.e. alternating Poissons), (4) randomly shuffling start positions in a self-avoiding fashion, and (5) randomly shuffling start positions in a self avoiding fashion, where feature lengths are sampled from the empirical feature-instance-length distribution.

The methods returned vastly different results. From simulation, we know that the p-value associated with the region overlap statistic for this observed data is $p \sim 0.005$. The GSC recapitulated the simulation distribution accurately, permitting correct significance estimation in this border-line case. Each of the other methods drastically overestimated the significance of the observed data.
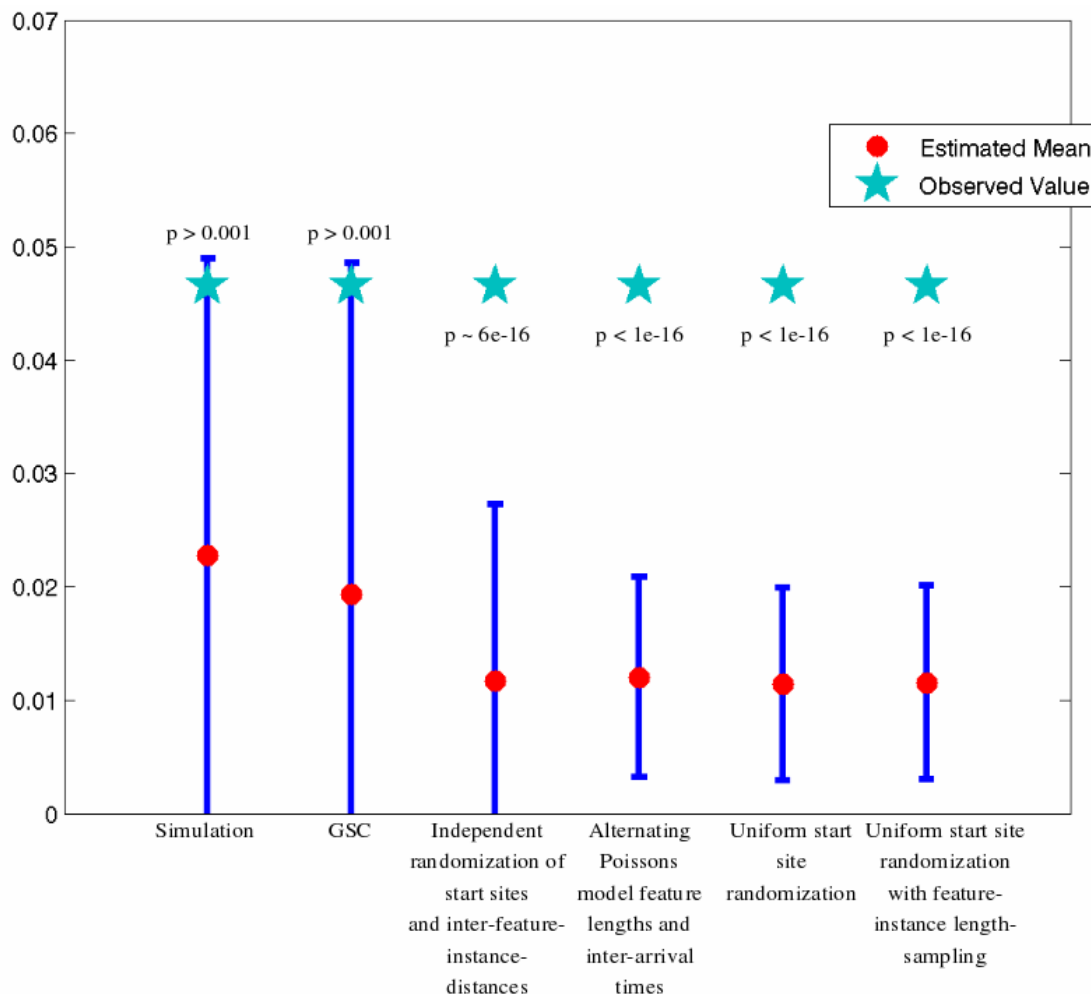
Supplementary Figure 2: The results from simulation and five methods of significance estimation

S2 Transcription

S2.1 TxFrag and Genome Tiling Arrays: Data generation and analysis

S2.1.1.1 Cell culture conditions and RNA preparation for Yale Samples

Total RNA from Human NB4 Cells:

NB4 cells were grown and maintained in RPMI-1640 medium (GIBCO, Grand Island, NY) supplemented with 10% heat-inactivated fetal calf serum, 2 mmol/L L-glutamine, 100 pg/mL penicillin and 100 U/mL of streptomycin. The cells were incubated at 37°C in a humidified air atmosphere supplemented with 5% CO_2. A fraction of these cells were grown to a concentration of 1 X 10e5/mL under the conditions described above and induced with 5 pmol/L all-trans-retinoic-acid (ATRA; Sigma, St Louis, MO) for 4 days which leading the cells to differentiate to

neutrophils. For the monocytes differentiation, a third fraction of the NB4 cells were grown to a concentration of 1 X 10e5/mL and pre-treated with 200-nM 1,25(OH)2D3 for 8 h, then with 200-nM TPA for a total treatment time of 72 h. For each biological replicate of NB4 cells (undifferentiated), NB4 cells treated with ATRA and NB4 cells treated with TPA; total RNA was extracted using the Qiagen RNA extraction kit according to the manufacturer's instructions.

Total RNA from Human Neutrophil Cells:
Human neutrophils were isolated from venous blood (freshly drawn at 8 to 9 AM) of healthy volunteers, using dextran sedimentation and centrifugation through Ficoll-Paque Plus (Pharmacia, Uppsala, Sweden), as described previously in Subrahmanyam et al[55]. Total RNA was extracted using the Qiagen RNA extraction kit.

PolyA+ RNA from Human Placental Tissue:
Triple selected polyA RNA for placenta was obtained from Ambion (Austin, TX). All RNA samples had an agilent ratio greater than 1 indicating that degradation had not occurred. All RNA samples were prepared from a pool of several different individuals.

S2.1.1.2 Cell culture conditions and RNA preparation for Affymetrix samples

Cell Lines:
The HL-60 acute myeloid lymphoma cell line was obtained from the American Type Culture Collection facility. Cell were maintained in Iscove's Modified Dulbecco's Medium with GlutaMAX (Invitrogen) containing 20% Fetal Bovine Serum (Invitrogen) and 1X penicillin/streptomycin (Invitrogen) in a humidified 37°C incubator with 5% CO_2. For each of the three biological replicates, cultures were seeded at approximately $3x10^5$ cells/ml and were induced with a final concentration of 1 μM ATRA (purchased from Sigma) after 2 days of growth when cultures had achieved a density of 10^6 cells/ml. These cultures (3 liters total for each time point) were then incubated for 2, 8, and 32 hours with ATRA or untreated (0 hour) before harvesting. Both cell viability and recovery after ATRA treatment were assessed by Trypan Blue exclusion as well as determining cell density by counting an aliquot on a hemocytometer.

HeLa cell line (ATCC accession number CCL-2) was grown in DMEM media (HyClone cat# SH30022.02) supplemented with 10% fetal bovine serum (HyClone cat# SH30070.03) and 1X penicillin-streptomycin (Invitrogen cat# 10378-016). GM06990 cell line (Coriell Institute) was grown in RPMI media (HyClone cat# SH30027.02) supplemented with 15% fetal bovine serum (HyClone cat# SH30070.03) and 1X penicillin-streptomycin (Invitrogen cat# 10378-016). All cell lines were grown at 37°C at 5% CO2.

CD11b Cell Surface Antigen Labeling:
ATRA treated HL-60 cells were monitored for differentiation by detection of CD11b expression. Triplicate samples for each time point in each biological replicate (10^6 cells per sample) were centrifuged at 300xg for 10 minutes, media aspirated, and resuspended in 100 μl Label Buffer (1x Hanks Buffered Saline, 2% filtered Fetal Bovine Serum, and 0.01% sodium azide). Cells were blocked with 5 μl unlabeled isotype matched mouse $IgG_{1\kappa}$ (BD Pharmingen) on ice for 15 minutes, then washed with 2 ml ice cold Label Buffer. Cells were pelleted at 300xg for 10

minutes and resuspended in 100 µl Label buffer. Five µl of anti-CD11b antibodies or isotype controlled mouse IgG$_{1\kappa}$ coupled to Alexa 488 (BD Pharmingen) were added to each sample and incubated on ice for 30 minutes. Cells were washed twice in 2 ml Label Buffer and fixed with 2% formaldehyde in PBS. Samples were stored packed in ice and in the dark until analyzed by flow cytometry using a FACScaliber bench top cell sorter (BD Biosciences) counting 10,000 events for each triplicate sample. IgG$_{1\kappa}$ labeled samples were used to determine the amount of background fluorescence and non-specific binding. Percent of CD11b positive cells were quantitated using Cellquest Pro software.

Nitroblue Tetrazolium (NBT) Reduction Assay:
NBT reduction assays were performed in triplicate for each time point for each of the 3 biological replicates. Approximately $5x10^5$ were collected by centrifugation at 300xg for 10 minutes at room temperature using a swing bucket rotor. Media was aspirated away and cells were resuspended in 100 µl of growth media. An equal volume of NBT (Roche) diluted 1:50 in PBS was then added to each sample containing 200 ng PMA (Calbiochem). Samples were incubated at 37°C for 30 minutes at which time cells were placed on microscope slides and cells were scored as either positive or negative based on the presence of dark blue formazin deposites. At least 1000 cells were counted for each of the triplicate samples and percent NBT positive cells was determined for each time point as a measure of differentiation.

RNA preparation:
Approximately $5x10^8$ cells per time point per biological replicate were harvested by centrifugation and total RNA was purified using RNeasy RNA extraction kit (Qiagen) as per manufacturer's specifications. Each sample required three columns in order to recover the majority of the RNA. PolyA RNA was then obtained from the total RNA using Oligo-tex purification kits (Qiagen) as per manufacturer's instructions.

Total RNA was isolated using Qiagen's RNeasy protocol. Where specified, the polyA+ fraction was isolated using Qiagen's Oligo-tex kits. Cytosolic polyA+ RNA was isolated following Qiagen's RNeasy protocol. Total or polyA+ RNA was treated with DNAse I and then converted into double-stranded cDNA as described in Cheng et al[56]. 2 mg of cDNA corresponding to polyA+ RNA or 10 mg of cDNA corresponding to total RNA were hybridized to ENCODE tiling arrays as described in Cheng et al[56].

S2.1.2   Description of RNA material used in the RNA mapping experiments

Supplementary Table 1: Description of RNA sources used in the RNA mapping experiments

Cell line/Tissue	Number of different biological sources[6]	Description	Stimulant (if applicable)	Time points Available	Cellular Compartment	Method of RNA profiling	Method of cDNA priming
HL60		promyeloblast,	retinoic acid	0, 2, 8	Whole-cell	TxFrag	random

[6] Refers to a number of different sources for primary cell lines or tissues assayed independently

		acute promyelocytic leukemia		and 32 hrs	polyA+ RNA		hexamer
HeLa		cervical adenocarcinoma			Cytosolic polyA+ RNA	TxFrag	random hexamer
GM06990		B-Lymphocyte, transformed with Epstein-Barr Virus			Cytosolic polyA+ RNA	TxFrag	random hexamer
NB4		Acute promyelocytic leukemia	retinoic acid	0 and 96 hrs	Whole-cell total RNA	TxFrag	random hexamer
			12-O-tetradecanoylphorbol-13 acetate	0 and 72 hrs			random hexamer
Primary Neutrophils from donor blood	10				Whole-cell total RNA	TxFrag	random hexamer
Placenta					Whole-cell polyA+ RNA	TxFrag, RxFrag	random hexamer - TxFrag, oligo dT - RxFrag
Brain					Whole-cell polyA+ RNA	RxFrag	oligo-dT
Colon					Whole-cell polyA+ RNA	RxFrag	oligo-dT
Heart					Whole-cell polyA+ RNA	RxFrag	oligo-dT
Kidney					Whole-cell polyA+ RNA	RxFrag	oligo-dT
Liver					Whole-cell polyA+ RNA	RxFrag	oligo-dT
Muscle					Whole-cell polyA+ RNA	RxFrag	oligo-dT
Small Intestine					Whole-cell polyA+ RNA	RxFrag	oligo-dT
Spleen					Whole-cell polyA+ RNA	RxFrag	oligo-dT
Stomach					Whole-cell polyA+ RNA	RxFrag	oligo-dT
Testis					Whole-cell polyA+ RNA	RxFrag	oligo-dT
MCF7		mammary gland adenocarcinoma	beta-estradiol	12 hrs	Whole-cell polyA+ RNA	PET	oligo-dT
					Whole-cell polyA+ RNA	PET	oligo-dT
HCT116		colorectal carcinoma	5-fluorouracil	6hrs	Whole-cell polyA+ RNA	PET	oligo-dT
kidney	3				Whole-cell total RNA	CAGE	random hexamer
cerebrum	4				Whole-cell total RNA	CAGE	random hexamer
renal artery					Whole-cell total RNA	CAGE	random hexamer
ureter					Whole-cell total RNA	CAGE	random hexamer
urinary bladder	2				Whole-cell total RNA	CAGE	random hexamer

prostate					Whole-cell total RNA	CAGE	random hexamer
mammary gland					Whole-cell total RNA	CAGE	random hexamer
epididymidis					Whole-cell total RNA	CAGE	random hexamer
adipose, processed lipoaspirate					Whole-cell total RNA	CAGE	random hexamer
			dihydrotestosterone	9 days	Whole-cell total RNA	CAGE	random hexamer
			TNF-alpha	48 hrs	Whole-cell total RNA	CAGE	random hexamer
preadipocyte	2				Whole-cell total RNA	CAGE	random hexamer
	2		dihydrotestosterone	9 days	Whole-cell total RNA	CAGE	random hexamer
	2		TNF-alpha	48 hrs	Whole-cell total RNA	CAGE	random hexamer
CCD-1112Sk		fibroblast, foreskin			Whole-cell total RNA	CAGE	random hexamer
Human stem cells HS181 p52 grown on the feeder layer of CCD-1112Sk cells					Whole-cell total RNA	CAGE	random hexamer
Hep G2		hepatocellular carcinoma			Whole-cell total RNA	CAGE	Two libraries: random hexamer and oligo-dT

S2.1.3   Scoring of TARs or Yale transfrags and Affymetrix transfrags

Affymetrix ENCODE microarrays have approximately 750,000 pairs of perfect-match (PM) and mismatch (MM) 25 mer oligonucleotide probes to tile all the ENCODE regions at an average spacing of 21 bp between probe starts. Technical replicas are scaled to each other using quantile normalization[57] and then median scaled to 25. The probe intensities from technical replicas are combined using a sliding genomic window of 100 bps centered on the genomic coordinate of each PM probe. All probe intensities for oligonucleotides within the genomic coordinates bounded by the window are combined to estimate the pseudomedian PM-MM intensity (the pseudomedian or Lehman-Hodges estimator is computed from the median of all pairwise average of PM-MM pairs). This intensity is then assigned to the probe at the center of the window. This is repeated for each biological replicate. After this step, biological replicas were quantile normalized to each other and then for each PM probe the median of normalized intensities from biological replicas is computed. An intensity threshold is determined from negative controls; bacterial probe sequences on each microarray, which should not show hybridization signal, from the intensity that corresponds to a 5% false positive rate. Transcribed regions or transfrags (transcribed fragments) were then established by requiring a genomic region longer than 40 bps (the minimum run of the transfrag), where probe intensities above threshold are spaced less than 50 bps apart (the maximum gap allowed within the transfrag).

Distances are computed from the center nucleotide of each PM oligonucleotide probe. This scoring methodology is based on what was used in Kampa *et al*[58] and Cheng *et al*[56].

S2.1.4   Verification of Affymetrix genome tiling array maps

Supplementary Table 2: Validation results of Affymetrix genome tiling array maps

	Index TF	Successful RACE reactions (%)				Transcription on both strands	No transcript detected
		5' RACE	3' RACE	5' and 3' RACE	5' or 3' RACE		
Exonic	20	19 (95)	19 (95)	16 (80)	20 (100)	19 (95)	0 (0)
Intronic	90	71 (79)	77 (86)	66 (73)	79 (88)	65 (72)	11 (12)
Intergenic	90	62 (69)	65 (72)	44 (49)	77 (86)	46 (51)	13 (14)
Non Transfrag Regions	100	66 (66)	60 (60)	45 (45)	75 (75)	44 (44)	25 (25)
Numbers represent transfrags. Numbers in () represent % of total number of regions tested.							

200 transfrags were randomly chosen from the map of HL60 cell line un-stimulated (00hr time point) with retinoic acid. The transfrags consisted of 90 intergenic transfrags, 90 intronic and 20 exonic transfrags. Intergenic or intronic transfrags were defined as correspondingly non-overlapping or overlapping the bounds of known genes from the UCSC Known Gene track on the hs.NCBIv35 version of the genome. Intergenic and intronic transfrags were selected not to overlap any mRNA or EST annotation. Information on the index transfrags, primers used for this analysis can be found at http://genome.imim.es/gencode/RACEdb. 100 non-transfrag regions that mimic transfrags in length were randomly selected throughout the non-repetitive portions of the ENCODE regions.

5' and 3' RACE analysis was performed on DNAseI-treated cytosolic polyA+ RNA from un-stimulated HL60 cell line for each transfrag for each strand of the genome totaling to 4 RACE reactions per transfrag. RACE reactions were performed essentially as described in Kapranov *et al*[59] with the following modifications. cDNA synthesis for the 5'RACE was performed with a pool of 12 gene-specific primers. cDNA synthesis was done with two reverse-transcriptases: Superscript II and Thermoscript (both form Invitrogen) in two separated reactions with 50 ng of polyA+ RNA each. The cDNA reactions were pooled for the RT-PCR step. cDNA synthesis for the 3'RACE was performed with oligo-dT 3' CDS primer as in Kapranov *et al*[59]. The cDNA was treated with RNAse A/T1 cocktail (Ambion) and RNAse H (Epicentre), purified over Qiagen's columns and pooled for the RT-PCR step. 40 ng of purified cDNA were used as starting material for each RT-PCR reaction. Three rounds of amplifications were performed at the RT-PCR step of the RACE utilizing 3 transfrag-specific nested RT-PCR primers for both 3' and 5' RACE. After each round, the RT-PCR reactions were purified using QIAquick 96 PCR purification system (Qiagen) and eluted in 70 μl. 1 μl of the first round amplification was used as a template for the second round and 0.01 μl of the second round RT-PCR reaction was used as a template for the third round. Oligonucleotides 3' CDS, UPL/UPS and NUP (Clontech SMART II RACE protocol) were used as common primes for the first, second and third round of RT-PCR. Each

round of amplification consisted of 25 cycles of PCR (94°C for 20 sec; 62°C for 30 sec; 72°C for 5 min) followed by 10 min at 72°C. Products of the final round of RT-PCRs were purified using QIAquick 96, pooled and hybridized to ENCODE arrays as described above. The maps were generated using the Tiling Analysis Software (TAS; http://www.affymetrix.com/support/developer/downloads/TilingArrayTools/index.affx) with bandwidth of 50. RACEfrags were generated using threshold of 100, maxgap =50 and minrun =50.

The Affymetrix RACEfrags were filtered so that each pool contains RACEfrags that are unique to the pool. GENCODE RACEfrags were filtered against Affymetrix RACEfrags. Regions overlapping RACEfrags from the Affymetrix pools were removed. Pooling was done so that the index transfrags within each pool are at least 40 kbp apart from each other. This is to facilitate the unambiguous assignment of the parent child relationships between the index transfrag and the RACEfrag. A region (transfrag or non-transfrag) was considered to be positive for presence of a transcript of either 5' or 3' RACE reaction was scored positive on either strand.

To control for genomic DNA contamination, 3' RACE reactions were conducted on the 100 non-transfrag regions with the omission of the reverse transcriptase. Only 1 region was scored as positive.

The data for the entire verification dataset can loaded from a centralized RACE database RACEdb located at this URL http://genome.imim.es/gencode/RACEdb. Also, the profile of each RACE reaction for each of the 300 index regions could be viewed via the links provided in this database in the UCSC browser or loaded as a BED file.

S2.1.5   Experimental reproducibility of RNA mapping using tiling arrays

The experimental reproducibility of the microarray data was measured by calculating a Pearson correlation coefficient (R) between individual microarray experiments. Three tiers of correlations were calculated: (1) tier 1: correlation among different technical replicas represented by different microarrays hybridized to the same sample; (2) tier 2: correlation among different biological replicas for the same cell line or tissue and (3) tier 3: correlation among different cell lines/tissues. The correlation coefficient R was calculated based on the perfect match (PM) intensity values. The values shown in the table are R2 * 100 and represent a percent similarity. 100 would be identical, anything less than 50 quite different, above 80 very similar. As expected, the reproducibility among the technical replicas is very high ~97, followed by somewhat lower biological reproducibility at ~92. The reproducibility among different cell lines/tissues is quite low ~54, as expected for different samples. These results are quite consistent with the observation that different biological samples are quite different in the extent of un-annotated transcription and that this observation is not caused by poor reproducibility of the array data.

Supplementary Table 3: Analysis of technical versus biological reproducibility of the RNA mapping experiment obtained with the tiling arrays

Cell Line/tissue	Number of Technical (Array) Replicas	Number of Biological Replicas	Technical reproducibility (Median R^2*100)	Biological reproducibility (Median R^2*100)	Reproducibility among different cell lines/tissues (Median R^2*100)
Summary					
Total			97.0	92.2	54.3
Individual Cell line/tissue					
GM06990	6	3	97.2	97.6	
HeLa	6	3	96.8	96.8	
Placenta	7	3	96.4	93.9	
HL60, 0 hours of retinoic acid treatment	6	3	92.4	93.5	
HL60, 2 hours of retinoic acid treatment	6	3	97.8	93.7	
HL60, 8 hours of retinoic acid treatment	6	3	97.6	94.1	
HL60, 32 hours of retinoic acid treatment	6	3	98.6	92.2	
NB4, Untreated	8	4	97.3	88.9	
NB4, Treated with retinoic acid	8	4	97.9	91.3	
NB4, treated with 12-O-tetradecanoylphorbol-13 acetate	6	3	97.6	98.4	
Primary Neutrophils from donor blood	20	10	96.4	89.5	

S2.2 5'-Specific Cap Analysis Gene Expression (CAGE)

CAGE libraries[60] were prepared using a protocol based on the described procedures in Kodzius *et al*[61]. A wide variety of human RNA libraries was used (29 distinct RNA libraries corresponding to 15 tissues) for CAGE sequencing: the content of the CAGE data repository has been described in detail elsewhere[33, 62, 63] (http://fantom31p.gsc.riken.jp/cage/).

CAGE technology is based on priming the first strand cDNA with an oligo-dT or a random primer, starting from total RNA and synthesize the first-strand cDNA at high temperature (55-60°C) in presence of trehalose and sorbitol to increase the full-length cDNA rate even in presence of strong secondary RNA structure. Full-length cDNA is enriched by cap-trapping, as reviewed in Harbers *et al*[64]. After chemical biotinylation, RNAseI (cleaving only single strand mRNA at any base) is used to remove any ssRNA linking the biotinylated cap and the double-strand RNA/truncated cDNA. RNA molecules hybridized with full-length cDNA molecules are left undigested, and are subsequently captured with streptavidin beads. After several stringent washings of the beads, full-length cDNAs are removed with mild alkali treatment. Following the addition of a specific linker, which contains the class-IIs restriction enzyme *Mme*I site next to the ligation junction with the 5' end of cDNAs, the second strand cDNA is synthesized. Next, the cDNA is cleaved with *Mme*I: only the initial 20-21 nucleotides of the cDNA are left attached to the 5'-end linker, while cDNA is removed. After addition of appropriate linkers and cycles of PCR and purification, restriction-digested double strand sequencing tags are obtained. After formation of concatenamers, these are cloned and sequenced. The whole procedure is described in details elsewhere[61].

S2.2.1   Mapping CAGE tags to the genome

The sequenced CAGE tags were extracted and aligned to the genome by using BlastN. Only CAGE tags without base-calling problems (no "N" nucleotides in the sequence) were used for mapping, and tags mapping on multiple genomic regions (such as tags consisting of repeats) were not used for the current analysis. Only best-scoring alignments of at least 18 nucleotides length or more were chosen: if two or more alignments were best-scoring, the tag was ignored.

S2.3 Gene Identification Signature – Paired End DiTAGS (GIS-PET)

S2.3.1   Cell lines, Growth condition and RNA preparation

Two human cancer cell lines were used for GIS-PET analysis. HCT116 is a human colorectal cancer cell line (ATCC#: CCL-247(tm)) and MCF7 is a human breast cancer cell line (ATCC# HTB-22(tm)). Cells grown in three ways were harvested; the log phase of MCF7 cells, MCF7 cells treated with estrogen (10nM beta-estradiol) for 12 hours and HCT116 cells treated with 5FU (5-fluorouracil) for 6 hours. Total RNA and polyA+ RNA were prepared by Trizol method and oligo-dT using standard molecular biology procedures.

S2.3.2   Full length library and PET library construction for GIS analysis

Full length cDNA library was made by a modified biotinylated cap-trapper approach[32, 65]. Briefly, the 5' cap structure of mRNA was first biotinylated and the 5' intact first-strand cDNA was selected by streptavidin affinity to biotin. After second-strand synthesis, the double-strand cDNAs were cloned into a cloning vector, pGIS1, to form a full-length DNA library. This vector contains only two MmeI recognition sites in its multiple cloning sites and therefore introduces MmeI recognition sites directly flanking both ends of cDNA inserts. Purified plasmid prepared from the full-length cDNA library was digested with MmeI, end-polished with T4 DNA polymerase; and the resulting plasmids containing a pair of end tags from each terminal of the original cDNA insert were self-ligated, which were then transformed to form a transitional single-PET library. Plasmid DNA extracted from this library was digested with BamHI to release the 50bp PETs. The PETs were concatenated and cloned into the BamHI-cut pZErO-1 to form the final GIS-PET library for sequencing analysis[32].

S2.3.3   PET sequencing and mapping

PET sequences were extracted from vector trimmed and based called high quality sequence reads. The extraction algorithm included: 5' vector/insert interface, a fixed size internal spacer and 3' vector/insert interface with PET length ranged from 34 to 40 bp. The extracted PETs were then filtered to remove low-complexity sequences. Each of the PET sequences was split into 5' tag and 3' tag, and the tags were searched independently for matches in the compressed suffix array (CSA) of human genome assembly hg17. We mandated a minimum 16-nucleotide contiguous match for the 5' (from nucleotide position 1 to 19) and 3' (from 18 to the last) tags of PET to accommodate most possible variations from type II restriction enzyme slippage. The mapped tags were then paired based on the criteria that the mapping locations of 5' and 3' signatures of a PET sequence must be on the same chromosome, in the correct order and orientation (5'→3'), and within appropriate genomic distance (one million base pairs)[32, 66]. Each PET library sequencing read generates about 10-15 PET sequences.

S2.3.4   Generation and Mapping of DiTag Sequences

With respect to the ditags and polyA sequences, the RNA samples used in the ditag experiments were purified using polyT-affinity columns. The majority of the RNA species in the samples were polyA+ RNA, and since we used an oligo-dT primer (NV[T]16, N=A, T, G, C; V=T, G, C) for first-strand cDNA synthesis, the presence of a polyA stretch is guaranteed. All cDNA fragments generated for ditag analysis should thus be either derived from the polyA tail of mRNA or from internal polyA stretches. We found that 98% of ditags mapping to known transcripts matched the known 5' and 3' ends, and all the characterized 3' ends showed some kind of polyA signals in the defined region (10-30 bp upstream of 3' end), and mostly the canonical ones (like AATAAA or ATTAAA). A similar observation was reported by us previously[32]. There are a number of ditag-mapped 3' ends that are different from the known 3' ends. They are possible alternative 3' ends or they resulted from internal priming of the oligo-dT primer. To distinguish these two possibilities, we manually checked about 100 such "alternative" 3' ends by looking at the genomic DNA sequences +/- 50 bp from the ditag-mapped 3' ends. If it was derived from internal priming, we would see a stretch of A's immediately after the ditag site. We

found that none (0) has such a polyA stretch, suggesting that none are due to internal priming. However, we cannot completely rule out such possibility. For this group of sequences, we did observe that a large proportion of the polyA signal is not a canonical ones (AATAAA or ATTAAA). It is known that other combinations of nucleotides can also be used as the polyA signal.

S2.4 The GENCODE Annotation

Available sequence data has been used to delineate an annotation of the known genes and transcripts in the ENCODE regions by the GENCODE consortium. Details on the annotation pipeline can be found in Harrow *et al*[29]. In summary, the ENCODE regions were first subjected to a detailed manual annotation by the Havana group at the Sanger Institute; the annotators build coding transcripts based on alignments of known mRNA, EST and protein sequences to the human genome. The initial gene map delineated in this way was then experimentally refined through RT-PCR and RACE, which essentially confirmed the existence of the mRNA sequences of the hypothesized genes. Finally, the initial annotation was refined by the annotators based on these experimental results.

To assess the completeness of the GENCODE annotation, and the ability of the automatic methods to reproduce it, the EGASP community experiment was organized[26]. EGASP was organized in two phases. In January 2005, the GENCODE annotation of 13 regions, among the 44 ENCODE regions, was publicly released: Gene and other DNA feature prediction groups world-wide were asked to submit genome annotations on the remaining 31 regions. Eighteen groups participated by submitting 30 prediction sets within four months. When the annotation of the entire set of ENCODE regions was released in May, participants, organizers and a committee of external assessors met at the Wellcome Trust Genome Campus, Hinxton, UK, for a workshop sponsored by the National Human Genome Research Institute (NHGRI) to compare the GENCODE annotation, with the predictions by the groups. While the computational methods were accurate to predict the individual exons, they were less accurate when linking exons together into gene structures, with the best of the programs being able to resolve about 40% of the complete gene structures inferred by the human annotators. On the other hand more than 12,000 unique exons were predicted by the programs, which were not included in the GENCODE annotation. Experimental verification of a subset of them by RT-PCR yielded only about 3% verification rate (see Guigó *et al*[26] for details).

S2.4.1   The GENCODE Consortium

The GENCODE consortium (http://genome.imim.es/GENCODE) was formed to identify and map all protein-coding genes within the ENCODE regions. This is achieved by a combination of initial manual annotation by the HAVANA team (http://www.sanger.ac.uk/HGP/havana/), experimental validation by the GENCODE consortium, and a refinement of the annotation based on these experimental results. The HAVANA group divides gene features into eight different categories of which only the first two (known and novel CDS) are confidently predicted to be protein-coding genes. The common factor between all annotated gene structures is that they must be supported by transcriptional evidence, through homology to cDNA, EST and/or protein sequences. Eight different loci categories were used to fully classify the annotation produced for the ENCODE project[29].

Extensive experimental validation was used to confirm the initial manual annotation. First, 5' raid amplification of cDNA ends (RACE) was performed on 420 coding loci in 12 different tissues and resulted in 229 loci being confirmed by sequenced RACE products. In addition RT-PCR was used to verify all 360 splice junctions representing 161 novel and putative transcripts, resulting in 37% of novel transcripts being confirmed and 19% or the putative transcripts. RT-PCR verification of 1215 splice junctions identified by computational gene prediction algorithms, but not manually annotated by GENCODE, revealed only 2 (0.2%) splice junctions could be confirmed, suggesting that few intergenic coding loci remained unannotated[29].

S2.4.2   GENCODE Loci classification as defined in Harrow, et al[29]

-**known genes** are identical to human cDNA or protein sequences and identified by a GeneID in Entrez Gene (http://www.ncbi.nlm.nih.gov/entrez/query .fcg?db=gene).
-**novel CDSs** (CoDing Sequence) have an open reading frame (ORF) and are identical, or have homology, to cDNAs or proteins but do not fall in the above category; these mRNA sequences are submitted to public databases, but they are not yet represented in Entrez Gene or have not yet received an official gene name from the nomenclature committee ((http://www.gene.ucl.ac.uk/nomenclature/). They can also be novel in the sense that they are not yet represented by an mRNA sequence in the species concerned.
-**novel transcripts** are as above but no ORF can be unambiguously assigned; these can be genuine non-coding genes or they may be partial protein-coding genes supported by limited evidence. They should be supported by at least three ESTs from independent sources (not originating from the same clone identifier).
-**putative genes** are identical, or have homology, to spliced ESTs but lack a significant ORF and polyA features; these are generally short two or three exon genes or gene fragments.
-**pseudogenes** (assumes no expressed evidence) have homology to proteins but generally suffer from a disrupted CDS and an active homologous gene can be found at another locus. This category can be further subdivided into processed or unprocessed pseudogenes. Sometimes these entries have an intact CDS or an open but truncated ORF, in which case there is other evidence used (for example genomic polyA stretches at the 3' end) to classify them as a pseudogene.
-**transcribed pseudogene**s are not currently given a separate tag within GENCODE and are handled by creating a pseudogene object and an overlapping transcript object with the same locus name.
-**TEC** (To be Experimentally Confirmed). This is used for non-spliced EST clusters that have polyA features. This category has been specifically created for the ENCODE project to highlight regions that could indicate the presence of novel protein coding genes that require experimental validation, either by 5' RACE or/RT-PCR to extend the transcripts or by confirming expression of the putatively-encoded peptide with specific antibodies.
-**artefact gene** is used to tag mistakes in the public databases (Ensembl/SwissProt/ Trembl). Usually these arise from high-throughput cDNA sequencing projects, which submit automatic annotation sometimes resulting in erroneous CDSs that are, for example, 3' UTRs.

S2.4.3   Expression levels of GENODE transcripts

We investigated the expression levels of GENCODE transcripts using the signal levels from the 11 experiments used to detect TxFrags.(http://genome.ucsc.edu/cgi-

bin/hgTables?org=Human&db=hg17&hgsid=86335460&hgta_doMainPage=1&hgta_group=enc odeTxLevels ; tracks Yale Tar, Yale RNA, Affy RNA Signal, Affy Transfrags)

Each experiment was analysed separately because the threshold level used for calling TxFrags could vary substantially from experiment to experiment. Each probe was classified according to its coverage by both the TxFrags detected in the particular experiment under consideration and the GENCODE annotated exons. The exon type classes were single-cover ie annotated as being involved in only a single transcript, multi-cover ie covered by annotation from multiple transcripts, coding ie covered by annotation from a transcript with a CDS region and non-coding (NC) ie covered by a transcript with no identified CDS. Probes partially overlapping a particular exon type were assigned that type hence any given probe could fall into none, any or all four of the exon classes. This allowed us to omit boundary-overlapping probes and probes belonging to more than one class from the analyses.

We looked at the distribution of signal levels for the probes which fell both in transfrags and in only one of the following annotation classes 'single-cover NC', 'single-cover coding', 'multi-cover NC' and 'multi-cover coding' in order to compare the expression levels of the different exon classes. The distributions of signal level were broadly similar for the four annotation classes in all the tissues and cell lines examined. For an example see Supplementary Figure 3.
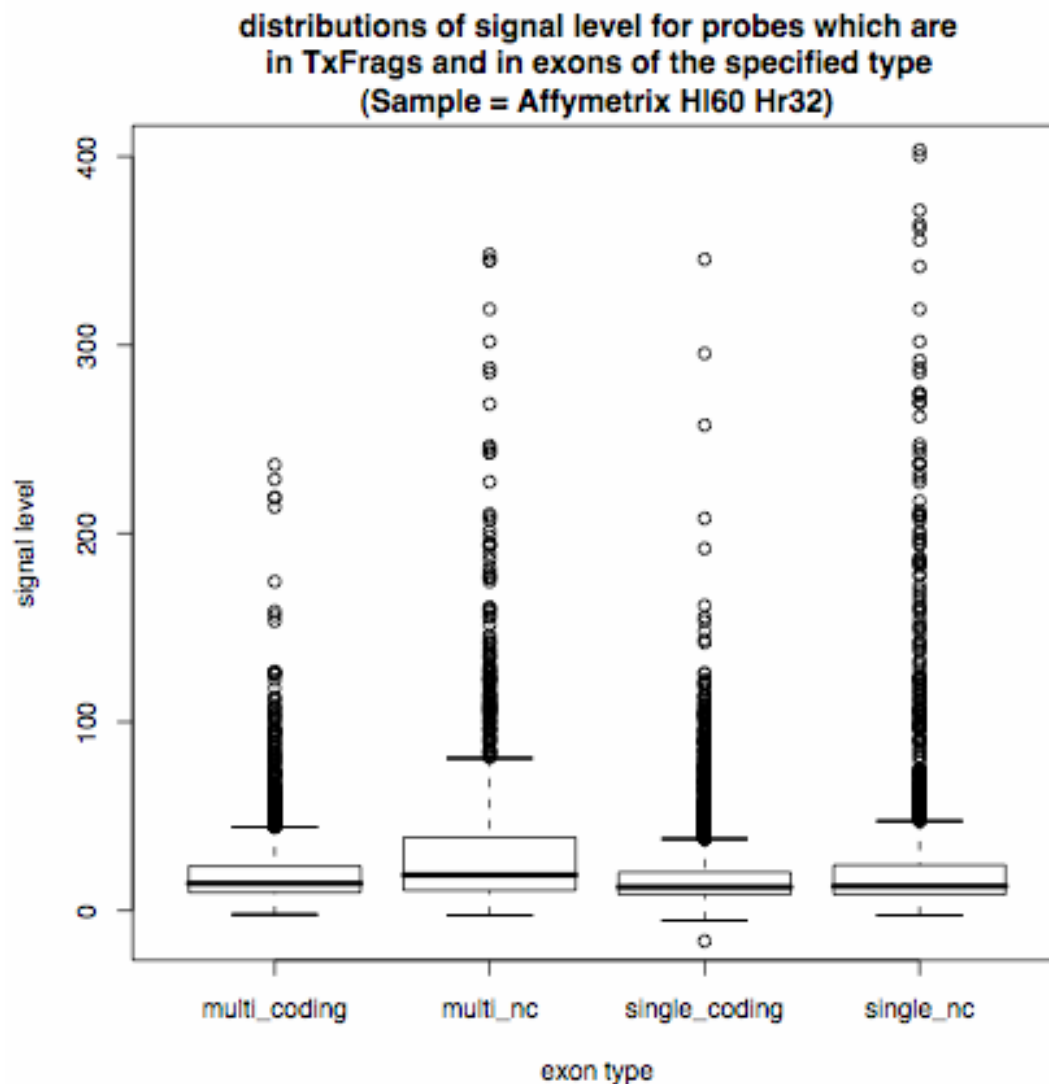
Supplementary Figure 3: Distributions of affymetrix genome tiling microarray probe signal levels for probes which fall both in TxFrags and in exons with different types of GENCODE annotation. 'Single' indicates the exon is unique to the transcript; 'multi' indicates the exon occurs in more than one transcript; 'coding' indicates the exon belongs to a transcript which is annotated as having a protein coding open reading frame (CDS); 'nc' indicates the exon belongs to a transcript with no known CDS. Only values for probes which belong to a single class are plotted. Signal levels and TxFrags obtained from tracks encodeAffyRnaHl60SignalHr32 and encodeAffyRnaHl60SitesHr32 at http://genome.ucsc.edu

From this exon level assignment, we have also classified transcripts in a boolean "expressed or not" manner using the expression level of the single-cover exons alone. Single cover transcripts were considered expressed if they had one or more single-cover exons with at least 50% of the probes in a TxFrag. For each expressed transcript the median probe signal level for probes of the

specified type was extracted. The distributions of these median values for coding single-cover and NC single-cover transcripts were similar to one another in all the tissues and cell lines indicating similar levels of expression for the coding and NC transcripts (see Supplementary Figure 4).
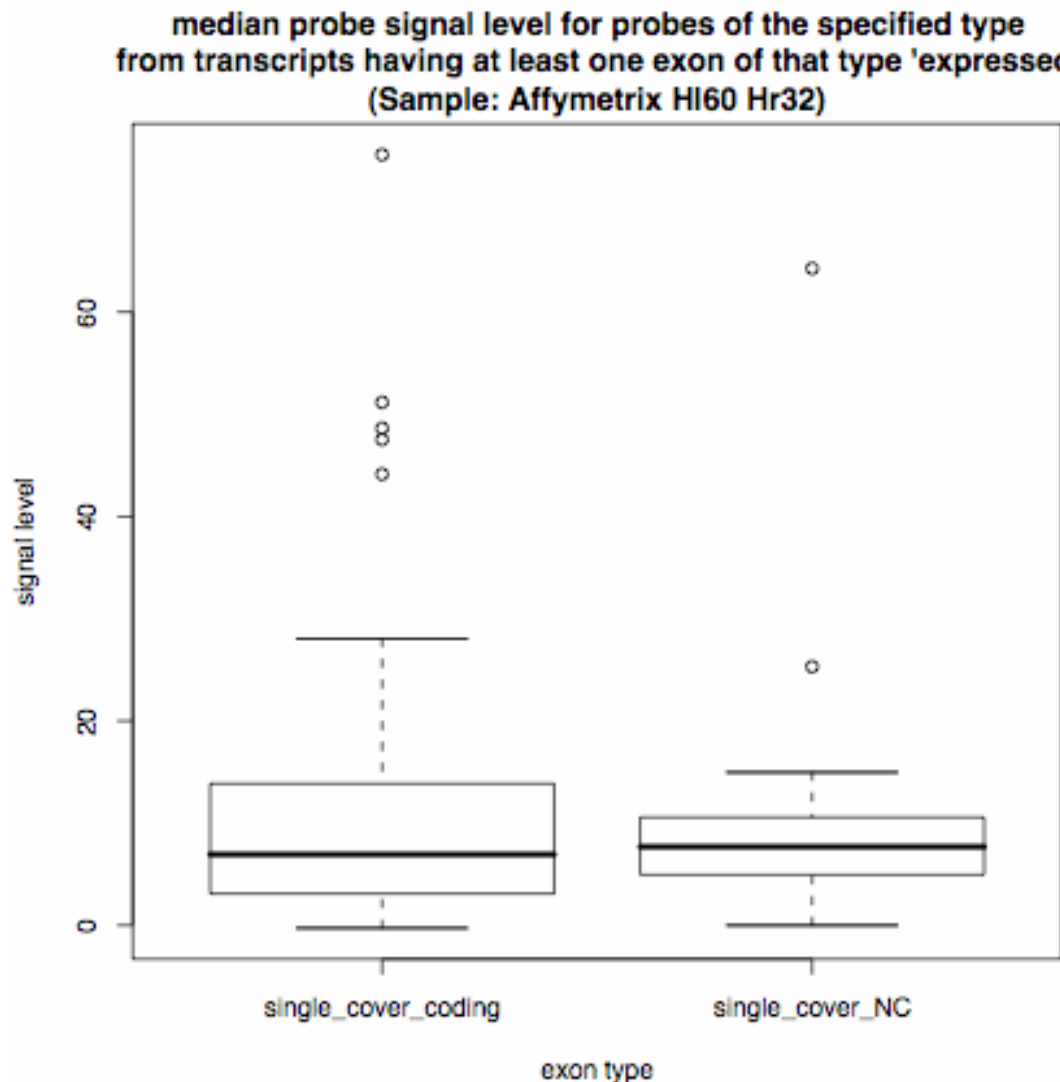
Supplementary Figure 4: Distributions of transcript median probe signal level of single-cover probes from transcripts having at least one exon annotated as unique to the transcript expressed. Exons were considered expressed if at least half the probes they contained were also contained in TxFrags. 'Coding' indicates the transcript is annotated as having a protein coding open reading frame (CDS); 'nc' indicates the transcript has no known CDS. Signal levels and TxFrags obtained from tracks encodeAffyRnaHl60SignalHr32 and encodeAffyRnaHl60SitesHr32 at http://genome.ucsc.edu

S2.5 Generation of Transcript Maps

S2.5.1   Generation of merged maps

28 maps were generated that describe the union of the following sources of annotations:
1. CAGE tags from Riken
2. PETs from Singapore
3. GENCODE exons (only exons of known and validated genes are considered here).
4. Filtered (see below for filtering process) TARS from Yale
5. Filtered (see below for filtering process) from Affymetrix.

The set of CAGE tags, PETs and GENCODE exons is same for each file. Only the TAR or transfrag content varied. There are 22 maps for each cell line/time point (11 for each strandless and stranded content). In addition, there are 2 maps for union of all Affymetrix and Yale array data, 2 files for polyA+ RNA data and 2 files for Total RNA data (see Table 2 for the list of cell lines and RNA sources). The strandless files were generated by ignoring strand information whereas the stranded files were generated on a strand-by-strand basis.

S2.5.2   Generation of 5' and 3' transcript end maps

Briefly, a comprehensive map of all nucleotides within the ENCODE regions that have evidence of being 5' or 3' ends of genes was generated. The source data for the generation was the GENCODE annotation of transcript boundaries (gives connected 5' and 3' edges), the PET dataset (gives connected 5' and 3' edges), and the CAGE dataset (gives only 5' edges).

For the maps, only the start or end nucleotide position of a transcript was considered. The confidence of ends identified by PET and CAGE data is increased with the number of tags mapping to the same position. Any nucleotide within the ENCODE regions that had a 5' or a 3'end indicated by any of the above data sources was included in the map, and the level of support for each data source was annotated.

In detail, the GENCODE transcripts were divided into their respective Havana categories, and the support level counted for each of these sets for 5' and 3' positions. The Ditag count is the total number of PETs starting (in the 5' case) or ending (3'case) at the position (including identical tags), regardless of cell line. The CAGE tag count is the total number of CAGE tags starting in the position (5' case), regardless of cell line or tissue source. For parsing issues, the cage count is reported in the 3' cases also, where it always is zero. In those cases where 3' ends and 5' ends can be connected by GENCODE or Ditag data, this is indicated.

The map should be considered a baseline of all evidence of 5' and 3' ends within the ENCODE regions, and sites corresponding to a given level of confidence can easily be extracted from the map. An important consideration is that the ends are at nucleotide level scale: there are many cases of multiple ends that are closely located (often the next nucleotide positions). This should be considered if the goal of extraction is to define promoter regions – in that case, clustering nearby locations into one unit is more relevant approach.

S2.5.3   Transcriptional Coverage of ENCODE regions

Supplementary Table 4: Summary of Transcriptional Coverage of ENCODE regions.

	PROCESSED TRANSCRIPTS (PT)						PRIMARY TRANSCRIPTS			
	Bases in All Exons [3]	Bases in CAGE tags [4]	Bases in PETs [5]	Bases in Tx Frags [6]	Total Bases in PT [7]	Bases in PT (ESTs included) [8]	Bases in Exons and Introns [9]	Bases with 5'RACE [10]	Bases between PETs [11]	Total Bases [12]
Total bases[1] 29998060 (percentage)*	1776157 (5.9%)	151149 (0.5%)	24939 (0.1%)	1369611 (4.6%)	2519280 (8.4%)	4826292 (16.1%)	17758738 (59.2%)	23318182 (77.7%)	19658563 (65.5%)	27325931 (91.1%)
Interrogated bases[2] 14707189 (percentage)*	1447192 (9.8%)	116013 (0.8%)	19629 (0.1%)	1369304 (9.3%)	2163303 (14.7%)	3545358 (24.1%)	9496360 (64.6%)	11763410 (80.0%)	9767311 (66.4%)	13618240 (92.6%)

1. Based on hg 35
2. Sequences interrogated by microarrays
3. Nucleotides in GENCODE exons from protein coding and noncoding transcripts (in whole regions or interrogated regions)
4. Nucleotides covered by CAGE tags
5. Nucleotides covered by PETs
6. Nucleotides covered by transfrags from polyA samples (TxFrags)
7. Nucleotides covered by GENCODE exons, CAGE tags, PETs and polyA transfrags present in processed transcripts : all processed transcription (PT)
8. Nucleotides covered by all sequences in 7. and non-spliced ESTs not included in GENCODE annotations
9. Nucleotides covered in GENCODE annotated exons and introns
10. Nucleotides covered by array detected RACE exons and newly detected introns
11. Nucleotides covered by 5' and 3' PET tags and intervening genomic sequences
12. Nucleotides covered by GENCODE exons and introns, RACE exons and introns, PET tags and intervening sequences, all transfrag samples, CAGE tags, and ESTs : all primary transcription
* Percent of ENCODE genomic regions for total and Percent of interrogated nucleotides for interrogated

S2.6 Analysis of protein coding evolution

S2.6.1   Evolution of protein-coding genes in the ENCODE loci

The protein-coding regions in the ENCODE loci are generally highly constrained, although the redundancy of the genetic code and the physico-chemical properties of different amino acids allow some flexibility in their exact nucleotide sequence. We sought to characterize the selective pressures that have been acting on the protein-coding genes in the ENCODE loci and investigated this via the ratio between the rate of non-synonymous (amino acid changing) and synonymous (silent) substitutions, defined here as ω, which we estimated for every codon in the GENCODE annotated (ftp://genome.imim.es/pub/other/GENCODE) transcripts. When neutral evolution is prevalent, ω is expected to be close to 1. The maintenance of biological function places the majority of codons under strong purifying selection ($\omega \ll 1$), while changes leading to

molecular adaptation between species may reveal themselves through excessive numbers of non-synonymous substitutions ($\omega > 1$). In the context of ENCODE, estimates of ω provide another useful function, which is to distinguish likely correct annotations of open reading frames from false ones.

Studies of selection are dependent on highly accurate alignments, as local alignment mistakes may cause an apparent excess of non-synonymous changes to be observed. The aligners used to align the ENCODE genomic sequences operate at the DNA level, and do not explicitly look for protein-coding sequence. To produce improved protein alignments, we assumed that the genome aligners correctly identified regions orthologous to the human exons and these were extracted, along with flanking sequences, and re-aligned using a protein-aware version of the prank aligner[67]. The resulting exon alignments were used to compute sitewise and exon-wide estimates of ω using SLR (see Section S2.6.3) Our results show that, in line with expectations, 45% and 72% of codons are under strong ($\omega < 0.05$) or moderately strong ($\omega < 0.25$) purifying selection, respectively. Additionally, 81% of exons are highly constrained, with an exon-wide mean ω estimate smaller than 0.05 (Supplementary Figure 5, histogram). Of these exons, 5.5% have at least one site estimated to have ω significantly greater than 1. A single site (at nucleotide position 1740) in a highly conserved exon of ACSL6, for example, was inferred to have undergone adaptive evolution (Supplementary Figure 5, upper panel).

In our analyses we noticed a small but significant fraction of exons where the expected pattern of substitution is not observed. A small fraction (3.3%) of exons have a mean ω estimate greater than 0.25, caused by aberrant estimates at multiple sites. A proposed exon within GRM8, for example (Supplementary Figure 5, lower panel), does not appear to evolve with the usual evolutionary dynamics associated with protein-coding sequences; only one of the three proposed alternative transcripts (variant 003) for this gene contains the unusual exon, and this transcript continues in a different reading frame from the others then terminates early. To further investigate our results, we devised a novel method to score each exon according to its overall tendency to conform to a 'background' distribution of sitewise ω values (see Section S2.6.3) Proposed exons or transcripts were ranked by this 'oddness score', allowing the easy identification of unusual exons. Aberrant patterns of selection may be explained by interesting biological phenomena, such as functionality in only a subset of species or exons having coding and non-coding functions, but are also consistent with errors in annotation and/or the identification of orthologous sequences. An arbitrary threshold for the 'oddness' score can be used to filter out the most implausible-looking exons/transcripts from further analyses. The results of our analyses are available via http://www.ebi.ac.uk/goldman-srv/encode, including prank alignments, sitewise estimates of ω, and lists of GENCODE annotated exons and transcripts ordered according to their 'oddness' score. Summarized versions of our protein analyses are also provided as custom tracks within the UCSC Genome Browser.
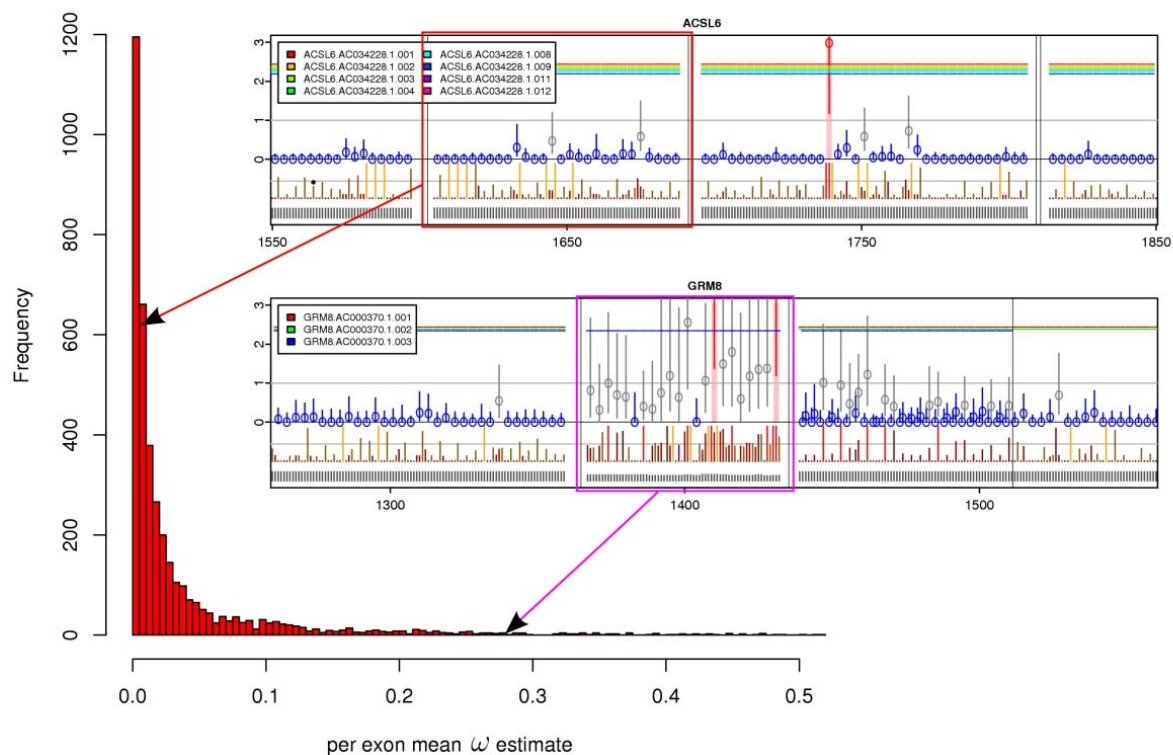
Supplementary Figure 5: Examples of sitewise ω analyses. The upper panel is from the ACSL6 gene of ENCODE target region ENm002. At the top, the colored horizontal lines and legend indicate the exons that contribute to each proposed transcript variant (001, ... , 012). The color of sitewise ω estimates (circles) and their confidence intervals (bars) denote the inferred mode of selection acting: blue: purifying selection; grey: unclassified; red: adaptive evolution (also highlighted with a pink background). Below this is a per-nucleotide measure of conservation, with abnormally fast sites colored orange (3rd codon positions) or red (1st or 2nd codon positions). The black bars at the bottom record the number of sequences available at each alignment position. The upper panel is typical of a good protein sequence alignment. The exon boxed in red has a typical exon-wide mean ω, indicated by the arrow showing its position relative to the distribution of the means from the full data. Note the single site (position 1740) for which significant positive selection is inferred. The lower panel is from GRM8 (Enm014). The exon boxed in purple (only present in transcript variant 003) has an atypical mean ω value, and comprises many sites inferred to have neutral or positively selected evolutionary dynamics. The preceding exon is not unusual; in the following one, variant 003 is in a different reading frame, terminates early and again has an unusual pattern of sitewise ω estimates. This is suggestive that variant 003 is under unusual selective pressures or is not protein coding.

S2.6.2   Consequences of the analysis

The availability of homologous sequence from many vertebrate species enables the evolutionary history of human proteins to be analyzed at the molecular level, giving insights into function and

adaptation. The depth of sequence provided by the ENCODE project enabled us to analyze all exons from proposed transcripts for selective pressures, providing useful estimates down to single codon resolution. Our results show that the majority (81%) of protein-coding exons in the ENCODE regions have evolved under strong purifying selection. A small fraction of these highly conserved exons (5.5%) have evidence of adaptive evolution at one or more of their codon sites, suggesting that continual adaptation is rare. A significant fraction of proposed protein-coding exons appear to evolve in an atypical manner, with aberrant patterns of selective pressures acting upon them. There is unlikely to be a single specific cause of such unusual patterns of selection. It may be attributable to interesting biological phenomena that induce unusual forms of selection, including the scenario that the annotated region is not functional in some target species. The aberrant patterns may also result from coding sequence overlapping other evolutionarily constrained features, leading to purifying selection acting on both synonymous and non-synonymous changes in a manner not captured by this analysis. Alternatively, the unusual patterns may result from methodological problems, including errors in transcript annotation, poor sequence coverage, and alignment mistakes. Differentiating between these possibilities is difficult and we have concentrated our methods to highlight unusual patterns for further study. Currently, we advocate caution with accepting all proposed transcript variants as protein-coding: a region that is transcribed and spliced, even when it contains an open reading frame, may not necessarily code for a protein.

S2.6.3   Method for determining the rates of evolution in protein-coding genes

To improve the quality of the protein alignments, protein-coding exons with 200 bases of upstream and downstream flanking regions were extracted from the TBA alignments, and the sequences were re-aligned using the prank aligner[67]. This aligner exploits gene structure, with its varying patterns of evolutionary dynamics, and ensures that the alignments satisfy certain biological requirements such as ensuring the sequences begin and end with a UTR, and that the protein-coding regions are flanked by start/stop codons or donor/acceptor splice sites. The new alignments were trimmed by removing the upstream and downstream UTR regions, the two nucleotides at the beginning and end of each exon that may be under strong selection for the splicing function, and possibly one or two nucleotides to correct the exon into the first reading frame. Columns having alignment gaps in the human sequence were removed, as were the incomplete codons, caused by (e.g.) non-reading frame alignment gaps, and stop codons. Only exons from complete transcripts were included in later analyses.

Taking the alignments and phylogenetic trees, estimates and confidence intervals for the non-synonymous to synonymous rate ratio, ω, were obtained for each aligned site using the SLR method[68]. The method requires quantities, such as the length of branches and codon composition, that are considered common to all sites and these were estimated on a per-gene basis by concatenating all constituent exons. Confidence intervals were calculated for each estimate to ensure that the results are useful. We devised a novel method to score each exon according to its constituent sites' overall tendency to conform to the 'background' distribution of sitewise ω values. We assume this background is largely representative of true protein-coding genes, and quantify the deviation of each exon's ω estimates from this background with Kolmogorov-Smirnov-like test statistics accounting for the uncertainty in these estimates. This provides an 'evolutionary oddness' score for each exon; gene transcripts can be scored according to the maximum oddness score attained by any of their exons.

S2.7 Expression and confirmation of GENCODE transcripts and unusual splice variants

S2.7.1   Confirmation of unusual splice variants

Reconfirmation of 144 unusual splice variant transcripts was experimentally attempted by RT-PCR and sequencing of a specific splice-junction in a panel of 24 human tissues. The selected splice junction could either be the result of exon-skipping (91 cases) or presence of an exon specific to the non-canonical transcript variant (53 cases). A positive amplification was found for 36 out of 144 cases (see section S2.7.3) This approach has been shown to confirm 87% (84/96) and 12% (6/50) of exon-exon junctions of known human genes and novel human genes identified using the chicken genome as reference[29, 69]. Thus the rate of confirmation observed here (25%), suggests that these transcripts might be less abundant than the canonical ones. However, exon-exon junction that yielded positive results were found expressed in an average of 8.9 tissues out of the 24 tested suggesting that the non-canonical splice variants do not present extremely restricted expression patterns.

S2.7.2   Materials and Methods

24 human cDNAs (brain, heart, kidney, spleen, liver, colon, small intestine, muscle, lung, stomach, testis, placenta, skin, PBLs, bone marrow, fetal brain, fetal liver, fetal kidney, fetal heart, fetal lung, thymus, pancreas, mammary glands, prostate) were independently mixed with JumpStart REDTaq ReadyMix (Sigma) and 4 ng/ul primers (Sigma-Genosys) using a BioMek 2000 robot (Beckman) as described and modified[70]. RT-PCR oligonucleotides were designed with primer 3 (http://frodo.wi.mit.edu/cgi-bin/primer3/primer3_www.cgi) with default parameters. The first 10 cycles of PCR amplification were performed with a touchdown annealing temperature decreasing from 60 to 50ºC; annealing temperature of the next 30 cycles was carried out at 50ºC. Amplimers were separated on Ready-to-Run precast gels (Pharmacia). When the tested exon-exon splice junction was the result of an exon specific to the non-canonical transcript the amplimers were sequenced directly. On the contrary tested exon-exon junction that result from exon-skipping were purified from gel. This procedure allowed separating and sequencing the two amplimers corresponding to both the canonical and the non-canonical transcripts

S2.7.3   Table in the supplemental Excel spreadsheet

This table is included in the attached Excel spreadsheet on the worksheet labeled Section S2.7.3.

S2.8 Analysis of unannotated transfrags

S2.8.1   Analyzing coding potential of transfrags

The structure of the genetic code gives conserved coding sequence a characteristic periodic pattern of evolutionary rates, which can be used to distinguish sequence that is coding (or historically coding) from non-coding. Following David *et al*[71], aligned sequences of DNA were analyzed by comparing two models: HKY+G[72, 73] was used as a null model for non-coding sequence and contrasted to an alternative model expanded to allow for a periodic "*…abcabcabc…*" pattern of rate variation; there are no additional restrictions on each of these three rates, so this formulation is frame-independent and tests all reading frames simultaneously. This choice of models takes into account the possibility of rate variation in non-coding sequence while allowing an explicit likelihood ratio test for the presence of periodic variation. The periodic pattern is extremely sensitive to shifts in reading frame, as might be caused by alignment error or alignment to non-coding sequence. To reduce the effect of frame changes, all alignments were humanized (columns with gaps in human were deleted).

Three sets of alignments were analyzed: intronic transfrags, intergenic transfrags and a non-redundant set of Havana-annotated exons. The composition of these sets is summarized in Supplementary Table 5. While the exon alignments tend to be longer and contain more species than either of the transfrag sets, there is not a huge disparity between the three sets of data analyzed.

Supplementary Table 5: Summary of three sets of data analyzed. Exon alignments tend to be longer and be composed of more species than intronic transfrags, which in turn are more informative than intergenic transfrags.

	Intergenic	Intronic	Havana-annotated exons
Number analyzed	658	672	3154
Median no. of species	11	14	17
IQR	(8,14)	(12,15)	(11,19)
Median no. of sites	74	84	123.5
IQR	(64,93)	(65,128)	(86,168.8)

The distribution of test statistics for the intergenic transfrags is indistinguishable from that expected by random variation under the null model (one-tailed Kolmogorov test *vs.* χ_2^2, pvalue 0.60) and similarly for intronic transfrags (pvalue 0.93). In comparison, the p-value for the same test for Havana-annotated exons is indistinguishable from zero; i.e., the Havana-annotated exon set gives a signal that comprehensively rejects the idea that there is no periodicity of rates.

In total, only 6 transfrags from 1330 analyzed (intergenic: 4 from 658, intronic: 2 from 672) showed any evidence of periodicity at the 99% significance level, and these can be safely dismissed once corrections for multiple comparisons are taken into account. In other words, there seems no reason to believe that the transfrag set contains any protein-coding DNA.

The corresponding numbers for the Havana exons are 2661 significant from 3154, with 2252 remaining significant after correcting for multiple comparisons using the procedure of Hochberg[74]. This is clearly a very different signal from the transfrags. The exons not significant represent some mixture of Havana-annotated exons that are not actually protein-coding; or that have poor Encode alignments; or where the statistical power of the test is not enough to find the coding signal (of course, there are also reasons why some of the transfrags could be coding but not indicated as such by these tests).

Supplementary Figure 6 shows that the estimated rates for the transfrags tend to be equal ($a = b = c$), consistent with being non-coding, whereas the Havana-annotated exons tend to be dominated by a single rate as might be occur if every third position is less constrained than its neighbours. Supplementary Figure 7 shows the performance of the periodicity test, if used to distinguish between annotated exon "coding sequence" and transfrags "non-coding".
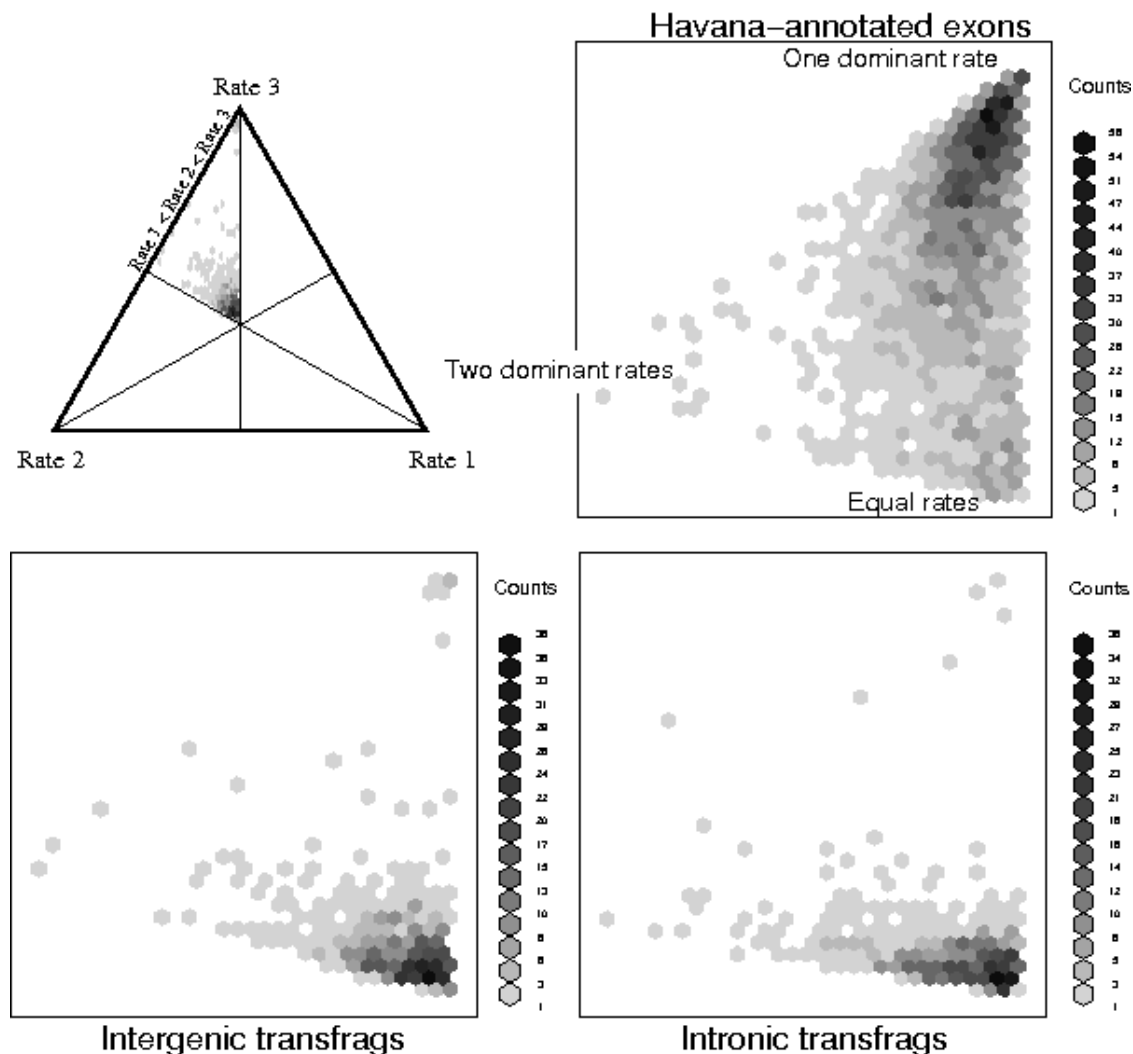
Supplementary Figure 6: Estimated rates for transfrags and Havana-annotated exons. Upper left: The three rates are constrained so each is positive and their sum is 3.0, and so lie in a simplex (an equilateral triangle). The ambiguity over reading frame is resolved by

sorting the rates according to magnitude, hence all points fall in the left upper portion of the simplex. Equal rates, the center of the simplex, is the bottom righthand corner of the region shown; the upper righthand corner corresponds to one dominant rate. The left upper portion of the simplex is expanded and shown for Havana-annotated exons (upper right), intergenic transfrags (lower left) and intronic transfrags (lower right).
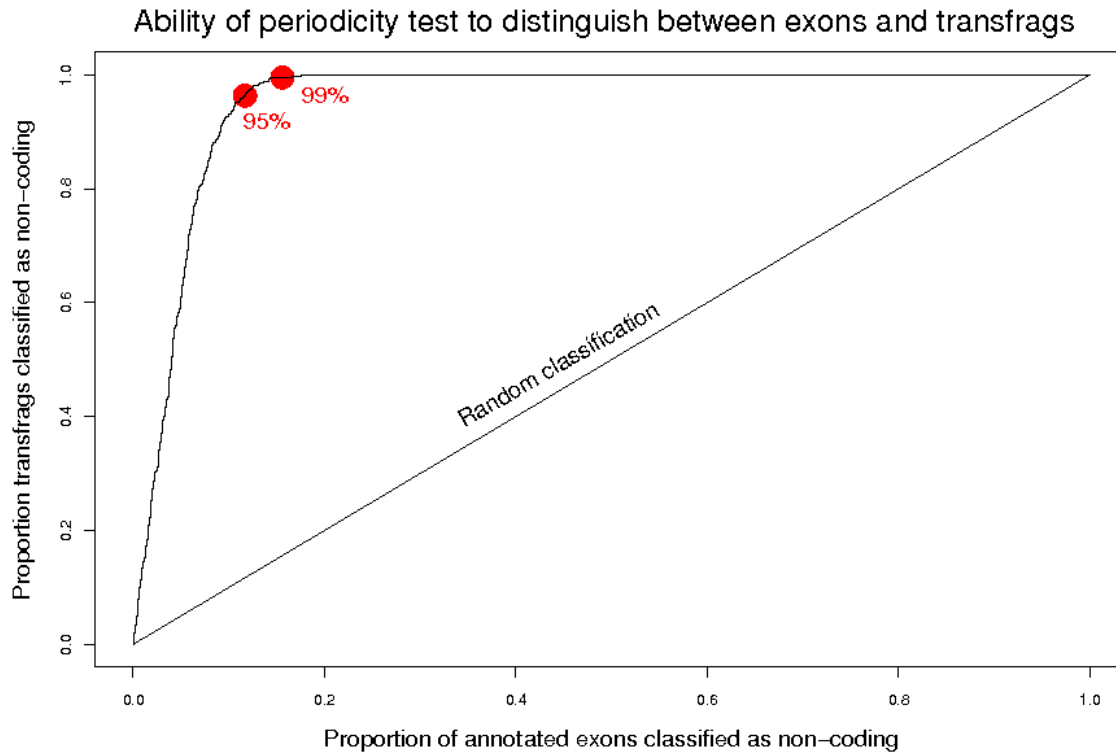
Supplementary Figure 7: Ability of periodicity test to separate exons and transfrags. Assuming that all transfrags are non-coding and all exons are correctly annotated, this curve shows the trade-off between specificity and sensitivity for different values of the likelihood-ratio test statistic. For comparison, the straight line represents random classification.

S2.8.2   Analysis of transfrag coordinated expression in the retinoic acid stimulated cell line HL60

We want to test the hypothesis that a non-negligible portion of transfrags (TxFrags) occurring next to each other in unannotated regions show a significant correlation in the pattern of expression across 4 time points in the retinoic acid stimulated cell line HL60. Taking the October 2005 release of the GENCODE annotation (track encodeGENCODEGeneKnownOct05 at the UCSC genome browser, hg17) we have built a set of unique internal CDS connected exon pairs out of the set of transcripts annotated with a complete CDS and at least 4 exons. We discard first and last exons as they have shown a higher variability in the hybridization signal due to a more frequent overlapping with exons of other transcripts.

Transfrags (TxFrags) occurring in the unannotated ENCODE regions generated from the HL60 cell line at each of the 4 time points have been filtered in order to obtain a set that includes:
1. the projected intersection across the 4 time points with a minimum length of 40nt.
2. the projected TxFrags that occur uniquely at one of the 4 time points with a minimum length of 40nt.

For each of the previously filtered TxFrags and exons, we have taken the hybridization values of the probes overlapping the TxFrag separately for each of the 4 time points of HL60 and assign the median of the probes discarding those TxFrags and exon pairs that were overlapped by less than 3 probes (an exon pair was discarded if just one of the two exons was overlapped by less than 3 probes).

In order to remove spurious correlations due to biases in expression within each different time point we take the logarithm of the hybridization values and standardize them ($[X-\mu]/SD$). Finally, we calculate the Pearson correlation between the following 5 pairs of sets:

unannotated TxFrag vs neighbor unannotated TxFrag,
unannotated TxFrag vs non-neighbor unannotated TxFrag randomly sampled from the same chromosome (intra-chr in the legend),
unannotated TxFrag vs non-neighbor unannotated TxFrag randomly sampled from a different chromosome (inter-chr in the legend),
exon vs exon (both connected in at least one transcript),
exon vs non-neighbor (not connected) exon randomly sampled from a different chromosome (inter-chr in the legend),

where a neighbor exon is defined as the one member of the same exon pair, while a neighbor unannotated TxFrag is defined as the closest unannotated TxFrag for which the genomic space in between is not occupied by an exon resulting of projecting the entire set of the GENCODE annotations on the genomic space. Thus neighbor unannotated TxFrags share a common intron or intergenic region.

Supplementary Table 6: Median correlations, (pseudo)median correlations and their 95% confidence interval for each of the five sets of neighbor and non-neighbor TxFrags and exon pairs.

	Neighbor unann TxFrags	non-neigh TxFrags intra-chr	non-neigh TxFrags inter-chr	neighbor exons	non-neigh exons inter-chr
Median	0.1690	0.0168	0.0029	0.6680	-0.0074
(pseudo)median	0.1160	0.0302	0.0064	0.5330	0.0002
95% CI ps.med.	0.0801:0.1550	-0.0042:0.0651	-0.0277:0.0406	0.4998:0.5667	-0.0304:0.0310

In Supplementary Table 6 we show the median correlation on each set and also the (pseudo)median and its confidence interval which have been calculated by using the Wilcoxon signed rank test. We observe that the neighbor exon set has the highest median as we expected. The neighbor unannotated-TxFrag set has the second highest median as we also expected,

although the strength of the median correlation is not very high (0.17) but it is about 10 times larger than the non-neighbor TxFrag intra-chromosomal set, about 58 times larger than the non-neighbor TxFrag inter-chromosomal set and about 23 times larger than the non-neighbor exon set. The confidence interval (CI) for the neighbor sets of exons and unannotated TxFrags does not include the value of 0 correlation meaning that the correlation, although small in the case of the unannotated TxFrags, can be considered significant, while the CIs for the other three non-neighbor sets do not overlap the CI of the neighbor sets and they do include the value 0 implying that the median correlation in these three sets cannot be considered significant.
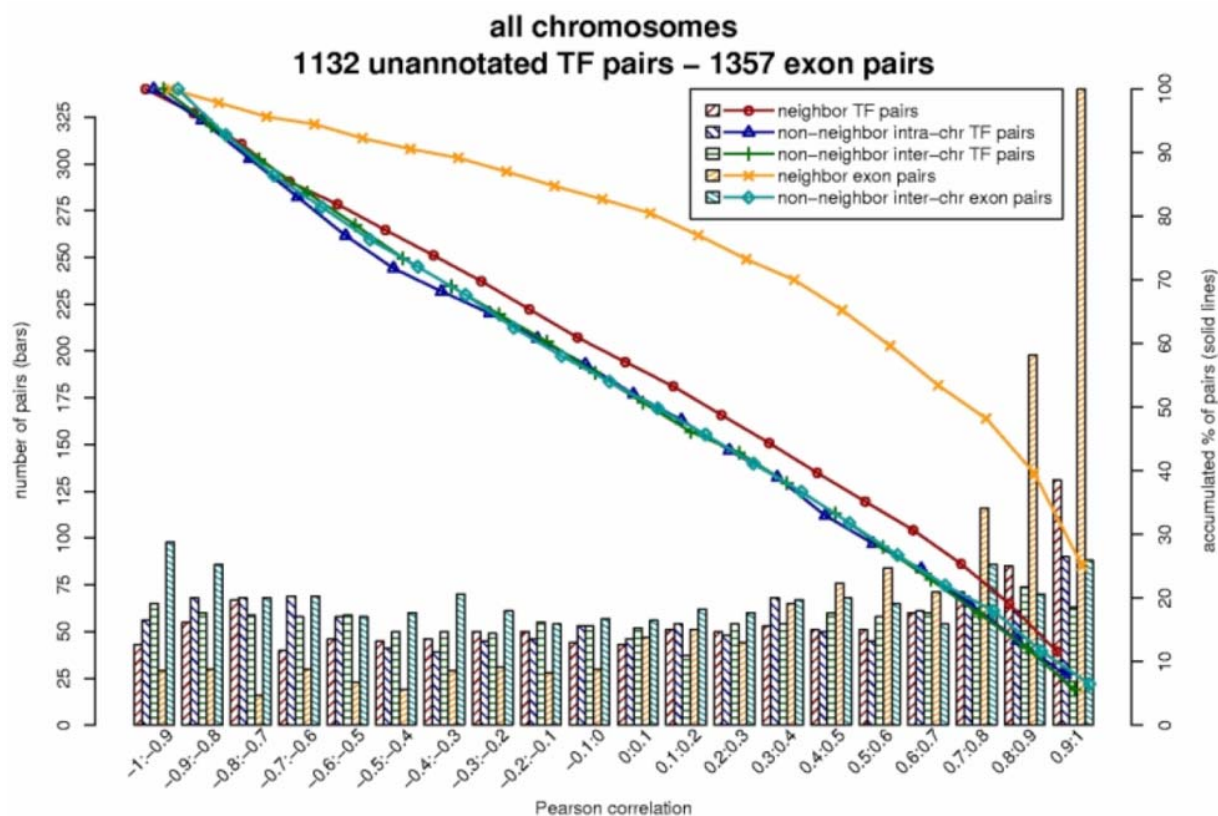
Supplementary Figure 8: Distribution of the median correlation throughout the five sets of neighbor and non-neighbor TxFrags and exon pairs

In Supplementary Figure 8 we show the distribution of the median correlation across the five sets (vertical bars) together with the accumulated minimum number of pairs at a particular median correlation (solid lines). For instance, about 40% of the neighbor exon pairs have at least a median correlation of 0.8 while this occurs to about 20% of the neighbor TxFrag pairs occurring in unannotated regions.

S2.9 RACE and Genome Tiling Arrays: Data generation and analysis

S2.9.1   Data generation for RACE/array of known protein-coding genes

5'-RACEs were performed on polyA$^+$ RNAs from 12 human tissues (brain, heart, kidney, spleen, liver, colon, small intestine, muscle, lung, stomach, testis, placenta, all BD Clontech) using the BD SMART^{TM} RACE cDNA amplification kit (BD Clontech Cat. No.634914). Double-stranded cDNA synthesis, adaptor ligations to the synthesized cDNA and 25 µl final volume RACE reactions were performed according to the manufacturers' instructions. RACE primers were designed with primer 3 (http://frodo.wi.mit.edu/cgi-bin/primer3/primer3_www.cgi) with the following parameters: $23 \leq$ primer size ≤ 27, optimal size=25, $68°C \leq$ primer Tm $\leq 72°C$, optimal Tm = 70°C, $50\% \leq$ primer GC percentage $\leq 70\%$. 15 µl aliquots of 80 to 100 RACE reactions performed with primers specific to non-neighboring genes and on the same tissue/cell line cDNA were assembled in pools, precipitated with ethanol and resuspended in water. 25 µg of RACE amplicons were fragmented with DNAse I to the size of 50-100 bp, denatured by heating to 99°C for 10 minutes and end labeled with biotin using terminal transferase (TdT; Roche) in 35 µl under the following conditions: 1X TdT reaction buffer (Roche), 2.5 mM CoCl$_2$, 1.15 nmoles of Affymetrix DNA Labeling Reagent (DLR, cat. # 900542) per 1 µg of fragmented DNA and 200 units of TdT. The reactions were incubated for 2 hrs at 37°C. 20 µg of labeled RACE DNA was hybridized to ENCODE tiling arrays as described in Kapranov *et al*[59]. RACE maps were generated using the one-sample, two-sample, and interval analysis methods described in details below and implemented in the Tiling Analysis Software suite (TAS,http://www.affymetrix.com/support/developer/downloads/TilingArrayTools/index.affx). The maps were generated with no smoothing (bandwidth = 1) and no CEL file normalization. The RACEfrags were generated using probe intensity threshold of 100; maxgap = 30 and minrun = 20. Thus, minimal RACEfrag would contain two consecutive positive probes.

One-sample Analysis
In a one-sample analysis, for example, used to generate TxFrag and RxFrag maps, Tiling Array Software (TAS) performs a Wilcoxon signed-rank test on the n probe intensity differences $\{PM_j-MM_j; i=1,...n\}$ by testing the null hypothesis of no shift between the distribution of PM intensities and MM intensities. The default alternative hypothesis is that there is a positive shift in the distribution of PM-MM, and therefore, a one-sided p-value is reported for the position. The p-value reported in the output file may be -10log10(p-value), which is a more suitable quantity for plotting against sequence position; higher values are more significant. This converts a p-value of 0.1 to a transformed p-value of 10, 0.01 to 20, 0.001 to 30, and so on (this is the same transform as the one used for Phred quality scores in the DNA sequencing literature). An estimate of signal intensity is also computed. The estimator used is the Hodges-Lehmann estimator[75] which is the usual estimator associated with the Wilcoxon signed-rank test, and which is also known as the pseudomedian. After forming all n values $\{D_i=PM_j-MM_j; i=1,...,n\}$, the n(n+1)/2 pairwise averages $(D_i-D_j)/2$, known as Walsh averages, are computed. The estimate s of signal location is taken to be the median of the n(n+1)/2 Walsh averages and is then transformed to log2(max(s,1)).

Two-sample Analysis

In two-sample analysis, for example, in the ChIP-chip analysis, there are two data sets, which are called a treatment (i.e. antibody to a specific factor) and a control group (a whole cell extract or non-specific antibody). Each group consists of the subset of data falling within the specified bandwidth as described above, resulting in nt treatment pairs of probe intensities $\{PM_{t,i}-MM_{t,i};$ $i=1,...nt\}$ and nc control pairs of probe intensities $\{PM_{c,i}-MM_{c,i}; i=1,...nc\}$. The log-transformed quantities $\{S_{g,i}=log2(max (PM_{g,i}-MM_{g,l,1})); g=t,c;i=1,...,ng\}$ are formed and a Wilcoxon signed-rank test is performed on the two samples $\{S_{t,i};i=1,...,nt\}$ and $\{t_{c,i};i=1,...,nc\}$. In the case of a PM only analysis, instead of using the log-transformed differences, the log-transformed PM signal intensities $\{S_{g,i}=log2(PM_{g,i});g=t,c;i=1,...,ng\}$ are used.

The default test type is a one-sided test, against the alternative that the distribution of the treatment data is shifted up with respect to the distribution of the control data. A two-sided or lower-sided test can be used instead of the one-sided lower. Similar to the one-sample p-values, by default, the -10log10 transform is applied to the output to enable visualization along the sequence.

An estimate of fold enrichment is also computed; the estimator used is the Hodges-Lehmann estimator associated with the Wilcoxon rank-sum test[75]. The estimator is computed by forming all ntnc values $\{D_{ij}=(S_{t,i}-S_{c,j});i=1,...,nt;j=1,...,nc\}$. The Hodges-Lehmann estimator is then the median of the D_{ij} and can be interpreted as the log2 fold change between the treatment and control group signals.

Interval Analysis

In both the one-sample and two-sample analysis, the Probe Analysis step described above will yield a p-value and a signal estimate associated with the location of each position in the sequence to which a probe pair aligns. TAS writes the resultant signals to output files, which can then be viewed in the Integrated Genome Browser (IGB). Additionally, these signals can be thresholded to produce discrete regions, which meet certain detection criteria, along the sequence of interest. The method involves three steps:

• In the first step, a threshold is applied to the value at each probe position, and a position is classified as positive if its value exceeds the threshold. The threshold can be applied to the signal, and a position can be classified as positive if it is either greater than or less than the threshold supplied. Alternatively, the threshold can be applied to the p-value associated with each position, in which case, one is typically interested in positions with p-values lower than the threshold.

 • In the second step, positive positions are separated by a distance of up to maxgap are joined together to form detected regions. The choice of maxgap is up to the user and depends on assay conditions. In general, making it larger is more permissive and will be more forgiving of positions which failed to make the threshold in a run of otherwise positive positions.

 • The final step is to process the list of all detected regions and reject any with a length of less than minrun. Again, the choice is dependent on the assay used, but generally making minrun smaller is more permissive and allows for shorter runs of positive positions to be classified as detected. The final set of all detection regions is written to an output file and can be used as a starting point for downstream analysis.

S2.9.2   Data generation of RACE/array of pseudogenes

5' RACEs to test expression of pseudogenes mapping within the ENCODE regions were performed on the same 12 tissues polyA$^+$ RNA and with the same conditions used for known protein-coding genes (see above). Similarly, pseudogene RACE primers were designed using the same parameters as with the known coding genes RACEs. In addition, pseudogene RACE primers were designed either to maximize or to minimize mismatches with pseudogene-parental gene pair, thus creating either pseudogene-specific primers and/or primers that recognize both the parental gene and the pseudogene, respectively. RACE reactions performed with these primers and on the same tissue cDNA were grouped in four pools: a pool of the RACE reactions performed with pseudogene-specific primers (5 to 14 mismatches between pseudogene and parental gene in the primer region), a pool with non-processed pseudogene-unspecific primers (0 to 3 mismatches), a pool with processed pseudogene unspecific primers (no mismatch), and a pool with processed pseudogene unspecific primers (1 to 3 mismatches). Pools of RACE reactions were precipitated, resuspended, digested, labeled and hybridized as described above for the known coding gene RACEs. The maps were generated using the TAS software with bandwidth of 50. RACEfrags were generated using threshold of 100, maxgap =50 and minrun =50. To assess pseudogene transcription, only pool-specific RACEfrags were considered. Furthermore, we only used RACEfrags if they were (i) from the pool with pseudogene-specific primers or (ii) uniquely mapped to a pseudogene locus or its close 5' upstream region (< 5 kbp). We have also compared pseudogenes with other transcriptional data. For example, we found that 56% of ENCODE pseudogenes overlapping with TxFrag, as comparison to a random expectation of 5%. The study of pseudogene transcription, including precise parameters and discussions of cross-hybridization, will be described in a separate paper[76].

S2.9.3   Data generation of RACE/array of ncRNA

Predicted ncRNA genes were tested for expression by RACE amplification and tiling-array hybridization as described above for known coding genes. However because a substantial fraction of ncRNA transcripts are not polyadenylated, RACEs reactions were performed independently with 12 human tissues cDNA prepared from both polyA+ and total RNA and oligo dT and random hexamers, respectively. Moreover whenever possible the RACE primer was designed in the most 3' portion of the predicted ncRNA. Aliquots of same tissue RACE reactions were grouped to create pools containing a single reaction per ENCODE region.

S2.9.4   Verification of 5' RACE/array results for known genes

551 RACEfrags were selected for independent verification of their connectivity with the original annotated gene. They are divided as follows: (set 1) 261 RACEfrags corresponding to the largest extension; (set 2a) 81 furthest RACEfrags supported by at least two tissues; (set 2b) 41 RACEfrags supported by the highest number of tissues (if not in set 2a); (set 3) 94 RACEfrags corresponding to the second largest tissue-specific extension; and (set 4) 33 intronic RACEfrags. RT-PCR were done either in Affymetrix Inc., Santa Clara (lab.A 300 RACEfrags) or the Universities of Geneva and Lausanne, Switzerland (lab.B 300 RACEfrags, 49 overlaps)

RT-PCRs in lab.B were performed on the oligo dT-primed cDNA using BD-advantage II polymerase mix and following the manufacturers' instructions (25 µl final volume). Note that the RNA used was the same as for the RACE reaction in which the RACEfrag was identified. The right primer was the original RACE primer and the left primer was designed with the same characteristics (see above) in the RACEfrag to be verified. ENCODE tiling arrays were used as a readout of the RT-PCR reactions. 15 µl aliquots of RT-PCR reactions were assembled in pools which contained a single reaction per ENCODE region. Pools of RT-PCR reactions were ethanol precipitated, resuspended in water, labeled and hybridized to the microarray as described above to control the connectivity between the RACEfrags and the original exon chosen to design the RACE primer.

Of the 300 RACEfrags, primers could only be selected for 283 by Lab A. The 283 reactions in lab A were performed using gene-specific primers for cDNA synthesis. cDNA synthesis was conducted on 10 ng of polyA+ RNA from a tissue where a corresponding RACEfrag was detected using the same oligonucleotide as used for 5' RACE analysis. The cDNA synthesis was performed with Thermoscript reverse transcriptase (Invitrogen) using the same conditions as described in Kapranov *et al*[59] for 5' RACE cDNA synthesis. The cDNA reactions were purified using QIAquick 96 (Qiagen) and ½ of each purified reaction was used as a starting material for RT-PCR. For each RACEfrag, two rounds of nested RT-PCR reactions were performed. The products of first round of RT-PCR were purified using QIAqucik 96 system, eluted in 80 µl and 0.01 µl of the first round reaction was used for the second round RT-PCR. Each round of amplification consisted of 30 cycles of PCR (94°C for 20 sec; 60°C for 30 sec; 72°C for 2 min) followed by 10 min at 72°C. Products of the final round of RT-PCRs were purified using QIAquick 96, pooled using the same strategy as in the lab B and hybridized to ENCODE arrays as described above.

In addition, RT-PCR reactions for 96 RACEfrags in lab A were done using oligo-dT cDNA as a substrate. PolyA+ RNA from brain, colon, heart, kidney, liver, lung and muscle were pooled and used for cDNA synthesis following the procedure used for cDNA synthesis for 3'RACE described above in section S2.1.4 The resulting cDNA was used for RT-PCR following the same PCR conditions as above.

The RT-PCRfrags were generated using the same parameters as the 5' RACEfrags for the known genes (see above) for both sets (Labs A & B).

S2.9.5   Assignment of RACEfrags to the target loci

The hybridization of the 5'RACE products on the tiling arrays was performed in 5 pools (each containing about 80 non adjacent loci) for each of the tissues. The RACEfrags were assigned to a particular locus using the following steps.

1) The RACEfrag maps were filtered to remove RACEfrags coming from non-specific amplicons. RACEfrags that are not specific to any particular pool of primers almost certainly represent non-specific amplicons that are often present in RACE reactions. To remove the products of such amplicons, RACEfrags that did not overlap GENCODE annotations and were non pool-specific were filtered out if they were overlapping RACEfrags from other pools by

more than 50% of their length. In addition, the RACEfrags that overlapped GENCODE exons were subdivided in fragments overlapping and non-overlapping exons. The fragmented RACEfrags overlapping exons were kept, whereas the ones not overlapping exons were filtered as above.

2) A RACE reaction was considered positive if at least one target exon was overlapping a RACEfrag. Target region was defined as genomic span between the index exon where the original 5'RACE oligonucleotide was designed and the GENCODE annotated 5' terminus of the locus[29]. Target exons were defined as annotated exons within the target region. With these criteria we found about 70% of positive reactions and ~90% of the loci were positive in at least one of the tissues tested. For the subsequent assignment procedure, only the target loci yielding positive reactions were considered.

3) The non-assignable RACEfrags, that map 3' to all target loci belonging to the pool, were discarded (~12%). Another group of RACEfrags were classified as ambiguous if they localized 5' to a pair of target loci mapping on opposite strands (Supplementary Figure 9). Overall, this resulted in 76% of assignable and 12% of ambiguous RACEfrags of the total number of RACEfrags kept after step 1. The final filter applied to all RACEfrags was to remove the ones overlapping target exons from other pools in order to rule out pooling errors. At the final assignment step, the remaining RACEfrags that were internal to the corresponding target locus were assigned to that target locus. RACEfrags found outside of the bounds of any target loci were assigned to the most proximal 3' target locus. The ambiguous RACEfrags were assigned to both possible loci, with high or low level of confidence: when the RACEfrag was closer to one loci than to the other (difference of distances greater than 100 kb), the assignment was considered as highly confident for the closest locus (provided that the RACEfrag was at less than 100 kb from the locus), otherwise, the assignments to both loci were considered as not confident. The final set of RACEfrags we describe contains only confidently assigned RACEfrags, they represent 70% of all the RACEfrags.
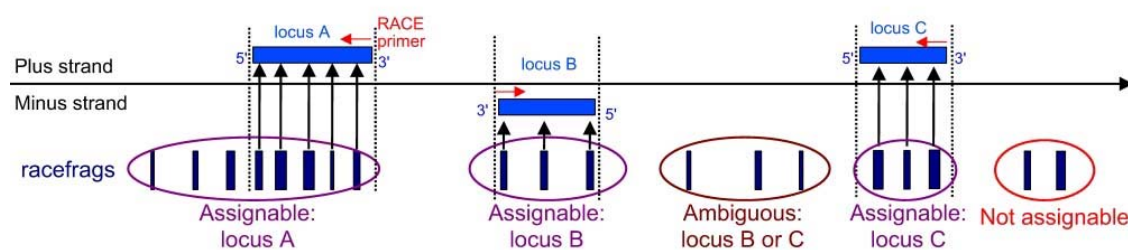
Supplementary Figure 9: Classification of RACEfrags for assignment to the target loci. The RACEfrags were classified as non-assignable RACEfrags, when they mapped 3' to all target loci belonging to the pool (circled in red). They were classified as ambiguous if they localized 5' to a pair of target loci mapping on opposite strands (circled in brown). The RACEfrags overlapping or localized in 5' of a single locus in the pool were classified as assignable (circled in purple): they were assigned unambigously to the locus they overlapped or the closest locus in 3'.

Supplementary Table 7: Summary of RACE/microarray experiments

	TOTAL	EXTERNAL TO THE LOCI		INTERNAL TO THE LOCI	
		ANNOTATED	UNANNOTATED	ANNOTATED	UNANNOTATED
RACEFRAGS	22,569	1,712	1,435	13,199	6,223
LOCI WITH RACEFRAG	359	180	213	356	247
5' MOST RACEFRAGS	3,282	483	548	2.077	174
LOCI WITH 5' MOST RACEFRAGS	359	165	195	324	76

Note that while the RACEfrags were assigned to the 3' most proximal target locus, we envision that scenarios where the RACEfrags could in fact be linked to target loci separated by other target loci might exist. We indeed observed numerous cases of extensions reaching across several loci (see main text and Supplementary Table 7). However, the verifications based on RT-PCRs reactions allowed to confirm the majority of connectivity between RACEfrags and target loci suggesting that the assignments were correct in most of the cases (see main text for results and below for procedure).

Furthermore, we were conservative as non-pool specific RACEfrags overlapping target exons from genes from other pools were discarded in case some pooling errors had occurred. As described in the main text section the RACE reactions revealed numerous cases of chimeric transcripts, thus some of these discarded RACEfrags could well have come from the correct target locus. Furthermore, as the target exons of other pools (i.e. the exons between the RACE primer and the 5'end of the locus) were discarded, the proportion of RACEfrags overlapping first exons is probably underestimated, and the RACEfrags reaching in 3'exons of genes are probably not the most distal ones; they were filtered out from the set of 157 RACEfrags the most likely to represent 5'ends (Supplementary Figure 10).

A — observed / random

Overlapping composite promoters
- 1390 external RACEfrags: 21.37%
- 584 most 5' external RACEfrags: 25.17%
- 157 RACEfrags the most likely to represent 5'ends: 38.22%

Less than 100 bp from TSS
- 1390 external RACEfrags: 16.04%
- 584 most 5' external RACEfrags: 20.89%
- 157 RACEfrags the most likely to represent 5'ends: 29.94%
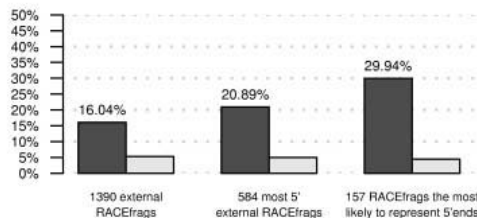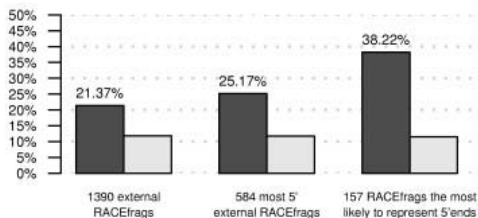
Less than 100 bp from Union HSS
- 1390 external RACEfrags: 12.01%
- 584 most 5' external RACEfrags: 14.38%
- 157 RACEfrags the most likely to represent 5'ends: 22.29%

Associated to TSS, promoter or HSS
- 1390 external RACEfrags: 34.1%
- 584 most 5' external RACEfrags: 38.36%
- 157 RACEfrags the most likely to represent 5'ends: 50.32%
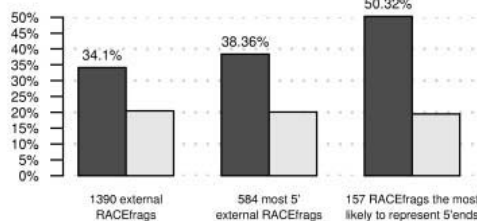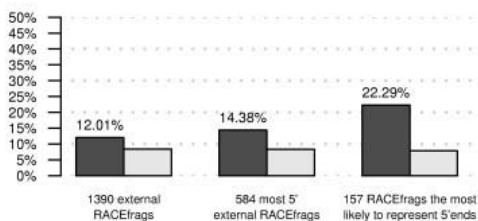
B

1,390 external RACEfrags
4%, 1%, 3%, 3%, 4%, 8%, 11%, 66%

584 most 5' external RACEfrags
7%, 1%, 4%, 4%, 3%, 9%, 11%, 62%
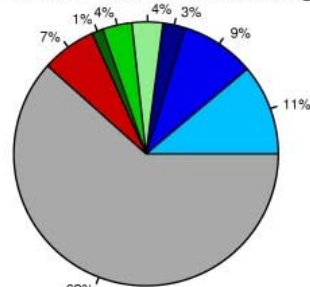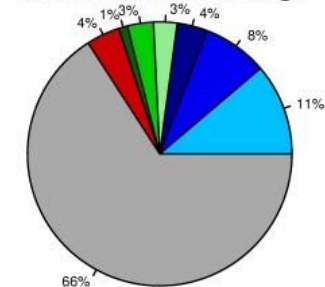
157 RACEfrags most likely
7%, 1%, 10%, 11%, 50%, 12%, 1%, 8%

Legend:
- Promoter only
- TSS only
- HSS only
- Promoter and TSS
- Promoter and HSS
- TSS and HSS
- Promoter TSS and HSS
- No overlap
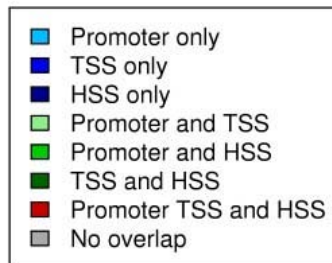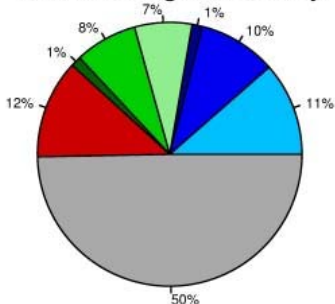
Supplementary Figure 10: Overlap of RACEfrags with 5' ends related datasets. Three sets of RACEfrags were overlapped with other datasets.

- 1390 projected RACEfrags: all projected RACEfrags external to the locus, not yet annotated as 5' ends (i.e not overlapping annotated first exons): they represent a mixture of 5'ends and internal new exons.

- 584 projected RACEfrags : from the first set, the subset of the RACEfrags that are the most distal for each locus per tissue was extracted: this set does not necessarily contain only 5'ends because the length of the ENCODE regions and the distance between genes in the pools limit the size of the observable extensions, and also because of the conservative filtering of RACEfrags, that could have discarded the most distal ones. However, this set is likely to be enriched in 5'ends compared to the previous set.

- 157 projected RACEfrags: from the 584 RACEfrags, the subset of RACEfrags that are the most likely to correspond to 5'ends was extracted. They correspond to loci where the length of the maximal extension observed is much lower than the length of the maximal possible extension possibly observable (<=50% of the distance to the next locus in the pool or encode region) -i.e. no limitation by the size of the interrogated region and pooling- and for which there is no limitation by the filtering strategy (upstream exons are not likely to have been filtered out).

The overlaps (stranded when the dataset contained a strand information) were calculated for the 3 RACEfrags sets as well as for random sets (200 random sets mimicking each of the 3 sets) to compare the random overlap to the observed overlap. All overlaps are significant (P-values<0.005).

A. proportion of RACEfrags in the real (black) and random (grey) sets overlapping the different datasets. As expected, there is an enrichment in objects supported by TSS, promoters, or Hss from the set of all external RACEfrags to the set of RACEfrags we expected to contain more 5'ends.

B. Pie charts of the different supports found for the RACEfrags in the three sets. Red:supported by three datasets, green; supported by two of the sets, blue: supported by one of the sets, grey: not supported by the other sets.

S2.9.6   Assignment of RTPCR-frags to the RT-PCR experiments

The pooling of RT-PCR reactions for array hybridizations was done such that assignment of RTPCR-frags to the each target locus would be un-ambiguous, i.e. each pool contained RTPCR reactions derived from different ENCODE regions. RTPCRfrags mapping between forward and reverse RT-PCR primers were assigned to the corresponding RT-PCR reaction.

To score an RTPCR as positive based on the profile of microarray hybridization, we used a two-way approach. First, an RT-PCR reaction was considered as positive if RTPCRfrags could be found within 1 kb from both forward and reverse RTPCR primer. 33% of the reactions were positive under this criteria. A separate scoring stretgy was used on the reactions that did not pass this filter to account for the cases where an RTPCR oligonucleotide was picked close to the boundary of the target RACEfrag or the target exon, thus resulting in the absence of RTPCRfrags

immediately proximal to the primer position: if 3 or more of the RTPCR frags were overlapping the original RACEfrags from the tissue where the RT-PCR was performed, the reaction was recalled positive (Supplementary Figure 11). Using both scoring strategies combined, about 58% of RTPCRs were scored positive.
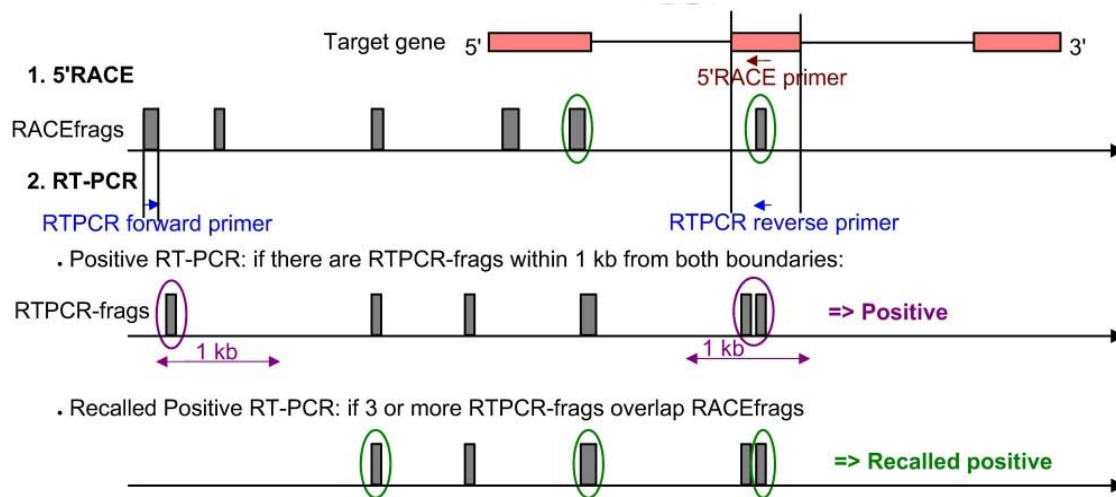
Supplementary Figure 11: Positive call of RT-PCR from array analysis. The figure represents a locus that was targetted for RACE with the position of the RACE primer (upper panel) and the RACEfrags that were obtained (middle panel). An RT-PCR was performed between the target exon used for the 5'RACE and one of the RACEfrags, providing RTPCRfrags (lower panel). Two cases of positive RT-PCR are represented. First, an RT-PCR reaction was considered as positive if RTPCRfrags could be found within 1kb from both forward and reverse RT-PCR primers. Second, for the the reactions that did not pass this filter, the reaction was recalled positive if 3 or more of the RTPCR frags were overlapping the original RACEfrags from the tissue where the RT-PCR was performed

S2.9.7   Cloning and sequencing of the RACE/array products

Two different strategies were employed to sequence the amplified transcripts that link tested RACEfrags and known exons. The RT-PCR reactions that appeared as single bands on agarose gel were selected for direct sequencing, while the others were cloned into pDRIVE following manufacturer's instructions (Qiagen) before sequencing of a minimum of eight clones. The reads were assembled after masking of the vector and mapped to the human genome using exonerate (unmasked, max intron length=1.5 Mb) to identify the best hit. The hit has to be more than 100 bp long, and with a %identity greater than 95%. From 2354 assembled sequences, 703 were spliced and mapped in the right target, corresponding to 353 non-redundant sequences (when several sequences were identical or included in each other, only one representative was kept). The following two filtering steps were applied to remove truncated sequences and those not reaching the borders of the target regions (the cloning could lead to a partial loss of the insert). First, at least 90% of the genomic span of a target region has to be covered by the RT-PCR sequence. Secondly, the RT-PCR sequence must not extend further than 100 bp outside the target genomic span. After these filtering steps, 175 unique sequences remained. They are deposited in

GenBank under accession numbers DQ655905-DQ656069 and EF070113-070122. They were inspected manually by the annotators who provided the GENCODE annotation[29] and dubious mappings were discarded, leading to a final set of 132 unique sequences. They correspond to 89 RT-PCR reactions and 69 loci. None of these sequences belong to the set of RT-PCR unconfirmed by the array approach, suggesting that this approach is efficient to classify the RT-PCR reactions.

S2.10 Pseudogene Annotation

In addition to the pseudogenes annotated by the GENCODE consortium, four computational methods designed specifically for identifying pseudogenes were also applied to the ENCODE regions. They were developed independently by research groups in the Genome Institute of Singapore (GIS), University of California Santa Cruz (UCSC) and Yale University. Details of individual methods have been described elsewhere[28, 29] or can be found with the corresponding data under the ENCODE pseudogenes track in the UCSC genome browser. These five methods differ in (i) queries used to search for pseudogenes (two used known proteins, one used human mRNAs, one used known human genes and one used genes derived from GIS-PETs) and (ii) parameters used to define and classify pseudogenes. They resulted in distinct lists of pseudogenes ranging from 56 to 172, some of which were method-specific. We have subsequently developed a consensus procedure to consolidate individual pseudogene annotation with the aim of providing a uniform pseudogene definition and one comprehensive list of pseudogenes. Our current approach built pseudogene annotation based on known proteins in the UniProt database and classified pseudogenes based on nearby genomic content and evidence of retrotransposition (e.g., lack of introns and polyA tails). In the end, we annotated 201 pseudogenes (77 non-processed and 124 processed pseudogenes). The list of pseudogenes and detailed description of our methods are available at http://www.pseudogene.org/ENCODE and http://genome.ucsc.edu/ENCODE/. Full characterizations of these pseudogenes will be described in a separate paper[76].

S2.11 Non-protein coding RNAs

S2.11.1   Expression of known non-coding RNAs and RNA pseudogenes

There is no comprehensive annotation of non-coding RNAs available for the human genome. Blast similarity search with sequences contained in the Rfam database yields appr. 6,200 hits in the human genome, 76 of these within the ENCODE regions. 60 of these belong to highly repetitive pseudogene RNA families (e.g. Y-RNAs, SRP-RNAs, rRNAs) some of which have thousands of copies in the genome. These are masked by RepeatMasker and not represented on the oligonucleotide arrays. As a consequence, they are not subject of analysis in this study.

There are eight well known non-coding RNAs in the ENCODE regions: 4 microRNAs (mir-192, mir-194-2, mir-196, mir-483), three H/ACA box snoRNAs (U70, ACA36, ACA56), and H19 a mRNA-like spliced non-coding transcript. All of them with the exception of mir-483 could be detected by the oligonucleotide experiments in at least one of the 11 tested tissues. mir-483 might be specific in fetal liver tissue which is not among the tested tissues.

In addition there are 8 sequences in the ENCODE regions that are similar to well-known functional ncRNAs . These are putative pseudogenes. Six are related to snoRNAs (ACA33-

related, ACA42-related, ACA44-related, U70-related, ACA36-related, E2-related), one is related
to the 28S rRNA, and one is related to the U6 snRNA. Expression was observed in tiling-array
data for all but the ACA36-related and E2-related sequences. The six putative pseudogenes that
were detected on the tiling-arrays were further analyzed using RACE/tiling-array analysis in
brain and testis (see Supplement S2.9.2). We could verify the expression of the ACA33-related,
ACA42-related, ACA44-related, and the 28S rRNA related sequences in both brain and testis.
Transcription of the U6-related sequence could not be detected in either brain or testis.

S2.11.2　　Prediction of structural non-coding RNAs

Three different approaches were used to predict ncRNAs with conserved and thus potentially
functional secondary structures. The complete non-repeat regions of the ENCODE regions were
screened with RNAz 0.1.1[77] and EvoFold 1.1[78]. In addition, an RNAz based screen was
conducted specifically on regions overlapping with TARs/Transfrags. For the EvoFold and
RNAz screen, human (hg17) referenced 28-way TBA alignments were used. Different pre-
processing steps and scoring protocols were used to meet the specific requirements of the two
programs.

S2.11.2.1　EvoFold

For the EvoFold analysis, sequences with more than 20% gaps relative to human were first
removed. Second, alignments with sequence from less than six species were eliminated. Third,
TBA alignment blocks consecutive relative to human were concatenated. Fourth, non-syntenic
sequences that include segments from disparate genomic regions (more than twice the length of
the human reference sequence apart) were removed; however, if the resulting alignment had less
than six sequences, none were removed. EvoFold was then applied to the concatenated
alignments, and their reverse complements, in 120 long overlapping windows each offset by 40.
Weak predictions (less than ten pairing bases or an average stem-length of less than three) as
well as predictions overlapping repeats or retro-genes (as defined by tracks of the UCSC
browser) were eliminated. Finally, the set was reduced to single coverage, by removing the
lowest scoring candidates when overlap occurred, and ranked according to score. The final
prediction set was defined based on the top-50% of the candidates.

S2.11.2.2　RNAz

Also for the RNAz screen alignments were sliced in overlapping windows of size 120 and slide
40. Each series of windows was started at the beginning of a TBA block. In cases of windows
exceeding the end of a block the adjacent block was tried to be concatenated to the current block.
Two blocks were only merged if all sequences were exactly or almost consecutive (up to 10
bases were allowed to be missing). Sequences with more than 25% gaps with respect to the
human sequence were discarded. Only alignments with more than four sequences, a minimum
size of 50 columns and at most 1% repeat masked letters were considered. RNAz can only
handle alignments with up to six sequences. From alignments with more than six sequences we
chose a subset of six sequences optimized for a mean pairwise identity of 80%. In cases of
alignments with more than 10 sequences we sampled three different of such subsets. The

windows were finally scored with RNAz in the forward and reverse complement direction. Overlapping hits were combined to a single genomic region. Two prediction sets of different significance (P>0.5 and P>0.9) were defined based on the RNA class probability calculated by RNAz.

S2.11.2.3 TARs/Transfrag centered RNAz screen

Non-repetitive chromosomal segments with evidence for transcription based on an analysis of high-density oligonucleotide tiling-arrays (i.e. segments matching to TARs/Transfrags) were used as a start point for an alternative search for structural ncRNAs using RNAz. TARs were first collected and extended by 50 nucleotides across their boundaries on either side in order not to miss RNA sequences with tight secondary structures, parts of which may hybridize poorly to the microarrays. Furthermore, TARs scored using less stringent scoring criteria (i.e. "low abundance" TARs with somewhat weaker evidence for transcription; all "low-abundance" TARs are available at http://homes.gersteinlab.org/people/rozowsky/low_abundance_tars) were utilized as a starting point in the analysis. All sequences were mapped to their corresponding TBA multiple sequence alignment blocks (23-way). In each case, the human sequence together with the five most distant sequences, each sharing an overall sequence identity of at least 70% with the human sequence, were kept and analyzed using RNAz. Alignment blocks of 120 were subjected to RNAz, utilizing an offset of 40 and considering both DNA strands independently (smaller alignment blocks of a minimum size of 50 bp were analyzed without offset). Regions with an RNAz classification score P > 0.5 were collected.

On the highest significance levels (P>0.9 for RNAz, top 50% predictions for EvoFold) 3,707 and 4,986 structural elements were predicted by RNAz and EvoFold, respectively. This corresponds to 1.3% and 1.4% of the ENCODE regions. To estimate the statistical significance of these predictions, we repeated the screen on randomized alignments that were created using a shuffling procedure which preserves base composition, sequence conservation and gap-patterns but removes any correlations arising from secondary structures[79]. As observed previously, both programs have a specificity of around 98%-99% on such random alignments. However, in this setting where a large number of alignments was scored, this corresponds to a false discovery rate of appr. 50% and 71% for RNAz and EvoFold, respectively. The overlap between RNAz and EvoFold is surprisingly low. There are only 268 overlapping hits (7% and 5%). This is only an enrichment of 1.6 over random. One reason is the generally low signal-to-noise ratio in this screen. The high false positive rate and the fact that false positives arise for different reasons for the two programs, limit the best possible overlap to about 1/3. Moreover, we found that the predicted RNA structures by RNAz and EvoFold differ dramatically with respect to sequence conservation and GC content. RNAz preferentially predicts regions of relatively high GC content and moderate sequence conservation, while EvoFold has its peak sensitivities in AT rich regions which are highly conserved. Since there exists examples of true functional RNA structures in both categories, predictions of both programs are of relevance despite the small overlap. On the panel of known ncRNAs, both programs agree perfectly. Both RNAz and EvoFold are able to detect the three H/ACA snoRNAs and the 4 microRNA precursors. In the long H19 transcript, RNAz and EvoFold predict 3 and 8 regions with conserved secondary structure, resp., one region is predicted by both programs.

The expression of 50 predicted targets was tested using RACE/array analysis (see Supplement S2.9.2). We manually picked promising candidates based on a variety of different criteria (absence of alignment artifacts or peculiar gap patterns, sequence conservation, structure conservation, compensatory mutations, overall appearance, genomic context etc.) We tested 16 targets from the EvoFold screen, 17 from the RNAz screen and 9 from the TAR centered RNAz screen. In addition, we tested 8 targets that were predicted by both RNAz and EvoFold. The experiments were carried out in brain and testis tissues. These tissues show the greatest and most varied transcriptome thus increasing our chances to identify potential expression of the predicted ncRNA even by restricting ourselves to only two tissues. We could verify expression in either brain or testis for 32 of the 50 candidates (64%). Results for the single sets: EvoFold: 9/16 (56%), RNAz: 11/17 (65%), RNAz screen of TAR/transfrag 7/9 (78%), overlapping EvoFold/RNAz: 5/8 (63%). Although not specifically selected, it should be added that 3 of the 16 EvoFold targets, 6 of the 17 RNAz targets, and 3 of the 8 overlapping RNAz/EvoFold targets have also some overlap with TARs/Transfrags. Out of these targets that showed expression on the tiling arrays, 1 of 3, 2 of 6, and 1 of 3 targets, respectively for the three sets, were detected also in the RACE experiments limited to brain and testis.

Details of the computational analysis and additional verification experiments using RT-PCR are described in a companion paper[34].

S2.12 Genome Rearrangements of ENCODE Cell lines

S2.12.1 Comparative Genomic Hybridization Analysis of the ENCODE common cell lines

Two cell lines were chosen as ENCODE consortium common cell lines. These were a human lymphoblastoid cell line from one of the HapMap CEPH pedigrees (GM06990) and the widely used human cervical carcinoma line HeLa S3. The rationale behind these choices was that the lymphoblastoid cell line would be as near as possible to a normal karyotype for a cultured line and would have high density SNP data from resequencing, while HeLa S3 is a commonly used cell line in many studies with specific properties essential for certain technologies e.g. cell cycle synchronisation protocols for study of replication time.

However, it is also well know that cell lines in culture are subject to chromosomal rearrangements which are sometimes substantial. In order to assess the extent of chromosomal rearrangement in the ENCODE consortium common cell lines we conducted comparative genomic hybridisation analysis (CGH) using large-insert clone arrays. For GM06990, genomic DNA was extracted from cultured cells and compared by array-CGH to a reference lymphoblastoid cell line DNA (HRC575) using a complete tiling path large-insert clone microarray in four replicates including two dye reversals as previously described[80]. Only a single region of copy number difference was identified between the cell lines at the telomere of 14q (data not shown), but no rearrangement, insertion or deletion was identified at this resolution which affected any of the ENCODE regions.

CGH was also performed on HeLa S3 using DNA from a large central culture supplied by Ambion to the consortium as well as extracted from HeLa S3 cultured at the Wellcome Trust Sanger Institute, compared to DNA from a pool of 20 normal females using a 1Mb resolution BAC microarray as previously described[81]. The results for the two sources of DNA were the same and are summarised in see Supplementary Table 8 and Supplementary Figure 12. Most copy number changes identified involve single copy losses/gains in a hypertriploid background. Examining in detail the ENCODE regions , in addition to the hypertriploid nature of the cells, up to 9 larger regions (more than 2 consecutive clones) are subject to additional chromosomal gain while at least 14 regions (more than 2 consecutive clones) are subject to chromosomal loss (Supplementary Table 9).

Supplementary Table 8: Ambion/suspension cell line vs. female pool of 20 normal individuals, analyzed on the basis of the Ambion cell line results

Chromosome 1	Gain from 110-209 Mb and from 235Mb to q-ter
Chromosome 2	Region of loss from 100 Mb to q-ter
Chromosome 3	Region of loss 64-100 Mb from, gain from 147-178 Mb
Chromosome 4	Loss of one copy of the entire chromosome in a hypertriploid background
Chromosome 5	Gain equivalent of two extra copies from p-ter to 45 Mb
Chromosome 6	Region of loss 65-68 Mb and from 118 Mb to q-ter
Chromosome 7	Gain from p-ter to 44 Mb
Chromosome 8	Region of loss from p-ter to 116 Mb
Chromosome 9	Region of loss from –pter to to 30 Mb, gain from 119 Mb to q-ter
Chromosome 10	Region of loss from p-ter to 38 Mb
Chromosome 11	Region of loss from p-ter to 7 Mb, regions of gain 27-27 Mb, 33-35 Mb, 46-48 Mb and 59-82 Mb, region of loss from 88 Mb to q-ter
Chromosome 12	Gain from 37-54 Mb
Chromosome 13	Region of loss from p-ter to 54 Mb, gain from 109 Mb to q-ter
Chromosome 14	Modal
Chromosome 15	Gain from 39 Mb to q-ter
Chromosome 16	Potential gain of a single copy of the entire chromosome
Chromosome 17	Modal
Chromosome 18	Region of loss from 18 Mb to q-ter
Chromosome 19	Region of loss from 5-9 Mb, 46-53 Mb, and 57-59 Mb, region of gain from 16-18 Mb
Chromosome 20	Region of loss from p-ter to 26 Mb, gain from 30 Mb to q-ter
Chromosome 21	Modal
Chromosome 22	Loss of one copy of the entire chromosome in a hypertriploid background
Chromosome X	Loss from 100 Mb to q-ter
Chromosome Y	N/A
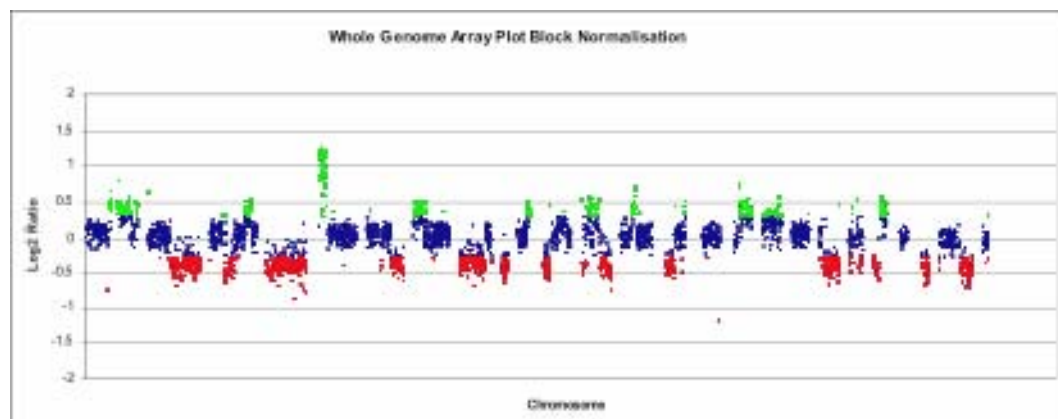
Supplementary Figure 12: Whole genome profile (cell line Ambion)

Supplementary Table 9: State of ENCODE regions in HeLa S3 as judged by array-CGH

Build	May 2004	hg17 (NCBI35)		
Chromosome	**Start**	**End**	**Region**	**Hela CGH analysis**
chr1	147971133	148471133	ENr231	Gain 110-209 Mb
chr2	51570355	52070355	ENr112	
chr2	118010803	118510803	ENr121	Loss 100 to q-ter
chr2	220102850	220602850	ENr331	Loss 100 to q-ter
chr2	234273824	234773888	ENr131	Loss 100 to q-ter
chr4	118604258	119104258	ENr113	Loss of one copy of the entire chromosome 4
chr5	55871006	56371006	ENr221	
chr5	131284313	132284313	ENm002	
chr5	141880150	142380150	ENr212	
chr6	41405894	41905894	ENr334	
chr6	73789952	74289952	ENr223	
chr6	108371396	108871396	ENr323	
chr6	132218539	132718539	ENr222	Loss 118 Mb to q-ter
chr7	26730760	27230760	ENm010	Gain from p-ter to 44 Mb
chr7	89428339	90542763	ENm013	
chr7	113527083	114527083	ENm012	
chr7	115404471	117281897	ENm001	
chr7	125672606	126835803	ENm014	
chr8	118882220	119382220	ENr321	
chr9	128764855	129264855	ENr232	Gain from 119 Mb to q-ter
chr10	55153818	55653818	ENr114	
chr11	1699991	2306039	ENm011	
chr11	4730995	5732587	ENm009	Possible gain
chr11	63940888	64440888	ENr332	Possible gain

chr11	115962315	116462315	ENm003	Loss from 88 Mb to q-ter
chr11	130604797	131104797	ENr312	Loss from 88 Mb to q-ter
chr12	38626476	39126476	ENr123	Gain from 37-54 Mb
chr13	29418015	29918015	ENr111	Loss up to 54 Mb
chr13	112338064	112838064	ENr132	Gain from 109 Mb to q-ter
chr14	52947075	53447075	ENr311	
chr14	98458223	98958223	ENr322	
chr15	41520088	42020088	ENr233	Gain from 39 Mb to q-ter
chr16	0	500000	ENm008	
chr16	25780427	26280428	ENr211	
chr16	60833949	61333949	ENr313	
chr18	23719231	24219231	ENr213	Loss from 18 Mb to q-ter
chr18	59412300	59912300	ENr122	Loss from 18 Mb to q-ter
chr19	59023584	60024460	ENm007	Loss from 57-59 Mb
chr20	33304928	33804928	ENr333	Gain from 30 Mb to q-ter
chr21	32668236	34364221	ENm005	
chr21	39244466	39744466	ENr133	
chr22	30128507	31828507	ENm004	Loss of one copy of the entire chromosome
chrX	122507849	123007849	ENr324	Loss from 100 Mb to q-ter
chrX	152635144	153973591	ENm006	Loss from 100 Mb to q-ter

CGH analysis was not conducted on additional cell lines beyond the consortium common cell lines. However information is available for other cell lines used from other analyses such as SKY-FISH. HL60 has been mapped by SKY-FISH (data available at http://www.ncbi.nlm.nih.gov/sky/skyquery.cgi - query for HL60) and shows substantial rearrangement[82]. However it is not possible to precisely determine how these rearrangements affect the ENCODE regions from the SKY-FISH results which are presented by chromosome band. More recent analyses of HL60 are also available[83].

S3 Regulation of Transcription

S3.1 ChIP-Chip and ChIP-PET experimental methodology

S3.1.1   Yale Group

S3.1.1.1 Preparation of ChIP DNA from HeLaS3 cells
For c-Fos, c-Jun, BAF155 and BAF170 HeLaS3 cells were grown by the National Cell Culture Center in Joklik's modified minimal essential medium (MEM), supplemented with 5% FBS at 37°C in 5% CO_2, to a density of 6 x10^5 cells/ml. Cells were fixed with 1% formaldehyde at room temperature for 10 min and fixation was terminated with 125 mM glycine. The cells were washed twice in cold 1x Dulbecco's PBS and then stored and shipped as frozen cell pellets. For

STAT1, HeLaS3 cells were grown in Dulbecco's modified Eagle's medium for suspension (SMEM) supplemented with 5% FBS at 37°C in 5% CO_2, to a density of 6 x10^5 cells/ml. The cultures were divided in half and were either induced with 5 ng/ml human recombinant IFN-γ (R&D Systems #285-IF), or left untreated, for 30 min at 37°C, 5% CO_2 and then fixed with 1% formaldehyde final concentration at room temperature for 10 min. Fixations were quenched by addition of glycine to 125 mM final concentration and cells were washed twice in cold 1x Dulbecco's PBS. All ChIP DNA samples were isolated from nuclear extracts. Nuclei were prepared by swelling cells for 10 min in hypotonic lysis buffer (20 mM HEPES, pH 7.9, 10 mM KCl, 1 mM EDTA, pH 8, 10% glycerol, 1 mM DTT, 0.5 mM PMSF and protease inhibitors). Following dounce homogenization nuclear pellets were collected and lysed in 1x RIPA buffer (10 mM Tris-Cl, pH 8.0, 140 mM NaCl, 1% Triton X-100, 0.1% SDS, 1% deoxycholic acid, 0.5 mM PMSF, 1 mM DTT, and protease inhibitors). Nuclear lysates were sonicated with a Branson 250 Sonifier to shear chromatin to approximately 0.5 to 1 kb in size. Clarified lysates were incubated overnight at 4°C with factor-specific antibodies. Protein-DNA complexes were precipitated with RIPA-equilibrated protein A agarose beads and immunoprecipitates were washed three times in 1x RIPA, once in 1x PBS, and then eluted from the beads by addition of 1% SDS, 1x TE (10 mM Tris-Cl at pH 7.6, 1 mM EDTA at pH 8), and incubation for 10 min at 65°C. Crosslinks were reversed overnight at 65°C. All samples were purified by treatment first with 200 μg/ml RNase A for 1 h at 37°C, then with 200 μg/ml Proteinase K for 2 h at 45°C, followed by extraction with phenol:chloroform:isoamyl alcohol and ethanol precipitation at -70°C.

S3.1.1.2 Labeling and Hybridization of ChIP DNA samples

Full details are available through GEO or are published in Euskirchen et al[22]. Briefly, for each array to be hybridized ChIP DNA isolated from 1 x 10^8 cells was directly random primed with Klenow and labeled with either Cy5 (ChIP DNA prepared with a specific antibody) or with Cy3 (reference DNA). The reference DNA samples varied for each factor. For c-Fos and c-Jun, total genomic DNA was used as reference samples. For BAF155 and BAF170 the reference samples were ChIP DNA prepared using normal rabbit IgG. STAT1 ChIP DNA prepared from IFN-γ stimulated cells was compared to STAT1 ChIP DNA prepared from uninduced cells, where STAT1 is nuclear excluded. Labeled ChIP DNA samples were applied to high density oligonucleotide arrays synthesized by maskless photolithography and arrays were hybridized in MAUI hybridization stations (BioMicro Systems) with mixing. Datasets consist of 3 or more biological replicates (defined as ChIP DNA prepared from distinct cell cultures grown, harvested and processed on separate days) and each biological replicate was hybridized to a separate array.

S3.1.1.3 Array Data Processing

The array data was processed using the Tilescope tool (tilescope.gersteinlab.org; Zhang et al[24]). Array data is first quantile normalized and median scaled between replicate arrays (both Cy3 and Cy5 channels). Using a 1000 bp sliding window centered on each oligonucleotide probe, a signal map (estimating the fold enrichment [log2 scale] of ChIP DNA) was generated by computing the pseudo-median signal of all log2(Cy5/Cy3) ratios (median of pairwise averages) within the window, including replicates. Similarly, a P-value map (measuring significance of enrichment of oligonucleotide probes in the window) for all sliding windows was made using the

Wilcoxon paired signed rank test comparing fluorensent intensity between Cy5 and Cy3 for each oligonucleotide probe. A binding site was determined by thresholding oligonucleotide positions with -log10(P-value) (>= 4), extending qualified positions upstream and downstream 250 bp, and requiring 1000 bp space between two sites. The top 200 sites are reported.

S3.1.2   Affymetrix Group

S3.1.2.1 Cell Lines

The HL-60 acute myeloid lymphoma cell line was obtained from the American Type Culture Collection facility. Cell were maintained in Iscove's Modified Dulbecco's Medium with GlutaMAX (Invitrogen) containing 20% Fetal Bovine Serum (Invitrogen) and 1X penicillin/streptomycin (Invitrogen) in a humidified 37°C incubator with 5% CO_2. For each of the three biological replicates, cultures were seeded at approximately $3x10^5$ cells/ml and were induced with a final concentration of 1 μM all-trans-retinoic-acid (ATRA – purchased from Sigma) after 2 days of growth when cultures had achieved a density of 10^6 cells/ml. These cultures (3 liters total for each time point) were then incubated for 2, 8, and 32 hours with ATRA or untreated (0 hour) before harvesting. Both cell viability and recovery after ATRA treatment were assessed by Trypan Blue exclusion as well as determining cell density by counting an aliquot on a hemocytometer.

S3.1.2.2 CD11b Cell Surface Antigen Labeling

ATRA treated HL-60 cells were monitored for differentiation by detection of CD11b expression. Triplicate samples for each time point in each biological replicate (10^6 cells per sample) were centrifuged at 300xg for 10 minutes, media aspirated, and resuspended in 100 μl Label Buffer (1x Hanks Buffered Saline, 2% filtered Fetal Bovine Serum, and 0.01% sodium azide). Cells were blocked with 5 μl unlabeled isotype matched mouse $IgG_{1\kappa}$ (BD Pharmingen) on ice for 15 minutes, then washed with 2 ml ice cold Label Buffer. Cells were pelleted at 300xg for 10 minutes and resuspended in 100 μl Label buffer. Five μl of anti-CDllb antibodies or isotype controlled mouse $IgG_{1\kappa}$ coupled to Alexa 488 (BD Pharmingen) were added to each sample and incubated on ice for 30 minutes. Cells were washed twice in 2 ml Label Buffer and fixed with 2% formaldehyde in PBS. Samples were stored packed in ice and in the dark until analyzed by flow cytometry using a FACScaliber bench top cell sorter (BD Biosciences) counting 10,000 events for each triplicate sample. $IgG_{1\kappa}$ labeled samples were used to determine the amount of background fluorescence and non-specific binding. Percent of CD11b positive cells were quantitated using Cellquest Pro software.

S3.1.2.3 Nitroblue Tetrazolium (NBT) Reduction Assay

NBT reduction assays were performed in triplicate for each timepoint for each of the 3 biological replicates. Approximately $5x10^5$ were collected by centrifugation at 300xg for 10 minutes at room temperature using a swing bucket rotor. Media was aspirated away and cells were resuspended in 100 μl of growth media. An equal volume of NBT (Roche) diluted 1:50 in PBS was then added to each sample containing 200 ng PMA (Calbiochem). Samples were incubated at 37°C for 30 minutes at which time cells were placed on microscope slides and cells were

scored as either positive or negative based on the presence of dark blue formazin deposites. At least 1000 cells were counted for each of the triplicate samples and percent NBT positive cells was determined for each time point as a measure of differentiation.

S3.1.2.4 RNA preparation

Approximately $5x10^8$ cells per time point per biological replicate were harvested by centrifugation and total RNA was purified using RNeasy RNA extraction kit (Qiagen) as per manufacturer's specifications. Each sample required three columns in order to recover the majority of the RNA. Poly-A RNA was then obtained from the total RNA using Oligo-tex purification kits (Qiagen) as per manufacturer's instructions.

S3.1.2.5 Formaldehyde Crosslinking and Soluble Chromatin Preparation

Cell culture remaining after removing cells for RNA processing was crosslinked using 1% final concentration formaldehyde for 10 minutes at room temperature with gentle swirling. The formaldehyde was quenched using 1/20 culture volume 2.5 M glycine at room temperature for 5 minutes. Cells were pelleted at 500xg for 8 minutes, washed twice with ice cold PBS, and washed three times in Run-on lysis buffer (10 mM Tris pH 7.5, 10 mM NaCl, 3 mM $MgCl_2$, and 0.5% NP40). Recovered nuclei were aliquoted, flash frozen in liquid nitrogen and stored at –80°C until use. Micrococcal nuclease (MNase) digestions were then performed such that there were the equivalent of approximately $2x10^8$ cells per digestion. Frozen pellets were resuspended to a volume of 1.5 ml MNase reaction buffer (10 mM Tris pH 7.5, 10 mM NaCl, 3 mM $MgCl_2$, 1 mM $CaCl_2$, 4% NP40, 1 mM PMSF). Fifteen units of MNase (USB) were added to each reaction, samples were incubated at 37°C for 10 minutes, and the digestion halted by the addition of 30 µl 200 mM EGTA. Forty µl of 100 mM PMSF, 150 µl of protease inhibitors (Roche mini-EDTA free inhibitor pellet resuspended in 500 µl MNase reaction buffer), 200 µl 10% sodium dodecyl sulfate, and 80 µl 5 M NaCl were subsequently added to each reaction. Next, samples were sonicated using a Branson Sonifier-450 four times for 1 minute at a power level setting of 4 and 60% duty. The cellular debris were then cleared by centrifugation on high speed for 10 minutes at 4°C. The supernatant was then removed to a new tube, aliquoted to volumes equivalent to $2x10^7$ cells per tube, flash frozen on liquid nitrogen, and stored at -80°C until use. For each sample, a small aliquot was treated with Pronase, the crosslinks reversed, and run on a 1% TAE-agarose gel to monitor MNase digestion. The average size fragments for each chromatin preparation were 500-1000 base pairs.

S3.1.2.6 Chromatin Immunoprecipitation

Chromatin immunoprecipitation were performed using a volume of soluble chromatin equivalent to $2x10^7$ cells. Chromatin was diluted 1:5 using IP Dilution Buffer (20mM Tris pH 8.0, 2mM EDTA, 1% TritonX-100, 150mM NaCl, and Roche mini-EDTA free inhibitor pellet) and pre-cleared with a mix of Protein A (Amersham) and Protein G (Amersham) sepharose beads for 15 minutes at 4°C on a rotator. The pre-cleared diluted chromatin was then incubated with the appropriate amount of antibody of interest overnight at 4°C (see below). Fifty µl of protein A/G mixed sepharose was then added to each IP and incubated for 3 hours at 4°C. IPs were washed in 1 ml Dilution Buffer, centrifuged, the beads resuspended in 0.7 ml Dilution Buffer and

transferred to a Spin-X centrifuge column (Costar). Samples were washed for 5 minutes at room temperature on a rotator using the following buffers respectively: ChIP Wash Buffer 1 (20mM Tris pH 8.0, 2mM EDTA, 1% TritonX-100, 0.1% SDS, 150mM NaCl, 1mM PMSF), ChIP Wash Buffer 2 (20mM Tris pH 8.0, 2mM EDTA, 1% TritonX-100, 0.1% SDS, 500mM NaCl, 1mM PMSF), ChIP Wash Buffer 3 (10mM Tris pH 8.0, 1mM EDTA, 0.25 M LiCl, 0.5% NP-40, 0.5% deoxycholate), and 3 times in TE. Samples were eluted in 200 µl Elution buffer (25mM Tris pH 7.5, 5mM EDTA, 0.5% SDS) at 65°C for 30 minutes. Eluates were collected by centrifugation and an additional 100 ml Elution Buffer was washed through the column. Pronase was added to each sample and to pre-cleared input chromatin samples to a final concentration of 1.5 µg/µl. Samples were incubated at 42°C for 2 hours and at 65°C for at least 6 hours to reverse the crosslinks. Precipitated DNA was then recovered using QIAquick PCR purification columns (Qiagen) as per manufacturer specifications and eluted in 100 µl 10 mM Tris pH 8.5

S3.1.2.7 Antibodies

The following antibodies were used per individual IP for the ChIP-Chip experiments: 15 µl anti-tetraacetylated H4 (Upstate 06-866); 3 µg anti-Brg1 (Santa Cruz sc-10768); 3 µg anti-CTCF (Abcam 10571); 12 µl anti-diacetylated H3 (Upstate 06-599); 3 µg anti-Pu.1 (Santa Cruz sc-22805); 3 µg anti-Retinoic acid receptor alpha (Santa Cruz sc-551); 4 µg anti-TFIIB (Santa Cruz sc-225); 4 µg anti-p300 (Santa Cruz sc-584); 4 mg anti-C/EBPε (Santa Cruz sc-158); 3 mg anti-trimethylated H3K27 (a gift from Thomas Jenuwein)

S3.1.2.8 Random Primer Amplification

In the first round of amplification (Round A), 30 µl of IP or Input samples, 10 µl dH$_2$O, 12 µl 5X Sequenase Buffer (USB), and 4 µl of 40 µM Primer A (GTTTCCCAGTCACGATCNNNNNNNNN) were mixed in 0.2 ml thin wall PCR tubes. Samples were heated to 95°C for 4 minutes and then flash frozen in liquid nitrogen. The samples were then transferred to 10°C for 5 minutes during which time 0.5 µl 10 mg/ml BSA, 3 µl 0.1 M DTT, 1.5 µl 25 mM dNTPs, and 1.5 µl Sequenase (USB) diluted 1:10 (1.3 U/µl final) were added. Temperature was then raised 1 degree every 20 seconds until it reached 37°C where it was held for an additional 8 minutes. This entire process was then repeated with the exception that only sequence was added during the 5 minutes at 10°C. Next the samples were purified using QIAquick PCR purification columns (Qiagen) as per manufacturer specifications and eluted in 100 µl 10 mM Tris pH 8.5. In the next round of PCR amplification (Round B), 85 µl "Round A" DNA was mixed with 2 µl 100 µM Primer B (GTTTCCCAGTCACGATC) in a standard 100 µl PCR reaction. Samples were then amplified using the following cycler program: 95°C for 3 minutes then 30 cycles of 95°C for 30 seconds, 40°C for 30 seconds, 50°C for 30 seconds, and 72°C for 1 minute. The resulting amplified material was then purified using QIAquick PCR purification columns and eluted in 100 µl 10 mM Tris pH 8.5. One last round of PCR amplification was performed using 90 µl of "Round B" to set up three 300 µl standard PCR reactions using Primer B similar to Round B with the exception that 25 cycles are performed instead of 30 cycles. The three PCR reactions were then combined, purified using 10 QIAquick PCR purification columns, and eluted in a total of 1 ml 10 mM Tris pH 8.5. Eluted samples were precipitated on ice using 1/10 volume NaOAc pH 5.2 and 3 volumes of 100% EtOH.

Precipitated pellets were washed once with 70% EtOH, dried, and resuspended in 40 µl 10 mM Tris pH 8.5.

S3.1.2.9 Microarray Hybridizations and Generation of Maps of Binding Sites

The precipitated amplified DNA from the chromatin immunoprecipitation experiments was fragmented with DNAse I to an average size of 100 nucleotides, end labeled with biotin using terminal transferase and hybridized to ENCODE tiling oligonucleotide microarrays (Affymetrix cat. No. 900544) at concentration of 10 µg/ml or 2 µg per array as described earlier[25, 56]. Arrays were scanned on an in-house made scanner with a laser spot size of 3.5 µm and pixel size of 1 µm. The procedure for generation of binding of sites is described in Ghosh *et al*[84].

S3.1.3　　Farnham Data -UC Davis-Farnham lab methods

S3.1.3.1 Chromatin Immunoprecipitation (ChIP) Assays

HeLa cells were grown and crosslinked with formaldehyde as previously described[85]. A complete protocol can be found on our website at http://genomics.ucdavis.edu/farnham/ and in Oberley *et al*[86]. A mixed monoclonal antibody against E2F1 (KH20/KH95) was purchased from Upstate Biotechnology Incorporated (Lake Placid, NY), a rabbit polyclonal antibody against MYC (N-202; cat#sc-764x was purchased from Santa Cruz Biotechnology, rabbit IgG (cat# 210-561-9515) was purchased from Alpha Diagnostic, and the secondary rabbit anti-mouse IgG (cat# 55436) was purchased from MP Biomedicals. For analysis of the ChIP samples prior to amplicon generation, immunoprecipitates were dissolved in 50 µl of water, except for input samples that were dissolved in 100 µl. Each PCR reaction mixture contained 2 µl of immunoprecipitated DNA, 1X Taq reaction buffer (Promega, Madison, WI), 1.5 mM MgCl$_2$, 50 ng of each primer, 1.7 U of Taq polymerase (Promega, Madison, WI), 200 µM deoxynucleotide triphosphates (Promega, Madison, WI) and 1 M betaine (Sigma, St, Louis, MO) in a final reaction volume of 20 µl. PCR mixtures were amplified for 1 cycle of 95°C for 5 min, annealing temperature of the primers for 5 min, and 72°C for 3 min followed by 31-33 cycles of 95°C for 1 min, annealing temperature of the primers for 1 min, and 72°C for 1 min and 1 cycle of 72°C for 7 min. PCR products were separated by electrophoresis through 1.5% agarose gels and visualized by ethidium bromide intercalation.

S3.1.3.2 Amplicon Preparation

Briefly, two unidirectional linkers oligoJW102 (5'gcg gtg acc cgg gag atc tga att c 3') and oligoJW103 (5' gaa ttc aga tc 3') were annealed and blunt-end ligated to the ChIP samples. Amplicons were created by PCR; each sample consisted of 5 µl 10X Taq polymerase buffer, 7 µl 2mM dNTPs, 3 µl MgCl$_2$, 6.5 µl betaine, 2.5 µl oligoJW102 (20µM), 1 µl Taq (Promega, M1861), and 25 µl of the blunted and ligated chromatin. PCR was run with one cycle at 55°C for 2 min, 72°C for 5 min, and 95°C for 2 min. 15 cycles were then run at 95°C for 0.5 min, 55°C for 0.5 min, and 72°C for 1 min. Finally the products were extended at 72°C for 4 min, then held at 4°C until purified using the Qiaquick PCR purification kit according to the manufacturer's instructions. 2.5 µl of the first round of amplicons were used as described above to generate a

second round of amplicons. DNA was quantitated and stored -20°C until sent to NimbleGen. For more details, see http://genomics.ucdavis.edu/farnham/ and Oberley *et al*[86].

S3.1.3.3 Array Hybridization

High density ENCODE oligonucleotide arrays were created by NimbleGen Systems (Madison, WI, USA) and contained ~380,000 50mer probes per array, tiled every 38 bp. The regions included on the arrays encompassed the 30 MB of the repeat masked ENCODE sequences, representing approximately 1% of the human genome. The labeling of DNA samples for ChIP-chip analysis was performed by NimbleGen Systems, Inc. Briefly, each DNA sample (1 µg) was denatured in the presence of 5'-Cy3- or Cy5-labeled random nonamers (TriLink Biotechnologies, San Diego) and incubated with 100 units (exo-) Klenow fragment (NEB, Beverly, MA) and dNTP mix [6 mM each in TE buffer (10 mM Tris/1 mM EDTA, pH 7.4; Invitrogen)] for 2 h at 37°C. Reactions were terminated by addition of 0.5 M EDTA (pH 8.0), precipitated with isopropanol, and resuspended in water. Then, 13 µg of the Cy5-labeled ChIP sample and 13µg of the Cy3-labeled total sample were mixed, dried down, and resuspended in 40 µl of NimbleGen Hybridization Buffer (NimbleGen Systems) plus 1.5 µg of human COT1 DNA. After denaturation, hybridization was carried out in a MAUI Hybridization System (BioMicro Systems, Salt Lake City) for 18 h at 42°C at the NimbleGen Service Laboratory. The arrays were washed using NimbleGen Wash Buffer System (NimbleGen Systems), dried by centrifugation, and scanned at 5-µm resolution using the GenePix 4000B scanner (Axon Instruments, Union City, CA). Fluorescence intensity raw data were obtained from scanned images of the oligonucleotide tiling arrays using NIMBLESCAN 2.0 extraction software (NimbleGen Systems). For each spot on the array, log2-ratios of the Cy5-labeled test sample versus the Cy3-labeled reference sample were calculated. Then, the biweight mean of this log2 ratio was subtracted from each point; this procedure is approximately equivalent to mean-normalization of each channel. Sites bound by E2F1 and Myc were identified using the peak calling algorithm described in Bieda *et al*[19] and available at http://genomics.ucdavis.edu/farnham/.

S3.1.4   Sanger Group (PCR Arrays)

We assayed H3k4me1, H3k4me2, H3k4me3, H3Ac, and H4Ac across ENCODE in both GM06990 cells and Hela S3 cells using a modified chromatin immunoprecipitation followed by microarray read-out ('chip-on-chip') procedure[16].

S3.1.4.1 Generation of chromatin immunoprecipatation (ChIP) samples

Human cell line GM06990 (CEPH/UTAH PEDIGREE 1331) was cultured in RPMI640, 15% fetal calf serum, 1% penicillin-streptomycin and 2 mM L-glutamine. Human cell line HeLa-S3 was cultured in Joklic's DMEM, 5 % newborn bovine serum by the National Cell Culture Center Minneapolis, USA. 108 cells were collected by centrifugation, resuspended in 50 ml pre-warmed serum free media in a glass flask. Formaldehyde (BDH) was added to final concentrations of 0.37 or 1%. After incubating the cells for 10 minutes with gentle agitation at room temperature, glycine (Sigma) was added to a final concentration of 0.125M followed by again incubating for 5 minutes at RT with agitation. Cells were collected at 4°C, resuspended in 1.5 ml ice-cold PBS and centrifuged at 2000 rpm for 5 min at 4°C (Sorval Heraeus). The cell pellet was resuspended in ~1.5X pellet volume of cell lysis buffer (10mM Tris-HCl pH 8.0, 10mM NaCl, 0.2% Igepal

CA-630, 10mM sodium butyrate, 50µg/ml PMSF, 1µg/ml leupeptin) and incubated for 10 minutes on ice. The cell nuclei were collected by centrifugation at 2500 rpm for 5 minutes at 4°C. The nuclei were resuspended in 1.2 ml of nuclear lysis buffer (NLB 50mM Tris-HCl pH 8.1, 10mM EDTA, 1% SDS, 10mM sodium butyrate, 50µg/ml PMSF, 1µg/ml leupeptin) and incubated on ice for 10 minutes. After adding 0.72 ml of immunoprecipitation dilution buffer (IPDB 20mM Tris-HCl pH 8.0, 150mM NaCl, 2mM EDTA 1% Triton X-100, 0.01% SDS, 10mM sodium butyrate, 50µg/ml PMSF, 1µg/ml leupeptin) the chromatin was transferred to a 5ml tube (falcon) and sheared to a fragment size of ~ 500 bp by sonication (Branson sonifier using settings of time: 8 min, amplitude: 16 %, pulse on 0.5 s, pulse off 2.0 s, 450 digital,). During sonication samples were cooled in an ice water bath. Debris was removed from the sheared chromatin by centrifugation in a cooled bench centrifuge (Eppendorf) at 14000 rpm for 5 minutes at 4°C. The supernatant was diluted with 4.1 ml of IPDB to a final ratio of NLB:IPDB of 1:4. The chromatin was precleared by adding 100µl of normal rabbit IgG (Upstate) and incubating for 1 hour at 4°C on a rotating wheel. 200 µl of homogeneous protein G-agarose suspension was added (Roche) and incubation continued for 3 hours to overnight at 4°C on a rotating wheel. The protein G-agarose was spun down at 3000 rpm for two minutes at 4°C. 1.35 ml of supernatant (chromatin) was used to set up each ChIP assay while 270 µl were used as input control. Ten micrograms of antibody was used in each ChIP assay. Antibodies used were di-acetylated histone H3 (06-599, Upstate), tetra-acetylated histone H4 (06-866, Upstate), histone H3 mono-methyl lysine 4 (ab8895, Abcam), histone H3 di-methyl lysine 4 (ab7766, Abcam), histone H3 tri-methyl lysine 4 (ab8580, Abcam). The chromatin and antibody were incubated on a rotation wheel overnight at 4°C, then 100 µl of homogeneous protein G-agarose suspension was added (Roche) and incubation continued for 3 hours. The protein G-agarose was spun down and the pellet washed twice with 750 µl of IP wash buffer 1 (20 mM Tris-HCl pH 8.1, 50 mM NaCl, 2 mM EDTA, 1% Triton X-100, 0.01% SDS), once with 75 EPAL CA630, 1% deoxycholic acid) and twice with 10 mM Tris-HCl 1 mM EDTA pH80 µl of IP wash buffer 2 (10 mM Tris-HCl pH 8.1, 250 mM LiCl, 1 mM EDTA, 1% IG.0. The immune complexes were twice eluted from the beads by adding 225 µl of IP elution buffer (100mM NaHCO3, 0.1% SDS). After adding 0.2 µl of RNase A (10 mg/ml, ICN) and 27 µl of 5M NaCl to the combined elutions and adding 0.1µl of RNAse A and 16.2 µl of 5M NaCl to the input sample, the samples were incubated at 65°C for 6 hours. Then 9 µl of proteinase K (10 mg/ml, Invitrogen) was added and the samples incubated at 45°C overnight. Immediately before the DNA was recovered using phenol chloroform extraction, 2 µl tRNA (5 mg/ml stock/ Invitrogen) was added. The aqueous layer was extracted once with chloroform. Then 5 µg of glycogen (Roche), 1 µl of tRNA (5 mg/ml Invitrogen), 50 µl of 3M sodium acetate pH 5.2 and 1.25 ml of ice-cold ethanol was added to precipitate the DNA at -20°C over night. The DNA pellets were washed with 70% ethanol, air dried and resuspended in 100 µl of water for input samples and 50 µl of water for ChIP samples.

S3.1.4.2 Fluorescent DNA labeling, microarray hybridization and data analysis

Fluorescently labelled DNA samples were prepared using a modified Bioprime labelling kit (Invitrogen) in 150 µl reaction volumes containing 450 ng Input DNA or 40% of ChIP DNA, dNTPs (0.2 mM dATP, 0.2 mM dTTP, 0.2 mM dGTP, and 0.1 mM dCTP), 0.01 mM Cy5/Cy3 dCTP (GE Healthcare) , 60 µl 2.5x random primer solution (750 µg/ml, Invitrogen) and 3 µl of Klenow fragment (Invitrogen) . Input DNA samples were labeled with Cy5, and ChIP DNA samples were labelled with Cy3 over night at 37°C. Labelling reactions were purified using

Micro-spin G50 columns (Pharmacia-Amersham) in accordance with the manufacturer's instructions. Input and ChIP sample were combined and precipitated with 3 M sodium acetate (pH 5.2) in 2.5 volumes of ethanol with 135 μg human C_{ot} DNA (Invitrogen). The DNA pellet was resuspended in 80μl hybridization buffer containing 50% deionized formamide (Sigma), 10 mM Tris-HCl (pH 7.4), 5% dextran sulphate, 2× SSC, 0.1% Tween-20. Two combined labeling reactions were denatured for 10 minutes at 100°C, snap frozen on ice and used for one microarray hybridisation. Microarrays were hybridized on an automatic hybridization station (HS4800, Tecan) for 45h at 37°C with medium agitation, washed 10 times for 1 minute with PBS 0.05% Tween20 (BDH) at 37°C, 5 times for 1 minute with 0.01x SSC at 52°C, 10x 1 minutes with PBS 0.05% Tween20 at 23°C, followed by a final wash with HPLC-grade water (BDH) at 23°C and drying under nitrogen flow for 4 minutes. Microarrays were scanned using a ScanArray 4000 confocal laser-based scanner (Perkin Elmer). Mean spot intensities from images were quantified using ScanArray Express (Perkin Elmer) with background subtraction. Spots affected by dust were manually flagged as "not found" and subsequently excluded from the analysis.

S3.1.4.3 ENCODE tiling array construction

The final Encode array spanned 23.8 Mb and contained 24005 array elements (average size 992 bp). Primers pairs used to amplify PCR products for the arrays were designed using primer 3 including repetitive elements where possible. (The primer sequences for amplicons used as array elements are available at ftp://ftp.sanger.ac.uk/pub/encode/microarrays/). In order to generate arrays containing single-stranded array elements, all amplicons used in this study were prepared and printed on arrays as previously described (see Dhami et al[87] and www.sanger.ac.uk/Projects/Microarrays/arraylab/methods.shtml). All PCR products were prepared as follows. A 5'-(C6) amino-link was added to all forward primers. The primer pairs (final concentration 0.5 μM) were used to amplify PCR products in a 60-μl final volume PCR containing 50 mM KCl, 5 mM Tris HCl (pH 8.5), 2.5 mM MgCl2, 10 mM dNTPs (Pharmacia), 0.625 U *Taq* polymerase (Perkin Elmer), and 50 ng of human genomic DNA (Roche). The PCR products were amplified with the following program: 1x 5 min 95°C, 35 x 95°C 1.5 min, 65°C 1.5 min (-0.3°C per cycle), 72°C 3 min, 1x 72°C 5 min. For arraying of PCR products, spotting buffer was added at final concentrations of 0.25 M sodium phosphate buffer pH 8.5 and 0.00025% sodium sarkosyl (BDH). The PCR products were filtered through multiscreen-GV 96-well filter plates (Millipore), aliquoted into 384-well plates (Genetix), and were arrayed onto Codelink slides (GE) in a 48-block format using a Microgrid II arrayer (Biorobotics/Genomic Solutions). Slides were processed to generate single-stranded array elements, as described at http://www.sanger.ac.uk/Projects/Microarrays/, and were stored at room temperature until hybridized.

S3.1.4.4 Data processing for analysis

The data of the ratio of the background corrected ChIP signal divided through the background corrected input signal, both globally normalised were used for the HMM analysis. Ratios of duplicated spots were averaged. Ratios of spots defined as "not found" and ratios with a value below zero were excluded from the analysis and also excluded from the median track of technical replicates. Each median track of technical replicates was automatically generated with an individual R script (i.e.

ftp://ftp.sanger.ac.uk/pub/encode/H3K4me3_GM06990_2/H3K4me3_GM06990_2.R) which combines only positive values of technical replicates not classified as "not found".

S3.1.4.5 Comprehensive annotation of peaks using hidden Markov model analysis

A two-state HMM3 was used to analyze the Sanger ChIP-chip data. The states of the HMM represent regions of the tile path corresponding to locations either consistent or inconsistent with antibody binding. The emission probabilities of the states are derived from the probability that a point is part of a normal distribution fitted from the 45% of the data with the lowest enrichment values. The fitted distribution is calculated separately for each of the ENCODE regions using the Levenberg-Marquart curve-fitting technique. The optimal state sequence for the observed data was calculated from the HMM using the Viterbi algorithm. The resulting list of tiles assigned to the state consistent with antibody binding was post-processed to develop a final hit list, which combined positive tiles within 1000bp of each other into "hit regions." The score of each hit region was determined by taking the summation of the median enrichment values of the tiles in the contiguous portions (i.e. the area under the peak). The center position of the PCR tile with the highest enrichment value in the hit region was deemed the center of the peak.

S3.1.4.6 Identification of significant peaks (p<0.01 level)

For the purposes of our analyses we defined significant peaks as those identified using the approach described above wherein the peak signal exceeded the 99th% confidence bound on outliers relative to the global distribution of each mark. To determine the 99% confidence bound, we analyzed log(2)-transformed microarray signal intensity ratios and computed the 99th percentile of values below log(2)=0. Such ratio values were considered to signify experimental noise. A standard assumption is that this noise is symmetric about the log(2)=0 baseline. We therefore reflected the 99th percentile values about the baseline for each mark. This established an empirical 99% confidence bound on outliers, which is equivalent to a p<0.01 threshold. We then identified, for each histone mark, the HMM-derived signal peaks in which the maximum signal exceeded the p<0.01 level.

S3.1.5   UT Austin ChIP-chip methods

S3.1.5.1 ChIP protocol for c-Myc and E2F4

Briefly, cells were cross-linked by addition of formaldehyde (1 % final concentration) directly to tissue culture plates for 7 min at room temperature. Cross-linking was terminated by adding glycine to a final concentration of 125 mM. Cells were washed with cold phosphate-buffered saline (PBS) containing PMSF, scraped off the plates, collected by centrifugation and washed again. After centrifugation, the pellet was resuspended in SDS lysis buffer (1 % SDS, 10 mM EDTA, 50 mM Tris-Cl pH 8.1, plus protease inhibitors) and incubated at room temperature for 20 min. Cells were sonicated on ice and centrifuged at 12000 rpm at 4 °C for 10 min. 10x ChIP dilution buffer (0.1 % SDS, 1 % Triton X-100, 2 mM EDTA, 20 mM Tris-Cl pH 8.1, 150 mM NaCl, plus protease inhibitors) was added to the collected supernatant. Sample was pre-cleared with protein A-agarose beads (previously washed with 10x ChIP dilution buffer) at 4 °C for 1 hr. Precleared chromatin was incubated with the corresponding specific antibody (anti-e2f4 antibody

sc-1082x, Santa Cruz for E2F4 and anti-myc antibody sc-764x, Santa Cruz for c-Myc) at 4 °C overnight. For the mock IP controls, the antibody was left out. Pre-washed protein A-agarose beads were added and protein-DNA complexes were recovered after a 2 hour incubation at 4 °C. Immunoprecipitated complexes were successively washed with Lowsalt wash buffer (0.1 % Deoxycholate, 1 % Triton X-100, 1 mM EDTA, 50 mM HEPES pH 7.5, 150 mM NaCl), High-salt wash buffer (0.1 % Deoxycholate, 1 % Triton X-100, 1 mM EDTA, 50 mM HEPES pH 7.5, 500 mM NaCl), LiCl wash buffer (250 mM LiCl, 0.5 % NP-40, 0.5 % Deoxycholate, 1 mM EDTA, 10 mM Tris-Cl pH 8.1) and TE buffer (10 mM Tris-Cl pH 7.5, 1 mM EDTA). SDS elution buffer was added and incubated at 65 °C for 30 min to recover protein-DNA complexes. Crosslinks were reversed by incubating at 65 °C overnight. The sample was treated with RNase A and Proteinase K, extracted with phenol:chloroform and precipitated. The pellet was resuspended in 25 µl of water. We used this ChIP DNA for STAGE as well as ChIP-chip.

S3.1.5.2 Hybridization of ChIP DNA to NimbleGen ENCODE arrays

ChIP and mock IP DNA samples were amplified and labeled for hybridization essentially using NimbleGen's recommended protocols. DNA was amplified by ligation mediated PCR as previously described[14]. The ChIP samples were labeled with Cy5 while the mock IP samples were labeled with Cy3 and used as a reference channel in two colour hybridizations. Hybridization was carried out at NimbleGen's service facility (Madison, WI) using their standard procedures. Microarray scanning, data acquisition, normalization and peak finding was done essentially as previously described for NimbleGen arrays[14].

S3.1.6   UCSD ChIP-chip methods

Three biological replicates of treated and untreated cells were crosslinked and harvested as previously described[14] with the following modifications. Cells were crosslinked for 20 minutes at 37ºC in normal culture media plus 1/10 volume formaldehyde crosslinking solution in large culture plates, followed by glycine quenching and PBS wash at room temperature. Crosslinked cells were collected by scraping and centrifugation. Chromatin was isolated and fragmented as previously described[14], though generating fragments of 1.5 Kbp in length required 12 x 30 sec cycles of sonication.

S3.1.6.1 Labeling procedure

One microgram (µg) of LM-PCR products were used for labeling and hybridization to each array. One microgram of immunoprecipitated or total genomic LM-PCR DNA was mixed with 40 µL of 1 µM Cy5 or Cy3 end labeled random prime nonamer oligonucleotides (TriLink Biotechnologies) respectively with the bacterial label control DNA in a total volume of 88 µL. The DNA and random primers were annealed by heating the sample to 98°C for 5 minutes and chilled quickly in ice water for 2-3 minutes. Two microliter of (100 units) of E. coli DNA polymerase Klenow fragment and 10 µL of 10 mM equimolar mixture of dATP, dTTP, dCTP, and dGTP were added to the annealed DNA sample and incubated at 37°C for 2 hours. The reaction was stopped by addition of 10 µL of 0.5 M EDTA. The labeled sample was ethanol precipitated by addition of 11 µL 5 M NaCl and 110 µL isopropanol. The precipitate was collected by centrifugation and the resulting labeled DNA pellet was washed with 80% ethanol

(V/V). The pellet was dried under vacuum for 5-15 minutes to remove any remaining liquid, and the resulting dry labeled DNA pellet was resuspended in 10 μL dH2O.

S3.1.6.2 Hybridization procedure and parameters

Equal amounts (12 μg) of Cy5 and Cy3 labeled DNA samples were mixed, and 4 μL 2.94 nM Xenohybe control oligos (an equimolar mixture of
5'　TTGCCGATGCTAACGACGCATCAGACTGCGTACGCCTAAGCAACGCTA3'　and
5'　CATTGCTGTGCGTACGCAGTCAAGTCGATCACGCTAACTCGTTGCGAC3'　) was added to the mixture. The sample was vacuum dried under low heat until the volume of sample was less than 14.4 μL. The final volume of DNA was adjusted to 14.4 μL with dH2O. To this sample, 11.25 μL 20X SSC, 18 μL 100% formamide, 0.45 μL 10% SDS, 0.45 μL 10X TE (100mM Tris, 10mM EDTA), and 0.45 μL equimolar mixture of Cy3 and Cy5 labeled CPK6 oligonucleotides
(5'　TTCCTCTCGCTGTAATGACCTCTATGAATAATCCTATCAAACAACTCA3'　and
5'　TTCCTCTCGCTGTAATGACCTCTATGAATAATCCTATCAAACAACTCA3'　,
respectively) were added to prepare the hybridization mixture. The hybridization sample was heated to 95 °C and was applied to the slide and incubated in the MAUI® Hybridization Station (BioMicro Systems, Inc.) at 42°C for 16-20 hours.

The hybridized slides from the MAUI® Hybridization Station were washed once in Wash 1 (0.2X SSC, 0.2% SDS, 0.1 mM DTT) for 10-15 seconds and followed by another wash in Wash 1 (0.2X SSC, 0.2% SDS, 0.1 mM DTT) for 2 minutes with gentle agitation. The slides were then washed in Wash 2 (0.2X SSC and 0.1mM DTT) for 1 minute and followed by a wash in Wash 3 (0.05X SSC and 0.1 mM DTT) for 15 seconds. The slides were dried by centrifugation

S3.1.6.3 Measurement data and specifications

The hybridized arrays were scanned on an Axon GenePix 4000B scanner (Axon Instruments Inc.) at wavelengths of 532nm for control (Cy3), and 635nm (Cy5) for experimental sample. PCR arrays were processed using GenePix 4.0 software while NimbleGen data were extracted from the scanned images using the NimbleScan 2.0 program (NimbleGen Systems, Inc.). The arrays were gridded using the automated gridding algorithm, and extracted in two channels using a mean intensity calculation of the interior of the gridded rectangular features upon extraction, and each pair of N probe signals were converted into a scaled log ratio using the function:

$$R(i) = Log (Experimental(i) / Control(i))$$

S3.1.7　　ChIP-PET method description

HCT116 Cells before and after 5-FU treatment were cross-linked with 1 % formaldehyde for 10 min at room temperature. Formaldehyde was inactivated by addition of 125 mM Glycine. Chromatin extracts containing DNA fragments of average size 500 bp were immunoprecipitated using anti-p53 DO1 monoclonal antibody (Santa Cruz Biotechnology). For all ChIP experiments, quantitative PCR analyses were performed in real time using ABI PRISM 7900 Sequence Detection System and SYBR Green master mix as described (Ng et al., 2003). Relative

occupancy values were calculated by determining the apparent immunoprecipitation efficiency (ratios of the amount of immunoprecipitated DNA over that of the input sample) and normalized to the level observed at a control region, which was defined as 1.0. The control region is a 279 bp region on chromosome 22 and is amplified using the following primers: 5'-GGACTCGGAAGAGGTTCACCTTCGG-3' and 5'-GTCGCCTCCGCTTGCTGAACTCAATGC-3'.

ChIP enriched DNA fragments were end-polished and ligated to the cloning vector pGIS3, which contains two MmeI recognition sites. The ligations were transformed into electrocompetent TOP10 bacterial cells to form the ChIP DNA library. Purified plasmid prepared from the ChIP DNA library was digested with MmeI, end-polished with T4 DNA polymerase to remove the 3'-dinucleotide overhangs, and the resulting plasmids containing a signature tag from each terminal of the original ChIP DNA insert were self-ligated to form single-ditag plasmids. These were then transformed into TOP10 cells to form a "single-ditag library". Plasmid DNA extracted from this library was digested with BamHI to release 50 bp paired end ditags. The PETs were PAGE-purified, then concatenated and separated on 4-20% gradient TBE-PAGE. An appropriate size fraction (1 kb-2 kb) of the concatenated DNA was excised, extracted and cloned into BamHI-cut pZErO-1 (Invitrogen) to form the final ChIP-PET library for sequencing.

PET sequences containing 18 bp from 5' and 18 bp from 3' ends of the original ChIP DNA fragments were extracted from the raw sequences obtained from the PET library, and mapped to human genome assembly (hg17). The process of PET extraction and mapping is essentially the same as previously described for cDNA analysis[32]. The specific mapping criteria are that both the 5' and 3' signatures must be present on the same chromosome, on the same strand, in the correct orientation (5'→3'), with minimal 17 bp match, and within 4 kb of genomic distance.

Based on the genomic coordinates, we took the center point of each PET cluster to measure the distances to the nearest genes on both sides of the cluster. The genes that had a distance from the nearest clusters of ≤ 100 kb were selected. We did not intend to absolutely associate the PET clusters with particular genes, but tried to provide the distance of the clusters to the nearest genes along the chromosomes.

S3.2 STAGE Data Generation Methods

The ChIP protocol is described in section S3.1.5.1

Generation of sequence tags from c-Myc ChIP DNA was carried out as described before[88]. Briefly, DNA was amplified using a biotinylated primer. We then essentially followed the LongSAGE protocol (http://www.sagenet.org/), but using amplified, biotinylated ChIP DNA as the starting material. Amplified DNA (1-2 µg) was digested with NlaIII. The terminal DNA fragments were bound to streptavidin-coated magnetic beads (Dynal) and separated into two tubes. After ligation with linker 1 or 2, which contain recognition sites for MmeI, the DNA fragments were released by MmeI digestion. The released tags were ligated to generate ditags. Ditags were amplified with nested primers, gel purified, and trimmed by NlaIII digestion. Trimmed ditags were gel purified, concatamerized by ligation, and cloned into the pZero 1.0 vector (Invitrogen). Insert sizes were assayed in recombinant clones and clones containing at

least 10 ditags were sequenced. For STAGE analysis of STAT1, we amplified gel purified ditags from an intermediate step of the STAGE protocol using linker specific primers and sequenced the population of ditags directly using bead-based pyrosequencing (454 Inc.). Analysis of STAGE tags was carried out as described in Kim et al[88] and Bhinge et al[17].

S3.3 DNaseI sensitivity and hypersensitivity: Data generation and analysis

S3.3.1   Mapping of DNaseI hypersensitivity sites with Quantitative Chromatin Profiling

DNaseI hypersensitive sites were mapped in ENCODE regions by applying the Quantitative Chromatin Profiling (QCP) methodology[4] to the following cell types: GM06990, HelaS3, CACO2, and SKnSH (all regions); K562, primary fetal and adult erythroblasts (ENm009); HepG2 and Huh7 (ENm003); PANC1, Calu3, primary large and small airway cells (ENm001); primary CD4 (ENm002). DNaseI sensitivity ratios were obtained for ~118,000 PCR amplicons (avg. length ~225bp) tiled end-to-end across the ENCODE regions. The tiling path covered approximately 86% of ENCODE sequence, encompassing all unique sequence and a large fraction of RepeatMasked sequence. DNaseI hypersensitive sites (DHSs) were identified by computing a moving baseline using a LOESS approach; determining the 95% confidence bound relative to the moving baseline; and identifying outliers (=DHSs).

S3.3.2   Mapping of DNaseI sensitivity and hypersensitivity with DNase/Array

DNaseI sensitivity and DHSs were mapped across ENCODE regions in GM06990 and HeLa S3 cells using the DNase/Array methodology[5].   We cultured cells using standard protocols. To remove background introduced from actively dividing cells, we synchronized cells in G1 by sequential temperature shifts. Cells were placed on ice for 1hr prior to nuclear harvest. We performed nuclear extraction, permeabilization, and DNaseI (Roche, Indianapolis, IN) digestions using a standard approach as described previously in Dorschner et al[4]. To isolate chromatin-specific and non-specific DNaseI fragments, we size fractionated both the control and treated samples using sucrose step gradients. We pooled fractions with fragments smaller than 1.5kb and cleaned the DNA using Qiagen (Valencia, CA) PCR purification columns according to the manufacturer's protocol. Samples were labeled and hybridized to a Nimblegen DNA microarray comprising ~390,000 50-mer probes tiled with 12-bp overlap across non-RepeatMasked regions of the ENCODE regions. DHSs were identified as peaks in the signal ratio that exceeded the P<0.01 level = 99th percent confidence bound on outliers. Results were extensively validated using conventional DNaseI sensitivity assays.

S3.3.3   Mapping of DNaseI hypersensitive sites with DNase-chip

DNaseI hypersensitive sites and DNaseI sensitivity were mapped across ENCODE regions with the DNase-chip methodology[2].

S3.3.3.1 Preparation of DNase treated nuclei for DNase-chip

Intact nuclei were isolated from GM06990 and Hela S3 cells using methods previously described[2]. Nuclei from 3 biological replicates were digested with 3 different optimized concentrations of DNaseI.   We blunt ended the DNase digested fragments using T4 DNA polymerase. Genomic DNA used for the random sheared reference control was purified from

each cell line (Gentra), vigorously pipetted and vortexed to generate randomly sheared DNA fragments, and blunt ended.

S3.3.3.2 Capture of DNase digested ends for DNase-chip

We ligated biotinylated linkers (5' Biotin-GCG GTG ACC CGG GAG ATC TGA ATT C and 5' Phos-GAA TTC AGA TC-3AmM) to DNase digested ends from DNase treated or randomly sheared DNA. The ligation mix was sonicated to generate 200-500 base pair fragments, and biotin-labeled fragments were enriched using streptavidin-coated magnetic beads (Dynal). The sonicated ends were made blunt using T4 DNA polymerase and ligated to nonbiotinylated linkers described above. The DNase captured material was amplified using ligation mediated PCR (5' GCG GTG ACC CGG GAG ATC TGA ATT C).

S3.3.3.3 Hybridization to tiled ENCODE microarrays and data analysis for DNase-chip

We labeled ligation mediated PCR products from DNase treated and random sheared DNA with Cy3- and Cy5-dUTP. Labeled samples were mixed, supplemented with a blocking cocktail (tRNA, Cot1 DNA, Poly A+ RNA, and Poly T+ RNA), and hybridized to Nimblegen ENCODE tiled arrays for >20 hours (Maui). The ENCODE array has approximately 385,000 x 50mer oligos spaced approximately every 38 base pairs of unique sequence (NimbleGen). Slides were washed, scanned (Agilent), and signals were normalized using Nimblescan software. We averaged normalized ratio data (DNase:random) from 9 hybridizations (3 DNase concentrations and 3 biological replicates). We used the ratios to perform a chi-square test on sliding 500 base pair windows to identify regions with a higher than expected number of oligos in the top 5% of the log-ratio distribution (p-values <0.001). Analysis software was written in R (http://www.r-project.org) and is available upon request.

S3.3.4 Generation of a common set of DHS for GM06990 lymphoblastoid cells

When applied to the same tissue type, the aforementioned methodologies have considerable overlap. Because the cell preparation procedures differ amongst the method, and because of minor intrinsic biological variability between preparations of the same cell type using the same methodology, some DHSs may be detected in one data set that are not present in the others. We therefore generated a common set of DHSs from lymphoblastoid cells (see section S3.3.5). First, thresholded all the individual DHS data sets at the P<0.01 level (i.e., we did not consider DHSs that did not contain signal or indensity ratios that exceeded their respective 99th percent confidence bound on outliers. We next performed a merging step in which overlapping DHSs were merged. In cases where two DHSs in the common data set might be separated by less than 200bp (approximately the size of a nucleosome plus linker DNA), these were merged into a single site.

S3.3.5 Table in supplemental Excel streadsheet

This table is included in the attached Excel spreadsheet on the worksheet labeled Section S3.3.5.

S3.4 FAIRE Data Generation methods

Formaldehyde Assisted Isolation of Regulatory Elements (FAIRE) was performed in foreskin fibroblast cells (CRL-2091). Cells were grown to 90% confluence in 245 x 245 mm plates and fixed in 1% formaldehyde at room temperature for 1, 2, 4, or 7 minutes. Glycine was added to a final concentration of 125 mM, the cells were spun down at 2K rpm for 4 minutes, and washed twice with cold 1 X PBS containing 100 mM phenylmethylsulphonylflouride. Cells were resuspended in 1 ml of lysis buffer (2% Triton X-100, 1% SDS, 100 mM NaCl, 10 mM Tris-Cl (pH 8.0), and 1mM EDTA) for every 0.1 g of cells and subjected to five 1-minute sessions of glass bead disruption with 2 minutes on ice between sessions. The extract was then sonicated for five sessions of 60 pulses (1 second on/1 second off, 15% amplitude), cooled for 2 minutes on ice between sessions. This yielded an average fragment size of 500 bp. The extract was spun at 15K rpm for 1 minute to clear cellular debris. An equal volume phenol/chloroform was added to the supernatant, vortexed, and spun at 15K rpm for 5 minutes. The aqueous phase was recovered and an additional extraction was performed by adding 1 ml of TE to the organic phase, vortexing, and spinning at 15K rpm for 5 minutes. An equal volume of phenol/chloroform was then added to the pooled aqueous sample, vortexed, and spun at 15K rpm for 5 minutes. Sodium acetate was added to the to a final concentration of 0.3 M. 2X volumes of 95% ethanol was added and incubated at -20°C overnight. The precipitated DNA was pelleted at 15K rpm for 5 minutes, washed with 70% ethanol, and pelleted. The DNA was dried in a speed-vac, resuspended in water, and were incubated at 65°C overnight. 2 μl of RNase A (100 μg/ml) was added and incubated at 37°C for 30 minutes. DNA fragments recovered from the aqueous phase were amplified by ligation-mediated PCR, fluorescently labeled, and hybridized to high-density tiling arrays (NimbleGen Inc., Madison, WI), which cover the non-repetitive portion of the ENCODE regions at 38 bp resolution. A more detailed description of the protocol and subsequent data analysis can be found in Giresi et al[3].

S3.5 Generation and categorization of 5' end clusters

One of the goals within the ENCODE projects is to find 5' ends of genes and thereby the core promoter regions. The dataset described above and recent studies[89] indicates that 5' ends of genes in many cases cannot be described as a single nucleotide position, but a cluster of closely located positions.

There are many ways of defining such TSS clusters. In our approach we started with two sets of 5' sites, those identified as the 5' ends of transcripts in the GENCODE annotation (ftp://genome.imim.es/pub/projects/GENCODE/data/TSS_to_share/GENCODE_all_TSS.gff) and those identified by either the CAGE or PET 5' end tag capture technologies (http://genome.ucsc.edu/encode/encode.hg17.html tables encodeGisRnaPetHCT116.bed, encodeGisRnaPetMCF7.bed, encodeGisRnaPetMCF7Estr.bed, encodeRikenCageMinus.bed, encodeRikenCagePlus.bed). In each set, sites located within 60 bp of each other and on the same strand were clustered. The 60 bp criterion was based on analyzing the distribution of distances between 5' end positions from the 5' and 3' map described above. Specifically, we investigated the distances between consecutive nucleotides labeled as TSS on the same strand by any of the

methods. The growth of the cumulative distribution of such distances drop rapidly at around 50-70 nts (see Supplementary Figure 13).
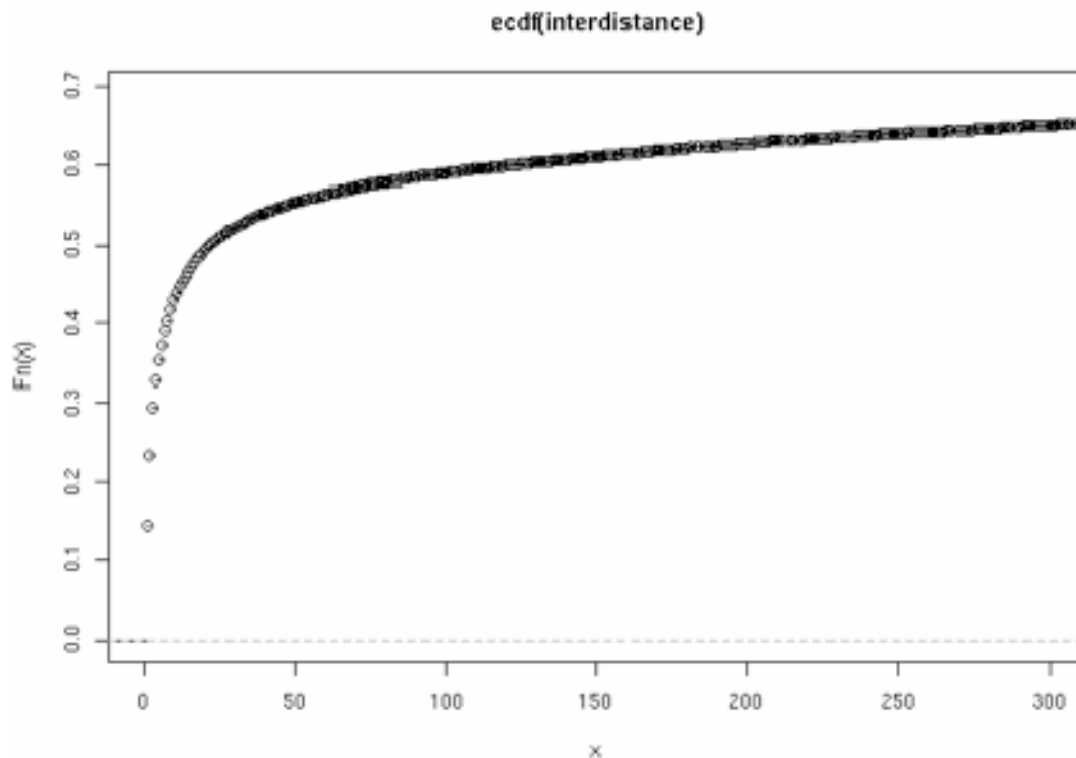
Supplementary Figure 13: Cumulative distribution of the shortest distances between consecutive nucleotides inferred as TSS on the same strand by GENCODE, CAGE and/or PETs. The Y axis shows the fraction of the whole population of distances that are <= x nucleotides

A single genomic coordinate was chosen to represent each cluster. For the GENCODE sites this was the most 5' site in the cluster and for the tag sites it was the site with the highest number of individual tags. There were 1730 GENCODE clusters and 6045 tag clusters.

The two sets of clusters were merged and categorised roughly in order of confidence, by determining what type of annotated genomic feature supported their validity. A TSS cluster was considered supported if it lay within the interval +/- 100bp of the given feature. Category A comprised all the GENCODE 5' site clusters. Category B comprised those tag clusters supported by the 5' end of GENCODE exons (ftp://genome.imim.es/pub/other/GENCODE/data/havana-encode/version02.2_14oct05/CHR_coord_hg17/global_files/44regions_CHR_coord.gtf.gz origin in 'VEGA_Antisense_val', 'VEGA_Known','VEGA_Novel_CDS','VEGA_Novel_transcript_val', 'VEGA_Putative_val') on the same strand as the tag cluster but not supported by Category A clusters. Category C comprised those tag clusters not in the previous categories and supported by GENCODE exons on the opposite strand. Category D comprised those tag clusters not in the previous categories and supported by any TxFrag (http://transcriptome.affymetrix.com/download/ENCODE/HS_v35/genes_transcripts/TARs_tran

sfrags/union_TARs_transfrags.bed) or RxFrag
(ftp://genome.imim.es/pub/projects/GENCODE/data/RxFrags/suppl_info/). Category E
comprised those tag clusters not in the previous categories and supported by a CpG island
(http://genome.ucsc.edu/encode/encode.hg17.html table cpgIslandExt) and Category F
comprised the remaining, unsupported tag clusters.

The Pvalue of the overlap between the Tag data and the supporting data was calculated using
overlap statistics based on the Genome Structure Correction method (see Supplement S1.3).

S3.5.1   Correlation of Singleton Tag clusters to other transcriptional evidence.

The Transcription Start Sites (TSSs) defined by CAGE or DiTags can be defined by one or tags.
Any technical false tags, or low level, random transcription is likely to provide single tag TSSs.
To assess whether the classifications of TSSs in different evidence catagories were inflated by
the presence of random, singleton tags, we repeated the statistical analysis of the overlap (within
100bp, as for the global tag set) between only singleton Tag clusters and each source of
supporting evidence. The Table below shows the P-value of seeing the evidence overlap by
chance, using the GSC statistic (see Supplement S1.3) which conservatively handles
heterogeneous distributions in the genome.

**Supplementary Table 10: Correlation of singleton tag clusters to other transcriptional
evidence**

Evidence Type	P-value to singleton clusters
Sense GENCODE exon	1e-273
Antisense GENCODE exon	1e-95
TxFrag or RxFrag	1e-263
CpG island	1e-313

As the table shows, there is no evidence to support the hypothesis that most of the singleton
clusters are randomly distributed around the genome with respect to any of these four
classifications of evidence.

S3.6 ChIP enrichment profiles for TSSs

These plots show the curves in Figure 5 individually and without smoothing. The x-axis is the
relative distance to the nearest anchor (either TSSs or DHSs). The y-axis is the averaged ChIP
signal at a certain distance to all anchors. For each plot the signal was first normalized with a
mean of 0 and standard deviation 1. The signal of each probe in the ChIP-chip dataset was
assigned a distance to its nearest anchor of a given class. Then all signals at the distance to all the
anchors were averaged. In order to examine the significance of differences in signal intensity
between positions proximal versus distal to anchors, P-values were calculated from two-sided
Student's t-test between intensity of all probes within 10Kb range from any anchor and those
within 1Kb range, or between outside 5Kb and within 1Kb.

A

-0.24, 0.23, p1=5.9e-05, p2=1.5e-48

B

-0.25, 0.16, p1=0.015, p2-1.8e-06

C

-0.15, 0.14, p1=2.6e-62, p2=8.9e-77

D

-0.99, 1.24, p1=1.6e-51, p2=7.1e-13

E

-0.3, 0.64, p1=6.8e-15, p2=4.4e-29

F

-0.14, 0.62, p1=0, p2=0
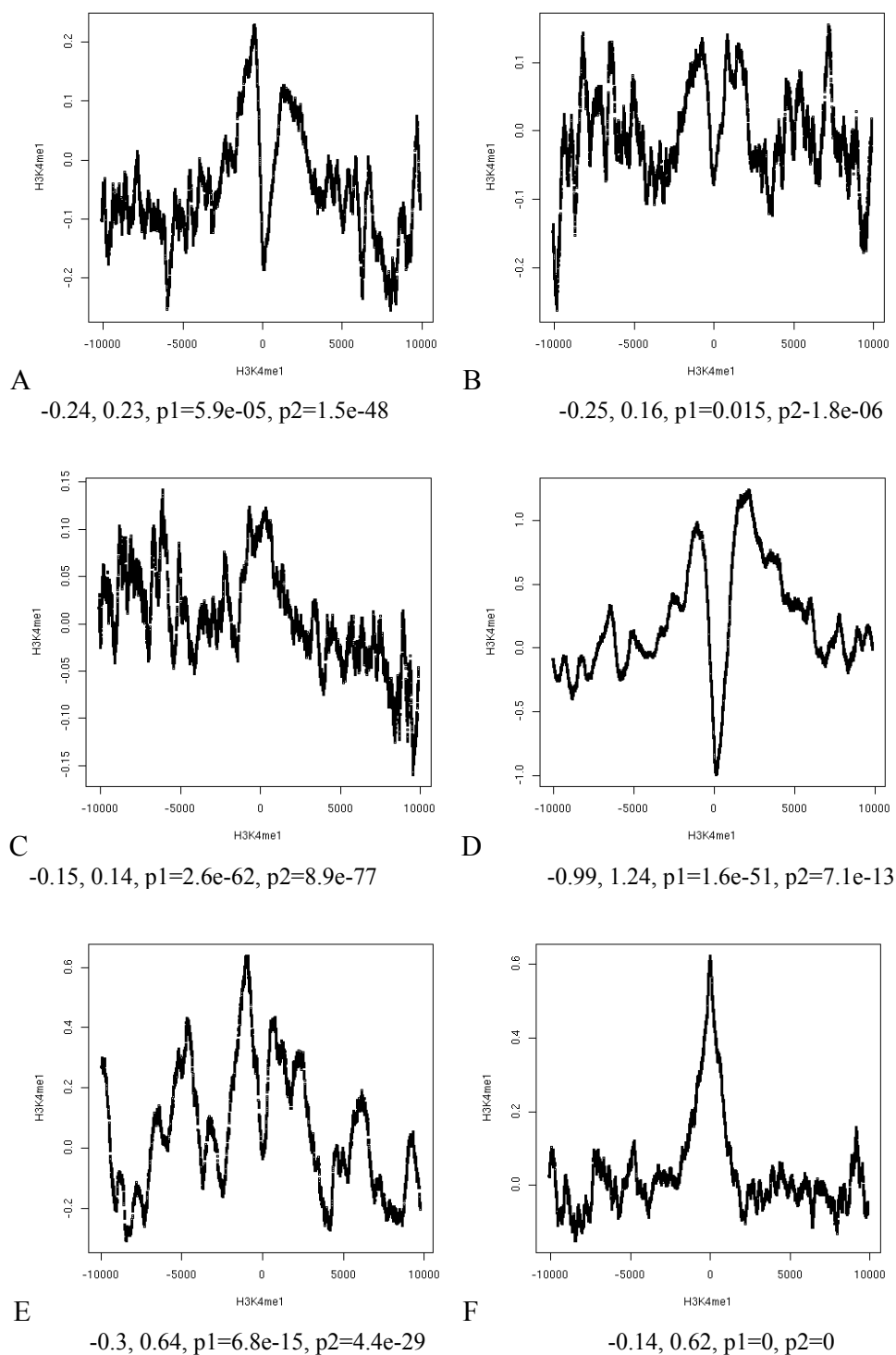
Supplementary Figure 14: Aggregate H3K4me1 ChIP-chip signals of (A) GENCODE TSS, (B) novel TSS, (C) unsupported tags, (D) GeneOnCpG, (E) GeneOffCpG, (F) distal DNS. Below each plot are the y-min, y-max, and the p-values from two-sided t-tests between intensity of all displayed probes and those within 1Kb (p1), and between probes outside 5Kb and within 1Kb (p2).

A   -0.27, 0.71, p1=0, p2=0   B   -0.32, 0.47, p1=0, p2=0

C   -0.15, 0.21, p1=6.1e-32, p2=8.3e-33   D   -0.31, 3.87, p1=0, p2=0

E   -0.23, 1.82, p1=1.7e-107, p2=3.5e-157   F   -0.18, 0.41, p1=1.2e-144, p2=7.7e-128
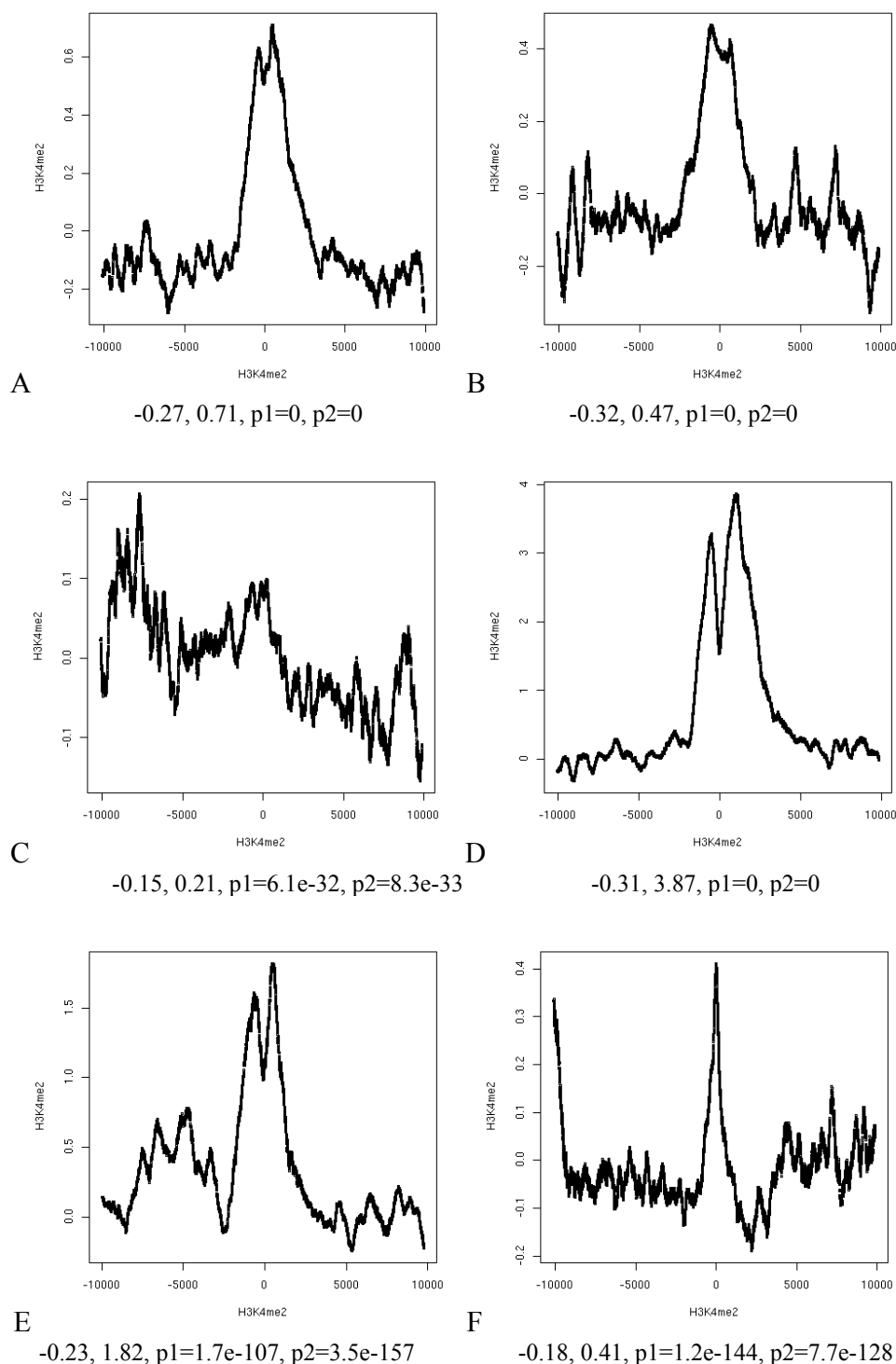
Supplementary Figure 15: Aggregate H3K4me2 ChIP-chip signals of (A) GENCODE TSS, (B) novel TSS, (C) unsupported tags, (D) GeneOnCpG, (E) GeneOffCpG, (F) distal DNS. Below each plot are the y-min, y-max, and the p-values from two-sided t-tests between intensity of all displayed probes and those within 1Kb (p1), and between probes outside 5Kb and within 1Kb (p2).

A

-0.25, 0.8, p1=0, p2=0

B

-0.26, 0.39, p1=1.3e-286, p2=0

C

-0.12, 0.15, p1=3e-06, p2=1.6e-12

D

-0.33, 4.91, p1=0, p2=0

E

-0.31, 1.32, p1=6e-67, p2=3.9e-90

F

-0.17, 0.2, p1=7.6e-05, p2=1.2e-16
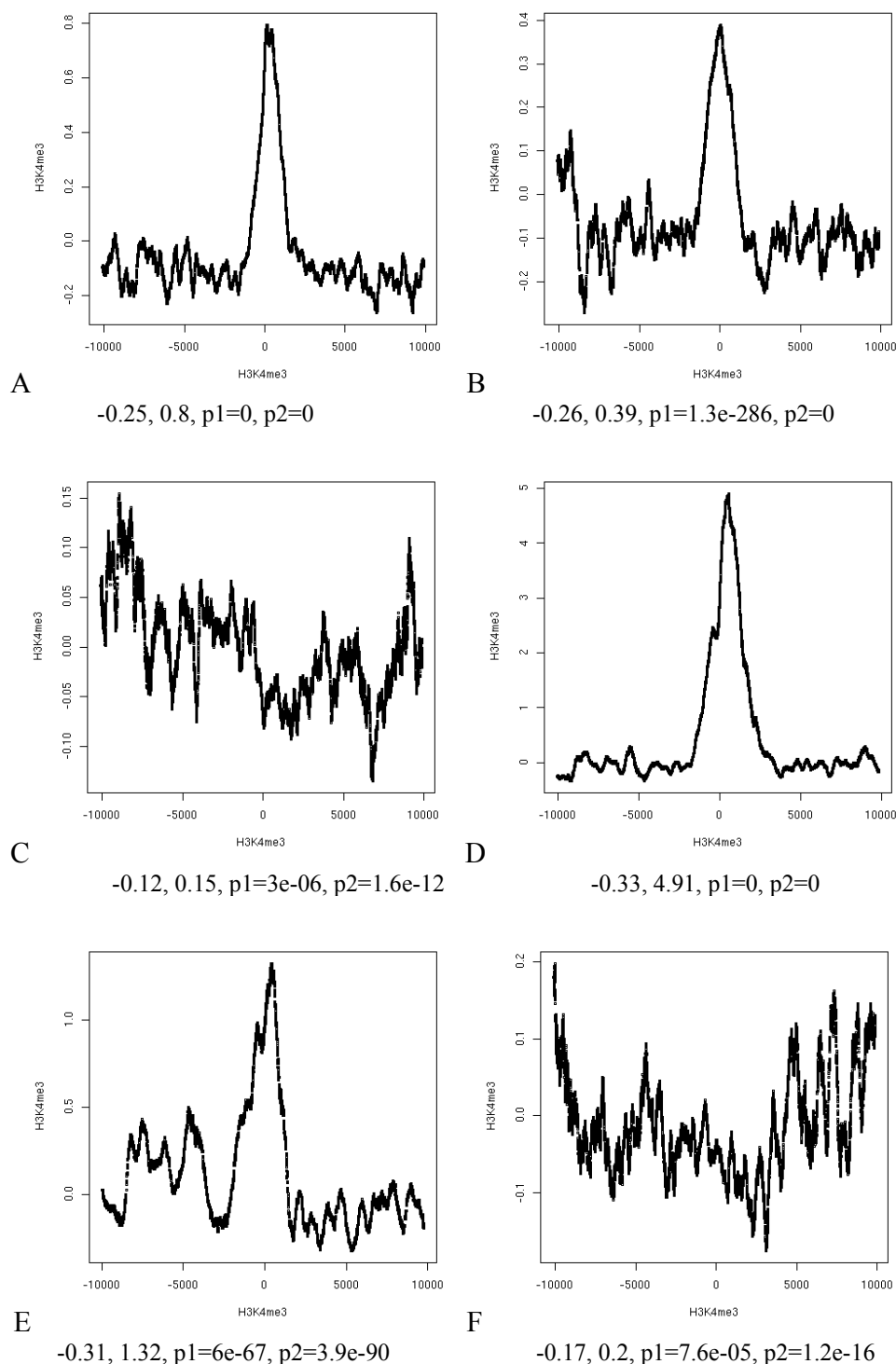
Supplementary Figure 16: Aggregate H3K4me3 ChIP-chip signals of (A) GENCODE TSS, (B) novel TSS, (C) unsupported tags, (D) GeneOnCpG, (E) GeneOffCpG, (F) distal DNS. Below each plot are the y-min, y-max, and the p-values from two-sided t-tests between intensity of all displayed probes and those within 1Kb (p1), and between probes outside 5Kb and within 1Kb (p2).

A

-0.25, 0.85, p1=0, p2=0

B

-0.38, 0.58, p1=0, p2=0

C

-0.14, 0.15, p1=8.3e-49, p2=3.4e-62

D

-0.01, 3.95, p1=0, p2=0

E

-0.09, 1.59, p1=6.3e-87, 6.3e-119

F

-0.21, 0.31, p1=8.1e-107, p2=3.5e-68

Supplementary Figure 17: Aggregate H3ac ChIP-chip signals of (A) GENCODE TSS, (B) novel TSS, (C) unsupported tags, (D) GeneOnCpG, (E) GeneOffCpG, (F) distal DNS. Below each plot are the y-min, y-max, and the p-values from two-sided t-tests between intensity of all displayed probes and those within 1Kb (p1), and between probes outside 5Kb and within 1Kb (p2).

A   -0.2, 0.49, p1=0, p2=0

B   -0.22, 0.36, p1=1.5e-250, p2=0

C   -0.14, 0.15, p1=2.3e-17, p2=5.5e-21

D   -0.29, 2.58, p1=0, p2=0

E   -0.23, 0.9, p1=1.9e-38, p2=3e-49
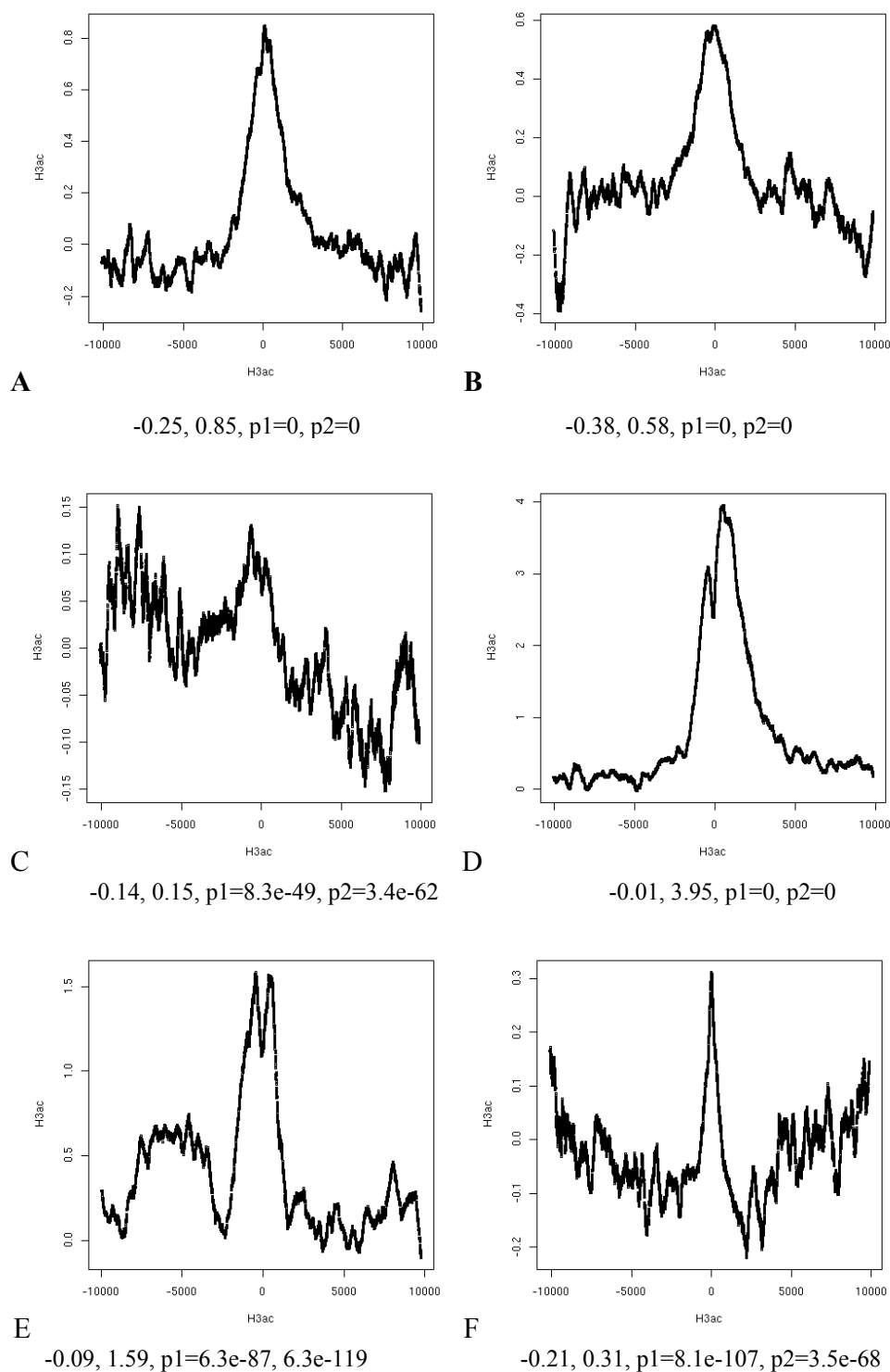
F   -0.14, 0.21, p1=1.7e-43, p2=1.2e-41

Supplementary Figure 18: Aggregate H3ac ChIP-chip signals of (A) GENCODE TSS, (B) novel TSS, (C) unsupported tags, (D) GeneOnCpG, (E) GeneOffCpG, (F) distal DNS. Below each plot are the y-min, y-max, and the p-values from two-sided t-tests between intensity of all displayed probes and those within 1Kb (p1), and between probes outside 5Kb and within 1Kb (p2).

A

-0.19, 0.58, p1=3.4e-160, p2=9e261

B

-0.15, 0.32, p1=1e-81, p2=1.8e-112

C

-0.09, 0.16, p1=3.3e-20, p2=2.6e-37

D

-0.12, 2.55, p1=5.5e-199, p2=5.3e-290

E

-0.21, 0.82, p1=1.2e-33, p2=1.5e-50

F

-0.13, 0.44, p1=8.6e-68, p2=9.3e-78

Supplementary Figure 19: Aggregate FAIRE signals of (A) GENCODE TSS, (B) novel TSS, (C) unsupported tags, (D) GeneOnCpG, (E) GeneOffCpG, (F) distal DNS. Below each plot are the y-min, y-max, and the p-values from two-sided t-tests between intensity of all displayed probes and those within 1Kb (p1), and between probes outside 5Kb and within 1Kb (p2).
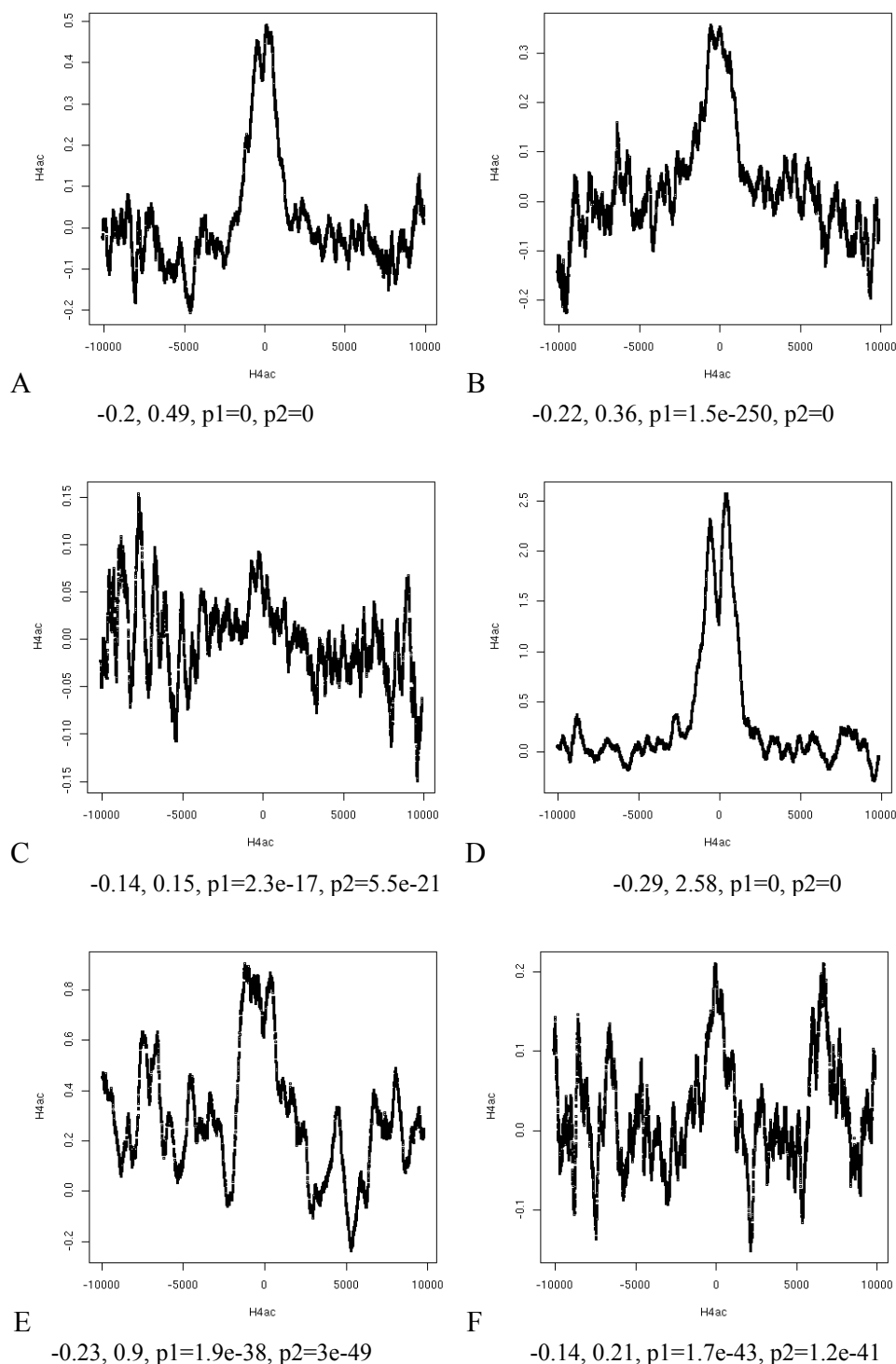
A

-0.15, 0.85, p1=0, p2=0

B

-0.13, 0.38, p1=5.2e-164, p2=1.2e-296

C

-0.11, 0.19, p1=2.9e-16, p2=1.8e-10

D

-0.16, 4.37, p1=0, p2=0

E

-0.2, 1.31, p1=2.9e-63, p2=1.7e-105

F

-0.1, 0.35, p1=4.7e-45, p2=6e-50

Supplementary Figure 20: Aggregate DNAseI signals of (A) GENCODE TSS, (B) novel TSS, (C) unsupported tags, (D) GeneOnCpG, (E) GeneOffCpG, (F) distal DNS. Below each plot are the y-min, y-max, and the p-values from two-sided t-tests between intensity of all displayed probes and those within 1Kb (p1), and between probes outside 5Kb and within 1Kb (p2).
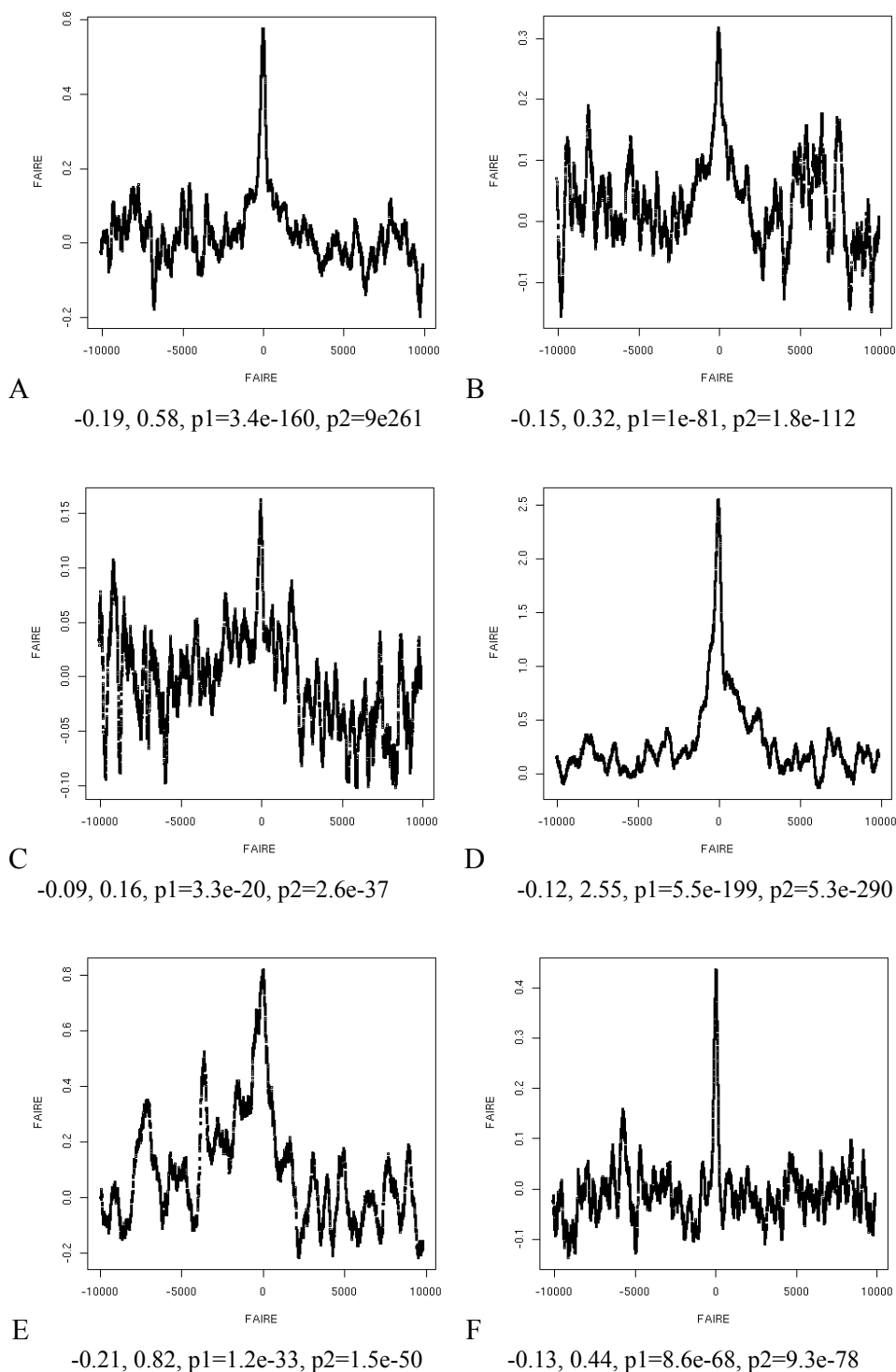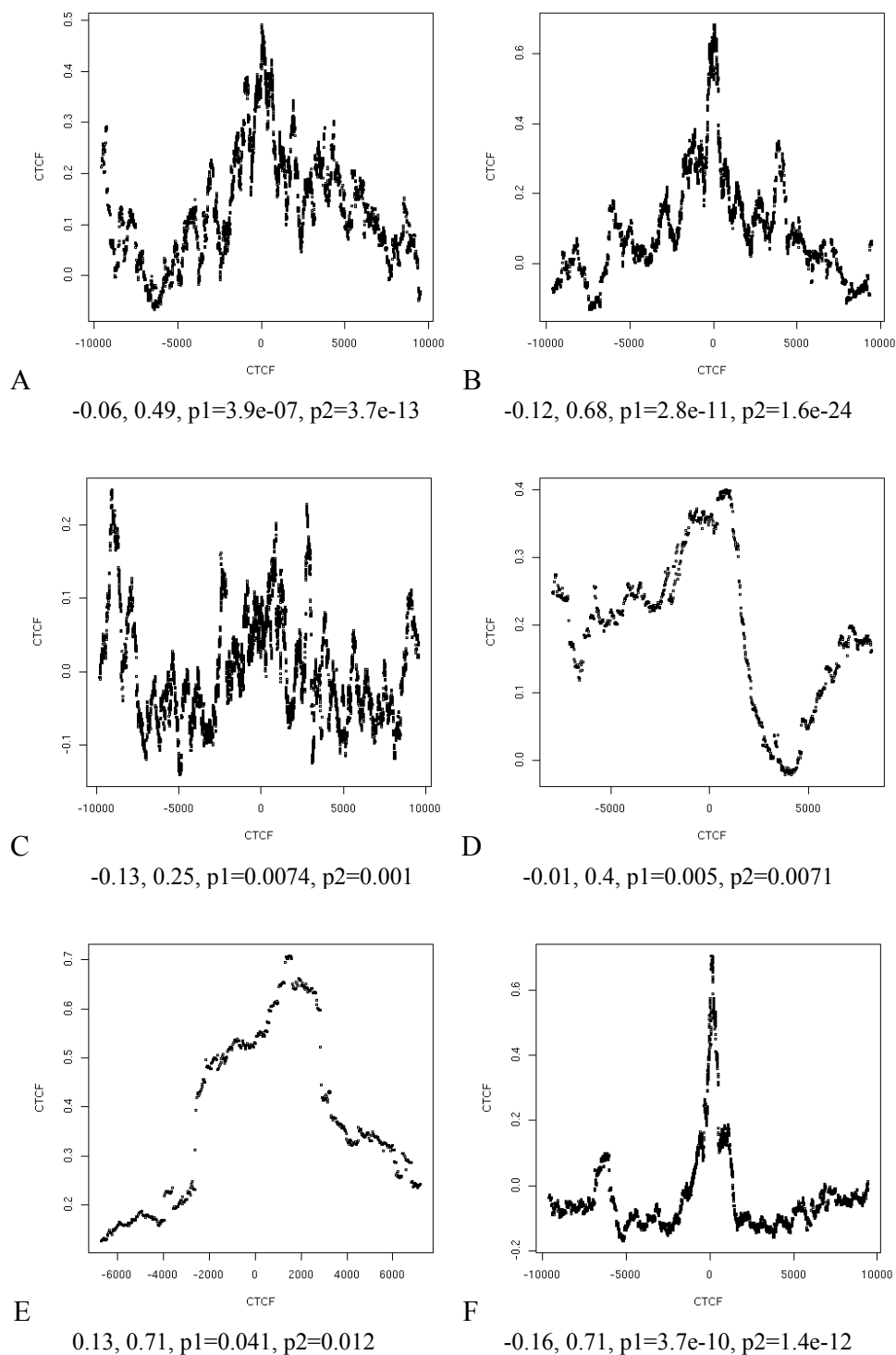
Supplementary Figure 21: Aggregate CTCF ChIP-chip signals of (A) GENCODE TSS, (B) novel TSS, (C) unsupported tags, (D) GeneOnCpG, (E) GeneOffCpG, (F) distal DNS. Below each plot are the y-min, y-max, and the p-values from two-sided t-tests between intensity of all displayed probes and those within 1Kb (p1), and between probes outside 5Kb and within 1Kb (p2).
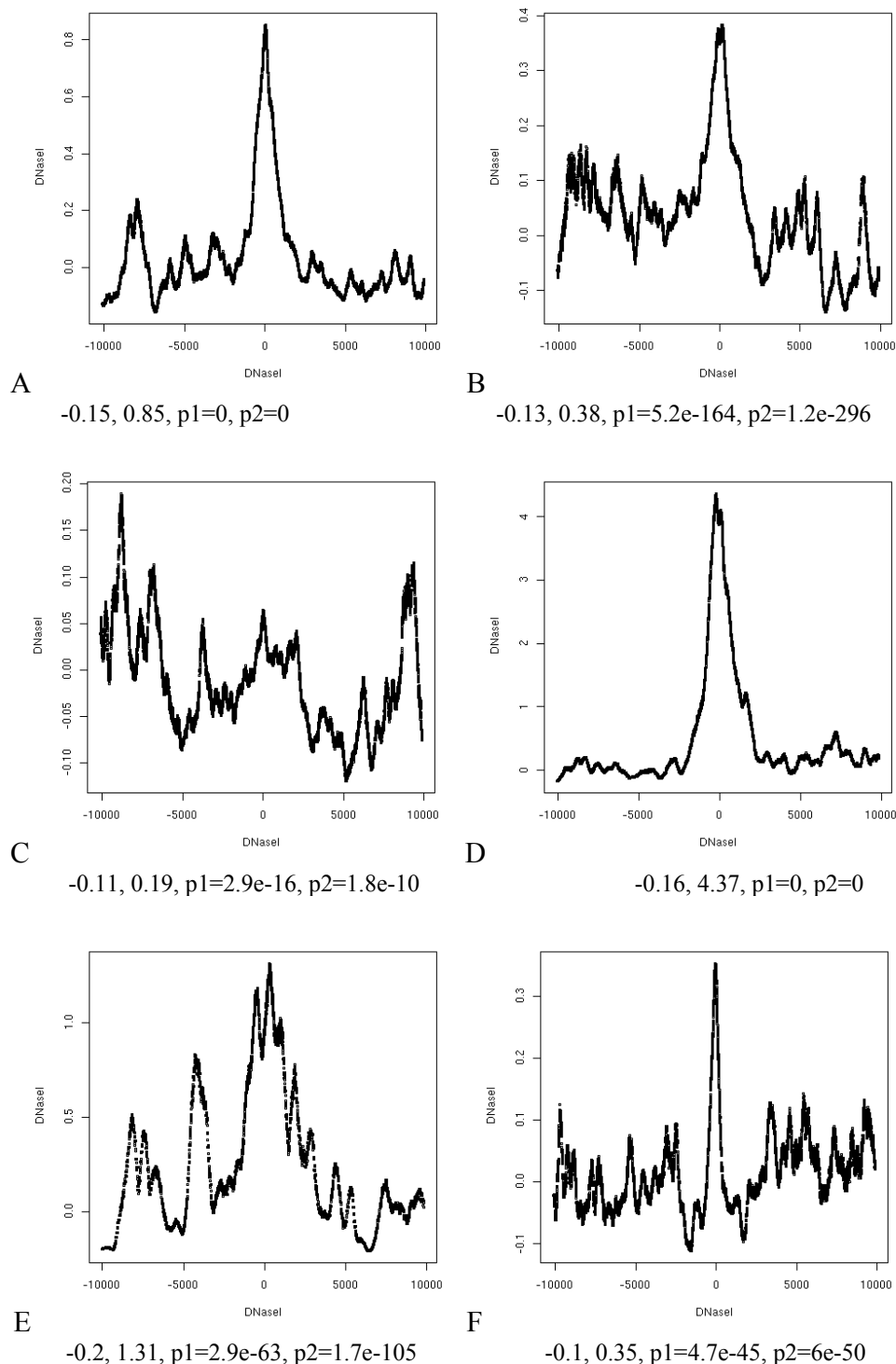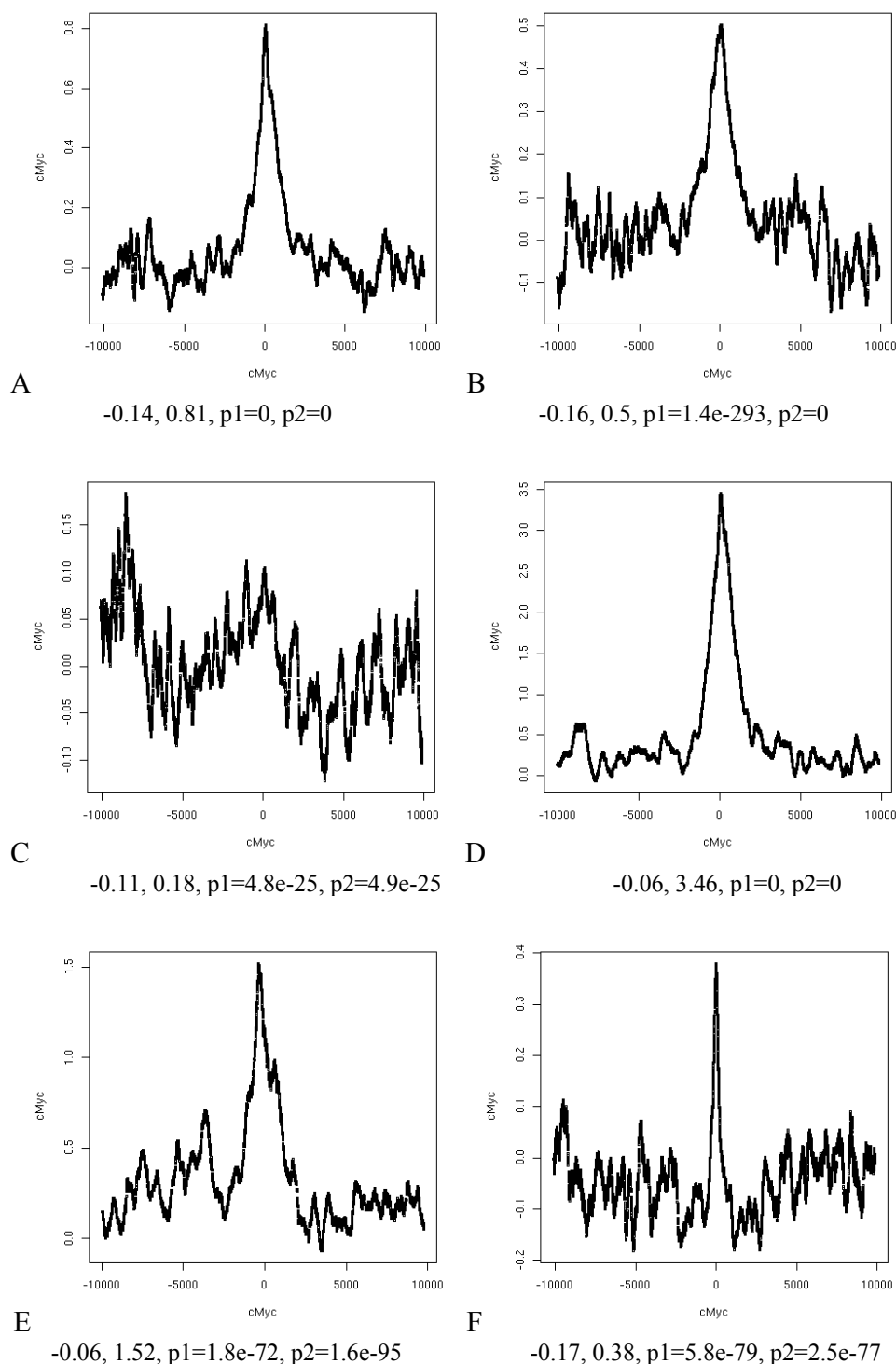
Supplementary Figure 22: Aggregate cMyc ChIP-chip signals of (A) GENCODE TSS, (B) novel TSS, (C) unsupported tags, (D) GeneOnCpG, (E) GeneOffCpG, (F) distal DNS. Below each plot are the y-min, y-max, and the p-values from two-sided t-tests between intensity of all displayed probes and those within 1Kb (p1), and between probes outside 5Kb and within 1Kb (p2).

A

-0.22, 1.14, p1=0, p2=0

B

-0.28,0.74, p1=0, p2=0

C

-0.09, 0.13, p1=3.9e-06, p2=2.6e-05

D

-0.14, 4.79, p1=0, p2=0

E

-0.12, 2.18, p1=1.6e-124, p2=1.8e-162

F

-0.22, 0.19, p1-5.8e-60, p2=4.1e-107

Supplementary Figure 23: Aggregate E2F1 ChIP-chip signals of (A) GENCODE TSS, (B) novel TSS, (C) unsupported tags, (D) GeneOnCpG, (E) GeneOffCpG, (F) distal DNS. Below each plot are the y-min, y-max, and the p-values from two-sided t-tests between intensity of all displayed probes and those within 1Kb (p1), and between probes outside 5Kb and within 1Kb (p2).
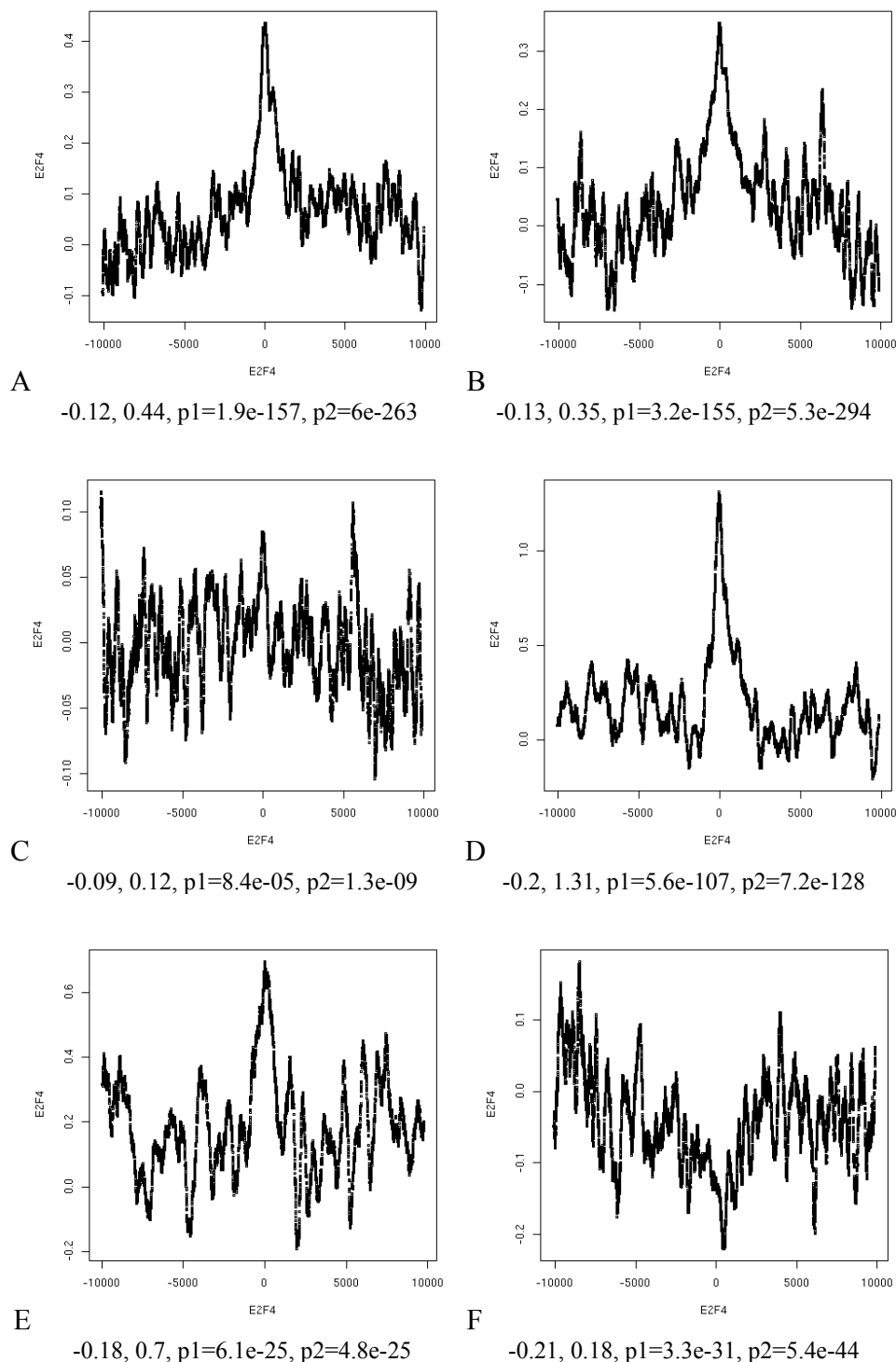
Supplementary Figure 24: Aggregate E2F4 ChIP-chip signals of (A) GENCODE TSS, (B) novel TSS, (C) unsupported tags, (D) GeneOnCpG, (E) GeneOffCpG, (F) distal DNS. Below each plot are the y-min, y-max, and the p-values from two-sided t-tests between intensity of all displayed probes and those within 1Kb (p1), and between probes outside 5Kb and within 1Kb (p2).

A   -0.12, 1.03, p1=0, p2=0

B   -0.21, 0.98, p1=0, p2=0

C   -0.21, 0.13, p1=5.5e-40, p2=3.7e-75

D   0.04, 1.72, p1=1.3e-212, p2=7.2e-226

E   0.05, 1.89, p1=3.6e-103, p2=1e-126

F   -0.3, 0.16, p1=9e-165, p2=6.5e-246

Supplementary Figure 25: Aggregate BAF155 ChIP-chip signals of (A) GENCODE TSS, (B) novel TSS, (C) unsupported tags, (D) GeneOnCpG, (E) GeneOffCpG, (F) distal DNS. Below each plot are the y-min, y-max, and the p-values from two-sided t-tests between intensity of all displayed probes and those within 1Kb (p1), and between probes outside 5Kb and within 1Kb (p2).
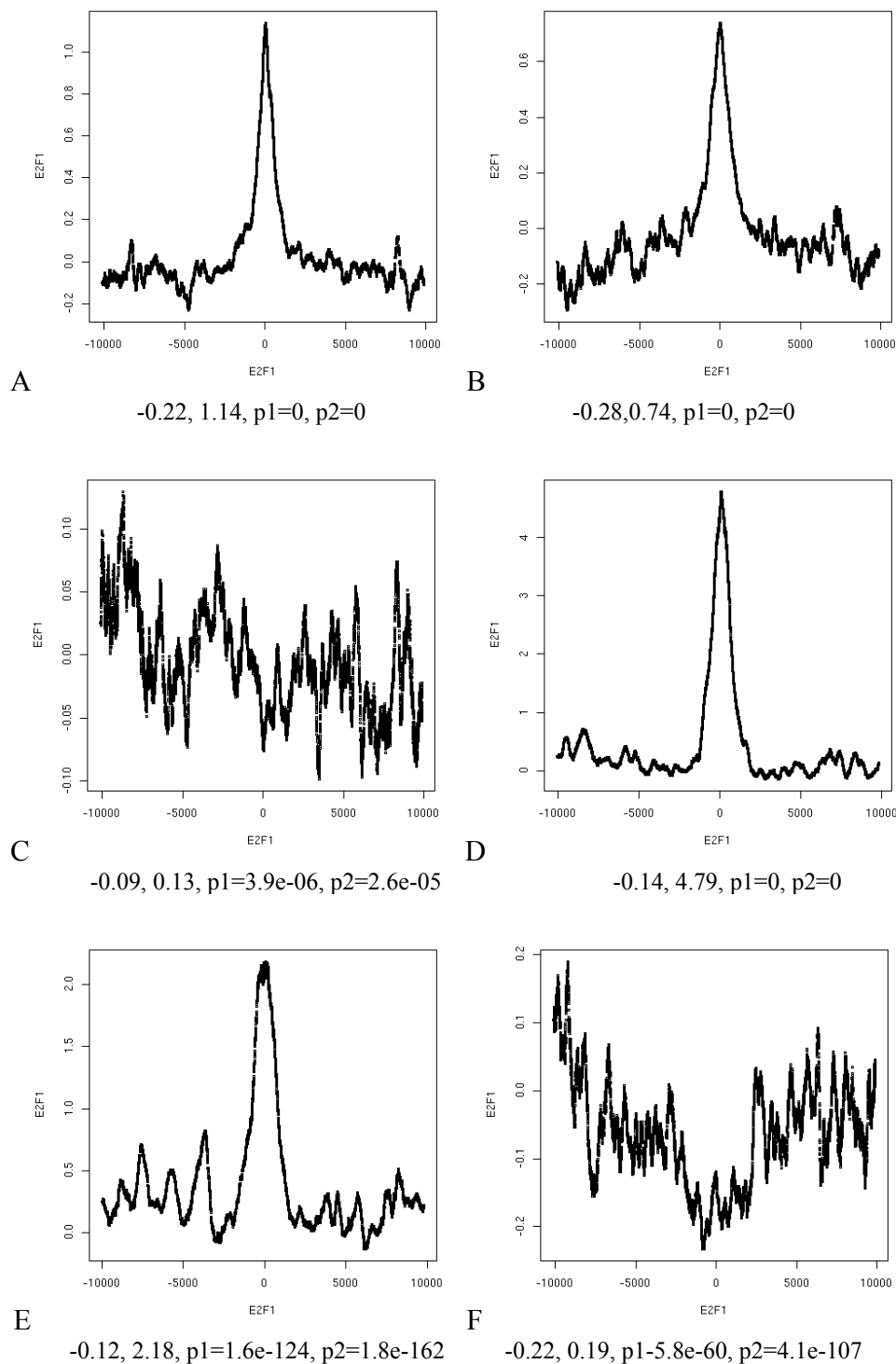
A

-0.22, 0.48, p1=1.6e-155, p2=3e-253

B

-0.16, 0.22, p1=2e-85, p2=2.4e-159

C

-0.12, 0.18, p1=0.00076, p2=3.1e-07

D

-0.31, 2.8, p1=1.4e-238, p2=0

E

-0.33, 0.32, p1=8.4e-15, p2=2.1e-20

F

-0.14, 0.24, p1=2.8e-08, p2=0.055

Supplementary Figure 26: Aggregate RNA PolII ChIP-chip signals of (A) GENCODE TSS, (B) novel TSS, (C) unsupported tags, (D) GeneOnCpG, (E) GeneOffCpG, (F) distal DNS. Below each plot are the y-min, y-max, and the p-values from two-sided t-tests between intensity of all displayed probes and those within 1Kb (p1), and between probes outside 5Kb and within 1Kb (p2).
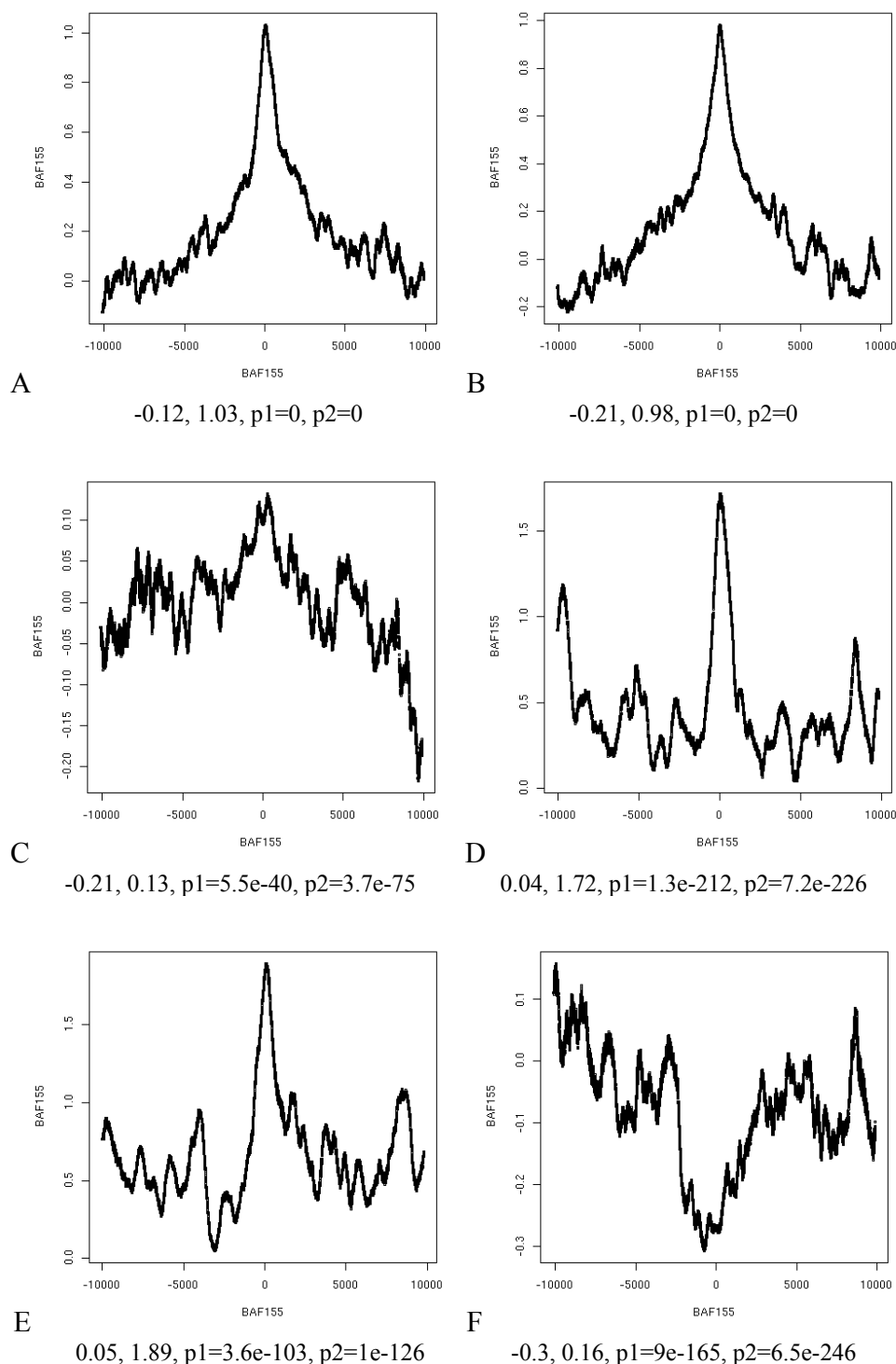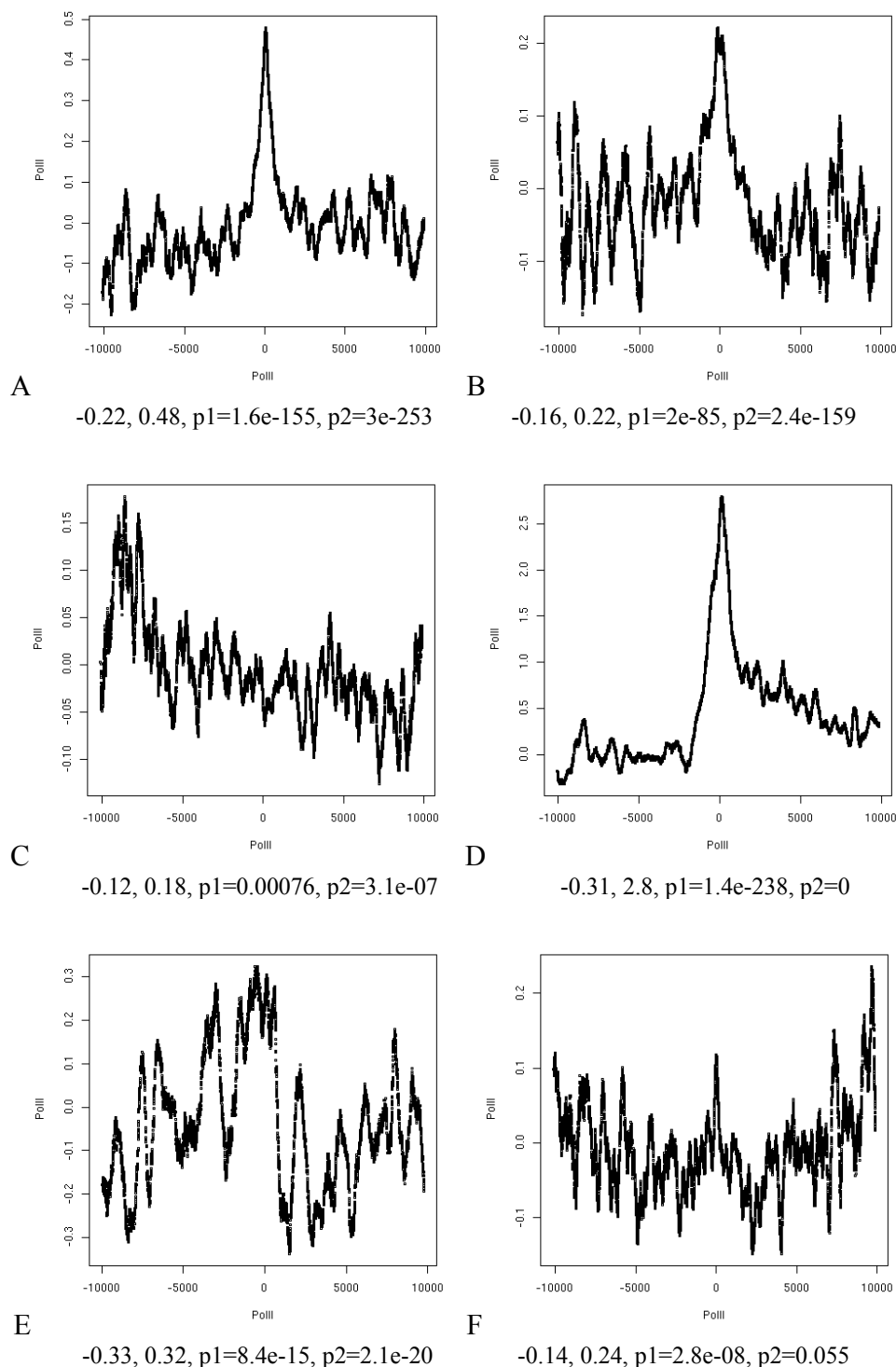
S3.7 Symmetrical Signal Analysis

All of the ChIP-chip analysis shows binding peaks both upstream and downstream of features such as the transcription start sites. These binding patterns are not exactly symmetrical on each side of the features, but there does not appear to be a preference for the upstream side of the TSS.

In an effort to determine if this effect is an artifact of the array platform or of the analysis, we first assume that the DNA is sheared randomly with respect to the location of the DNA-protein complex. We also assume that the antibodies used do not preferentially pull down sheared fragments in which the DNA-protein binding complex is located on either the 5` end or the 3` end of the fragment.

If these assumptions hold, the population of labeled DNA fragments to be hybridized to the tiling array can be considered a random distribution centered on the site of the DNA-protein binding site. There may still be some unintended directional bias if the TSSs considered in each of the categories are biased with respect to the position of the tiles. For example, TSS positions that are biased to the 3' end of the array tiles will, on average, result in a higher enrichment signal in tiles that are further downstream from the center tile. Similarly, if the TSS positions are located in gaps on the tile path and the positions of the TSSs within the gaps are preferentially toward the 5' or 3' end of the gap on the tile path, there will be an enrichment bias to the 3' or 5' the DNA-protein binding location, respectively.

Supplementary Figure 27 shows that the distribution of the distance of the category A TSSs from the center of the tiles on the Sanger PCR array as a fraction of the tile length is essentially flat. We do note that there is a small bias for category A TSSs to be toward the 3' end of the tiles and category B TSS- to be toward the 5' end of tiles. Indeed, the tendency for enrichments to be slightly shifted 3' appears in Figure 5 and section S3.6 but does not affect the symmetrical nature of the enrichment signatures.
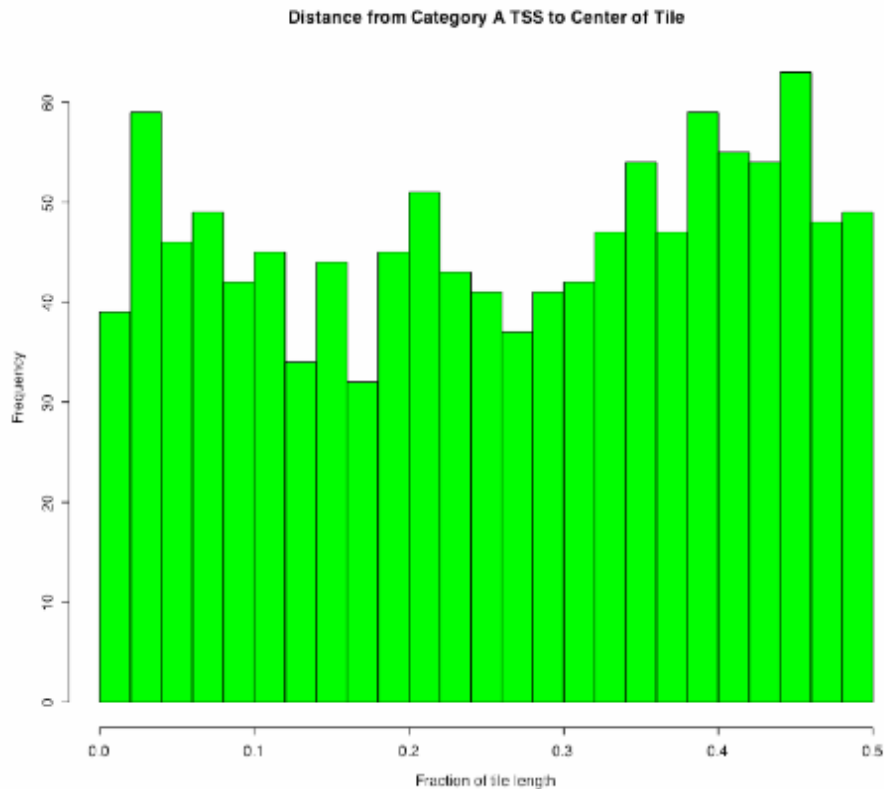
Supplementary Figure 8: Distribution of the distance of category A TSSs from the center of the array tile on the Sanger PCR array platform as a fraction of the total length of the tile.

Supplementary Figure 27: Distribution of the distance of category A TSSs from the center of the array tile on the Sanger PCR array platform as a fraction of the total length of the tile.

S3.8 BAF Analysis

S3.8.1 Computational Analysis

Both the BAF and CTCF signal show broad enrichment and depletion in aggregate around different positions in the genome. This could be due to a number of different phenomena; for example, enrichment could either be due to a general raising or lowering of the genomic background or due to more specific highly enriched regions near the sites. Broad depletion signals are more complex to understand; as aggregation takes normalised scores, this could be due to a shift in the overall mean signal due to a long tail of highly enriched sites, or a more general shift in the analysis.

To characterise this further, we considered the BAF155 signal partitioned into different genomic regions based on the following hierarchy; within 100bp of a Category A TSS, within 5KB of a Category A TSS, within a Gene extent (but outside of the TSS neighborhood), within 1KB of a distal DHS or intergenic. These are plotted in Supplementary Figure 28. The two gene centric regions have their entire distribution right shifted, with very few positions showing low BAF

signal in the close to TSS position (red) and an even distribution of the positions showing enriched BAF (blue) near TSSs. This suggests that the main features of the BAF signal is due to a broad region around each TSS having considerable enrichment across all tiles; this consequently raises the average mean position. The gentle depletion of BAF around distal sites is a more complex story (magenta curve vs black curve). A shift of the mean signal due to the enrichment around the TSS should give a reasonably flat depletion (without a peak) across distal sites. Although broad, the depletion does have a mode around the central site. This is either due to genuine low enrichment cases concentrated at this position (31% of the distal DHS probes are in the lowest quartile of the overall distribution whereas 39% of the intergenic probes), but also could be due to clustering effects of unrecognized TSSs, meaning that sites which are at least 5KB from any detected TSS are also more likely to be distant from undetected TSSs. Aggregate depletion of signal is hard to explain with simple models for the main Chip/Chip distribution being due to random, non biological variables and clearly these signals suggest a more complex view of Chip/Chip data with many biological variables influencing the signal readout across every tile.
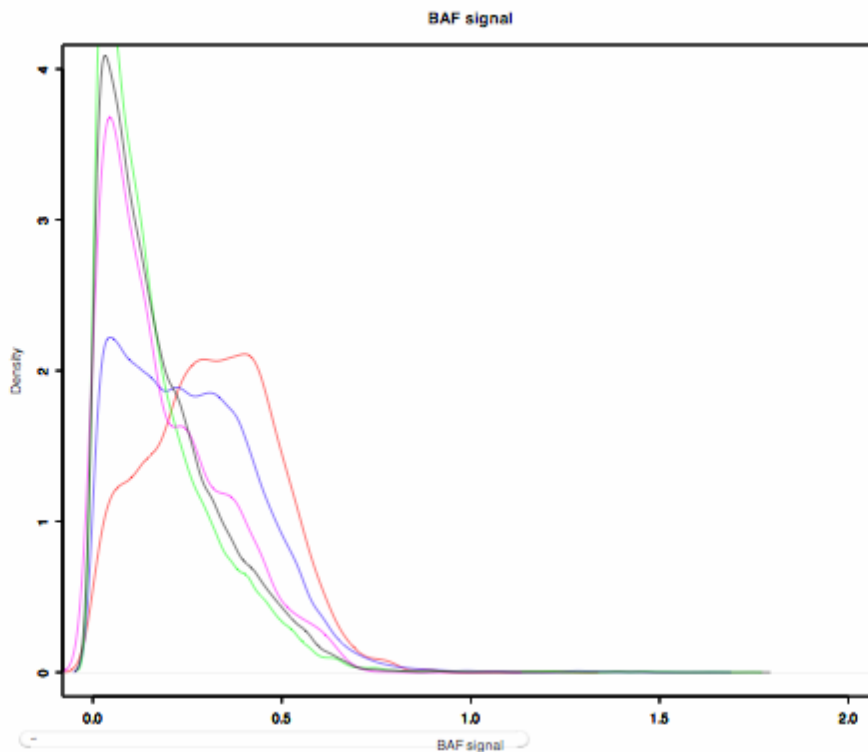
Supplementary Figure 28: BAF signal near different classes of genomic feature. Red is within 100bp of a TSS, blue within 5kb of a TSS, green within gene extents, magenta within 1kb of a distal DHS, and black intergenic.

S3.8.2   Sheared chromatin

This gel image in Supplementary Figure 29 displays sheared chromatin that was prepared from unstimulated HeLaS3 cells and used in BAF155 and BAF170 ChIP-chips (sample lanes 1 to 3,

with each lane containing a separate biological replicate). For comparison, lanes 4 and 5 show sheared chromatin that was prepared from interferon gamma-stimulated HeLaS3 cells and used in Stat1 ChIP-chips, a transcription factor characterized to have a point source binding profile.
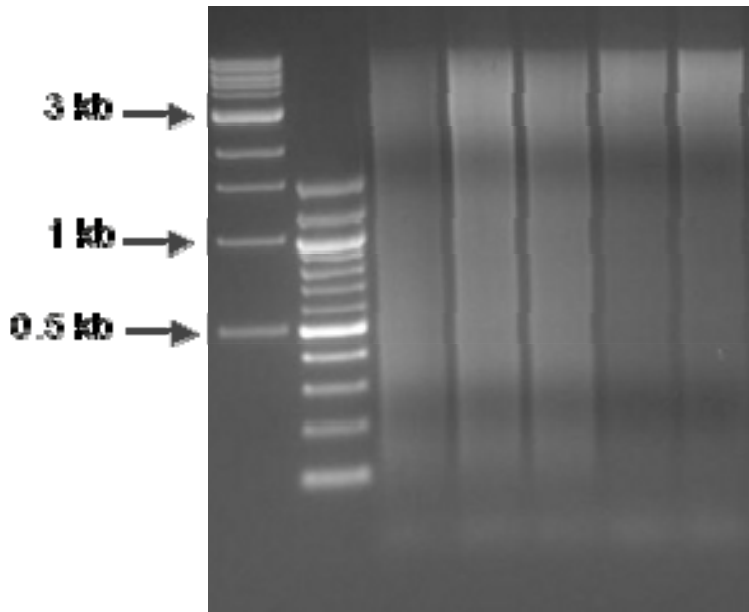
Supplementary Figure 29: Sheared chromatin used in BAF155, BAF170, and STAT1 ChIP Experiments

S3.9 Prediction of TSS activity from chromatin modifications

An SVM was used to predict the transcriptional state of the last exon in HeLa and GM06990 cells based on the presence of various histone modifications.

The SVM input data set contains individual training patterns labeled as positive or negative according to the assayed activity of transcripts measured by the activity of internal exons from the Affymetrix tiling arrays. Each pattern is a vector of individual measurements from five histone modification assays: H3K4me1, H3K4me2, H3K4me3, H3ac, H4ac. The data set is comprised of 529 patterns, of which 231 are negative and 298 are positive.

The performance of the SVM is measured using 10-fold cross-validation. This procedure involves splitting the data set at random into 10 equally sized parts. During each step of cross validation, the SVM is trained on 90% of the data, and the resulting classifier is evaluated on the remaining 10%. To compute the final accuracy, the predictions for all ten test sets are combined.

The SVM uses a radial basis kernel function $K(x,y) = e^{\gamma\|x-y\|^2}$. The width parameter \gamma as well as the SVM soft margin parameters C are selected via internal cross-validation within each training set, considering $C \in \{0.001, 0.1, 1, 10, 1000\}$ and $\gamma \in \{0.001, 0.1, 1, 10\}$.

The SVM produced an accuracy of 88% for HeLa, and 91% for GM06990.

S3.10 RFBR Identification Methods

S3.10.1   Identification of RFBRs in ChIP-chip experiments

All pre-processing steps were performed using existing methods (*normalizeWithinArrays, normalizeBetweenArrays, lmFit, and eBayes*) from the R package *limma* in Bioconductor[90]. After scanning and image extraction, Cy5 (ChIP DNA) and Cy3 (input) signal values were normalized within each array by applying either intensity-dependent Loess correction based on control probes or median-scaling normalization. To combine replicates, we used quantile-normalization between arrays and a linear model-fitting strategy to estimate an average log-ratio for each probe.

For NimbleGen platform arrays, we used a computational peak-finding strategy called *MPeak* which models binding profiles as triangles with peaks at binding sites, estimates a P-value for significance based on the average of the probe signals defining the triangle, and adjusts the P-value cutoff for multiple-testing by False Discovery Rate (FDR) control[91]. We applied *MPeak* on the average profile over replicates, as well as on individual array experiments. To define binding sites, we selected significant peaks at 1, 5, and 10% FDR predicted in the average profile that are supported by peak predictions (at the same FDR) in at least 2 out of 3 replicates.

For PCR arrays, a variation on the single-array error model was used to define PCR probes as significantly enriched[92]. Instead of assuming a standard normal distribution for the test statistics representing the PCR probes, we used the R package *locfdr* to estimate the parameters of the normal distribution which best fit the middle range of the test statistics[93-95]. We used this estimated distribution to assign P-values and FDR values for the test statistics based on individual array experiments and for the weighted-average test statistics based on combinations of replicate array experiments. To define enriched binding regions, we selected PCR probes at less than 1, 5, 10% FDR based on their weighted-average test statistics which are also defined as enriched in 2 out of 3 replicates based on P-value <0.01 for the UCSD PCR arrays and P-value <0.05 for the Sanger PCR arrays.

For both array platforms, binding sites within 1 kb of each other were combined to define binding regions. The midpoint of each binding region was then used to define a "point-source" binding peak.

For Affmetrix platform, differential behavior at four time points (0, 2, 8 and 32 hrs after treatment) was assessed by a modification of Significance Analysis of Microarrays (SAM)[96, 97].

S3.10.2   RFBR Identification in ChIP-sequencing experiments

Human cancer cell HCT116 and HeLa lines were cultured in DMEM containing 10% FCS and subjected to 5-FU and IF-g treatment followed by cross-linking and chromatin-immunoprecipitation using anti-p53 DO1 monoclonal antibody (Santa Cruz) and anti-STAT1 antibody, respectively. The end polished ChIP DNA fragments were ligated to the cloning vector pGIS3, which contains two MmeI recognition sites to form the ChIP DNA library. Purified plasmid prepared from the ChIP DNA library was digested with MmeI, end-polished with T4 DNA polymerase to remove the 3'-dinucleotide overhangs, and the resulting plasmids containing a signature tag from each terminal of the original ChIP DNA insert were self-ligated to form the

single-ditag library. 50 bp paired end ditags (PETs) were released by BamHI digestion, PAGE-purified, then concatenated and separated on a 4-20% gradient TBE-PAGE. An appropriate size fraction (1-2 kb) of the concatenated DNA was excised, extracted and cloned into BamHI-cut pZErO-1 (Invitrogen) to form the final ChIP-PET library for sequencing.

PET sequences containing 18 bp from 5' and 18 bp from 3' ends of the original ChIP DNA fragments were extracted from the raw sequences obtained from the PET library, and mapped to human genome assembly hg17. The process of PET extraction and mapping is essentially the same as previously described for cDNA analysis[32]. The specific mapping criteria are that both the 5' and 3' signatures must be present on the same chromosome, on the same strand, in the correct orientation (5'-3'), with a minimal 17 bp match, and within 4 kb of genomic distance.

S3.10.3 TSS Positional Specificity of RFBRs

The raw data of a ChIP-chip experiment was formatted so that each probe was represented as its mapped genomic coordinates associated with a measured signal level. Given a certain set of anchor coordinates, such as transcription start sites, the relative genomic distance between each probe and its nearest TSS was calculated. Then the signal associated with the probe was mapped to the specific distance, and signals at the distance were averaged across all TSSs. Smoothed plots for average ChIP-chip signals vs. distances to TSSs were made by stepping through distances by windows of 100 data points and taking the average. TSSs were separated according to whether they overlap with CpG islands or not (CpG+/-) and whether the transcript was detected according to Su *et al*[98] (the presence/absence calls). The TSS-averaged signal was plotted for cMyc, Sp3, cJun and STAT1.

S3.11 Detection of overrepresented motifs with *ab initio* methods

RFBRs bound by many sequence-specific factors are enriched for their motifs. We examined 31 ChIP-chip datasets generated for 18 sequence-specific factors for the presence of sequence motifs. For ten datasets, the cognate motif matrices in TRANSFAC[99] were found to be overrepresented in RFBRs compared to randomised genomic sequences (P-value 0.001; see Frith, M. C. et al[100]). Of the 18 factors assayed, nine have at least one dataset that is enriched for its corresponding motif. For seven datasets, the motif could be uncovered using an ab initio program. Supplementary Table 11 summarizes the enrichment and discovery results. Some of the ab initio-predicted matrices contain more conserved positions than those reported in TRANSFAC (Supplementary Figure 30), indicating that our RFBR datasets can be used to improve the motif definitions. However, the datasets for 9 factors were not found to contain an enriched TRANSFAC motif nor could any motif be identified using ab initio methods. There are a number of possible explanations for this lack of apparent sequence specificity – that the TRANSFAC motifs are not accurate; that in vitro binding preferences do not fully reflect the sites that are bound in vivo; and that the antibodies used in the ChIP-chip studies recognize other sequence-bound elements or other factors that may have caused experimental failure. It is important to remember that in a ChIP-chip experiment, protein-protein interactions can occur in addition to direct protein-DNA interactions; therefore, for complex interactions involving

multiple factors, not every identified DNA segment will have a sequence-specific motif that is associated with the particular factor under study in that experiment.
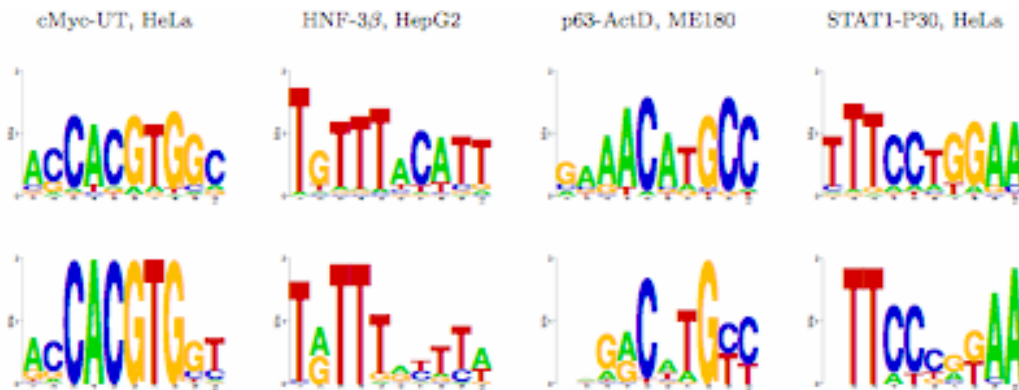
Supplementary Figure 30: Established and derived sequence motifs for selected sequence-specific protein factors. The upper and lower rows depict the TransFac motifs and motifs deduced ab initio from the RFBRs, respectively. The height of each letter corresponds to the relative information content at that position in the motif. Data are shown for the four indicated proteins, with the data in each case generated using the indicated cell lines.

Supplementary Table 11: Motif enrichment in RFBRs of sequence-specific transcription factors. The "Enriched in PSSM" column indicates whether the RFBRs of a factor as a she are enriched in the motif of the factor as described by the position specific scoring matrix (PSSM) in the "PSSM Accession in TRANSFAC" column. Enrichment is defined by using Clover[100] at P-values less that 0.001. The "Motif found ab initio" indicates whether any of the three programs BioProspector[101], MDscan[102], and WEEDER[103] could discover the cognate motif.

Dataset	PSSM available?	PSSM Accession in TRANSFAC	Enriched in PSSM?	Motif found *ab initio*?
ALL_STAT1gIF_HeLa	YES	STATx.M00223	YES	No
ALL_STAT1_HeLa	YES	STATx.M00223	NO	No
NG_STAT1-NASA_HeLa	YES	STATx.M00224	NO	No
NG_STAT1-P30_HeLa	YES	STATx.M00223	YES	Yes
NG_STAT1-Yale_HeLa	YES	STATx.M00223	NO	No
UCSD_STAT1-P30_HeLa	YES	STATx.M00223	YES	Yes
ALL_cMyc_HeLa	YES	Myc.M00799	NO	No
NG_cMyc-Qt_2091	YES	Myc.M00799	NO	No
NG_cMyc-St_2091	YES	Myc.M00799	NO	No
NG_cMyc-UCD_HeLa	YES	Myc.M00799	NO	No
NG_cMyc-UT_HeLa	YES	Myc.M00799	YES	Yes
ALL_p53_HCT116	YES	p53 decamer.M00761	YES	No
AFFX_p63-ActD_ME180	YES	p53 decamer.M00761	YES	Yes
AFFX_p63-noAD_ME180	YES	p53 decamer.M00761	NO	No
NG_Sp1_HCT116	YES	Sp1.M00196	NO	No

NG_Sp1_JURKAT	YES	Sp1.M00196	NO	No
NG_Sp1_K562	YES	Sp1.M00196	NO	No
NG_Sp3_HCT116	YES	Sp3.M00665	NO	No
NG_Sp3_JURKAT	YES	Sp3.M00665	NO	No
NG_Sp3_K562	YES	Sp3.M00665	NO	No
NG_E2F1_HeLa	YES	E2F.M00803	YES	No
NG_E2F4_2091	YES	E2F-4:DP-1.M00738	NO	No
NG_cJun_HeLa	YES	CRE-BP1:c-Jun.M00041	NO	No
Sanger_HNF3b_HePG2	YES	HNF-3.M00791	YES	Yes
Sanger_HNF4a_HePG2	YES	HNF-4.M00134	YES	Yes
Sanger_USF1_HePG2	YES	USF.M00217	YES	No
AFFX_CEBPe_HL60	YES	C/EBP.M00770	YES	Yes
AFFX_CTCF_HL60	See Below	N/A	NO	No
AFFX_PU1_HL60	YES	PU.1.M00658	NO	No
AFFX_RARecA_HL60	YES	RAR.M00762	NO	No
AFFX_p300_HL60	YES	p300.M00033	NO	No
NG_BAF155_HeLa	NO	N/A	N/A	N/A
NG_BAF170_HeLa	NO	N/A	N/A	N/A
UCSD_Suz12_HeLa	NO	N/A	N/A	N/A
AFFX_Brg1_HL60	NO	N/A	N/A	N/A
AFFX_SIRT1_HL60	NO	N/A	N/A	N/A
FOS	No RFBR at 5% FDR			

S3.12 Significance of RFBR enrichments near GENCODE TSSs

In order to assess the significance of enrichments of RFBRs near GENCODE TSSs, we have carried out a random simulation. First, we calculated the observed number of RFBRs near GENCODE TSSs for each ChIP experiment. Then, we randomly generated a set of fragments with their total number, length distribution, and ENCODE region distribution matching to those of the experimental RFBRs. This set was used to compute an expected number of RFBRs near TSSs. Repetitive elements were excluded in our simulation and the randomization was repeated 500 times to obtain the average expected number of RFBRs near TSSs. In the end, the observed number of RFBRs near GENCODE TSSs was divided by this expected number to yield the relative enrichment that is depicted on y-axis in Supplementary Figure 31. As shown in this figure, our simulation indicates that for most ChIP experiments the enrichment of their RFBRs near GENCODE TSSs is significant (>1.0). Each point in Supplementary Figure 31 represents one ChIP experiment.
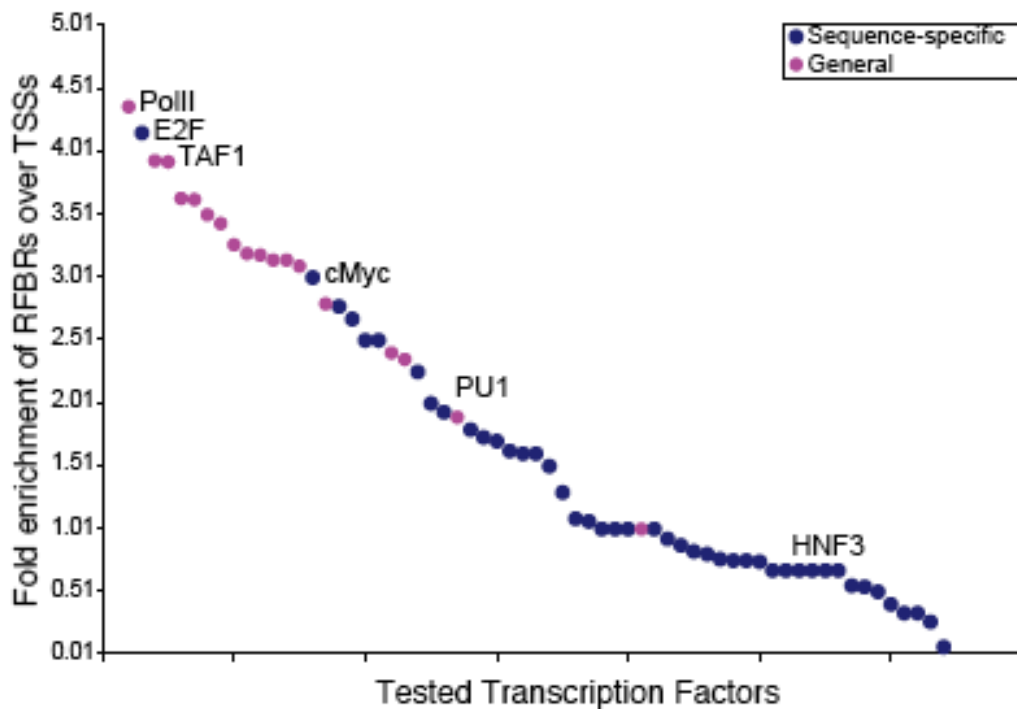
Supplementary Figure 31: Distribution of RFBRs relative to GENCODE TSSs. The y-axis depicts the relative enrichment of RFBRs at GENCODE TSSs, while the x-axis shows the order of factors tested by ChIP experiments with respect to this enrichment. Random expectation corresponds to an enrichment of 1.0. Pink circles represent factors expected to be general for many promoters (e.g., polymerase), whereas blue circles represent factors expected to be more sequence-specific. A handful of representative factors are labelled.

S3.12.1   Supplemental table provided in accompanying Excel spreadsheet

This table shows for each ChIP experiment the percentage of RFBRs in various distance (in a 1 kb increment) in relation to category A TSSs. Data in this table shows that more than half of RFBRs for SIRT1 are 20 kb away from TSSs and thus are generally in "gene deserts."

This table is provided in the included supplemental Excel spreadsheet on the worksheet labeled S3.12.1.

S3.13 Integration approaches to generate Regulatory Cluster lists

We implemented four complementary approaches to integrate the data from 129 ChIP datasets. The *Z-score method* (see Supplement S3.13.1) normalizes ChIP scores from individual experiments and assigns a cumulative normalised score to genomic intervals. The *Naïve Bayes method* (see Supplement S3.13.2) combines ChIP scores from different experiments after thresholding and weighting them based on a set of known promoters. Though both these methods use continuous ChIP scores, Naïve Bayes makes an assumption on how a typical promoter is

while Z-score treats all the datasets the same way. The third and fourth methods, *tree-weighting* (see Supplement S3.13.3) and *majority-voting* (see Supplement S3.13.4) use FDR thresholded ChIP scores. Tree-weighting method weights the counts from ChIP hits based on both the TSS enrichments of individual experiments and the correlation between experiments. The last method, majority-voting, evaluates the level of experimental support for each genomic position by taking into account the number of cross-lab, cross-platform or cross-factor ChIP hits matching that position.

Each of these integration methods is described in detail below. From these four methods we constructed two composite lists: A "small union list" of 965 regions from the union of approaches 1 and 2 (Z-score and Naive Bayes) and a "large union list" of 1393 regions from the union of the four methods. Both of these lists are available from the UCSC browser.

S3.13.1   Integration Approach 1: Z-score method

We first selected a set of promoter-specific experiments that we wished to integrate to identify potentially novel promoters[30]. We then matched corresponding datapoints between datasets. To accomplish this, we divided the ENCODE region into ~24,000 reference intervals that largely corresponded to the probes from the 2 PCR tiling arrays. The ChIP intensities were converted to Z-scores and assigned to the reference intervals.

To identify genomic regions identified by multiple experiments, we then summed the Z-scores for each interval across all the experiments (setting negative Z-scores to zero). To estimate a P-value for the summed score of each interval, we shuffled the data for each experiment within the ~24,000 reference intervals and then re-summed the values. We repeated this 10 times, to get a confidence value for each of the ~24,000 intervals. We used a cutoff of p<0.001 to define a list of putative promoters from this integrated analysis and merged regions that were within 100 bp of each other.

Supplementary Table 12: Experimental data in the "promoter" group used in the Z-score based method.

Experimental data in "promoter" group for the Z-score method:	
HCT116_Sp1_ChIP	H4ac_K562_1.wig.txt
HCT116_Sp3_ChIP	GM06990_61105_Regulome_ENCODE.txt
Jurkat_Sp1_ChIP	K562_061105_Regulome_ENCODE.txt
Jurkat_Sp3_ChIP	SKNSH_061105_Regulome_ENCODE.txt
K562_Sp1_ChIP	CACO2_061105_Regulome_ENCODE.txt
K562_Sp3_ChIP	encodeUcsdChipAch3Imr90_f.txt
CTCF_00hr	encodeUcsdChipHeLaH3H4acH3_p0.txt
Brg1_00hr	encodeUcsdChipHeLaH3H4acH4_p0.txt
CEBPe_00hr	encodeUcsdChipHeLaH3H4dmH3K4_p0.txt
HisH4_00hr	encodeUcsdChipHeLaH3H4RNAP_p0.txt

P300_00hr	encodeUcsdChipHeLaH3H4stat1_p0.txt
Pol2_00hr	encodeUcsdChipHeLaH3H4TAF250_p0.txt
PU1_00hr	encodeUcsdChipHeLaH3H4tmH3K4_p0.txt
RARecA_00hr	encodeUcsdChipMeh3k4Imr90_f.txt
H3K27T_00hr	encodeUcsdChipRnapHct116_f.txt
SIRT1_00hr	encodeUcsdChipRnapHela_f.txt
H3K4me1_GM06990_1.wig.txt	encodeUcsdChipRnapImr90_f.txt
H3ac_GM06990_1.wig.txt	encodeUcsdChipRnapThp1_f.txt
H3ac_K562_1.wig.txt	encodeUcsdChipTaf250Hct116_f.txt
H3K4me2_GM06990_1.wig.txt	encodeUcsdChipTaf250Hela_f.txt
H3K4me2_K562_1.wig.txt	encodeUcsdChipTaf250Imr90_f.txt
H3K4me3_GM06990_2.wig.txt	encodeUcsdChipTaf250Thp1_f.txt
H3K4me3_K562_1.wig.txt	encodeUcsdNgHeLaH3K4me3_p0.txt
H4ac_GM06990_1.wig.txt	encodeUcsdNgHeLaRnap_p0.txt

S3.13.2   Integration Approach 2: Naïve Bayes Method

Training Set: We trained a Naïve Bayes classifier to predict regulatory regions. A training set of real TSS and non-TSS regions was built as follows. The set of real TSS (*positive set*) was based on CAGE (5' Cap Analysis of Gene Expression) and GIS-PET (Gene Identification Signature Paired-End ditag) clusters. All the CAGE tags in ENCODE regions were clustered and only clusters with 4 or more tags were kept, producing 797 examples. These 797 examples were further filtered by intersecting them with the 5'-ends of GIS-PETs in either HCT116 or MCF7 cell lines to obtain 223 positive examples. The negative regions were selected from deep introns (3rd or deeper) and the CDS parts of deep exons. The introns were verified not to overlap with exons from other transcripts, TARs or transfrags. These selection criteria resulted in 225 regions, spanning approximately 450kb. All possible uniformly distributed and non-overlapping windows of 300bp were extracted, which gave 1365 negative examples (*negative set*).

Training of the Bayesian Model: For each region in the training set, the average ChIP enrichment scores corresponding to different ChIP experiments within a 1KB window around the TSS were extracted. Using these scores, each ChIP dataset was binarized at a cutoff that maximized the correlation between the training set and the binarized ChIP dataset. The training set thus consisted of positive and negative examples of a TSS, each associated with a binary vector describing the presence or absence pattern of each TF within that example region. The prediction of the model is the log odds of a TSS given data. The log odds of a TSS is defined as:

$$log\ odds_{TSS} = \log[\frac{P(TSS\ |\ all\ data)}{P(non-TSS\ |\ all\ data)}]$$

Under the Naïve-Bayes assumption that all datasets are independent, the log odds can be separated into two terms:

$$log\ odds_{TSS} = \log[\frac{P(TSS)}{P(non-TSS)}] + \sum_{all\ data} \log[\frac{P(D_i = x\ |\ TSS)}{P(D_i = x\ |\ non-TSS)}]$$

The first term is the prevalence of the TSSs. In the second term, D_i is a binary variable that denotes the ith dataset. If $x=1$ (i.e., the average score for ChIP dataset D_i around the given TSS is above its threshold and hence the represented factor is present in the example), we call the contribution to the second term PLL (positive log likelihood) and if $x=0$ we call it NLL (negative log likelihood). For each dataset, both PLL and NLL were measured empirically from the training set.

Scanning of ENCODE Regions with the Bayesian Model: Once the appropriate Bayesian weights were calculated (PLL and NLL), ENCODE regions were scanned using the model to predict new regulatory regions. To build a map of regulatory regions we calculated, for each base pair in the ENCODE regions, the log odds score of it being part of a TSS by summing contributions from individual ChIP datasets at that base pair. For each dataset, the contribution is either PLL or NLL depending on whether that base pair is called present or absent in that dataset based on the respective binarization cutoff. Contiguous base pairs with a log odds score above a chosen cutoff were joined to define putative regulatory regions. The final list of regions was obtained by pruning all the regions shorter than 300bp and by joining regions separated by less than 200bp. The score cutoff was calculated based on the expected prevalence of TSSs in the entire ENCODE region but was later made more stringent to obtain a higher confidence set of predictions.

S3.13.3 Integration Approach 3: Tree-weighting Method

In this method, we first calculated the fold-enrichment F_i of RFBRs near TSSs for each experiment i. Briefly, the fold-enrichment was defined as the number of RFBRs near a TSS (-2 kb to +200 bp) divided by a corresponding number derived from a simulation in which the RFBRs for experiment i were randomly shuffled and placed back on the individual ENCODE regions (excluding repeats). Separately, we constructed a cluster tree of all ChIP experiments based on their similarities with regard to the genomic distribution of RFBRs. This is very similar to the construction of the whole-track correlation scores (described above). A weight W_i was assigned to each leaf (i.e., experiment i) using a branch-length division method[104]. The primary purpose of this clustering and weight-assigning step was to minimize the bias introduced by the same factors being tested in multiple conditions and several platforms. In this analysis, the overall weight for a particular factor would be apportioned between individual experiments with a ratio between 1/n and 1, where n is the number of experiments in which this factor was probed. We then made a union list of RFBRs from individual experiments on the condition that overlapping (by $\geq$ 50 bp) RFBRs were merged into a single region. This union contained 3227 regions (average length ~1.1 kb). A score S_j was subsequently assigned to each region j in the union list. It was defined as $\sum (N_i \times F_i \times W_i)$ where N_i was the number of RFBRs within this region j from experiment i, and F_i and W_i were the fold-enrichment and weight computed for experiment i, respectively. Finally, in order to make this integrative list comparable with those from the other three methods we used a S_j threshold of 0.05 to generate a total of 714 regions, based on the distribution of scores in these regions. This cutoff approximately corresponded to 2 ChIP hits per region.

S3.13.4   Integration Approach 4: Voting Method

We developed a voting method to identify genomic regions that were determined by at least two ChIP datasets from different labs, or on different factors, or on different platforms. Each experiment was given a weight based on two measures: 1) the number of different investigators within ENCODE who studied the sequence-specific transcription factor, histone modification, PolII, or TAF1, 2) the number of different platforms used in these studies. An experiment would be assigned a maximum weight of one if the factor, modification, or binding in question was studied by a single investigator using a single platform type. Otherwise, a weight smaller than one and inversely proportional to the multiplicity was assigned. Supplementary Table 13 shows the weights used for each experiment.

We used the weighted RFBRs to determine genomic regions marked by different groups of RFBRs at different FDR levels. The 129 experiments were stratified into two groups: those for sequence specific transcription factors (Sequence Specific Voting List) and the remaining ones for histone modifications, Pol2, and TAF1 binding. For each experiment, all the base pairs within an RFBR were assigned the same weight and for each base pair these weights were summed across all the experiments in each of the two groups. This gave a continuous score over the ENCODE regions. The score at a given base position is i) zero if that base doesn't appear in any of the RFBRs, ii) above zero if that base gets support from at least one experiment, iii) above one if that base is supported by at least two experiments done either using the same platform by different investigators or using different platforms by the same investigator. For each group, two different thresholds were used (zero and one) to convert the continuous scores to genomic regions. All the base pairs above the threshold were clustered together to define a genomic region whose score was the mean score for all the base pairs contained within it.

Supplementary Table 13: Weights used in the voting method.

Peakfile	designfile	Inverse Weight	Weight	lab	TR	HisPol TAF	TF
AFFX_Brg1-00_HL60	Affy.all	8	0.125	Affy	1	0	1
AFFX_Brg1-02_HL60	Affy.all	8	0.125	Affy	1	0	1
AFFX_Brg1-08_HL60	Affy.all	8	0.125	Affy	1	0	1
AFFX_Brg1-32_HL60	Affy.all	8	0.125	Affy	1	0	1
AFFX_CEBPe-00_HL60	Affy.all	8	0.125	Affy	1	0	1
AFFX_CEBPe-02_HL60	Affy.all	8	0.125	Affy	1	0	1
AFFX_CEBPe-08_HL60	Affy.all	8	0.125	Affy	1	0	1
AFFX_CEBPe-32_HL60	Affy.all	8	0.125	Affy	1	0	1
AFFX_CTCF-00_HL60	Affy.all	8	0.125	Affy	1	0	1
AFFX_CTCF-02_HL60	Affy.all	8	0.125	Affy	1	0	1
AFFX_CTCF-08_HL60	Affy.all	8	0.125	Affy	1	0	1
AFFX_CTCF-32_HL60	Affy.all	8	0.125	Affy	1	0	1
AFFX_H3ac-00_HL60	Affy.all	8	0.125	Affy	1	1	0
AFFX_H3ac-02_HL60	Affy.all	8	0.125	Affy	1	1	0
AFFX_H3ac-08_HL60	Affy.all	8	0.125	Affy	1	1	0
AFFX_H3ac-32_HL60	Affy.all	8	0.125	Affy	1	1	0
AFFX_H4ac-00_HL60	Affy.all	8	0.125	Affy	1	1	0
AFFX_H4ac-02_HL60	Affy.all	8	0.125	Affy	1	1	0

AFFX_H4ac-08_HL60	Affy.all	8	0.125	Affy	1	1	0
AFFX_H4ac-32_HL60	Affy.all	8	0.125	Affy	1	1	0
AFFX_P300-00_HL60	Affy.all	8	0.125	Affy	1	0	1
AFFX_P300-02_HL60	Affy.all	8	0.125	Affy	1	0	1
AFFX_P300-08_HL60	Affy.all	8	0.125	Affy	1	0	1
AFFX_P300-32_HL60	Affy.all	8	0.125	Affy	1	0	1
AFFX_p63-ActD_ME180	Affy.all	4	0.25	Affy	1	0	1
AFFX_p63-noAD_ME180	Affy.all	4	0.25	Affy	1	0	1
AFFX_PolII-00_HL60	Affy.all	8	0.125	Affy	1	1	0
AFFX_PolII-02_HL60	Affy.all	8	0.125	Affy	1	1	0
AFFX_PolII-08_HL60	Affy.all	8	0.125	Affy	1	1	0
AFFX_PolII-32_HL60	Affy.all	8	0.125	Affy	1	1	0
AFFX_PU1-00_HL60	Affy.all	8	0.125	Affy	1	0	1
AFFX_PU1-02_HL60	Affy.all	8	0.125	Affy	1	0	1
AFFX_PU1-08_HL60	Affy.all	8	0.125	Affy	1	0	1
AFFX_PU1-32_HL60	Affy.all	8	0.125	Affy	1	0	1
AFFX_RARecA-00_HL60	Affy.all	8	0.125	Affy	1	0	1
AFFX_RARecA-02_HL60	Affy.all	8	0.125	Affy	1	0	1
AFFX_RARecA-08_HL60	Affy.all	8	0.125	Affy	1	0	1
AFFX_RARecA-32_HL60	Affy.all	8	0.125	Affy	1	0	1
AFFX_SIRT1-00_HL60	Affy.all	16	0.0625	Affy	1	0	1
AFFX_SIRT1-02_HL60	Affy.all	16	0.0625	Affy	1	0	1
AFFX_SIRT1-08_HL60	Affy.all	16	0.0625	Affy	1	0	1
AFFX_SIRT1-32_HL60	Affy.all	16	0.0625	Affy	1	0	1
AFFX_TFIIB-32_HL60	Affy.all	4	0.25	Affy	1	1	0
Ng_TAF1-Yale_HeLa	Ng.all	1	1	Ng	1	1	0
Ng_Sp1_HCT116	Ng.all	3	0.333333333	Ng	1	0	1
Ng_Sp1_Jurkat	Ng.all	3	0.333333333	Ng	1	0	1
Ng_Sp1_K562	Ng.all	3	0.333333333	Ng	1	0	1
Ng_Sp3_HCT116	Ng.all	3	0.333333333	Ng	1	0	1
Ng_Sp3_Jurkat	Ng.all	3	0.333333333	Ng	1	0	1
Ng_Sp3_K562	Ng.all	3	0.333333333	Ng	1	0	1
Ng_STAT1-NASA_HeLa	Ng.all	2	0.5	Ng	1	0	1
Ng_STAT1-P30_HeLa	Ng.all	1	1	Ng	1	0	1
Ng_STAT1-Yale_HeLa	Ng.all	2	0.5	Ng	1	0	1
Ng_BAF155_HeLa	Ng.all	2	0.5	Ng	1	0	1
Ng_BAF170_HeLa	Ng.all	2	0.5	Ng	1	0	1
Ng_E2F1_HeLa	Ng.all	1	1	Ng	1	0	1
Ng_E2F4_2091	Ng.all	1	1	Ng	1	0	1
Ng_cMyc-UCD_HeLa	Ng.all	1	1	Ng	1	0	1
Ng_cMyc-UT_HeLa	Ng.all	1	1	Ng	1	0	1
Ng_cMyc-Qt_2091	Ng.all	2	0.5	Ng	1	0	1
Ng_cMyc-St_2091	Ng.all	2	0.5	Ng	1	0	1
Ng_cJun_HeLa	Ng.all	1	1	Ng	1	0	1
Ng_Fos_HeLa	Ng.all	1	1	Ng	1	0	1
ALL_STAT1_HeLa	ALL.all	2	0.5	PET	1	0	1
ALL_STAT1gIF_HeLa	ALL.all	2	0.5	PET	1	0	1

ALL_cMyc_HeLa	ALL.all	1	1	PET	1	0	1
ALL_p53_HCT116	ALL.all	1	1	PET	1	0	1
Sanger_H3ac_GM06990	Sanger.all	3	0.333333333	Sanger.PCR	1	1	0
Sanger_H3ac_HeLa	Sanger.all	3	0.333333333	Sanger.PCR	1	1	0
Sanger_H3ac_K562	Sanger.all	3	0.333333333	Sanger.PCR	1	1	0
Sanger_H4ac_GM06990	Sanger.all	3	0.333333333	Sanger.PCR	1	1	0
Sanger_H4ac_HeLa	Sanger.all	3	0.333333333	Sanger.PCR	1	1	0
Sanger_H4ac_K562	Sanger.all	3	0.333333333	Sanger.PCR	1	1	0
Sanger_H3K4me1_GM06990	Sanger.all	2	0.5	Sanger.PCR	1	1	0
SUZ	Sanger.all	2	0.5	Sanger.PCR	1	1	0
Sanger_H3K4me2_GM06990	Sanger.all	3	0.333333333	Sanger.PCR	1	1	0
Sanger_H3K4me2_HeLa	Sanger.all	3	0.333333333	Sanger.PCR	1	1	0
Sanger_H3K4me2_K562	Sanger.all	3	0.333333333	Sanger.PCR	1	1	0
Sanger_H3K4me3-2_GM06990	Sanger.all	3	0.333333333	Sanger.PCR	1	1	0
Sanger_H3K4me3_HeLa	Sanger.all	3	0.333333333	Sanger.PCR	1	1	0
Sanger_H3K4me3_K562	Sanger.all	3	0.333333333	Sanger.PCR	1	1	0
Ng_H3ac-P0_HeLa	Ng.all	2	0.5	UCSD.Ng	1	1	0
Ng_H3ac-P30_HeLa	Ng.all	2	0.5	UCSD.Ng	1	1	0
Ng_H4ac-P0_HeLa	Ng.all	1	1	UCSD.Ng	1	1	0
Ng_H3K4me2-P0_HeLa	Ng.all	2	0.5	UCSD.Ng	1	1	0
Ng_H3K4me2-P30_HeLa	Ng.all	2	0.5	UCSD.Ng	1	1	0
Ng_H3K4me3-P0_HeLa	Ng.all	2	0.5	UCSD.Ng	1	1	0
Ng_H3K4me3-P30_HeLa	Ng.all	2	0.5	UCSD.Ng	1	1	0
Ng_PolII-P0_HeLa	Ng.all	2	0.5	UCSD.Ng	1	1	0
Ng_PolII-P30_HeLa	Ng.all	2	0.5	UCSD.Ng	1	1	0
UCSD_H3ac_IMR90	UCSD.all	2	0.5	UCSD.PCR	1	1	0
UCSD_H3ac-P0_HeLa	UCSD.all	4	0.25	UCSD.PCR	1	1	0
UCSD_H3ac-P30_HeLa	UCSD.all	4	0.25	UCSD.PCR	1	1	0
UCSD_H4ac-P0_HeLa	UCSD.all	2	0.5	UCSD.PCR	1	1	0
UCSD_H4ac-P30_HeLa	UCSD.all	2	0.5	UCSD.PCR	1	1	0
UCSD_H3K4me2_IMR90	UCSD.all	2	0.5	UCSD.PCR	1	1	0
UCSD_H3K4me2-P0_HeLa	UCSD.all	4	0.25	UCSD.PCR	1	1	0
UCSD_H3K4me2-P30_HeLa	UCSD.all	4	0.25	UCSD.PCR	1	1	0
UCSD_H3K4me3-P0_HeLa	UCSD.all	2	0.5	UCSD.PCR	1	1	0
UCSD_H3K4me3-P30_HeLa	UCSD.all	2	0.5	UCSD.PCR	1	1	0
UCSD_PolII-P0_HeLa	UCSD.all	8	0.125	UCSD.PCR	1	1	0
UCSD_PolII-P30_HeLa	UCSD.all	8	0.125	UCSD.PCR	1	1	0
UCSD_PolII_HCT116	UCSD.all	4	0.25	UCSD.PCR	1	1	0
UCSD_PolII_IMR90	UCSD.all	4	0.25	UCSD.PCR	1	1	0
UCSD_PolII_THP1	UCSD.all	4	0.25	UCSD.PCR	1	1	0
UCSD_TAF1_HCT116	UCSD.all	4	0.25	UCSD.PCR	1	1	0
UCSD_TAF1_IMR90	UCSD.all	4	0.25	UCSD.PCR	1	1	0
UCSD_TAF1_THP1	UCSD.all	4	0.25	UCSD.PCR	1	1	0
UCSD_TAF1-P0_HeLa	UCSD.all	8	0.125	UCSD.PCR	1	1	0
UCSD_TAF1-P30_HeLa	UCSD.all	8	0.125	UCSD.PCR	1	1	0
UCSD_STAT1-P30_HeLa	UCSD.all	2	0.5	UCSD.PCR	1	0	1
Sanger_HNF3b_HePG2	Sanger.all	1	1	Sanger.PCR	1	0	1

Sanger_HNF4a_HePG2	Sanger.all	1	1	Sanger.PCR	1	0	1
Sanger_USF1_HePG2	Sanger.all	1	1	Sanger.PCR	1	0	1

S3.13.5 Site detection algorithm

The site detection algorithm employs a rank statistics based paradigm where all enrichment sites are ranked based on their intra-replicate ranks and inter-replicate rank consistency. The two fundamental parameters of the site detection model are: (a) signal enrichment; (b) pScore where $pScore = \sigma_p = -10(\log_{10}(pValue))$. The first step in the algorithm entails the application of a lenient threshold, approximating a signal to noise ratio (SNR) slightly greater than 1. This estimate, based on either a fixed pScore (20) or a signal enrichment (log(2)) threshold, captures the maximal number of candidate intervals or seed sites. The second step refines the seeding process and associates statistical significance to each site. This optimization is governed by the following parameters determined both on an intra and inter array basis. Specifically on a per site basis, they comprise of: (a) Rank of pScore per replicate; (b) Sum of the absolute pair-wise rank difference (SAD) across replicates; (c) χ^2 based composite P-value estimate across replicates; The basic optimization in the model involves: minimization of the above three parameters with simultaneous maximization of signal enrichment. Ultimately, seed sites with superior intra-replicate ranks as well as high rank consistency across replicates are expected to dominate the highly significant set of the final sites. The site rankings are accompanied by site-level *meta* P-value and composite signal enrichment across replicates. Further segmentation of the ranked sites is possible via P-value or signal enrichment criteria individually or by a criterion derived from the composite. Sensitivity (reported for H4ac data) obtained following segmentation of data using the filters: (a) *meta* P-value of 10^{-5}: 88%; (b) array enrichment of 0.2: 87%; (c) composite of (a) and (b): 95%.

Numbers not shown include 6 between NB and TW and 19 between V and Z. All numbers sum up to 1393 non-overlapping regions.
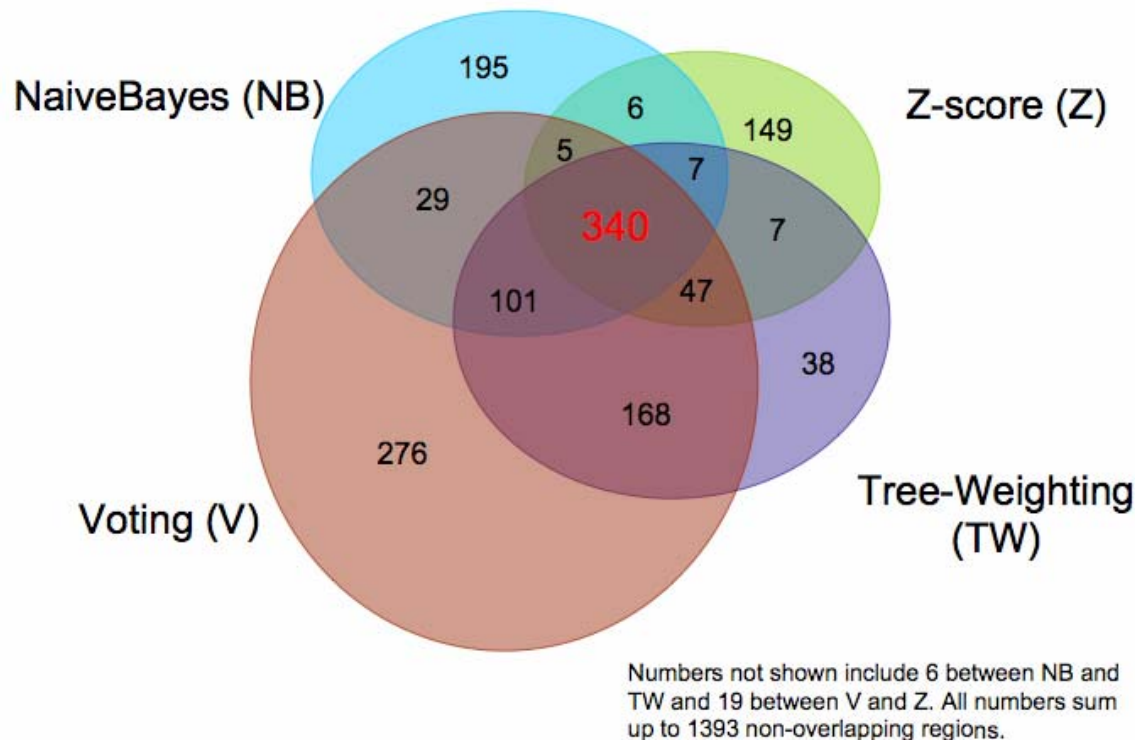
Supplementary Figure 32: Comparison of the composite Regulatory Cluster lists generated by four methods. The four methods independently generated 793 (NB), 656 (Z), 828 (TW), and 1327 (V) Regulator Clusters respectively. To make the data directly comparable and resolve the caveat that a region from one method could overlap with multiple regions in another method, we had collapsed all regions from these four methods into 1393 non-overlapping regions. This process resulted in 689, 580, 714, and 985 regions respectively for the four methods above. Shown in this Venn diagram is the partition of these 1393 regions into different sets according to how many methods identified them. For instance, 340 regions were identified by all four methods. Numbers not shown include 6 between NB and TW only and 19 between V and Z only. All numbers sum up to 1393 non-overlapping regions.

S3.14 The overlap of Regulatory Clusters with different TSS evidence classes.

The correspondence of the regulatory clusters with the previously categorized TSSs was investigated by examining the numbers of clusters falling within 2.5kb of TSSs from each category. The table below shows the number and percent of 1393 Regulatory Clusters located within 2.5kb of a Transcription Start Site (TSS) from one of categories. TSS Categories as defined in Table 3 of the main paper. Because a given Regulatory Cluster can fall within 2.5kb of more than one TSS the total of the percents exceeds 100.

Supplementary Table 14: Overlap of Regulatory Clusters with different TSS evidence classes.

| TSS Category (number of TSS in category)	NUMBER OF REGULATORY CLUSTERS	PERCENT OF REGULATORY CLUSTERS
GENCODE 5' ends (1730)	595	42.7
Novel: Sense exon (1437)	405	29.1
Novel: Antisense exon (521)	283	20.3
Novel: TxFrag/RxFrag (639)	363	26.1
Novel: CpG (164)	128	9.2

As Supplementary Table 14 shows, there is a bias towards the GENCODE 5' ends, but not obviously across the other classes.

S3.15 Cloning putative novel promoters

Of the 233 putative promoters that were cloned and tested, 186 had at least one CAGE or GIS-PET supporting a TSS in that region (of these 186, 113 had only one tag). The remaining 47 putative promoter fragments had no transcript data that supported a TSS in that region. For the 186 that had CAGE or GIS-PET support, we used the 5' end of the CAGE or GIS-PET sequence as the predicted TSS. We then used Primer3 software to design primers by inputting 600 bp of upstream sequence and 100bp downstream of the predicted TSS[105]. Each primer pair was required to flank the transcription start site. For the 47 promoters that lacked transcripts we designed primers to amplify a 1000 bp fragment so that we could clone it in both directions. To the 5' end of each primer, we added 16 basepair tails to facilitate cloning by the Infusion Cloning System (BD Biosciences, Clontech cat no. 639605). (Left primer tail: 5'-CCGAGCTCTTACGCGT-3', Right primer tail: 5'-CTTAGATCGCAGATCT-3') We amplified the fragments using the touchdown PCR protocol previously described[106] and Titanium Taq Enzyme (BD Biosciences, Clontech, cat no 639210). To clone our PCR amplified fragments using the Infusion Cloning System, we combined 2 μl purified PCR product and 100 ng linearized pGL3-Basic vector (Promega). We added this mixture to the Infusion reagent and incubated at 42°C for 30 minutes. After incubation, the mixture was diluted and transformed into competent cells (Clontech cat. No. 636758). We screened clones for insert by PCR and positive clones were prepared as previously described. We quantified DNA with a 96-well spectrophotometer (Molecular Devices, Spectramax 190) and standardized concentrations to 50 ng/μl for transfections.

Supplementary Table 15: Overlap of Experimentally Tested Regulatory Clusters with TSS Categories. The table lists experimental validation results for all the regulatory clusters that were tested by transient-transfection reporter assay (TFXN) and/or RACE. A regulatory cluster might overlap with more than one type of TSS category

			TSS Categories							
			A	B	C	D	E	F	no_ABCDE	no_ABCDEF
Both	Pos	3	1	0	1	0	1	1	1	0
	Neg	17	3	4	7	8	2	3	4	3
	Tested (Pos+Neg)	20	4	4	8	8	3	4	5	3
Either	Pos	85	24	19	14	28	9	23	29	21
	Neg	120	13	13	10	20	9	30	78	59
	Tested (Pos+Neg)	205	37	32	24	48	18	53	107	80
TFXN	Pos	41	8	9	4	12	5	14	16	10
	Neg	122	13	12	12	25	10	31	76	57
	Tested (Pos+Neg)	163	21	21	16	37	15	45	92	67
RACE	Pos	47	17	10	11	16	5	10	14	11
	Neg	15	3	5	5	3	1	2	6	5
	Tested (Pos+Neg)	62	20	15	16	19	6	12	20	16
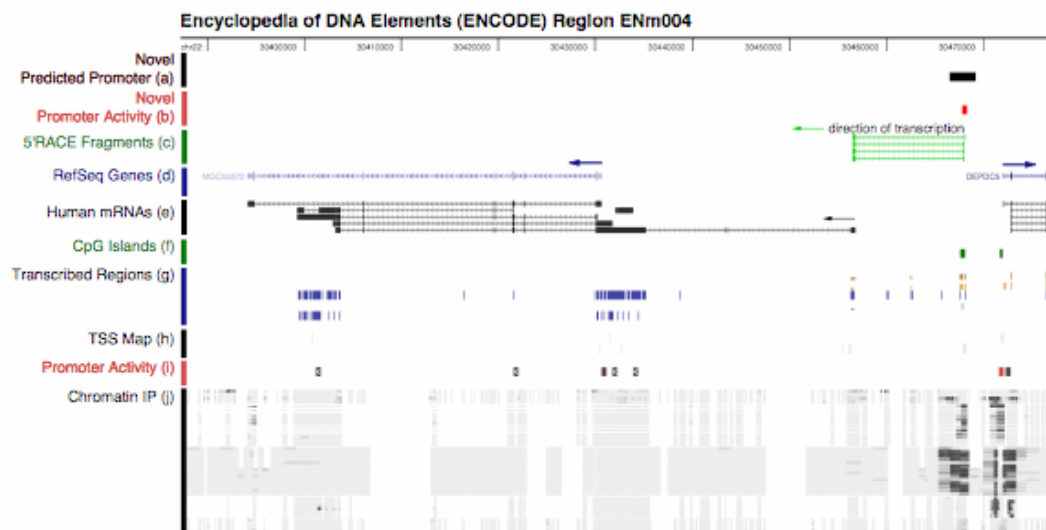
Supplementary Figure 33: Example of a novel promoter supported by the reporter assay and RACE products. a) Region predicted to contain a novel promoter based on the integrated analysis b) Activity of the novel predicted promoter as assayed by the transient

transfection reporter assay c) 5' RACE products show the 5' end of a novel transcript occurs in the novel promoter region d) Annotated RefSeq genes e) Annotated human mRNAs f) Computationally predicted CpG islands g) Transcribed regions experimentally identified with genomic tiling microarrays h) Maps of experimentally identified transcription start sites based on CAGE and GIS-PET sequences i) Fragments assayed for promoter activity by transiently transfected reported constructs (intensity of red is proportional to promoter activity) j) Binding sites of various transcription factors identified by chromatin IP and tiling microarrays. This figure was adapted from the UCSC genome browser.

S3.15.1   Cell culture, transient transfections, and reporter gene activity assays

We performed transfections in 4 cultured human cell lines (Hela, HCT116, HT1080, and CRL1690) as previously described[106]. We seeded 5,000-10,000 cells per well in 96-well plates. Twenty-four hours after seeding, we co-transfected 50 ng of each experimental luciferase plasmid with 10 ng of renilla control plasmid (pRL-TK, Promega Cat. No. E2241) in duplicate using 0.3 µl of FuGene (Roche) transfection reagent per well. We also transfected 24 random genomic fragments as negative controls. Cells were lysed 24-48 hours post-transfection, depending on cell type. We measured luciferase and renilla activity using the PE Wallac Luminometer and the Dual Luciferase Kit (Promega, Cat. No. E1960). We followed the protocol suggested by the manufacturer with the exceptions of injecting 60 µl each of the luciferase and renilla substrate reagents and reading for 5 seconds.

S3.15.2   Data Analysis

The activity data is reported as a transformed ratio of luciferase to renilla. The mean ratio and standard deviation in the 4 cell lines were computed for 24 negative controls. The final promoter activity was computed as the number of standard deviations from the mean for each promoter in each cell line. All the promoters which were at least three standard deviations above the mean ratio of the negatives were called significantly positive.

S3.16 Control for the Ascertainment Bias

The raw enrichment signal of 23 ChIP-chip datasets were compiled for 28 non-GENCODE based clusters. The signals from multiple ChIP-chip regions matching the same regulatory cluster were averaged. For each ChIP-chip dataset, a Mann-Whitney test was performed to compare the signal for 22 RACE-positive and 6 RACE-negative clusters. Supplementary Table 16 lists the two-tailed p-values. None of the datasets suggests that there is a difference in the raw signal for positives vs. negatives.

Supplementary Table 16: Significance from rank sum test for 22 Novel RACE Positive and 6 Novel RACE Negative regulatory clusters.

ChIP-chip Dataset	pvalue

ChIP-chip Dataset	pvalue
Stanford_Sp1_HCT116	0.112
Stanford_Sp1_Jurkat	0.892
Stanford_Sp1_K562	0.088
Stanford_Sp3_HCT116	0.395
Stanford_Sp3_Jurkat	0.427
Stanford_Sp3_K562	0.157
UCDavis_E2F1_HeLa	0.723
UCDavis_Myc_HeLa	0.978
UCSDNg_H3ac_HeLa_p0	0.604
UCSDNg_H3ac_HeLa_p30	1
UCSDNg_H3K4me2_HeLa_p0	0.892
UCSDNg_H3K4me2_HeLa_p30	0.978
UCSDNg_H3K4me3_HeLa_p0	0.764
UCSDNg_H3K4me3_HeLa_p30	0.494
UCSDNg_H4ac_HeLa_p0	0.643
UCSDNg_Pol2_HeLa_p0	0.530
UCSDNg_Pol2_HeLa_p30	0.806
UCSDNg_STAT1_HeLa_p30	0.039
UCSD_STAT1_HeLa_p0	0.764
UCSD_STAT1_HeLa_p30	0.604
UCSD_Suz12_HeLa	0.654
UT_cMyc_HeLa	0.460
UT_E2F4_2091Fibroblast	0.643

S3.17 Classification of functional elements

S3.17.1   SVM Classification of functional elements

We used the Support Vector Machine algorithm to classify DHS segments on the basis of histone modification data. We designed classifiers to distinguish the signature or histone modifications patterns in distal and proximal distance with respect to GENCODE transcriptional start sites.

S3.17.1.1 SVM discrimination of proximal DHS vs. non-proximal DHS

(1) We begin by determining the distance between each DHS and the nearest GENCODE Gene. The GENCODE gene used in the analysis are an aggregate of the known, pseudo, and putative GENCODE subtracks.
(2) Once the distance is calculated, each DHS is placed into a proximal or non-proximal category. In order to be considered proximal, a DHS must be within +/- 2500 bases of a GENCODE Tx start. We place all other DHSs in the nonproximal category. Each DHS is now

assigned an SVM training 'label', representing whether or not it is proximal to a GENCODE Gene.

(3) All DHS segments are then expanded in each direction until the total segment length is 1000bp.

(4) We assign the mean score of each histone modification is assigned to each 1000bp expanded DHS. This produces a vector of 5 scores for each DHS.

(5) All histone scores are translated to standard units (Zscores) by using the mean and standard deviation of all results from a given assay over the entire ENCODE regions.

(6) If a DHS does not contain a full set of histone modification scores (due to gaps in the underlying assay), the entire DHS is eliminated from the analysis.

(7) We prepare the SVM input by placing each labeled DHS, and the associated histone modification scores, into a matrix.

(8) Training and cross-validation results are generated by running a grid of SVM simulations using the freely available SVM implementation, PyML toolkit (http://pyml.sourceforge.net). We choose the best SVM resulting from 10-fold cross-validation of the training set. Each round of cross validation consists of training the SVM on a randomly selected 90% of the data, and then measuring the results against the held out 10%. An individual iteration of cross-validation performs model selection to select the best combination of SVM parameters. The specific parameters evaluated during model selection are Gaussian kernel gamma values of 0.01,0.1,1,10, and kernel 'C' values of 0.1,1,10,100.

S3.17.1.2 SVM discrimination of proximal DHS from random background

We perform step #1 as in section S3.17.1.1

(2) We assign positive labels to all DHSs within +/- 2500bp of a GENCODE Tx Start. These DHSs are considered proximal-DHSs.

(3) Next, we begin collecting the negative SVM training examples. First, all ENCODE regions are broken into contiguous 250bp segments. Segments located within 2kb of a proximal-DHS are removed from the data set.

(4) All segments are expanded to 1kb.

(5) We assign the mean score from each histone assay to the corresponding 1kb segment. Any segments that do not have an associated score are removed from the data set.

(6) Since the resulting negative data set is quite large, we randomly sample segments until we have satisfied a ratio of 2 negatives examples for every positive example.

We then perform steps 7-10 as above.

S3.17.1.3 SVM discrimination of distal DHSs from background

We perform step #1 as in section S3.17.1.1.

We then assign positive labels to all DHSs that are more than 10kb from the nearest GENCODE Tx Start. These DHSs are considered distal-DHSs.

We then perform steps 3-7 as in section S3.17.1.2

S3.17.1.4 ROC curves for individual histone marks (simple classifiers)

The individual feature ROCs are determined by comparing the distribution of individual feature data to the training labels. The feature data is sorted in reverse order, and then the list of labels is traversed. Each time a label occurs out of order, the false positive count increases. If labels are in

consecutive order, the true positive count increases. The entire list is traversed in this manner. The resulting labels are plotted. The area under this curve is the feature-roc 'score'.
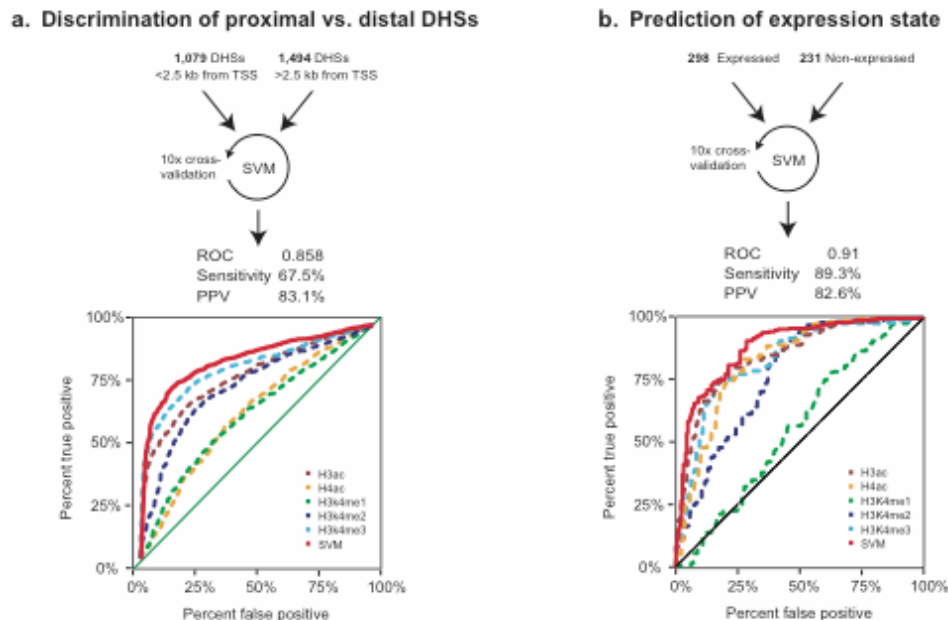
Supplementary Figure 34: Inputs to the two SVMs for discriminant training and their resulting performance. Panel A shows the classifier for distinguishing proximal from distal sites. Panel B shows the classifier for distinguishing TSSs from expressed vs non expressed transcripts. In each case, the upper portion summarizes the training data, while the lower portion consists of the Receiver Operating Characteristic (ROC) curves, in which the percent true-positive results (y-axis) are plotted as a function of the percent false-positive results (x-axis). A perfect classifier would have a step function that immediately achieves 100% true-positive results with no false predictions. A random classifier is a diagonal line between the bottom left and top right. The thick red line in each case shows the ROC curve of the SVM, whereas the different dashed lines show the curves for each individual mark independently.

S3.17.1.5   Correspondence of SVM identified TSSs with Gencode and Tag derived TSS categories.

The correspondence of the 110 top scoring TSSs identified by the SVM on the basis of Histone signals around DHSs to the category A-F TSSs in Table 3 (of the main paper) was investigated.

The category A-F TSSs were characterised by a single genomic coordinate and the SVM-TSSs by an arbitrary 250bp region.

As the methodologies underlying the SVM-TSS identification have a poor resolution in base-pair coordinates we considered overlap to have occurred if features from the two classes fell within 2500bp of one another.

Overlap analysis of the SVM-TSSs with the category A-F TSSs using the Genome Structure Correction (see section S1.3) for probability estimation is shown in Supplementary Table 17. The total number of SVM-TSSs located within 2500bp of a category A-F TSS was 93.

Supplementary Table 17: Counts of the numbers of SVM-TSSs falling within +/- 2500 bp of Category A-F TSSs and the probability of this occurring by chance – calculated using the GSC statistic. Note: the sum of the counts totals more than 110 as a given SVM-TSS can lie within 2500bp of more than one Category TSS.

TSS Category	Observed Overlay (count of SVM-TSSs)	p value
A	73	4.52E-018
B	51	3.05E-005
C	42	1.11E-016
D	32	9.87E-008
E	18	2.62E-043
F	38	1.26E-006

S3.17.2   CART Analysis of gene status

CART as employed here is a classification algorithm – its background and theory are given in Classification and Regression Trees[107]. Like all such algorithms it constructs a rule for prediction of a particular label from a given set of variables. Again, like all such algorithms, CART needs to be provided with a training set, that is, a set of labeled examples from which to construct the rule. Once constructed, the rule's performance is ideally judged on a test set for which the predictions of the classifier can be compared to known, true labels. CART is a tree structured algorithm. How it works is best illustrated when there are only two possible labels, for example, 0 and 1. Say we are given a categorical prediction variable with 10 possible categories and a real valued prediction variable. CART considers two types of rules based on one variable.

For the categorical variable Y, the possible rules are an assignment of one of the two classes to each category. For instance, "If Y is category v, then assign label 0, else, assign label 1." For the real variable X, the rules are of the form, "Assign label 0 if $X < c$ and 1 if $X > c$, where c and the label identities are free. Each such rule can be framed as a question, such as above, with an answer: Yes, say, for a label 0, and No for a label 1.

The program picks the "best" question (according to a purity measure described[107] based on any one of the predictor variables, represents it as the root of the tree, and places the cases according to their answers. The resulting nodes are then subjected to the same procedure until all nodes

contain cases with the same label. The tree is then "pruned" back, since the pure tree, which, by construction, behaves optimally on the training sample, performs poorly on the test sample. Various methods of pruning are described in Breiman *et al*[107]. Performance on the test sample yields estimates of misclassification probabilities. Care has to be taken if the proportional sizes of the sets of examples corresponding to each label in the training set do not reflect their expected values in the population. Modifications to take care of such cases and the parallel situation that misclassification of one label is more serious than that of the others are available in the CART program.

Tree structured rules have the advantage, which we try to employ, that, if the signal is strong, the order of the variables used in the "best" questions and their success in classification at the appropriate node give an indication of which variables may be important.

Here, we have utilized CART to predict gene expression status based on several genomic and epigenomic variables, both categorical and real valued. We discovered that histone 3 lysine 4 methylation status (i.e. H3K4me1, H3K4me2, and H3K4me3), along with a measure of DNase sensitivity was sufficient to build high-quality predictors of gene expression status within, and to a lesser extent, between cell lines. Some of the input variables, such as CpG status (a 1,0 categorical variable indicating whether the transcription start site of the given gene occurs in a CpG island), appear to hold little to no predictive value in the presence of the other predictors, while others provide highly incisive questions, whose answers result in accurate labels for both training set and test set data.

S4 Chromatin architecture

S4.1 Replication Timing: Data generation and Analysis

S4.1.1　　　Determination of replication time of ENCODE regions

HeLa cells were synchronized by a thymidine aphidicolin block and released from the block. As cells passed synchronously through a 10 hr S phase, they were labeled for 2 hr intervals with Bromodeoxyuridine starting at 0, 2, 4, 6 and 8 hrs. The BrdU labeled DNA was purified by two cycles of CsCl density gradient centrifugation, labeled and hybridized to the genome tiling arrays. Details of protocols and data processing are published in Jeon *et al*[7] and Karnani *et al*[8].

S4.2 Correlations between continuous chromatin and replication datatypes

S4.2.1　　　Sliding window correlations

S4.2.1.1 Background

"Continuous" datatypes refer to those data that take on real values at nearly regularly-spaced intervals along the genome. Examples incude DNaseI sensitivity and DNA replication timing. This is in contrast to "discrete" datatypes that are elemental in nature, such as locations of DNaseI hypersensitive sites. The primary challenge for continuous analysis is the issue of scale. As inputs to the analysis, we are dealing with apparently disparate datatypes, collected at different resolutions and scales. Sanger histone modification strength data, for instance, is

available at a resolution of approximately 1kb, while PhastCons conservation scores are available at every base. We also have an issue of scale on the output side, in that we want to uncover trends in the data that may be occurring at multiple scales.

The primary tool we use to address the challenge of scale is wavelets[108], a mathematical tool pioneered in the field of signal processing. Wavelets provide a framework for decomposing a given data type into increasingly coarse scales, allowing broader and broader trends in the data to reveal themselves. As opposed to Fourier analysis, which also provides a decomposition of a given signal in terms of multiple scales (frequencies), wavelet analysis localizes behavior in both frequency and "time" (genomic position, in our case), and is thus better suited to pick up transient behavior. Wavelets have been used for the analysis of genomic data to uncover local periodic patterns in DNA bending profiles[109] and gene expression data[110, 111], to predict protein structures[112], and to correlate a variety of genomic data on multiple scales in microbial genomes[113]. We use wavelets to visually represent individual datatypes on multiple scales at once, using wavelet scalograms, or heatmaps. Wavelets also provide a method to normalize pairs of datatypes to a common set of scales, allowing us to perform quantitative correlations on a scale-by-scale basis.

S4.2.1.2 Continuous wavelet transformation

Wavelet analysis makes use of two types of transform, the continuous wavelet transform (CWT) and the discrete wavelet transform (DWT). The CWT is defined for a time series $x(t)$ at each time t and scale a by

$$W(a,t) = \frac{1}{\sqrt{a}} \int_{-\infty}^{\infty} x(u)\, \psi\left(\frac{u-t}{a}\right) du$$

where $\psi(t)$ is the wavelet function of choice. For this analysis we use the first derivative of Gaussian (DOG) wavelet, implemented in the R package `Rwave`. In this implementation the DOG wavelet is complex-valued, and the absolute value $|W(a,t)|$ can be taken to represent the strength of the change in the original function x at scale a and location t. Thus for fixed a, $|W(a,t)|$ can be thought of as a representation of $x(t)$ at scale a. The `Rwave` wavelet functions are scaled so that the wavelet scale a is approximately equal to the *equivalent Fourier period* of a periodic feature in the original data, a fact we verified experimentally.

S4.2.1.3 Discrete wavelet transformation

The discrete wavelet transform (DWT) is essentially defined by restricting the CWT to time series sampled at discrete, equally-spaced time points, and by restricting the scales to the dyadic intervals $a_j = 2^j \delta$, where δ is the resolution of x. The DWT requires that the input sample x be of length equal to a power of two. A key feature of the DWT, not available for generic CWTs, is the *multiresolution analysis*. This gives, for each user-defined maximal level J corresponding to scale $2^J\delta$, a scale-by-scale decomposition of x into separate components,

$$x = \sum_{j=1}^{J} D_j + S_J$$

Here the D_j, or *details,* represent the local change in x at the scale $2^j\delta$, and the *smooth* S_J represents a smoothed version of x at the scale $2^J\delta$. The D_j and S_J are each the same length as x. For this analysis, we use a variant of the DWT called the maximal overlap DWT (MODWT), which allows x to be of arbitrary length. We use MODWT smooths for computing higher-order functional domains (see section S4.7) and for smoothing datasets in preparation for further analysis (see section S4.2.1.4). For all calculations we use the R package waveslim, and its implementation of the Daubechies "least asymmetric" LA(8) wavelet filter. We use reflection boundary conditions for computing multiresolution analyses.

S4.2.1.4 Preparation of ENCODE data sets for wavelet analysis

Implementations of the CWT and MODWT require input datasets to be equally-spaced. We thus define a nominal scale for each ENCODE dataset based on the assay used in each case (50bp for DNaseI sensitivity, 1kb for Sanger histone modifications, for instance). We then construct equally-spaced datasets at the nominal scale using the following interpolation scheme. Gaps less than 2kb are filled using linear interpolation between the existing flanking data points. For gaps greater than 2kb, a linear loess curve is fit at each interpolated position, using data within a centered window of width equal to 50 times the gap length. We use R function loess with default weights. To compare datasets with disparate nominal scales, we transform the dataset with the finer nominal scale by computing its MODWT wavelet smooth (see section S4.2.1.3) at the dyadic scale closest to coarser scale.

S4.2.1.5 Wavelet correlations and correlation heatmaps

Wavelet correlation heatmaps quantify the degree of local correlation between two genomic series on a scale-by-scale basis. For fixed scale a and genomic position t_0 the wavelet coefficients at scale a for the two series are computed in a 20kb window centered at t_0. The Pearson correlation coefficient is then computed on the two 20kb segments. The color in the correlation heatmap at location (t_0,a) represents the correlation coefficient so computed, ranging from red (high) to yellow (none) to green (low). We use the DOG wavelet for computing wavelet correlations.

Supplementary Table 18: Significance of differences in sliding window correlation distributions. Wavelet sliding window correlation values between DNaseI and five activating histone modifications were computed as described above, and accumulated at the 16kb scale across all of ENCODE. The resulting distributions of correlation values were compared pairwise using the one-sided Kolmogorov-Smirnov test (R function ks.test). P-values, included below, were computed for the null hypothesis that the distribution for one mark (given by the row labels) is not greater than the distribution for the other mark (given by the column labels).

	H3K4me2	H3K4me3	H3K4me1	H3ac	H4ac
H3K4me2		3.367152e-02	1.890608e-59	0.00982103	5.696281e-35
H3K4me3	0.008147442		1.391836e-63	0.01158146	1.667976e-36
H3K4me1	0.995825313	9.582033e-01		0.98030121	5.423018e-01

| H3ac | 0.001563221 | 2.519860e-06 | 1.118025e-55 | | 1.465513e-33 |
| H4ac | 0.997792115 | 9.950358e-01 | 6.036933e-05 | 0.98488594 | |

S4.2.1.6 Non-wavelet sliding window correlation for TR50 comparisons

Correlations with DNA replication timing data, as represented by the TR50 curve, are handled separately. This is due to the highly smoothed nature of the TR50 data, which gives features that are of a scale beyond those used for the wavelet analyses of other datatypes. To reach the apparent scale of the TR50 data, we performed loess smoothing on the other datatypes. We experimented with a number of different window widths for loess smoothing -- a visual check revealed that a 100kb smoothing window produced features comparable to those of the TR50 data. Local correlations between TR50 and the loess smoothed datatypes are computed using a sliding window of 250kb, as in the previous section. This gives a vector of correlation values at a single scale (that of the loess smoothed data) as opposed to the multiple scales computed for other datatypes using wavelets.

S4.3 Correlations of histone modifications with TR50 at discrete points in the genome

In addition to the sliding window correlation analysis reported in Figure 7a, we computed a histogram of correlation values obtained for each histone modification vs. TR50 across all of ENCODE, and plotted these as a function of correlation value (Supplementary Figure 35). As expected, the activating marks were mostly negatively correlated with TR50, although there were occasional areas of positive correlation. H3K27me3 displays a greater heterogeneity of correlation , with the positive correlation slightly predominating. Indeed, experiments on random data indicate that the observed fraction of highly positive correlations of H3K27me3 (> 0.5) is statistically significant, with empirical p-value of 0.005 (see Supplement S4.3.1). The positive correlation is consistent with the enrichment of H3K27me3 in late replicating regions , and its depletion in early replicating regions, illustrated in Figure 7b. In mouse histone modification H3K27me3 is targeted to the promoters of genes that also exhibit high levels of H3K4 methylation in stem cells where repressed promoters are held poised for activation[114]. Intriguingly, this bivalent state disappeared in differentiated cells. A reappearance of the bivalent state in cancer cells could provide a potential explanation for the appearance of H3K27Me3 in early replicating regions in HeLa cells. An alternative explanation might be based on the interallelic variation in time of replication (pan-S replication) and interallelic variation in chromatin structure described in the text.

S4.3.1   Statistical significance of positive correlations between H3K27me3 and TR50
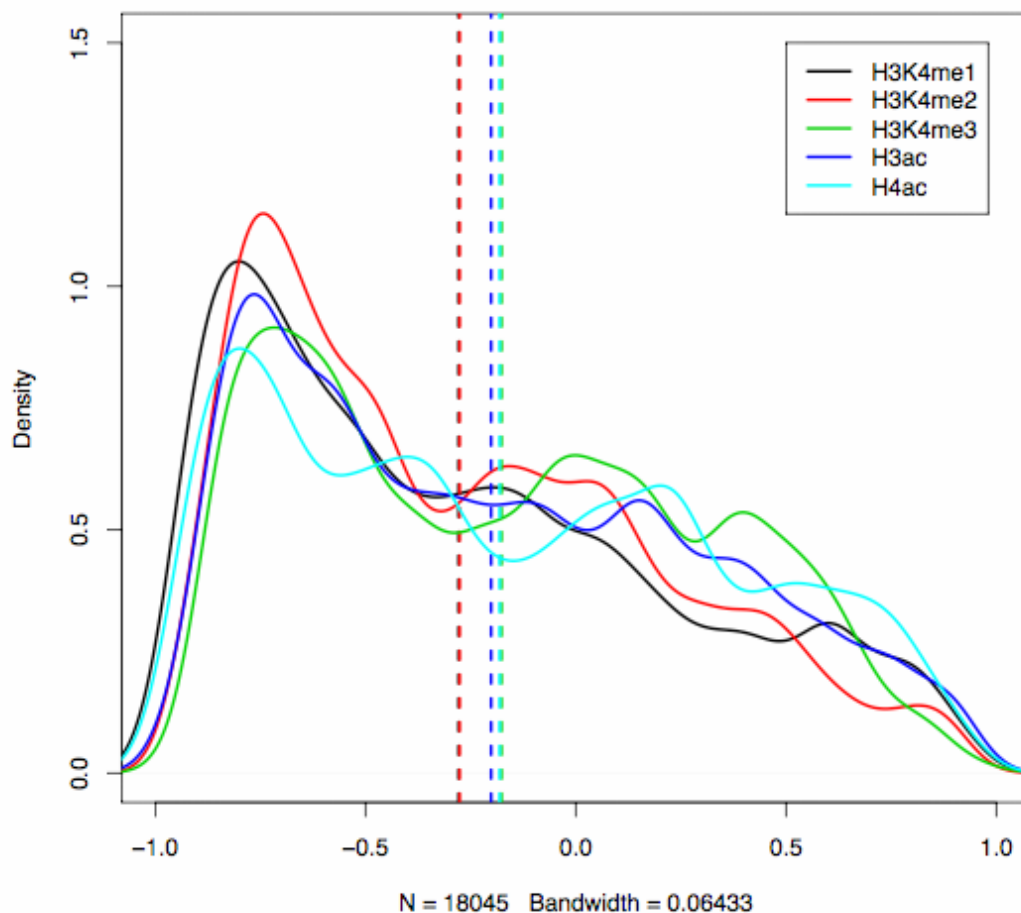
Sliding window correlations between TR50 and loess-smoothed H3K27me3 were computed as in section S4.2.1.6 and the resulting distribution of correlation values is displayed in Supplementary Figure 36. We observed that 28.3% of all ENCODE-wide sliding correlation values were greater than 0.5. To test the statistical significance of this result we performed sliding window correlation analysis on random data, simulated by randomly sampling the

H3K27me3 and TR50 datasets separately. Specifically, data for each of H3K27me3 and TR50 are concatenated across all of ENCODE to form two master datasets. Each sample experiment consisted of choosing, for each ENCODE region, a chunk of contiguous data of the same size as the given ENCODE region but starting from a random location in the H3K27me3 master dataset, and a separate same-sized chunk from a different random location in the TR50 master dataset. This was repeated for all 43 ENCODE regions (the TR50 data does not cover ENm011), and sliding window correlation was performed on the resulting 43 paired datasets. The sample experiment concluded by comparing the accumulated distribution of correlation values against the observed distribution. Out of 1000 such experiments, five produced distributions whose fraction of highly-positive correlations (>0.5) exceeded the observed fraction of 28.3%, for an empirical p-value of 0.005.

S4.3.2 Details of data analysis for Figure 7a

Data for H3K4me2 and H3K27me3 are loess smoothed as described in section S4.2.1.6 and local correlations with TR50 are computed in a sliding 250kb window. The graphs are colored at each position to reflect the value of the local correlation at that point, with red representing positive correlation, green for negative correlation, and yellow for no correlation. Enrichment in Fig. 7a measures the strength of the signal for a particular mark at that location relative to the negative control ChiP. For H3K4me2 this is measured as the fold-enrichment while for H3K27me3 the measure is the negative log P value of the significance of enrichment.

Supplementary Figure 35: Smoothed histograms of all sliding window correlation values (of indicated histone modification enrichment versus TR50) computed as described in Section S4.3.2 and accumulated across all of ENCODE. The indicated histone modifications are largely anti-correlated with TR50. The vertical dashed lines indicate the mean correlation value for that mark. The smoothed histogram was computed and plotted using R function density(), using default optional arguments.
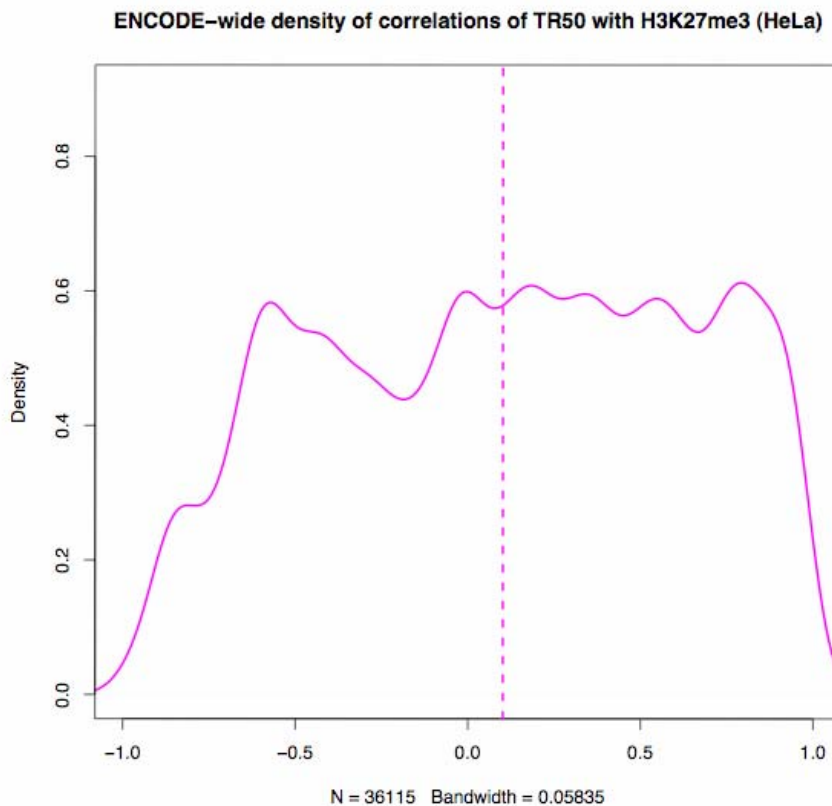
Supplementary Figure 36: A smoothed histogram similar to that in Supplementary Figure 35 for the correlation of H3K27me3 with respect to TR50.

S4.4 Chromatin:Replication enrichment analysis

S4.4.1   Distribution of active chromatin elements in regions with different replication timing

When we compare active chromatin elements with replication timing, we can determine how many base pairs of a given modification fall into each of the replication classes. If there were no relationship, then at random distribution would expect the active chromatin elements to fall into roughly the same percentages given above. However, this is not the case. For example, roughly 34% of the base pairs of the Sanger H3K4me1 HeLa data set fall into early replicating segments. So we see a ratio of 34%/23.36% = 1.45 of what we would expect at random. This means that H3K4me1 elements are +45% enriched in early replicating segments. We can calculate a p-value for this enrichment by randomizing the positions of the H3K4me1 elements in the ENCODE regions in order to calculate a distribution of expected overlap. By doing so we find that this enrichment is significant at better than 1 in 10,000 iterations, corresponding to a p-value of less than 0.0001.

The H3K27me3 data covered 1,230,522 base pairs in the ENCODE regions (which total. approximately 30,000,000 base pairs). The corresponding numbers for the other marks are H3K4me1.HeLa 1,931,448, H3K4me2.HeLa 932,980,H3K4me3.HeLa 743,454, H3ac.HeLa 833,122, H4ac.HeLa 869,186. Thus the different behavior of H3K27me3 cannot be explained as an artifact from the statistics of small numbers.

S4.4.2 P-value calculation for enrichment analysis

In order to calculate significance values for the enrichment of active chromatin elements in early, mid, late, and panS replicating segments, we randomized each set of active chromatin elements within the ENCODE regions. For the Sanger data, 43 of the ENCODE regions (excluding ENm011 for which replication data is not available) were included in the random model. For a given iteration of the model, each interval in the active chromatin element set in question was randomly placed within the 43 ENCODE regions. These randomly placed segments were not allowed to overlap or to 'hang over' the end of an ENCODE region. Then the amount of overlap with each replication category was calculated. This randomization was repeated for 10,000 iterations producing a distribution of overlaps for the active chromatin element in question. Then the actual amount of overlap was compared with the distribution in order to calculate a p-value for this enrichment. For example, if only 1 of the 10,000 iterations produced an amount of overlap greater than the actual overlap, then this enrichment has a p-value of 1/10000 or 0.0001. Generating a distribution where the actual overlap is greater than all of the 10,000 iterations would indicate a p-value less than 0.0001, and this is the limit of our analysis with 10,000 iterations. In order to fairly assess our p-values in the presence of multiple tests, we used Bonferroni correction to ascertain a level of p-value beyond which there would be a 0.05 probability that any of the reported significant p-values were actually insignificant. This level corresponded to p-values of 0.0013 or less. Hence all of the enrichments reported significant are significant at a p-value of 0.0013 or less which leads to a probability of 0.05 or less that any of the reported significant enrichments are actually insignificant.

S4.5 Histone modification patterns of DHSs

S4.5.1 Distribution of histone modification signals around DHSs

Our aim was to determine the average distribution of activating histone marks around DHSs centroids. A DHS centroid is the genomic coordinate marking the midpoint of a DHS segment, around which the DNaseI sensitivity signal is approximately symmetric by mass. We used the common DHS set described above as inputs. Because we wished to examine a 10kb window (+/- 5kb on either side of the DHS centroid), we filtered the DHS data to select only a single DHSs within a 10kb interval. Next, the 10kb segments are broken into contiguous bins of 100 bases, producing 100 bins for each 10kb segment. We now determine the distribution of Histone scores by assigning each 100bp bin the mean value of the corresponding segment in the Sanger histone assays. In the same manner, we map the underlying score from the DNase/Array data to each corresponding 100bp bin. Each expanded DHS is now associated with 100 scores from each of the 5 Histone mod assays and the DNase/Array data. In the next step, we average each bin from the entire set of expanded DHSs to produce an aggregate 100bp distribution. If a 100bp segment did not contain any underlying data from a particular assay, the value is not considered in the

average. This provides a comparison of the distribution of histone marks and DNaseI sensitivity averaged over a large group of DHSs.

S4.5.2   Histone modification patterns of proximal and distal DHSs

For each DHS, we first calculate the distance to the nearest GENCODE gene TSS. We then filtered DHSs according to their distance from the TSS. For example, all DHSs within 2.5kb of any GENCODE tx start are considered one group, and DHSs greater than 10kb from any DHS are considered another group. We perform the analyis using the following distances <2.5kb, >2.5kb, >5000, >10000, >12500, >15000, >20000, >25000, and >30000. Using this selection strategy, the input data at each increasingly larger distance is a subset of all smaller distances. We then perform the following steps on each distance grouped DHS set: First, we calculate the centroid position of each DHS. Next, we expand all centroids by 5000bps in the 5' and 3' directions, creating a set of segments of length 10kb, centered on the DHS centroid. In a second pass, all overlapping segments are considered. If a segment overlaps a segment that has a higher average DHS score, the lower scoring segment is removed from the analyis. In this way, the analysis considers only 10kb segments with the strongest underlying DHS signal. The DHS score used to resolve overlaps is the score associated with each DHS in the underlying DNase/Array data set. Next, the 10kb segments are broken into contiguous bins of 100 bases, producing 100 bins for each 10kb segment. We now determine the distribution of Histone scores by assigning each 100bp bin the mean value of the corresponding segment in the Sanger histone assays. In the same manner, we map the underlying score from the UW-CAP array to each corresponding 100bp bin. All mapped scores are transformed to z-scores by using the mean and standard deviation of all data points in the underlying ENCODE assay. The purpose of converting to z-scores is to enable relative comparisons between the different histone marks. Each expanded DHS is now associated with 100 scores from each of the 5 Histone mod assays and the UW CAP DNaseI array. In the next step, we average each bin from the entire set of expanded DHSs to produce an aggregate 100bp distribution. If a 100bp segment did not contain any underlying data from a particular assay, the value is not considered in the average. For each assay the resulting data is 100, 100bp bins of average score covering the 10kb DHS segment. # of DHSs in each dataset (+/- 5kb sets): <2500: 355; >2500: 639; >5000: 489; >7500: 410; >10000: 355; >12500: 305; >15000: 271; >20000: 218; >25000: 183; >30000: 158.

S4.6 Identification and analysis of CORCS

S4.6.1   Alignment of hydroxyl radical cleavage patterns Gibbs sampling

Hydroxyl radical cleavage patterns were predicted for the 3,150 DNA sequences in the Union DHS dataset using data from experimentally determined cleavage patterns. The values in each pattern were then binned into 50 levels of cleavage intensity and aligned by a Gibbs sampling algorithm[115]. In order to improve efficiency, the dataset was divided at random into smaller subsets of 300 sequences prior to alignment. The motif width was fixed to a length of 8 bp. The sampler was run until there was no further improvement in the aligment score for 5 complete iterations through the dataset. This process was repeated 10,000 times. Motifs exhibiting a high cleavage intensity to sequence conservation ratio[116] were retained for further analysis. To determine the enrichment of the CORCS profile for DNase hypersensitive sites relative to the complete ENCODE regions, we used an algorithm similar to MatInspector[117] to assess the

similarity between the candidate CORCS profiles and each overlapping window of the predicted hydroxyl radical cleavage patterns of the ENCODE regions. The top-scoring 0.001% of these windows were recorded to a BED-format file and analyzed for enrichment.

S4.7 Identification of higher order domains by multi-track HMM segmentation

We define functional domains by segmenting the ENCODE regions using hidden Markov Models (HMMs). The basic premise of HMMs is that observed data are generated stochastically from a pre-determined number of hidden background probability distributions, or *states*. In our case we set the number of states to two, in the hopes of distinguishing between functionally active and inactive domains, and perform simultaneous, multi-variate HMM segmentation on six, ENCODE-wide datasets: TR50, H3K4me2, H3K27me3, Affy RNA Signal, DHS (DNaseI hypersensitive site) density, and RFBR density. The first four of these datasets are measured in the HeLa cell-line. DHS density is computed by first merging HS detected in HeLa using all three methods described in S3.3, and then computing the fractional occupancy of the HS in a 5kb window sliding every 1kb along the genome. RFBR density is computed by first considering the RFBRs defined at the 5% FDR (see section S3.10 and then computing the fractional occupancy of those RFBRs in a 5kb window sliding every 1kb along the genome. We choose to represent each of the two HMM states by four independent Gaussian distributions (the emission probabilities). These parameters, plus the four transition probabilities between states, are learned via unsupervised expectation-maximization. The final state values (0 or 1, interpreted a posteriori as "inactive" or "active") for each genomic position are then computed using the Viterbi algorithm.

To normalize the six datasets, we use MODWT wavelet smoothing (see section S4.2.1.3) to bring all datasets out to a common scale. As described in Thurman et al[118], as the scale increases, individual segment lengths generally increase. We desire that the median functional domain segment length be larger than the average gene size of 25kb, and that the minimum segment length be larger than 10kb (still larger than ~50% of human genes). After performing segmentations on individual and combined wavelet-smoothed datasets at a variety of scales, we used these criteria to arrive at 60kb for the common wavelet scale for smoothing all datasets. All datasets are preprocessed before wavelet smoothing as described in S4.2.1.4 The nominal resolutions after preprocessing are: TR50, 50bp; H3K4me2, 1000bp, H3K27me, 1000bp, Affy RNA Signal, 50bp, DHS density, 1000bp; RFBR density, 1000bp. The closest dyadic scale to 60kb for each dataset is then used for final wavelet smoothing. The final scales are: TR50, 51.2kb; H3K4me2, 64kb; H3K27me3, 64kb; Affy RNA Signal, 51.2kb; DHS density, 64kb; RFBR density, 64kb.

S5 Evolution and Population Genetics

S5.1 Conservation of regulatory elements

The possibility that MCSs within RFBRs preferentially occur at Transcription-Factor binding sites was investigated.

Transcription factor motif Position Weight Matrices were obtained from TRANSFAC[99] except for E2F1, Mycn, Sp1 and HNF4 which were obtained from JASPAR[119]. The potential transcription factor binding sites in the encode regions were identified as follows. For each matrix all possible string permutations of the nucleotides were generated where the frequency of occurrence of the nucleotide at that position in the string exceeded 0% and the bit-score for the string exceeded 0.8 * the number of nucleotides in the motif. The collection of strings for each motif were then mapped by exact matching to the ENCODE regions.

For each transcription-factor-associated RFBR in the 1% and 5% hitlists three coverage statistics were determined. A. The number of nucleotides occupied by the associated motif in the region +/- 150 bp around the hit peak coordinate, B. The number of nucleotides occupied by the the moderate MCSs contained within the RFBR region and C. The number of nucleotides occupied by the associated motif within the contained MCSs. The enrichment of the motif in the MCS was then calculated as 100 * (100 * C/B)/(100 * A/301) for each RFBR which contained the relevant motif.

Although all 17 motifs used had mappings in the ENCODE regions, only 12 had mappings which fell inside the associated 1% FDR RFBRs. For 6 of these 12, the MCSs were enriched with respect to the RFBR for the motif (Supplementary Table 19). The same motifs exhibited enrichments in the 5% FDR RFBRs and in addition the motif RAR was found in a number of the RFBRs and showed enrichment in the MCSs (Supplementary Table 20).

Supplementary Table 19: The relative percentage cover with the named motif of MCSs relative to the RFBRs in which they occur, together with the number of nucleotides in the RFBRs containing mapped motifs and the number of nucleotides in the MCSs in those RFBRs. RFBRs identified as ChIP-chip defined binding regions at 1% FDRP Values above 100% indicate enrichment

motif_name	Enrichment_of_Motif_in_MCS	bases_in_FDR	bases_in_MCS
C/EBP.M00770	681.7	3913	41
CRE-BP1:c-Jun.M00041	24.1	1204	312
E2F-4:DP-1.M00738	684.1	602	44
E2F.M00803	95.6	18361	2890
HNF-3.M00791	93.2	15050	1643
HNF4	144	6622	368
Mycn	129	121604	17536
p53.M00761	0	301	71
PU.1.M00658	150.2	3612	347
SP1	90.1	43344	4799
STATx.M00223	129.5	6923	1443
USF.M00217	34.7	14147	697

Supplementary Table 20: The relative percentage cover, with the named motif, of MCSs relative to the RFBRs in which they occur, together with the number of nucleotides in the RFBRs containing mapped motifs and the number of nucleotides in the NCSs in those RFBRs. RFBRs identified as ChIP-chip defined binding regions an 5% FDC. Values above 100% indicate enrichment.

| motif_name	Enrichment_of_Motif_in_MCS	bases_in_FDR	bases_in_MCS
C/EBP.M00770	245	6020	117
CRE-BP1:c-Jun.M00041	39.4	4515	606
E2F-4:DP-1.M00738	327.2	1505	230
E2F.M00803	93.1	22575	3794
HNF-3.M00791	94.9	24381	2108
HNF4	174.4	10836	1056
Mycn	123.2	173978	22424
p53.M00761	0	301	71
PU.1.M00658	157.5	8127	553
RAR.M00762	163.1	2408	328
SP1	79.9	74347	7534
Sp3.M00665	0	1806	126
STATx.M00223	134.9	9632	1648
USF.M00217	66.6	24381	1335

S5.2 Genetic Variation and experimentally-identified functional elements

S5.2.1   Feature-based Modified McDonald Kreitman MK and HKA tests

For the MK test a 2 x 2 contingency table was generated for each feature with one column containing the number of non 4-fold degenerate (4D) polymorphic and divergent sites within a feature and the other the number of polymorphic and divergent sites within 4D sites. A chi-square value was calculated on the resulting 2 x 2 contingency table. To infer the direction of selection, the neutrality index[120] was calculated for each 2 x 2 table as follows: NI = (Non-4D Poly / Non-4D Div) / (4D Poly / 4D Div). NI = 1 indicates neutrality. NI > 1 indicates an excess of polymorphism or deficit of divergence and NI < 1 indicates an excess of divergence or deficit of polymorphism.

To test specific ENCODE region features sets against expectations from neutral theory; we performed multi-locus Hudson-Kreitman-Agaudé tests[121], comparing the observed versus expected numbers of segregating sites and fixed differences within and between humans and chimpanzees respectively. We have performed a modified version of the original HKA test, which generalizes the original 2x2 approach of Hudson *et al*[121] to a multilocus setting in which loci consist of those ENCODE regions that belong to the same feature. Parameter estimates for the model (locus-specific mutation rates, and a genome-wide speciation time) were obtained by numerically solving the system of equations n + 1 equations, where n is the number of loci, as described in Hudson *et al*[121]. Numerical analysis of this system of equations was performed

using open source routines implemented in the Gnu Scientific Library (GSL; http://www.gnu.org/software/gsl/).
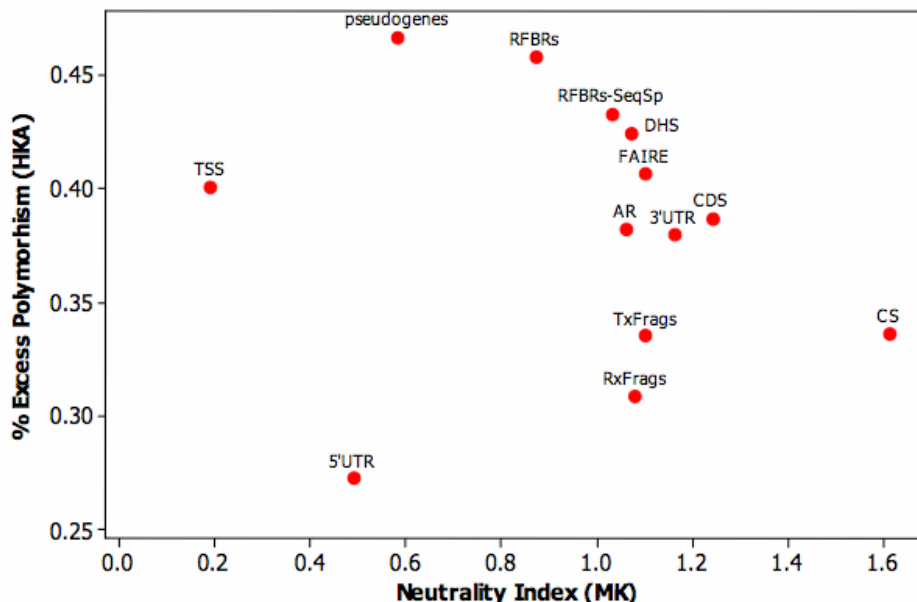
Supplementary Figure 37: The contrast of mMK neutrality index (NI)[120] on the x-axis to the percent of elements that had an excess of polymorphism per ENCODE feature set based on the HKA test on the y-axis.

It is important to note that we expect the complicated nature of human demography to cause genome-wide deviations from the standard neutral model and it will generate statistically significant signals with the MK and HKA tests. However this deviation should affect all loci to approximately the same extent[122], thus loci which have also been influenced by the historical actions of natural selection should be expected to deviate to a greater degree from our model's expectations.

Principle of the multilocus HKA test:
N individual loci of the same feature
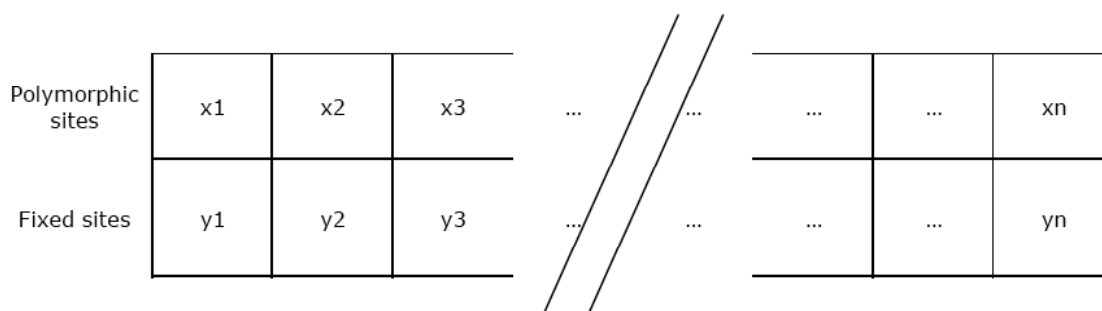
Test of heterogeneity on a 2xn table by solving the n+1 equations as mentioned in the methods

Principle of the MK test:

Fisher's exact test or chi2 test on a 2x2 table

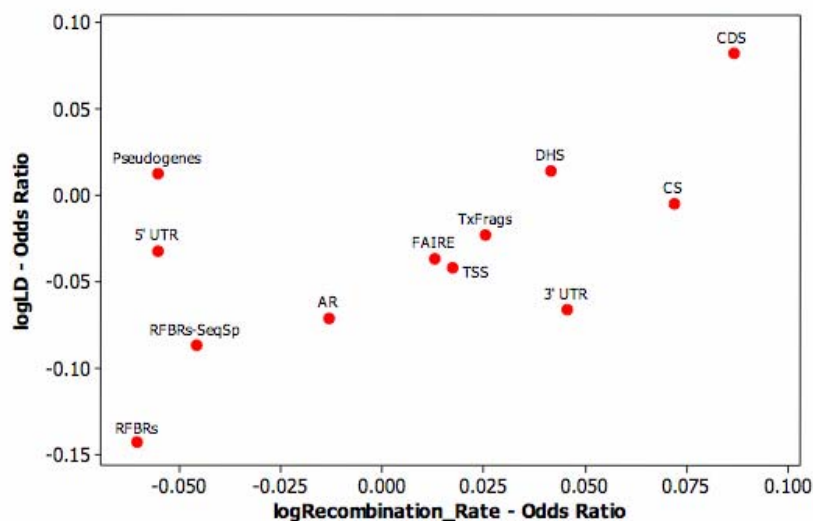### S5.2.1.1 Linkage Disequilibrium and Recombination Rate analysis

Recombination events can cluster within precisely localized recombination hotspots[123], and intermarker intervals exhibiting rapid breakdown of linkage disequilibrium can be used to localize these hotspots without direct measurement of recombination rates[124]. To identify intervals with rapid breakdown of linkage disequilibrium, we systematically evaluated intervals defined by a pair of consecutive SNP markers separated by <10,000 bps. For each interval, we considered the two SNPs and five equally-spaced flanking markers spanning 40 kb on either side of the interval (for a total of 12 markers) and calculated the maximum spanning r^2 coefficient by considering all 36 pairings of flanking markers[125]. Intervals without six genotyped markers within the flanking 40 kb on either side were deemed to be inadequately covered and were excluded from this analysis.

We then categorized each interval between markers using two criteria: whether or not the region included a feature of interest and whether or not the spanning r2 value was greater than 0.20 in the YRI population. We then used logistic regression to determine the level of association between the two characteristics (i.e. to determine whether the presence or absence of a particular feature made an interval more or less likely to exhibit rapid breakdown of disequilibrium). We summarized effect size in an odds ratio. We controlled for ENCODE region, GC content, and interval length by including appropriate covariates in our regression model. Approximately 8% of the total ENCODE sequence was in intervals with spanning r^2 less than 0.2. We chose 0.2 as our cut-off because it captured a low level of LD and it gave us enough power to detect an association. We repeated the analysis with a spanning r^2 cut-offs of 0.1 (3% of all sequence) and 0.4 (19% of all sequence) and obtained similar results.

We also included in our analysis estimated recombination rates computed as part of the International HapMap Project[37]. These recombination rates were made on the basis of data from

all four populations. We performed a similar logistic regression comparing the odds of having a recombination rate greater than 3 per feature. Roughly 11% of the sequence was included in intervals with recombination rate estimates of 3 cM/Mb. Again, we controlled for ENCODE region and interval length. The use of different recombination rate thresholds, of 10 cM/Mb (3%) and 1 cM/Mb (25%), did not appreciably change the results. Results using recombination rate estimated from Perlegen were consistent with the results from the HapMap data.

To assess the significance of our results, we performed simulation analyses. Since we wanted to preserve the underlying structure of the ENCODE regions, we circularly permuted the features within each region. To do this, we increased the start position of all features by a given value. The resulting features that fell outside the ENCODE region were pushed around to the start of the region. We then repeated our initial analysis a hundred times with the original LD (or recombination rate) pattern and the permuted features.

Supplementary Figure 38: The contrast of the log10 of the odds ratio of the Linkage Disequilibrium (LD) measure (y-axis) vs. the log10 of the odds ratio for the Recombination Rate measure (x-axis) for each ENCODE feature.

S5.2.2   Segmental duplications (SDs) and Copy Number Variants (CNVs) in the ENCODE regions

Segmental duplication mapping information was obtained from the University of California at Santa Cruz (UCSC; http://genome.ucsc.edu/) and from The Centre for Applied Genomics (TCAG; http://projects.tcag.ca/humandup/). Mapping information for copy number variants was obtained from the Database of Genomic Variants at TCAG (http://projects.tcag.ca/variation/). Information regarding annotated genes was obtained from the UCSC. All descriptive information regarding gene content in SDs and CNVs in ENCODE regions was obtained by matching genome coordinates in the different tables.

The assessment of the content of gene and transcript features in CNVs and SDs was performed after obtaining projections of the genomic localizations of CNVs and SDs. The assessment of statistically significant differences in their content was obtained using a permutation test in which positions of the features were randomly assigned 1000 times by Perl's random number generator, initialized using random seeds obtained from the /dev/random device. The p-value was calculated as the number of times that the data in the simulated set equals or exceeds the observed value from the real data, divided by the total number of permutations plus one. Analysis of the raw data generated by Perl scripts was performed using the statistical package R (http://www.r-project.org/).

S5.3 Unexplained constrained sequences

The distribution of constrained sequences is complex and highly clustered. If the constrained sequences were distributed, in some sense, uniformly throughout the genome, we would expect their placement to appear as an alternating Poisson process. In order to verify our visual intuition, we fitted exponential distributions to the distributions of constrained sequences in each ENCODE region. Hence, we generated a null distribution
for the start positions of constrained sequences. A 1-sample KS-test was sufficient to discern between the two distributions in each region at a confidence level of $p \sim 0.0001$.

We next sought to distinguish between the distribution of constrained sequences that overlap annotations from those that do not. This can be done with a 2-sample KS-test. However, the annotated constrained sequences (ACSs) and the unannotated constrained sequences (UCSs) are not, by definition, independently distributed. Hence, the D-statistic in the 2-sample test will not have its usual null distribution.

In order to compute the distribution of the D-statistic given the underlying genomic structure, we utilized a boot-strap sampling procedure detailed elsewhere in the supplement. This procedure entailed choosing two samples of b blocks of length L from each region. In either sample, the labels of the ACSs and the UCSs were ignored, and ascribed simply as general, or dummy, annotations. This represents the hypothesis that both the ACSs and UCSs are being drawn from the same distribution. The blocks were then concatenated to form samples of length R, where R is the length of the ENCODE region. We performed a 2-sample KS-test on the start positions of the general annotations from their respective bootstrap samples. Each iteration of this process provided one sample from the true null distribution of the D-statistic. We performed 1000 iterations, and computed the empirical p-values.

We tested UCSs against ACSs, conserved sequences overlapping Exons, conserved sequences overlapping CDSs (exons excluding UTRs), and conserved sequences overlapping annotations excluding exons (Other). In most regions we were able to discern between the distributions of the UCSs and the annotated conserved sequences, but, in many, no such discernment was possible. Data for each pairing, in each region, is shown below. P-values greater than 1 indicate insufficient sample size to perform any tests.

Supplementary Table 21: KS 2-sample test results: Comparing the distribution of Annotated and Unannotated constrained sequences by ENCODE region.

Region	UCS vs ACS	UCS vs Exon	UCS vs CDS	UCS vs Other
ENm001	0.0100	0.0010	0.0010	0.1279
ENm002	0.0220	0.0010	0.0120	0.0360
ENm003	0.0010	0.0010	0.0010	0.0010
ENm004	0.0010	0.0010	0.0010	0.0010
ENm005	0.0010	0.0010	0.0010	0.0010
ENm006	0.1239	0.0959	0.1688	0.1389
ENm007	0.0010	0.0010	0.0010	0.0010
ENm008	0.0619	0.0260	0.0969	0.0969
ENm009	0.0010	0.0010	0.0010	0.0010
ENm010	0.0080	0.0050	0.0010	0.0010
ENm011	0.8162	0.9471	0.2138	0.4705
ENm012	0.0629	0.1049	0.0010	0.0010
ENm013	0.0010	0.0010	0.0010	0.0010
ENm014	0.0010	0.0010	0.0010	0.0010
ENr111	0.0559	0.2248	0.0010	0.0010
ENr112	2.0000	2.0000	2.0000	2.0000
ENr113	2.0000	2.0000	2.0000	2.0000
ENr114	0.0929	0.0010	0.2488	0.2278
ENr121	0.0010	0.0010	0.0010	0.0010
ENr122	0.0010	0.0010	0.0010	0.0010
ENr123	0.0010	0.0010	0.0010	0.0010
ENr131	0.0010	0.0010	0.0010	0.0010
ENr132	0.0010	0.0110	0.0010	0.0010
ENr133	0.0240	0.0430	0.0070	0.0070
ENr211	0.0010	0.0010	2.0000	2.0000
ENr212	0.2378	0.1998	0.0010	0.0360
ENr213	0.0060	0.0030	0.0010	0.0010
ENr221	0.0010	0.0010	0.0010	0.0010
ENr222	0.0010	0.0040	0.0010	0.0010
ENr223	0.0010	0.0120	0.0010	0.0010
ENr231	0.0020	0.0010	0.0040	0.0010
ENr232	0.0010	0.0010	0.0010	0.0010
ENr233	0.0010	0.0010	0.0270	0.0170
ENr311	0.1279	0.1259	2.0000	2.0000
ENr312	0.0020	0.0010	2.0000	2.0000
ENr313	0.0010	0.0010	2.0000	2.0000
ENr321	0.0120	0.0110	0.0010	0.0010
ENr322	0.0140	0.0370	0.0010	0.0010
ENr323	0.0050	0.0040	0.0619	0.0080
ENr324	0.3816	0.6893	0.0549	0.0470
ENr331	0.0010	0.0010	0.0010	0.0010
ENr332	0.0010	0.0010	0.0010	0.0010
ENr333	0.0010	0.0010	0.0010	0.0010
ENr334	0.0899	0.1648	0.0010	0.0010

S5.4 Unconstrained experimentally-identified functional elements

S5.4.1 Diversity, Indel, and derived allele frequency (DAF)

S5.4.1.1 Diversity Analysis

Whole genome sequence data totaling one fold coverage of the human genome from DNA derived from a pool of cell lines from 8 unrelated adult African Americans, 4 male and 4 female enrolled in Houston, TX was used in these variation analyses[37]. The SSAHASNP software package[126] was used to align these reads to the build 35 of the human reference sequence, generating polymorphism calls while keeping track of total bases aligned for each read. The subset of reads aligning to the 44 ENCODE regions were used in this analysis. Heterozygosity was calculated for each of the feature sets by totalling the number of single base substitutions within each feature, relative to the reference genome sequence, and normalizing by the number of aligned bases that agreed with the reference sequence.

#### S5.4.1.2 Insertion-Deletion (Indel) Analysis

Indel densities per base pair (bp) for the regions or feature of interest were estimated by calculating the number of indels within those regions or feature, as a proportion of the total size in base pairs of that region or feature. To ease interpretation, we multiplied the intensity by 100,000 to provide an estimate per 100kb. 99% confidence intervals for indel densities were estimated using a negative binomial model with the number of indels as the response, and the lengths of sequence as an offset. This approach allowed for potential over-dispersion.

S5.4.1.3 Derived allele frequency (DAF) in ENCODE features

SNP density and diversity offer a good estimate of selective constraint but it is the use of the frequency spectrum of SNPs that allows for more rigorous analysis and a better representation of levels of variation. We have aligned all SNP positions to the chimp genome and have inferred the ancestral allelic state (the one shared with chimp). We then estimated the allele frequency of the inferred derived allele (the one NOT shared with chimp). In regions with high selective constraint we expect that the new (or derived) allele generally remain in low frequencies and most likely disappears from the population.

We mapped all SNPs and their respective DAFs onto the ENCODE features and estimated the mean and frequency distribution of DAF values for different functional elements. To assess the statistical significance of the differences observed among features, we have performed two different statistical analyses: a) we compared the distribution of DAF SNP values for each functional element against the distribution in Ancestral Repeats (AR) using two non-parametrical statistical tests (Kolmogorov-Smirnov (KS) and Mann-Whitney (MW) tests). b) We performed 10000 randomisations of elements within the same ENCODE region to analyse the average DAF for each group compared to the background. The randomisations allowed calculation of the Z-score and empirical p-value. These analysis were performed separately for the 10 resequenced regions of ENCODE and the remaining 34 regions. Standard tests that explore the whole DAF

spectrum to infer selective sweeps[127] are not appropriate in this case since the whole set of regions is being used and this violates assumptions of the tests about uniformity of recombination and mutation.
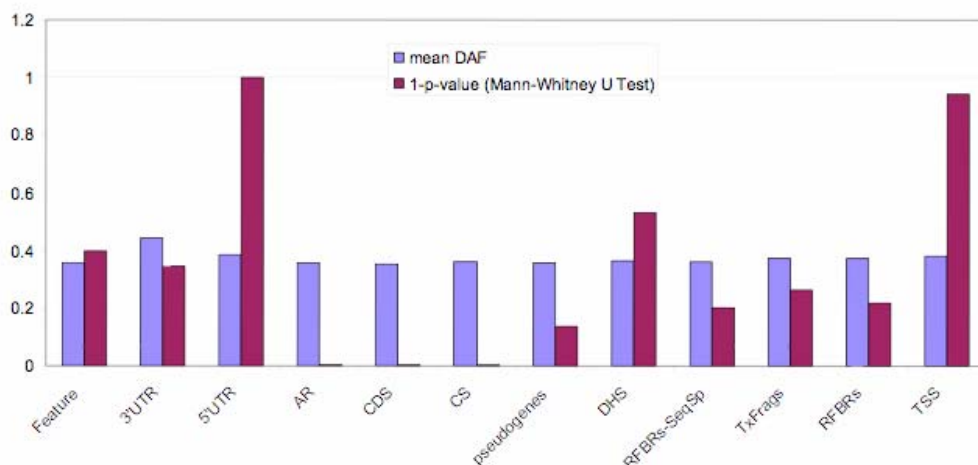
Supplementary Figure 39: Mean Derived Allele Frequency (blue bars) with 1-P-values indicating deviation (upwards or downwards) from the DAF spectrum of ancestral repeats (ARs).

We investigated whether there is a correlation between the DAF and the Genomic Evolutionary Rate Profiling (GERP) score from the Threaded Block Aligner (TBA). Using the Spearman's rank correlation coefficient, rho, we quantified correlation between the mean DAF for all SNPs in each functional element and the GERP scores calculated for two groupings of species; mammals ,and primates excluding the human sequence from the calculation to avoid any biases the polymorphism data has to the estimation of the conservation score.
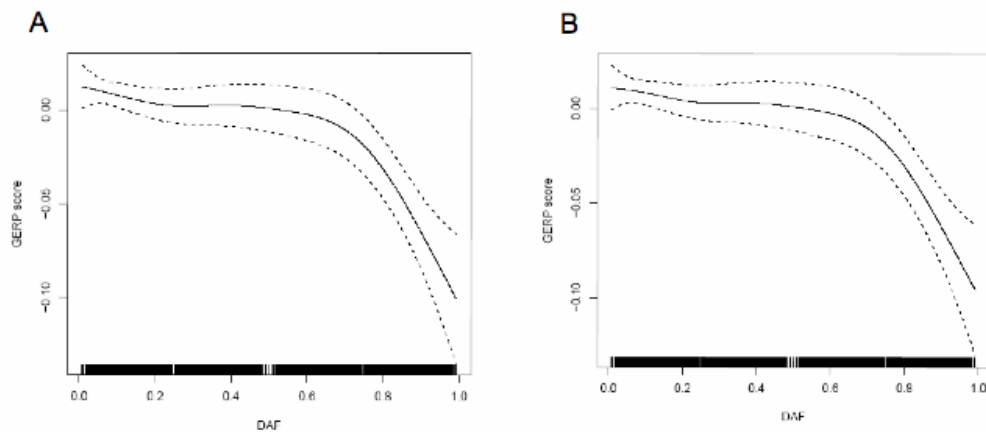
Supplementary Figure 40: Derived allele frequency (DAF) vs. GERP conservation score.
(A). DAF vs. GERP primate score in all ENCODE SNP positions; (B). DAF vs. GERP primate score in all ENCODE SNP positions excluding SNPs in all CS feature sequences

S5.5 Sensitivity of identifying evolutionary conserved bases

To address the question of the sensitivity of our methods for identifying evolutionary constrained bases, we used the mixture decomposition methods employed in the comparative analysis of the human and mouse genomes[128, 129] to estimate the fraction of bases that are constrained in regions outside of predicted MCSs. For this analysis, we used average GERP scores in non-overlapping windows of 10bp. In order to avoid biases due to alignment gaps and missing data, we only considered sites having enough aligned bases that the neutral branch length of the associated phylogeny was at least 0.5 substitutions/site, and we only considered windows with at least 8 such sites. We empirically characterized the score distribution for (1) windows in ancestral repeats ("AR") and (2) windows outside of "moderate" MCSs, ARs, and Alu transposons ("other"), using Gaussian kernel smoothing methods as described in Chiaromonte *et al*[129] (Supplementary Figure 41). Treating the AR distribution as a proxy for the distribution in neutrally evolving sites, we estimated a lower bound of 0.20 for the fraction of "other" sites that cannot be explained by the neutral (AR) distribution.
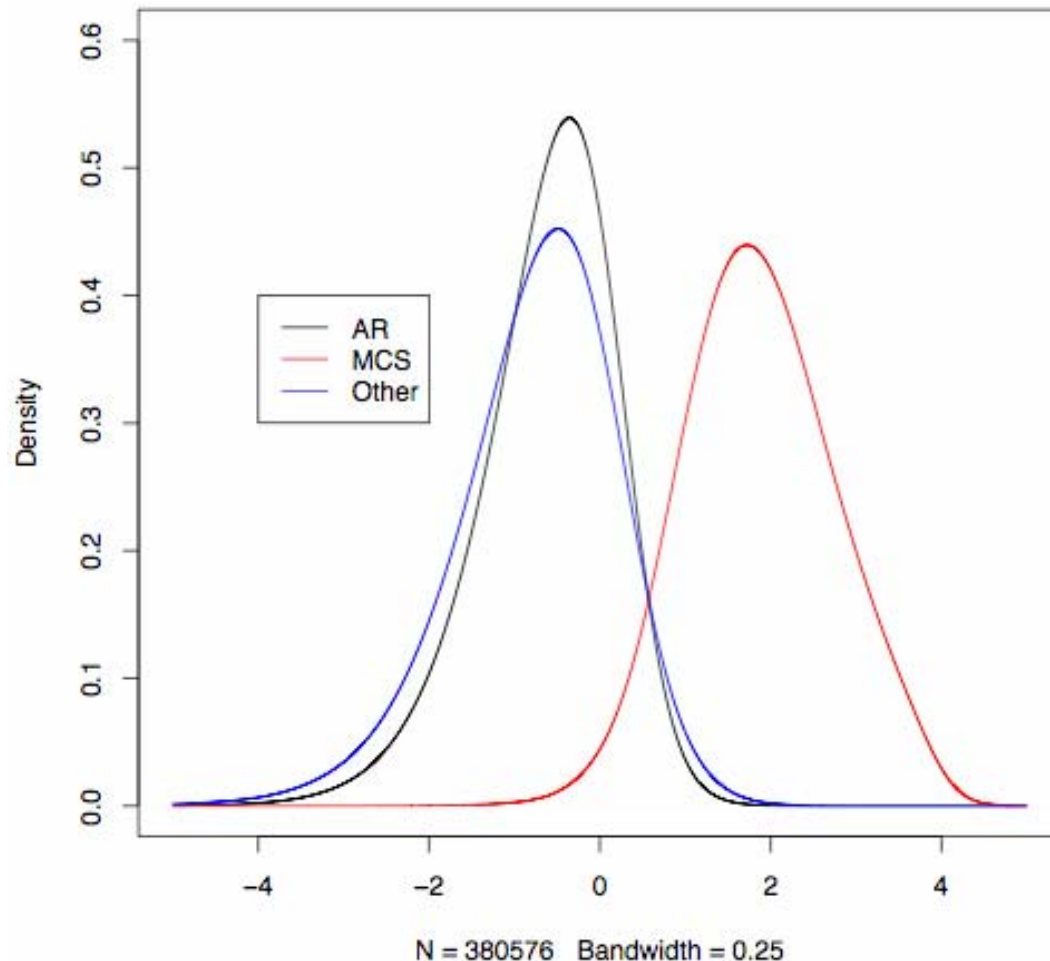
Supplementary Figure 41: Distributions of average GERP scores in 10bp windows in ancestral repeats (AR), multispecies conserved sequences (MCS; the "moderate" set is shown here), and sequences outside of ARs, MCSs, and Alu repeats (Other). Only windows with at least 8 phylogenetically informative sites were considered. The distributions were smoothed using the 'density' function in the R statistical computing package (Gaussian kernel, bandwidth 0.25, grid of 10000 equally spaced points)

It is apparent visually from the distributions, however, that more of these non-neutral sites have low scores (hence are evolving faster than expected) than have high scores (Supplementary Figure 41), so 20% may be a substantial overestimate of the fraction of sites in the "other" category that have been missed by our methods. It is not possible, without making assumptions about the score distributions for sites under selection, to decompose the "other" distribution into "fast", "slow", and "neutral" components. However, if we are willing to assume that the slow

sites contribute negligibly to the left tail of the distribution and that the fast sites contribute negligibly to the right tail, then the two-part decomposition employed above can be applied separately to the right and left halves of the distributions. We performed this analysis, cutting the "AR" and "other" distributions at the mode of the AR distribution, and arrived at approximate lower bounds of 3.9% of the "other" sites evolving slower and 12.7% evolving faster than expected under neutrality. If we use our more inclusive set of MCSs (the "loose" set), then the slow fraction decreases substantially, to 1.4%, and the fast fraction increases slightly, to 14.3%. However, with the Loose set, there is still considerable proportion of elements which are not overlapping – 37% of DHSs, 64% of RaceFrags (see Table below)

Element type	Elements	Bases	Overlapping	Bases	%Overlapping	%bp conserved
3UTR	503	435996	412	163215	0.819085487	0.374349765
5UTR	679	115905	517	41745	0.761413844	0.360165653
AFFX_Brg1_HL60_seqsp	14	4470	11	984	0.785714286	0.220134228
AFFX_CEBPe_HL60_seqsp	56	17091	42	2579	0.75	0.150898134
AFFX_CTCF_HL60_seqsp	35	10800	24	2450	0.685714286	0.226851852
AFFX_p63-ActD_ME180_seqsp	51	15578	43	4966	0.843137255	0.318782899
AFFX_p63-noAD_ME180_seqsp	7	2100	6	777	0.857142857	0.37
AFFX_PU1_HL60_seqsp	10	3000	6	350	0.6	0.116666667
AFFX_RARecA_HL60_seqsp	9	2700	4	410	0.444444444	0.151851852
AFFX_SIRT1_HL60_seqsp	9	3096	7	600	0.777777778	0.19379845
AFFX_TFIIB_HL60_seqsp	9	3096	7	600	0.777777778	0.19379845
ALL_cMyc_HeLa_seqsp	26	7800	15	613	0.576923077	0.078589744
ALL_p53_HCT116_seqsp	10	16373	8	3605	0.8	0.220179564
ALL_STAT1gIF_HeLa_seqsp	28	140343	28	21043	1	0.14993979
ALL_STAT1_HeLa_seqsp	9	67527	9	11104	1	0.164437929
CDS	3891	671166	3679	568852	0.945515292	0.847557832
HisPolTAF	1043	1074493	891	252087	0.854266539	0.234610184
LateRepSeg	472	7990358	319	833825	0.675847458	0.104353898
Ng_BAF155_HeLa_seqsp	352	105600	248	26854	0.704545455	0.254299242
Ng_BAF170_HeLa_seqsp	246	73800	160	17019	0.650406504	0.230609756
Ng_cJun_HeLa_seqsp	137	41100	81	7170	0.591240876	0.174452555
Ng_cMyc-Qt_2091_seqsp	45	13500	38	4245	0.844444444	0.314444444
Ng_cMyc-St_2091_seqsp	463	138900	365	38440	0.788336933	0.27674586
Ng_cMyc-UCD_HeLa_seqsp	254	76200	170	14966	0.669291339	0.196404199
Ng_cMyc-UT_HeLa_seqsp	330	99000	261	29078	0.790909091	0.293717172
Ng_E2F1_HeLa_seqsp	77	23100	64	7086	0.831168831	0.306753247
Ng_E2F4_2091_seqsp	27	8100	18	1921	0.666666667	0.237160494
Ng_Sp1_HCT116_seqsp	119	35700	89	8367	0.74789916	0.234369748
Ng_Sp1_Jurkat_seqsp	288	86400	168	14694	0.583333333	0.170069444
Ng_Sp1_K562_seqsp	68	20400	44	3629	0.647058824	0.177892157

Ng_Sp3_HCT116_seqsp	76	22800	62	6266	0.815789474	0.274824561
Ng_Sp3_Jurkat_seqsp	58	17400	37	3861	0.637931034	0.221896552
Ng_Sp3_K562_seqsp	49	14700	22	1780	0.448979592	0.121088435
Ng_STAT1-NASA_HeLa_seqsp	16	4800	8	498	0.5	0.10375
Ng_STAT1-P30_HeLa_seqsp	24	7200	19	2120	0.791666667	0.294444444
Ng_STAT1-Yale_HeLa_seqsp	49	14700	22	2217	0.448979592	0.150816327
Sanger_HNF3b_HePG2_seqsp	413	123900	259	21780	0.627118644	0.175786925
Sanger_HNF4a_HePG2_seqsp	443	132900	289	20342	0.652370203	0.153062453
Sanger_USF1_HePG2_seqsp	262	78600	150	12015	0.572519084	0.152862595
seq_specific	2896	1171558	2025	236942	0.699240331	0.202245215
TR	1494	1589195	1271	342513	0.850736278	0.2155261
TR-H3K4mUnique	1163	1308181	998	290212	0.858125537	0.221843919
TSS	1119	60041	677	31274	0.605004468	0.5208774
UCSD_STAT1-P30_HeLa_seqsp	41	12300	30	2970	0.731707317	0.241463415
UCSD_Suz12_HeLa_seqsp	298	89400	190	18201	0.637583893	0.203590604
uncFAIREsites	4017	1368211	2777	333444	0.691311924	0.243708025
dhs_all	2817	883862	1791	172906	0.635782748	0.195625561
Racefrags	2249	161188	827	22995	0.367718986	0.142659503
Transfrags	6965	645153	2381	75550	0.341852118	0.117104005

Overlap of Elements to MCS Loose definition of conservation

In summary, it appears that a substantial fraction of sites outside of MCSs, ARs, and recent transposons may be evolving in a nonneutral manner, but most of these sites are evolving faster, rather than slower, than expected, and of the remaining (slow) sites, roughly 2/3 seem to be near the threshold for detection by our methods. Even if we use our most inclusive set of MCSs, we find that roughly one and a half percent or more of sites in our "other" category may actually be under negative selection. We speculate that most of these cannot be detected by our methods because they are weakly conserved and/or occur as isolated bases or very short constrained elements. However, when we take this inclusive set of MCSs, many biochemically defined features remain absent from these conservation measures, suggesting that there is still a set of unconserved elements remaining outside of our most aggressive definition of constrain, which shows a small (1.5%) set of uncaptured constrained bases.

The same mixture decomposition methods can be used to estimate an upper bound on the fraction of bases in MCSs that are evolving neutrally. We estimate this fraction at less than 0.2% for the "moderate" MCS set (Supplementary Figure 41) and at 13% for the "loose" MCS set.

S6 References

1. Greenbaum, J. A., Parker, S. C. J. & Tullius, T. D. Detection of DNA structural motifs in functional genomic elements. Genome Res (2006 (in press)).

2.　　Crawford, G. E. et al. DNase-chip: a high-resolution method to identify DNase I hypersensitive sites using tiled microarrays. Nat Methods 3, 503-9 (2006).

3.　　Giresi, P. G., Kim, J., McDaniell, R. M., Iyer, V. R. & Lieb, J. D. FAIRE (Formaldehyde-Assisted Isolation of Regulatory Elements) isolates active regulatory elements from human chromatin. Genome Res (2006 (in press)).

4.　　Dorschner, M. O. et al. High-throughput localization of functional elements by quantitative chromatin profiling. Nat Methods 1, 219-25 (2004).

5.　　Sabo, P. J. et al. Genome-scale mapping of DNase I sensitivity in vivo using tiling DNA microarrays. Nat Methods 3, 511-8 (2006).

6.　　Cooper, G. M. et al. Distribution and intensity of constraint in mammalian genomic sequence. Genome Res 15, 901--913 (2005).

7.　　Jeon, Y. et al. Temporal profile of replication of human chromosomes. Proc Natl Acad Sci U S A 102, 6419-24 (2005).

8.　　Karnani, N., Taylor, C. Malhotra, A.& Dutta, A. Pan-S replication patterns and chromosomal domains defined by genome tiling arrays of human chromosomes. Genome Res (2006 (in press)).

9.　　Ding, C. & Cantor, C. R. Direct molecular haplotyping of long-range genomic DNA with M1-PCR. Proc Natl Acad Sci U S A 100, 7449-53 (2003).

10.　　Ding, C. & Cantor, C. R. A high-throughput gene expression analysis technique using competitive PCR and matrix-assisted laser desorption ionization time-of-flight MS. Proc Natl Acad Sci U S A 100, 3059-64 (2003).

11.　　Halees, A. S., Leyfer, D. & Weng, Z. PromoSer: A large-scale mammalian promoter and transcription start site identification service. Nucleic Acids Res 31, 3554-9 (2003).

12.　　Halees, A. S. & Weng, Z. PromoSer: improvements to the algorithm, visualization and accessibility. Nucleic Acids Res 32, W191-4 (2004).

13.　　Kim, T. H. et al. Direct isolation and identification of promoters in the human genome. Genome Res 15, 830-9 (2005).

14.　　Kim, T. H. et al. A high-resolution map of active promoters in the human genome. Nature 436, 876-80 (2005).

15.　　Heintzman, N. D. et al. Global analysis of chromatin signatures of transcriptional promoters and enhancers in the human genome. Nature Genetics (2006 (submitted)).

16.　　Koch, C. M. et al. The Landscape of Histone Modifications across 1% of the Human Genome in Five Human Cell Lines. Genome Res (2006 (accepted)).

17.　　Bhinge, A. A., Kim, J., Euskirchen, G., Snyder, M. & Iyer, V. R. Mapping the chromosomal targets of STAT1 by Sequence Tag Analysis of Genomic Enrichment (STAGE). Genome Res (2006 (in press)).

18.　　Cooper, S. J., Trinklein, N. D., Anton, E. D., Nguyen, L. & Myers, R. M. Comprehensive analysis of transcriptional promoter structure and function in 1% of the human genome. Genome Res 16, 1-10 (2006).

19.　　Bieda, M., Xu, X., Singer, M. A., Green, R. & Farnham, P. J. Unbiased location analysis of E2F1-binding sites suggests a widespread role for E2F1 in the human genome. Genome Res 16, 595-605 (2006).

20.　　Rada-Iglesias, A. et al. Binding sites for metabolic disease related transcription factors inferred at base pair resolution by chromatin immunoprecipitation and genomic microarrays. Hum Mol Genet 14, 3435-47 (2005).

21. ENCODE Project Consortium. The ENCODE pilot project: identification and analysis of functional elements in 1% of the human genome. Nature (2006 (submitted)).

22. Euskirchen, G. M. et al. Mapping of transcription factor binding regions in mammalian cells by ChIP: Comparison of array and sequencing based technologies. Genome Res (2006 (in press)).

23. Cawley, S. et al. Unbiased mapping of transcription factor binding sites along human chromosomes 21 and 22 points to widespread regulation of noncoding RNAs. Cell 116, 499-509 (2004).

24. Zhang, Z. D. et al. Statistical analysis of the genomic distribution and correlation of regulatory elements in the ENCODE regions. Genome Res (2006 (in press)).

25. Kapranov, P. et al. Large-scale transcriptional activity in chromosomes 21 and 22. Science 296, 916-9 (2002).

26. Guigó, R. et al. EGASP: The human ENCODE Genome Annotation Assessment Project. Genome Biology 7, S2.1-S2.31 (2006).

27. Bajic, V. B. et al. Performance assessment of promoter predictions on ENCODE regions in the EGASP experiment. Genome Biol 7 Suppl 1, S3 1-13 (2006).

28. Zheng, D. & Gerstein, M. B. A computational approach for identifying pseudogenes in the ENCODE regions. Genome Biology 7, S13.1-S13.10 (2006).

29. Harrow, J. et al. GENCODE: producing a reference annotation for ENCODE. Genome Biol 7 Suppl 1, S4 1-9 (2006).

30. Trinklein, N. D. et al. Integrated analysis of experimental datasets reveals many novel promoters in 1% of the human genome. Genome Res (2006 (submitted)).

31. Wei, C. L. et al. A global map of p53 transcription-factor binding sites in the human genome. Cell 124, 207-19 (2006).

32. Ng, P. et al. Gene identification signature (GIS) analysis for transcriptome characterization and genome annotation. Nat Methods 2, 105-11 (2005).

33. Carninci, P. et al. Genome-wide analysis of mammalian promoter architecture and evolution. Nature Genetics 38, 626-35 (2006).

34. Washietl, S. et al. Structured RNAs in the ENCODE Selected Regions of the Human Genome. Genome Res (2007 (in press)).

35. Emanuelsson, O. et al. Assessing the performance of different high-density tiling microarray strategies for mapping transcribed regions of the human genome. Genome Res (2006).

36. Rozowsky, J. et al. The DART classification of unannotated transcription within ENCODE regions: Associating transcription with known and novel loci. Genome Res (2006 (in review)).

37. International HapMap Consortium. A haplotype map of the human genome. Nature 437, 1299-320 (2005).

38. Stranger, B. E. et al. Genome-wide associations of gene expression variation in humans. PLoS Genet 1, e78 (2005).

39. Thomas, D. J. et al. The ENCODE Project at UC Santa Cruz. Nucleic Acids Res 35, D663-7 (2007).

40. Kent, W. J. et al. The human genome browser at UCSC. Genome Res 12, 996--1006 (2002).

41. Karolchik, D. et al. The UCSC Genome Browser Database. Nucleic Acids Res 31, 51-4 (2003).

42. Karolchik, D. et al. The UCSC Table Browser data retrieval tool. Nucleic Acids Res 32, D493-6 (2004).

43. Braun, J., Braun, R. & Muller, H. Multiple change-point fitting via quasi-likelihood, with application to DNA sequence segmentation. Biometrika 87, 301-314 (2000).

44. Braun, J. & Muller, H. Statistical methods for DNA segmentation. Statistical Science 13, 142-162 (1998).

45. Elton, R. A. Theoretical models for heterogeneity of base composition in DNA. J Theor Biol 45, 533-53 (1974).

46. Li, W., Bernaola-Galvan, P., Haghighi, F. & Grosse, I. Applications of recursive segmentation to the analysis of DNA sequences. Comput Chem 26, 491-510 (2002).

47. Li, W., Stolovitzky, G., Bernaola-Galvan, P. & Oliver, J. L. Compositional heterogeneity within, and uniformity between, DNA sequences of yeast chromosomes. Genome Res 8, 916-28 (1998).

48. Liu, J. S. & Lawrence, C. E. Bayesian inference on biopolymer models. Bioinformatics 15, 38-52 (1999).

49. Priestley, M. Spectral Analyses and Time Series (Academic Press, London, 1981).

50. Doukhan. Mixing: Properties and Examples (Springer, New York, 1995).

51. Bickel, P. J. & Doksum, K. A. Mathmatical Statistics: Basic Ideas and Selected Topics (Prentice Hall, New Jersey, 2001).

52. Politis, D. N., Romano, J. P. & Wolf, M. Subsampling (1999).

53. Künsch, H. R. The jackknife and the bootstrap for general stationary observations. Annals of Statistics 17, 1217--1241 (1989).

54. Buhlmann, P. & Kunsch, H. R. Block length selection in the bootstrap for time series. Computational Statistics and Data Analysis 31, 295-310 (1999).

55. Subrahmanyam, Y. V. et al. RNA expression patterns change dramatically in human neutrophils exposed to bacteria. Blood 97, 2457-68 (2001).

56. Cheng, J. et al. Transcriptional maps of 10 human chromosomes at 5-nucleotide resolution. Science 308, 1149-54 (2005).

57. Bolstad, B. M., Irizarry, R. A., Astrand, M. & Speed, T. P. A comparison of normalization methods for high density oligonucleotide array data based on variance and bias. Bioinformatics 19, 185-93 (2003).

58. Kampa, D. et al. Novel RNAs identified from an in-depth analysis of the transcriptome of human chromosomes 21 and 22. Genome Res 14, 331-42 (2004).

59. Kapranov, P. et al. Examples of the complex architecture of the human transcriptome revealed by RACE and high-density tiling arrays. Genome Res 15, 987-97 (2005).

60. Shiraki, T. et al. Cap analysis gene expression for high-throughput analysis of transcriptional starting point and identification of promoter usage. Proc Natl Acad Sci U S A 100, 15776-81 (2003).

61. Kodzius, R. et al. CAGE: cap analysis of gene expression. Nat Methods 3, 211-22 (2006).

62. Carninci, P. et al. The transcriptional landscape of the mammalian genome. Science 309, 1559-63 (2005).

63. Kawaji, H. et al. CAGE Basic/Analysis Databases: the CAGE resource for comprehensive promoter analysis. Nucleic Acids Res 34, D632-6 (2006).

64. Harbers, M. & Carninci, P. Tag-based approaches for transcriptome research and genome annotation. Nat Methods 2, 495-502 (2005).

65.   Wei, C. L. et al. 5' Long serial analysis of gene expression (LongSAGE) and 3' LongSAGE for transcriptome characterization and genome annotation. Proc Natl Acad Sci U S A 101, 11701-6 (2004).

66.   Chiu, K. P. et al. PET-Tool: a software suite for comprehensive processing and managing of Paired-End diTag (PET) sequence data. BMC Bioinformatics 7, 390 (2006).

67.   Loytynoja, A. & Goldman, N. An algorithm for progressive multiple alignment of sequences with insertions. Proc Natl Acad Sci U S A 102, 10557-62 (2005).

68.   Massingham, T. & Goldman, N. Detecting amino acid sites under positive selection and purifying selection. Genetics 169, 1753-62 (2005).

69.   Castelo, R. et al. Comparative gene finding in chicken indicates that we are closing in on the set of multi-exonic widely expressed human genes. Nucleic Acids Res 33, 1935-9 (2005).

70.   Reymond, A. et al. Human chromosome 21 gene expression atlas in the mouse. Nature 420, 582-6 (2002).

71.   David, L. et al. A high-resolution map of transcription in the yeast genome. Proc Natl Acad Sci U S A 103, 5320-5 (2006).

72.   Hasegawa, M., Kishino, H. & Yano, T. Dating of the human-ape splitting by a molecular clock of mitochondrial DNA. J Mol Evol 22, 160-74 (1985).

73.   Yang, Z. Maximum likelihood phylogenetic estimation from DNA sequences with variable rates over sites: approximate methods. J Mol Evol 39, 306-14 (1994).

74.   Hochberg, Y. A sharper Bonferroni procedure for multiple tests of significance. Biometrika 75, 800-803 (1988).

75.   Hollander, M. & Wolfe, D. A. Nonparametric Statistical Methods (John Wiley and Sons, 1999).

76.   Zheng, D. et al. Pseudogenes in the ENCODE regions: Consensus annotation, analysis of transcription and evolution. Genome Res (2007 (in press)).

77.   Washietl, S., Hofacker, I. L. & Stadler, P. F. Fast and reliable prediction of noncoding RNAs. Proc Natl Acad Sci U S A 102, 2454-9 (2005).

78.   Pedersen, J. S. et al. Identification and classification of conserved RNA secondary structures in the human genome. PLoS Comput Biol 2, e33 (2006).

79.   Washietl, S. & Hofacker, I. L. Consensus folding of aligned sequences as a new measure for the detection of functional RNAs by comparative genomics. J Mol Biol 342, 19-30 (2004).

80.   Fiegler, H. et al. Accurate and reliable high-throughput detection of copy number variation in the human genome. Genome Res 16, 1566-74 (2006).

81.   Fiegler, H. et al. DNA microarrays for comparative genomic hybridization based on DOP-PCR amplification of BAC and PAC clones. Genes Chromosomes Cancer 36, 361-74 (2003).

82.   Roschke, A. V. et al. Karyotypic complexity of the NCI-60 drug-screening panel. Cancer Res 63, 8634-47 (2003).

83.   Peiffer, D. A. et al. High-resolution genomic profiling of chromosomal aberrations using Infinium whole-genome genotyping. Genome Res 16, 1136-48 (2006).

84.   Ghosh, S., Hirsch, H. A., Sekinger, E., Struhl, K. & Gingeras, T. R. Rank-statistics based enrichment-site prediction algorithm developed for chromatin immunoprecipitation on chip experiments. BMC Bioinformatics 7, 434 (2006).

85. Weinmann, A. S., Bartley, S. M., Zhang, T., Zhang, M. Q. & Farnham, P. J. Use of chromatin immunoprecipitation to clone novel E2F target promoters. Mol Cell Biol 21, 6820-32 (2001).

86. Oberley, M. J., Tsao, J., Yau, P. & Farnham, P. J. High-throughput screening of chromatin immunoprecipitates using CpG-island microarrays. Methods Enzymol 376, 315-34 (2004).

87. Dhami, P. et al. Exon array CGH: detection of copy-number changes at the resolution of individual exons in the human genome. Am J Hum Genet 76, 750-62 (2005).

88. Kim, J., Bhinge, A. A., Morgan, X. C. & Iyer, V. R. Mapping DNA-protein interactions in large genomes by sequence tag analysis of genomic enrichment. Nat Methods 2, 47-53 (2005).

89. Carninci, P. et al. Promoting mammalian transcription. Nat Genet (2006 (in press)).

90. Smyth, G. K. & Speed, T. Normalization of cDNA microarray data. Methods 31, 265-73 (2003).

91. Zheng, M., Barrera, L. O., B., R. & Wu, Y. N. in Proceedings of the American Statistical Association, Statistical Computing Section (American Statistical Association., Alexandria, VA, 2005).

92. Ren, B. et al. Genome-wide location and function of DNA binding proteins. Science 290, 2306-9 (2000).

93. Efron, B. Correlation and large-scale simultaneous significance testing. (2005).

94. Efron, B. Local False Discovery Rates (http://www-stat.stanford.edu/~brad/papers/). (2005).

95. Efron, B. Large-scale simultaneous hypothesis testing: the choice of a null hypothesis. Journal of The American Statistical Association 99, 96-104 (2004).

96. Tusher, V. G., Tibshirani, R. & Chu, G. Significance analysis of microarrays applied to the ionizing radiation response. Proc Natl Acad Sci U S A 98, 5116-21 (2001).

97. Storey, J. D. & Tibshirani, R. Statistical significance for genomewide studies. Proc Natl Acad Sci U S A 100, 9440-5 (2003).

98. Su, A. I. et al. A gene atlas of the mouse and human protein-encoding transcriptomes. Proc Natl Acad Sci U S A 101, 6062-7 (2004).

99. Wingender, E. et al. TRANSFAC: an integrated system for gene expression regulation. Nucleic Acids Res 28, 316-9. (2000).

100. Frith, M. C. et al. Detection of functional DNA motifs via statistical over-representation. Nucleic Acids Res 32, 1372-81 (2004).

101. Liu, X., Brutlag, D. L. & Liu, J. S. BioProspector: discovering conserved DNA motifs in upstream regulatory regions of co-expressed genes. Pac Symp Biocomput, 127-38 (2001).

102. Liu, X. S., Brutlag, D. L. & Liu, J. S. An algorithm for finding protein-DNA binding sites with applications to chromatin-immunoprecipitation microarray experiments. Nat Biotechnol 20, 835-9 (2002).

103. Pavesi, G., Mauri, G. & Pesole, G. An algorithm for finding signals of unknown length in DNA sequences. Bioinformatics 17 Suppl 1, S207-14 (2001).

104. Gerstein, M., Sonnhammer, E. L. & Chothia, C. Volume changes in protein evolution. J Mol Biol 236, 1067-78 (1994).

105. Rozen, S. & Skaletsky, H. Primer3 on the WWW for general users and for biologist programmers. Methods Mol Biol 132, 365-86 (2000).

106.   Trinklein, N. D., Chen, W. C., Kingston, R. E. & Myers, R. M. Transcriptional regulation and binding of heat shock factor 1 and heat shock factor 2 to 32 human heat shock genes during thermal stress and differentiation. Cell Stress Chaperones 9, 21-8 (2004).

107.   Brieman, L., Friedman, J., Stone, C. J. & Olshen, R. A. Classification and Regression Trees (1984).

108.   Percival, D. B. & Walden, A. T. Wavelet methods for time series analysis (Cambridge University Press, 2000).

109.   Audit, B., Vaillant, C., Arneodo, A., D'Aubenton-Carafa, Y. & Thermes, C. Wavelet analysis of DNA bending profiles reveals structural constraints on the evolution of genomic sequences. J Biol Phys 30, 33-81 (2004).

110.   Allen, T. E. et al. Genome-scale analysis of the uses of the Escherichia coli genome: model-driven analysis of heterogeneous data sets. J Bacteriol 185, 6392-9 (2003).

111.   Jeong, K. S., Ahn, J. & Khodursky, A. B. Spatial patterns of transcriptional activity in the chromosome of Escherichia coli. Genome Biol 5, R86 (2004).

112.   Allen, T. E., Price, N. D., Joyce, A. R. & Palsson, B. O. Long-range periodic patterns in microbial genomes indicate significant multi-scale chromosomal organization. PLoS Comput Biol 2, e2 (2006).

113.   Torrence, C. & Compo, G. O. A practical guide to wavelet analysis. Bull Amer Met Soc 79, 61-78 (1998).

114.   Bernstein, B. E. et al. A bivalent chromatin structure marks key developmental genes in embryonic stem cells. Cell 125, 315-26 (2006).

115.   Lawrence, C. E. et al. Detecting subtle sequence signals: a Gibbs sampling strategy for multiple alignment. Science 262, 208-14 (1993).

116.   Schneider, T. D. & Stephens, R. M. Sequence logos: a new way to display consensus sequences. Nucleic Acids Res 18, 6097-100 (1990).

117.   Quandt, K., Frech, K., Karas, H., Wingender, E. & Werner, T. MatInd and MatInspector: new fast and versatile tools for detection of consensus matches in nucleotide sequence data. Nucleic Acids Res 23, 4878-84 (1995).

118.   Thurman, R. E., Day, N., Noble, W. S. & Stamatoyannopoulos, J. A. Identification of higher-order functional domains in the human ENCODE regions. Genome Res (2007 (in press)).

119.   Sandelin, A., Alkema, W., Engstrom, P., Wasserman, W. W. & Lenhard, B. JASPAR: an open-access database for eukaryotic transcription factor binding profiles. Nucleic Acids Res 32, D91-4 (2004).

120.   Rand, D. M. & Kann, L. M. Excess amino acid polymorphism in mitochondrial DNA: contrasts among genes from Drosophila, mice, and humans. Mol Biol Evol 13, 735-48 (1996).

121.   Hudson, R. R., Kreitman, M. & Aguade, M. A test of neutral molecular evolution based on nucleotide data. Genetics 116, 153-9 (1987).

122.   Lewontin, R. C. & Krakauer, J. Letters to the editors: Testing the heterogeneity of F values. Genetics 80, 397-8 (1975).

123.   Jeffreys, A. J., Kauppi, L. & Neumann, R. Intensely punctate meiotic recombination in the class II region of the major histocompatibility complex. Nat Genet 29, 217-22 (2001).

124.   McVean, G. A. et al. The fine-scale structure of recombination rate variation in the human genome. Science 304, 581-4 (2004).

125.   Smith, A. V., Thomas, D. J., Munro, H. M. & Abecasis, G. R. Sequence features in regions of weak and strong linkage disequilibrium. Genome Res 15, 1519-34 (2005).
126.   Ning, Z., Cox, A. J. & Mullikin, J. C. SSAHA: a fast search method for large DNA databases. Genome Res 11, 1725-9 (2001).
127.   Fay, J. C. & Wu, C. I. Hitchhiking under positive Darwinian selection. Genetics 155, 1405-13 (2000).
128.   International Mouse Genome Sequencing Consortium. Initial sequencing and comparative analysis of the mouse genome. Nature 420, 520-62 (2002).
129.   Chiaromonte, F. et al. The share of human genomic DNA under selection estimated from human-mouse genomic alignments. Cold Spring Harb Symp Quant Biol 68, 245-54 (2003).

SUPPLEMENTARY INFORMATION: DATA VALIDATION

Identification and analysis of functional elements in 1% of the human genome by the ENCODE pilot project.

This supplement provides the links to the key validation datasets, published separately for each class of experiments in the ENCODE project. In each case, a brief introduction of the data type is provided and then a DOI (Digital Object Identifier) and a URL which will resolve to the correct article. Where appropriate we have provided a short guide to which key figures or tables in the paper are used for validation. Most of the papers are found in the ENCODE special issue of Genome Research.

CONTENTS:

1. Quantitative real-time PCR (qRT-PCR) validation of ChIP-chip data from the NimbleGen platform (Ren Lab)

Validation of the Chip/chip data for the CTCF data was provided by qRT-PCR as described in the following paper:

Tae Hoon Kim, Ziedulla K. Abdullaev, Andrew D. Smith, Keith A. Ching, Dmitri I. Loukinov, Roland D. Green, Michael Q. Zhang, Victor V. Lobanenkov, and Bing Ren. 2007. Analysis of the Vertebrate Insulator Protein CTCF-Binding Sites in the Human Genome. *Cell* **128:** 1231-12 doi:10.1016/j.cell.2006.12.048.

DOI: doi:10.1016/j.cell.2006.12.048
URL: http://dx.doi.org/doi:10.1016/j.cell.2006.12.048

From the CTCF binding sites identified in the human genome, 84 sites were randomly selected for conventional ChIP analysis. For negative controls, 17 promoters sequences that were not near any CTCF binding sites were selected. Quantitative real-time PCR was performed with 0.5 ng of CTCF ChIP DNA and unenriched total genomic DNA. The quantitative real-time PCR of each sample was performed in duplicate using iCycler™ and SYBR green iQ™ SYBR green supermix reagent (Bio-Rad Laboratories). The threshold cycle (Ct) values were calculated automatically by the iCycle iQ™ Real-Time Dectection System Software (Bio-Rad Laboratories). Normalized Ct (ΔCt) values for each sample were then calculated by subtracting the Ct value obtained for the unenriched DNA from the Ct value for the CTCF ChIP DNA (ΔCt = Ctctcf – Cttotal). The fold enrichment of the tested promoter sequence in ChIP DNA over the unenriched DNA was then estimated. Primers used for this analysis and the data are found in http://dx.doi.org/doi:10.1016/j.cell.2006.12.048 in Supplement Table S1, S2 and S3.

The Validation of the histone modification, PolII, TAFI has not been published separately

To validate the ChIP/chip data for H3K4me2, H3K4me3, H3ac, H4ac, RNA PolII, TAF1, Chromatin from four biological replicates of HeLa S3 cells was isolated and immunoprecipitated using appropriated antibodies. ChIP DNA was purified, replicate samples were pooled and quantified, and 0.5 ng of ChIP DNA and corresponding input DNA were assayed in duplicate by quantitative real-time PCR using iCycler™ and SYBR-green iQ™ Supermix (Bio-Rad Laboratories, 170-8882). The cycle-number differences between ChIP DNA and input DNA were normalized using a pool of random controls, and were scored as positive if the differences were 2 standard deviations above the average of the controls. Three sets of genomic regions were selected and tested:

Group I: A. Between 11-13 of these were from the False Discovery Rate of 1% (FDR1);B. Between 6-12 of these were selected from fdr5, but did not overlap with fdr1; C. Between 2-13 of these were selected from fdr10, but did not overlap with fdr1 nor fdr5 lists; D. Between 1-4 of these were selected from results from the PCR product arrays, but did not overlap with the fdr1, fdr5, and fdr10 lists.

The validation rate for each category was computed as # of positives/ total tested.

Group II. To estimate the specificity of the results, 48 random genomic regions from the ENCODE sequences were selected, primers were designed and real-time quantitative PCR was performed to test their enrichment in ChIP DNA, compared to the input DNA. The number of negatives in this assay was compared to that of the ChIP-chip hit lists at different cutoffs. If the region is negative by qPCR but positive by ChIP-chip, then it is counted as a false positive (FP). It the region is negative by both methods then it is counted as true negatives (TN). The specificity is calculated as TN/(TN + FP).

Group III. To estimate the sensitivity of the results, 48 known promoters were selected. Primers were designed and real-time quantitative PCR was performed to test their enrichment in ChIP DNA, compared to input DNA. The number of positives in this assay was compared to that of the ChIP-chip hit lists at different cutoffs. If the region is positive by qPCR but negative by ChIP-chip, then it is counted as a false negative (FN). If the region is tested positive by both methods, then it is counted as a true positive (TP). The sensitivity is calculated as TP/(TP+ FN).

The results of the validation experiments are listed below:

	H3K4me2	H3K4me3	H3ac	H4ac	RNA PolII	TAF1
Random Controls						
1% FDR	45/45 100.00	46/46 100.00	44/44 100.00	45/47 95.74	47/47 100.00	46/47 97.87
5% FDR	45/45 100.00	46/46 100.00	44/45 97.78	45/47 95.74	47/47 100.00	46/47 97.87
10% FDR	45/45 100.00	46/46 100.00	44/46 95.65	45/47 95.74	47/48 97.92	46/47 97.87
Positive Controls						
1% FDR	28/30 93.33	30/31 96.77	30/33 90.91	13/26 50.00	18/30 60.00	16/33 48.48
5% FDR	30/30 100.00	31/31 100.00	33/33 100.00	18/26 69.23	22/30 73.33	20/33 60.61
10% FDR	30/30 100.00	31/31 100.00	33/33 100.00	20/26 76.92	25/30 83.33	22/33 66.67
PCR Arrays Only	30/30 100.00	31/31 100.00	33/33 100.00	76.92	25/30 83.33	22/33 66.67
Validation						
1% FDR	10/12 83.33	10/11 90.91	8/11 72.73	9/13 69.23	12/12 100.00	13/13 100.00
5% FDR	3/12 25.00	1/12 8.33	5/6 83.33	9/11 81.82	12/12 100.00	10/11 90.91
10% FDR	2/13	2/12	0/2	8/11	5/6	10/11

	15.38	16.67	0.00	72.73	83.33	90.91
PCR Arrays only	1/4 25.00	2/2 100.00	1/3 33.33	1/4 25.00	1/1 100.00	1/3 33.33

2. Validation of histone modification ChIP-chip data by qPCR (Dunham Lab)

Koch, C.M., Andrews, R.M., Flicek, P., Dillon, S.C., Karaöz, U., Clelland, G.K., Wilcox, S., Beare, D.M., Fowler, J.C., Couttet, P., et al. 2007. The landscape of histone modifications across 1% of the human genome in five human cell lines. *Genome Res*. doi: 10.1101/gr.5704207

DOI: 10.1101/gr.5704207
URL: http://dx.doi.org/10.1101/gr.5704207

In order to validate the ChIP-CHIP data, we identified and developed working assays for 74 enriched regions and 27 background signal regions for testing by quantitative PCR (qPCR) on anti-H3K4me3 ChIP material from the GM06990 cell line (for results, see Koch et al. doi:10.1101/gr.5704207).[2]
By designing qPCR assays tiling through six representative ChIP-CHIP enrichment peaks we were able to reproduce qualitatively the enrichment profiles observed on the microarray (see Figure S2, Koch et al. doi:10.1101/gr.5704207).

Real time PCR
The enrichment (relative copy number) was determined in real-time PCR reactions using either ChIP DNA or non enriched DNA as template. For primer pair design and methods see Koch et al. doi:10.1101/gr.5704207).

3. Validation of Replication Timing Data (Dutta Lab)

Karnani, N., Taylor, C., Malhotra, A., Dutta, A. 2007. Pan-S replication patterns and chromosomal domains defined by genome tiling arrays of ENCODE genomic areas. *Genome Res*. doi: 10.1101/gr.5427007.

DOI: 10.1101/gr.5427007
URL http://dx.doi.org/10.1101/gr.5427007

The tiling array based replication timing data from HeLa cells has been validated by interphase FISH and is detailed in Karnani et al. doi:10.1101/gr.5427007. Interphase FISH probes from ENCODE regions are listed alongside FISH results of replication time in HeLa cells released from thymidine/aphidicolin block in Karnani et al. Supplemental Table 2.

Tiling array data for time of replication and interphase FISH results for validating replication timing in HeLa are presented in Karnani et al. Figures 2 and 3, respectively.

4. Verification of HL60 cytosolic polyA+ RNA TxFrag results (Affymetrix Group - Phil Kapranov)

This section is taken from the Supplementary Information of the present manuscript: The ENCODE Consortium. The ENCODE pilot project: Identification and analysis of functional elements in 1% of the human genome and from Denoeud et al. doi:10.1101/gr.5660607.

Validation Supplement Table 2 Validation results of Affymetrix genome tiling array maps

	Index TF	Successful RACE reactions (%)				Transcription on both strands	No transcript detected
		5' RACE	3' RACE	5' and 3' RACE	5' or 3' RACE		
Exonic	20	19 (95)	19 (95)	16 (80)	20 (100)	19 (95)	0 (0)
Intronic	90	71 (79)	77 (86)	66 (73)	79 (88)	65 (72)	11 (12)
Intergenic	90	62 (69)	65 (72)	44 (49)	77 (86)	46(51)	13 (14)
Non Transfrag Regions	100	66 (66)	60 (60)	45 (45)	75 (75)	44 (44)	25 (25)
Numbers represent transfrags. Numbers in () represent % of total number of regions tested.							

200 transfrags were randomly chosen from the map of HL60 cell line un-stimulated (00hr time point) with retinoic acid. The transfrags consisted of 90 intergenic transfrags, 90 intronic and 20 exonic transfrags. Intergenic or intronic transfrags were defined as correspondingly non-overlapping or overlapping the bounds of known genes from the UCSC Known Gene track on the hs.NCBIv35 version of the genome. Intergenic and intronic transfrags were selected not to overlap any mRNA or EST annotation. Information on the index transfrags, primers used for this analysis can be found at http://genome.imim.es/gencode/RACEdb. 100 non-transfrag regions that mimic transfrags in length were randomly selected throughout the non-repetitive portions of the ENCODE regions.

5' and 3' RACE analysis was performed on DNAseI-treated cytosolic polyA+ RNA from un-stimulated HL60 cell line for each transfrag for each strand of the genome totaling to 4 RACE reactions per transfrag. RACE reactions were performed essentially as described in Kapranov et al[6] with the following modifications. cDNA synthesis for the 5'RACE was performed with a pool of 12 gene-specific primers. cDNA synthesis was done with two reverse-transcriptases: Superscript II and Thermoscript (both form

Invitrogen) in two separated reactions with 50 ng of polyA+ RNA each. The cDNA reactions were pooled for the RT-PCR step. cDNA synthesis for the 3'RACE was performed with oligo-dT 3' CDS primer as in Kapranov et al[5]. The cDNA was treated with RNAse A/T1 cocktail (Ambion) and RNAse H (Epicentre), purified over Qiagen's columns and pooled for the RT-PCR step. 40 ng of purified cDNA were used as starting material for each RT-PCR reaction. Three rounds of amplifications were performed at the RT-PCR step of the RACE utilizing 3 transfrag-specific nested RT-PCR primers for both 3' and 5' RACE. After each round, the RT-PCR reactions were purified using QIAquick 96 PCR purification system (Qiagen) and eluted in 70 μl. 1 μl of the first round amplification was used as a template for the second round and 0.01 μl of the second round RT-PCR reaction was used as a template for the third round. Oligonucleotides 3' CDS, UPL/UPS and NUP (Clontech SMART II RACE protocol) were used as common primes for the first, second and third round of RT-PCR. Each round of amplification consisted of 25 cycles of PCR (94°C for 20 sec; 62°C for 30 sec; 72°C for 5 min) followed by 10 min at 72°C. Products of the final round of RT-PCRs were purified using QIAquick 96, pooled and hybridized to ENCODE arrays as described above. The maps were generated using the Tiling Analysis Software (TAS; http://www.affymetrix.com/support/developer/downloads/TilingArrayTools/index.affx) with bandwidth of 50. RACEfrags were generated using threshold of 100, maxgap =50 and minrun =50. .

The Affymetrix RACEfrags were filtered so that each pool contains RACEfrags that are unique to the pool. GENCODE RACEfrags were filtered against Affymetrix RACEfrags. Regions overlapping RACEfrags from the Affymetrix pools were removed. Pooling was done so that the index transfrags within each pool are at least 40 kbp apart from each other. This is to facilitate the unambiguous assignment of the parent child relationships between the index transfrag and the RACEfrag. A region (transfrag or non-transfrag) was considered to be positive for presence of a transcript of either 5' or 3' RACE reaction was scored positive on either strand.

To control for genomic DNA contamination, 3' RACE reactions were conducted on the 100 non-transfrag regions with the omission of the reverse transcriptase. Only 1 region was scored as positive.

The data for the entire verification dataset can loaded from a centralized RACE database RACEdb located at this URL http://genome.imim.es/gencode/RACEdb. Also, the profile of each RACE reaction for each of the 300 index regions could be viewed via the links provided in this database in the UCSC browser or loaded as a BED file.

5. Validation experiments for DNase-chip (Crawford Group)

Crawford, G. E. et al. DNase-chip: a high-resolution method to identify DNase I hypersensitive sites using tiled microarrays. Nat Methods 3, 503-9 (2006)

DOI: doi:10.1038/nmeth888
URL: http://dx.doi.org/doi:10.1038/nmeth888

Validation was provided by Real time PCR on putative DNaseHS sites. 7 different catagories of sites were used depending on the presence of sites at different DNase concentrations. Data is shown in Figure 2a,b and in Supplementary Table 1.

6. Experimental Testing of Connectivity of Genomic Regions (Yale Group – Joel Rozowsky)

Rozowsky, J., Newburger, D., Sayward, F., Wu, J., Jordan, G., Korbel, J.O., Nagalakshmi, U., Yang, J., Zheng, D., Guigo, R., et al. 2007. The DART classification of unannotated transcription within the ENCODE regions: Associating transcription with known and novel loci. *Genome Res*. doi: 10.1101/gr.5696007.

DOI: 10.1101/gr.5696007
URL: http://dx.doi.org/10.1101/gr.5696007

RT-PCR and Sequencing was carried out for novel TARs expressed in placental RNA as described in Rozowsky et al. doi:10.1101/gr.5696007.[10] A table of the regions selected for RT-PCR validation testing for connectivity and their corresponding annotation and primer sequences are indicated in Rozowsky et al. Supplemental Table 1.

The sequences, forward and reverse primer sequences, the length of the unspliced genomic span between the primers and the length of the sequenced product obtained for PCR products that were sequenced is dispayed in Rozowsky et al. Supplemental Table 2.

7. Validation of STAT1 ChIP-chip and ChIP-PET (Yale Group – Mike Snyder)

Euskirchen, G.M., Rozowsky, J., Wei, C.-L., Lee, W.H., Zhang, Z.D., Hartmen, S., Emanuelsson, O., Stolc, V., Weissman, S., Gerstein, M., et al. 2007. Mapping of transcription factor binding regions in mammalian cells by ChIP: Comparison of array and sequencing based technologies. *Genome Res*. doi: 10.1101/gr.5583007

DOI: 10.1101/gr.5583007
URL: http://dx.doi.org/10.1101/gr.5583007

Yale Validation
Stat1 ChIP-chip and ChIP-PET datasets were validated in at least two biological replicate experiments using a quantitative PCR assay. Details of this analysis are available in Euskirchen et al. doi:10.1101/gr.5583007[11].

8. Validation of DnaseI hypersensitive site (DHS) mapping by DNase-array and QCP (Stamatoyannopoulos Lab)

Quantitative Chromatin Profiling (QCP)
Dorschner MO, Hawrylycz M, Humbert R, Wallace JC, Shafer A, Kawamoto J, Mack J, Hall R, Goldy J, Sabo PJ, Kohli A, Li Q, McArthur M, Stamatoyannopoulos JA. High-throughput localization of functional elements by quantitative chromatin profiling. Nat Methods 1, 219-25 (2004).

DOI: 10.1038/nmeth721
URL http://dx.doi.org/10.1038/nmeth721

To validate that DHSs identified by QCP correspond with classical DnaseI hypersensitive sites, we compared QCP data (high-throughput real-time quantitative PCR using end-to-end tiled ~225bp amplicons) with previously published DNaseI hypersensitivity Southern data from multiple loci (alpha- and beta-globin, T-cell receptor alpha, c-myc, adenosine deaminase, CD2) in erythroid, lymphoid, and hepatic cell types. 100% of known DHSs were detected. Novel sites were verified by conventional Southern blotting. Results are shown in Figs. 2-6, Supplementary Figs. 1-2, and Supplementary Table 1.

In unpublished studies during the ENCODE Pilot Project we additionally performed extensive conventional DnaseI hypersensitivity mapping in GM06990, CACO2, K562, HepG2, and SKnSH chromatin using conventional hypersensitivity Southerns. In total we performed 1,114 Southern end-label experiments. On the basis of these experiments the sensitivity of QCP was calculated to be 94.1% and specificity 99.8%.

Dnase-array
Sabo PJ, Kuehn MS, Thurman R, Johnson BE, Johnson EM, Cao H, Yu M, Rosenzweig E, Goldy J, Haydock A, Weaver M, Shafer A, Lee K, Neri F, Humbert R, Singer MA, Richmond TA, Dorschner MO, McArthur M, Hawrylycz M, Green RD, Navas PA, Noble WS, Stamatoyannopoulos JA. Genome-scale mapping of DNase I sensitivity in vivo using tiling DNA microarrays. Nat Methods 3, 511-8 (2006)

DOI: 10.1038/nmeth890
URL http://dx.doi.org/10.1038/nmeth890

To validate that DHSs identified by DNase-array correspond with classical DnaseI hypersensitive sites, we performed extensive conventional DnaseI hypersensitivity Southern mapping in lymphoblastoid (GM06990) cells. Results are shown in Fig. 2, Supplementary Fig. 1, Table 1 and Supplementary Table 2.

9. Validation of E2F1 ChIP-chip results (Farnham Lab)

Mark Bieda, Xiaoqin Xu, Michael A. Singer, Roland Green and Peggy J. Farnham Unbiased location analysis of E2F1-binding sites suggests a widespread role for E2F1 in the human genome

DOI : 10.1101/gr.4887606
URL: http://dx.doi.org/ 10.1101/gr.4887606

PCR quantification was performed using standard methods; in brief, primers were designed to test a subset of predicted binding sites. The PCR product for the ChIP sample was compared to the control sample. PCR confirmation experiments are described in Bieda et al. doi:10.1101/gr.4887606 Results of PCR confirmation of peak predictions are in Bieda et al. Supplemental Table 1.

10. Quantitative PCR (qPCR) validation of FAIRE sample (Iyer and Lieb Labs)

Paul G. Giresi, Jonghwan Kim, Ryan M. McDaniell, Vishwanath R. Iyer, and Jason D. Lieb. 2006. FAIRE (Formaldehyde-Assisted Isolation of Regulatory Elements) isolates active regulatory elements from human chromatin. *Genome Res.* Published December 19, doi:10.1101/gr.5533506.

DOI: 10.1101/gr.5533506
URL: http://dx.doi.org/10.1101/gr.5533506

The FAIRE procedure and qPCR validation is described in Giresi et al. 10.1101/gr.5533507.[14] FAIRE validation results for a portion of chromosome 21 are displayed in Giresi et al. Figure 3.

11. Quantitative PCR validation of ChIP-chip data (Struhl Lab)

The validation of this data has not yet been separately published.

The validation qPCR was performed a previously described in Beida etal, Genome Research, 16, 595-605. using an Applied Biosystems 7000 sequence detector and an Applied Biosystems 7700 sequence detector for SYBR green fluorescence. The PCR program was: 95 oC 10 min, followed by 40 cycles of 95 oC, 30 sec, 60 oC, 45 sec; 72 oC, 1 min. Fold enrichment for a for a called site from an array region was determined relative to a non-enriched region reference region determined for each factor. The formula used was: fold enrichment = $1.9-(\Delta CTexpt-\Delta CTref)$ where ΔCT is the cycle threshold (Ct) difference between ChIP DNA and input material, calculated for experimental and reference regions, and 1.9 is the mean primer slope. Sites tested were selected to encompass a large range of pValues as well as several array regions that were not called sites for a specific factor for use as negative controls. A called site was considered a true site if the qPCR fold enrichment value was greater than or equal to 3 standard deviations above the mean of the negative controls sites.

The pValue used to threshold the list of potential sites was determined by extrapolation qPCR results of true versus false sites along the list of pValues such that a 95% accuracy rate was required for qPCR. Therefore, by definition the final number of sites provided in table 1 are based on a 5% FDR. False negative rate was determined by calculating the percentage of true sites tested by qPCR that fall below

the pValue cutoff. This percentage was then applied to the original site lists to estimate the number of potential false negative sites for each factor.

Validation Supplement Table 6: Summary of threshold sites, false discovery, and false negative rates.

| Factor	Time Point	Original Number of Sites	Pvalue Threshold at 68%	Thresholded Sites	# True Positive Sites	# False Positive Sites	False Negative Rate	# False Negative Sites
Brg1	0 hour	1154		27	26	1		102
	2 hour	117	74	2	2	0	9.09%	10
	8 hour	717		16	15	1		64
	32 hour	417		15	14	1		37
C/EBPe	0 hour	1351		195	185	10		349
	2 hour	1176	70	163	155	8	30.20%	306
	8 hour	1521		234	222	12		389
	32 hour	535		187	178	9		105
H3 Ac **	0 hour	97		96	96			
	2 hour	99	36	99	99	NA	NA	NA
	8 hour	117		116	116			
	32 hour	102		100	100			
H4 Ac	0 hour	2371		1101	1046	55		546
	2 hour	891	56	508	483	25	43.30%	165
	8 hour	1914		727	691	36		513
	32 hour	1149		671	637	34		207
H3K27 Tri-ME	0 hour	1672		213	202	11		941
	2 hour	1525	50	285	271	14	64.50%	800
	8 hour	2769		513	487	26		1455
	32 hour	1439		233	221	12		778
Pol2	0 hour	1363		310	295	16		374
	2 hour	479	76	155	147	8	35.50%	115
	8 hour	819		242	230	12		205
	32 hour	1149		396	376	20		267
p300	0 hour	1251		11	10	1		620
	2 hour	2852	95	65	62	3	50.00%	1384
	8 hour	2506		60	57	3		1223
	32 hour	910		22	21	1		444
SirT1	0 hour	237		2	2	0		50
	2 hour	557	60	4	4	0	21.43%	118
	8 hour	219		2	2	0		46
	32 hour	505		11	10	1		106

**Pvalue Threshold of H3 is 100% as all predicted sites tested by qPCR were positive and thus a 0% FDR is used for this factor.
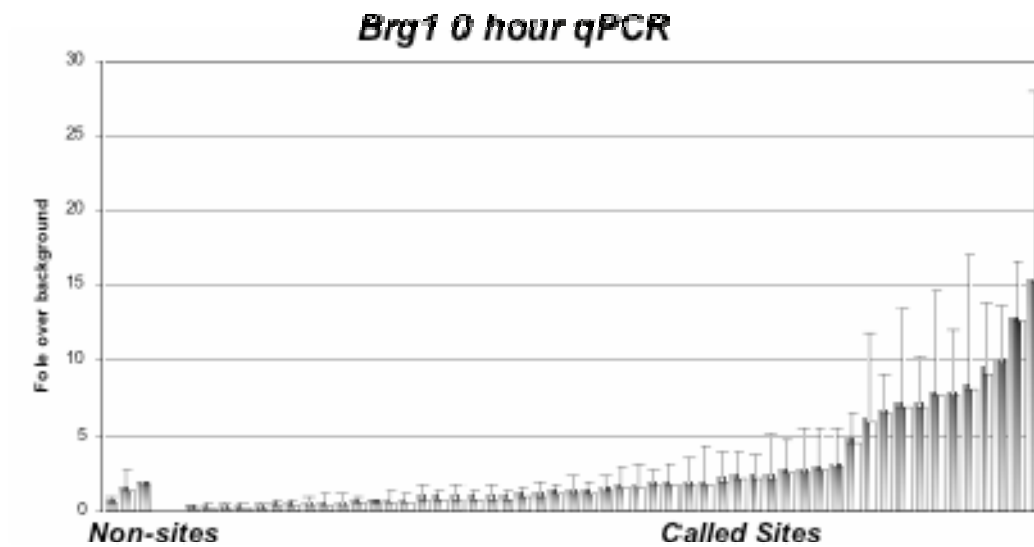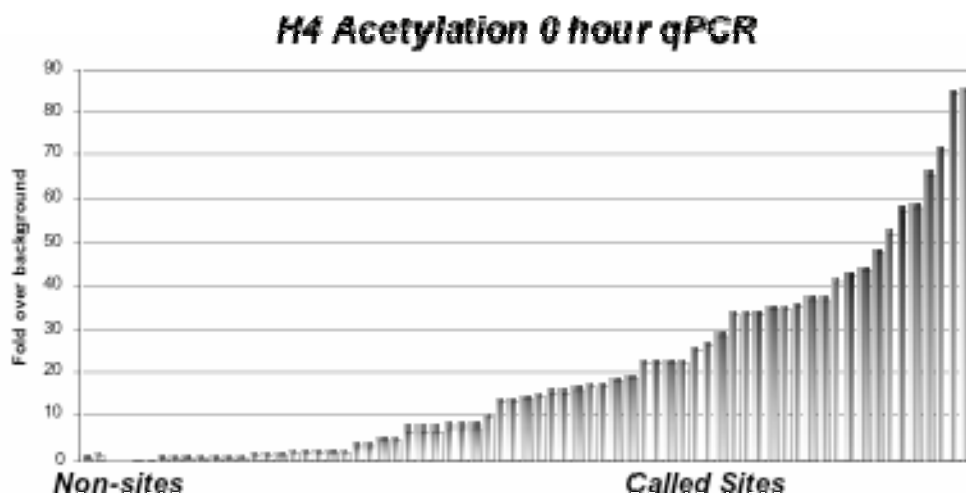
Validation Supplement Figure 1: QPCR validation of Brg1. 0 hour. 55 array regions were checked, including 52 called sites and 3 non-sites. The qPCR enrichment cut off is 3.17 fold.
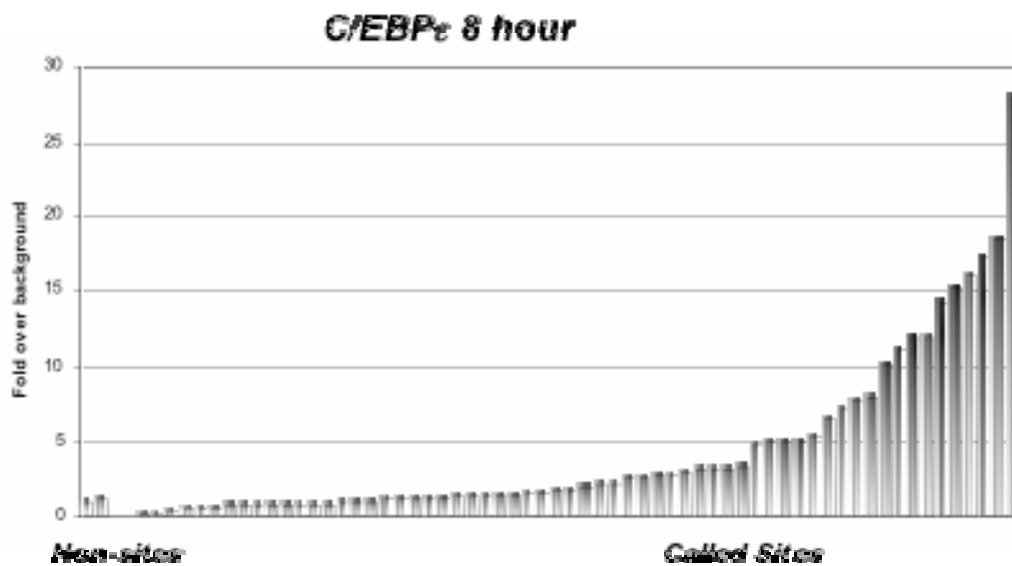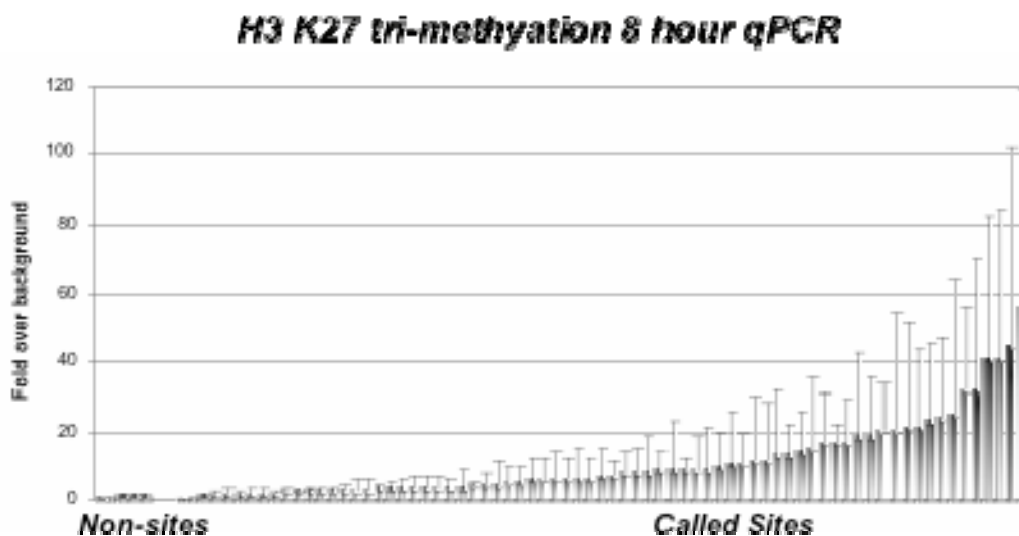

Validation Supplement Figure 2: QPCR validation of C/EBPε. 8 hour. 64 array regions were checked, including 62 called sites and 2 non-sites. The qPCR enrichment cut off is 2 fold.
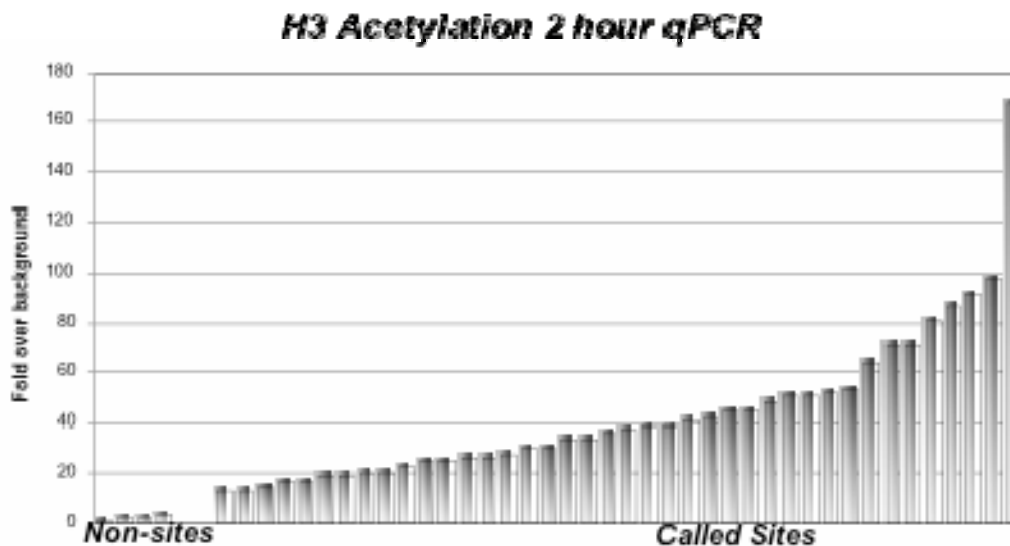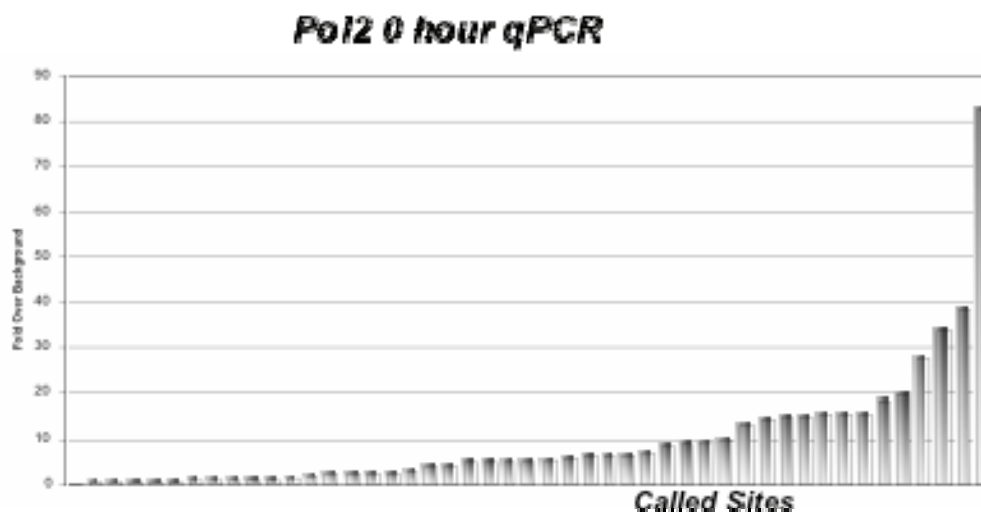
Validation Supplement Figure 3: QPCR validation of H3ac. 2 hour. 44 array regions were checked, including 40 called sites and 4 non-sites. The qPCR enrichment cut off is 6.8 fold.
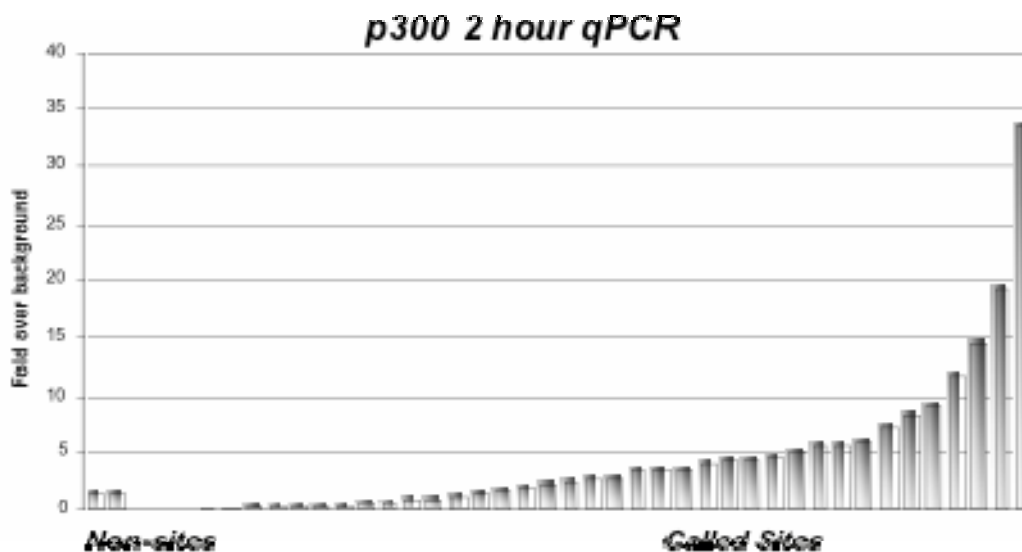

Validation Supplement Figure 4: QPCR validation of H4ac. 0 hour. 67 array regions were checked, including 65 called sites and 2 non-sites. The qPCR enrichment cut off is 3.4 fold.
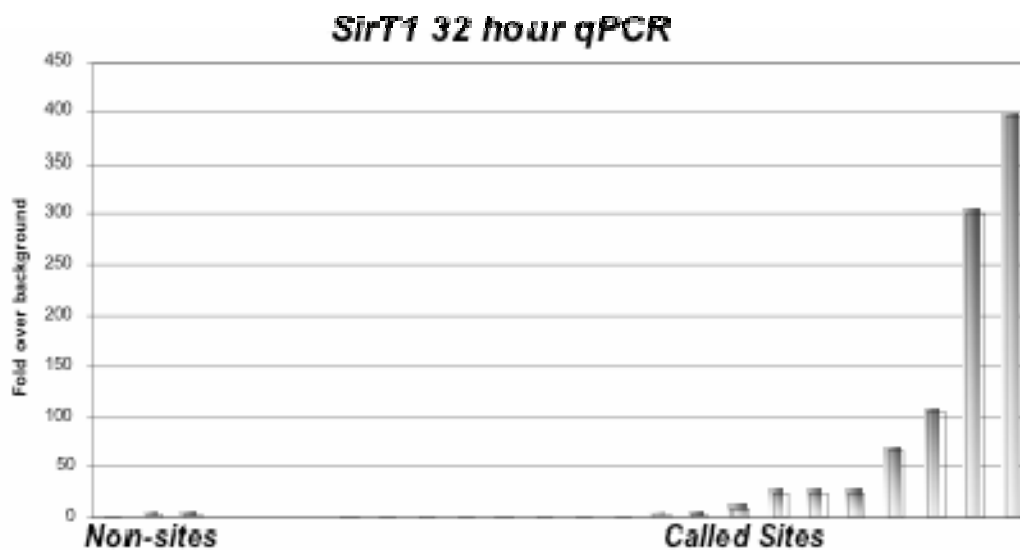
Validation Supplement Figure 5: QPCR validation of H3K27me3. 8 hour. 78 array regions were checked, including 73 called sites and 5 non-sites. The qPCR enrichment cut off is 2.34 fold.

Validation Supplement Figure 6: QPCR validation of RNA PolII. 0 hour. 52 array regions were checked including 47 called sites and 5 non-sites. The qPCR enrichment cut off is 3 fold.

Validation Supplement Figure 7: OPCR Validation of p300. 2 hour. 40 array regions were checked, including 38 called sites and 2 non-sites. The qPCR enrichment cut off is 2 fold.

Validation Supplement Figure 8: QPCR validation of SirT1. 32 hour. 22 array regions were checked, including 19 called sites and 3 non-sites. The qPCR cut off is 6.99 fold.